THE UNIVERSITY
of EDINBURGH

IMAGING CALCIFICATION IN AORTIC STENOSIS

Dr Tania Pawade

BMedSci (Hons) MB ChB (Hons) MRCP

A thesis presented for the degree of Doctor of Philosophy at the University of Edinburgh July 2017

To Joya, Ash, Vivien, Natasha, Lara and Kelly

ABSTRACT

BACKGROUND

Aortic stenosis is a common and potentially fatal condition in which fibro-calcific changes within the valve leaflets lead to the obstruction of blood flow. Severe symptomatic stenosis is an indication for aortic valve replacement and timely referral is essential to prevent adverse clinical events. Calcification is believed to represent the central process driving disease progression. 18F-Fluoride positron emission tomography computed tomography (PET-CT) and CT aortic valve calcium scoring (CT-AVC) quantify calcification activity and burden respectively. The overarching aim of this thesis was to evaluate the applications of these techniques to the study and management of aortic stenosis.

METHODS AND RESULTS

REPRODUCIBILITY

The scan-rescan reproducibility of 18F-fluoride PET-CT and CT-AVC were investigated in 15 patients with mild, moderate and severe aortic stenosis who underwent repeated 18F-fluoride PET-CT scans 3.9±3.3 weeks apart. Modified techniques enhanced image quality and facilitated clear localization of calcification activity. Percentage error was reduced from ±63% to ±10% (tissue-to-background ratio most-diseased segment (MDS) mean of 1.55, bias -0.05, limits of agreement -0·20 to +0·11). Excellent scan-rescan reproducibility was also observed for CT-AVC scoring (mean of differences 2% [limits of agreement, 16 to -12%]).

AORTIC VALVE CALCIUM SCORE: SINGLE CENTRE STUDY

Sex-specific CT-AVC thresholds (2065 in men and 1271 in women) have been proposed as a flow-independent technique for diagnosing severe aortic stenosis. In a prospective cohort study, the impact of CT-AVC scores upon echocardiographic measures of severity, disease progression and aortic valve replacement (AVR)/death were examined. Volunteers (20 controls, 20 with aortic sclerosis, 25 with mild, 33 with moderate and 23 with severe aortic stenosis) underwent CT-AVC and echocardiography at baseline and again at either 1 or 2-year time-points. Women required less calcification than men for the same degree of stenosis ($p<0.001$). Baseline CT-AVC measurements appeared to provide the best prediction of subsequent disease progression. After adjustment for age, sex, peak aortic jet velocity (Vmax) ≥ 4m/s and aortic valve area (AVA)<1 cm^2, the published CT-AVC thresholds were the only independent predictor of AVR/death (hazard ratio = 6.39, 95% confidence intervals, 2.90-14.05, $p<0.001$).

AORTIC VALVE CALCIUM SCORE: MULTICENTRE STUDY

CT-AVC thresholds were next examined in an international multicenter registry incorporating a wide range of patient populations, scanner vendors and analysis platforms. Eight centres contributed data from 918 patients (age 77±10, 60% male, Vmax 3.88±0.90 m/s) who had undergone ECG-gated CT within 3 months of echocardiography. Of these 708 (77%) had concordant echocardiographic assessments, in whom our own optimum sex-specific CT-AVC thresholds (women

1377, men 2062 AU) were nearly identical to those previously published. These thresholds provided excellent discrimination for severe stenosis (c-statistic: women 0.92, men 0.88) and independently predicted AVR and death after adjustment for age, sex, Vmax ≥4 m/s and AVA <1 cm^2 (hazards ratio, 3.02 [95% confidence intervals, 1.83-4.99], p<0.001). In patients with discordant echocardiographic assessments (n=210), CT-AVC thresholds predicted an adverse prognosis.

BICUSPID AORTIC VALVES

Within the multicentre study, higher continuity-derived estimates of aortic valve area were observed in patients with bicuspid valves (n=68, 1.07±0.35 cm) compared to those with tri-leaflet valves (0.89±0.36 cm p<0.001,). This was despite no differences in measurements of Vmax (p=0.152), or CT-AVC scores (p=0.313). The accuracy of AVA measurments in bicuspid valves was therefore tested against alternative markers of disease severity. AVA measurements in bicuspid valves demonstrated extremely weak associations with CT-AVC scores (r^2=0.08, p=0.02) and failed to correlate with downstream markers of disease severity in the valve and myocardium and against clinical outcomes. AVA measurements in bicuspid patients also failed to independently predict AVR/death after adjustment for Vmax ≥4 m/s, age and gender. In this population CT-AVC thresholds (women 1377, men 2062 AU) again provided excellent discrimination for severe stenosis.

CONCLUSIONS

Optimised 18F-fluoride PET-CT scans quantify and localise calcification activity, consolidating its potential as a biomarker or end-point in clinical trials of novel therapies. CT calcium scoring of aortic valves is a reproducible technique, which provides diagnostic clarity in addition to powerful prediction of disease progression and adverse clinical events.

LAY SUMMARY

Aortic Stenosis is a condition whereby one of the major heart valves through which blood exits the heart (the aortic valve) becomes progressively narrowed (stenosed) over a number of years. It is already the commonest form of valve disease in the western world and is set to become increasingly common. It is usually caused by the formation of calcium (calcification) on the valve leaflets and can eventually put a strain on the heart which has to work harder to pump blood through a narrowed valve. Presently, the only available treatment involves replacing the heart valve with an artificial valve once a patient with severe aortic stenosis develops symptoms such as breathlessness, chest pain or blackouts.

It was previously believed that calcium simply settled on the valve in a passive manner however it is now becoming increasingly apparent that the calcification process actually resembles that of bone formation and is now considered to be the central driver of disease progression. The overarching aim of this thesis was to explore whether advances in cardiac imaging could be harnessed to measure valve calcification and subsequently improve patient care.

Positron emission tomography (PET) is an imaging technique used to study calcification processes at a molecular level within the bone. We have recently shown that PET can also be to measure the amount of calcium actively forming within the aortic valve. In this thesis, I have refined this technique such that it is currently being used in a clinical trial examining whether medical treatments currently used to treat bone disorders, can slow the progression of aortic stenosis.

Ultrasound technology (echocardiography) is relied upon heavily by clinicans to grade the severity of the valve narrowing as mild, moderate or severe thereby identifying those patients who should be referred for surgery. However in approximately a quarter of cases, the different measurements used to grade severity can give conflicting information creating uncertainty as to the best course of action. Computed Tomography (CT) is a scanning technique which creates detailed pictures using X-rays, it can be used to measure the amount of established calcium on the valve (calcium scoring). I have shown how CT calcium scoring only provides an alternative method for identifying patients with severe disease, but also identifies those at risk of faster disease progression and worse clinical outcomes. We therefore believe it should be used as an additional test in cases of uncertainty to provide clarity with respect to diagnosis and management of patients with aortic stenosis. Indeed CT calcium scoring has recently been included in the European Society of Cardiology guidelines for the management of aortic stenosis.

CONTENTS

FIGURES INDEX

TABLES INDEX

DECLARATION

This thesis represents research undertaken at the Clinical Research Facility, University of Edinburgh, Clinical Research Imaging Centre, University of Edinburgh and the Royal Infirmary of Edinburgh between March 2014 and July 2017.

This thesis was supported by the British Heart Foundation scholarship SS/CH/09/02 and then the British Heart Foundation Clinical PhD training fellowship FS/16/19/31982. I was personally responsible for the setup, recruitment and conduct of Saltire 2 which features in all 4 chapters. Data has also been contributed by the following investigators; Dr William Jenkins, Dr Marc Dweck, Dr Calvin Chin and Dr Russell Everett. These have been appropriately acknowledged throughout the thesis.

At the time of writing, chapters 1 and 3 have been published in peer-reviewed journals, appropriate permissions have been obtained for reproduction. This thesis has not been accepted in any previous applications for a degree and all sources of information have been acknowledged. All studies were undertaken in accordance with the declaration of Helsinki of the World Medical Association and the regulations of the South East Scotland Ethics Committee.

13h May 2017

ACKNOWLEDGEMENTS

I would like to thank Professor David Newby (Professor of cardiology and consultant cardiologist) for giving me the opportunity to undertake my research under his guidance. I would also like to thank Marc Dweck (senior lecturer in cardiology) who co-supervised this thesis. Both of these individuals have provided me with a huge amount of advice, encouragement and support for which I am indebted.

I am extremely grateful to the British Heart Foundation for their generosity in supporting both myself and this research.

I would like to thank the staff at the clinical research facility who have worked incredibly hard to support the Saltire 2 study and who have had to accommodate me, often at short notice! I would also like to thank all the staff at the Clinical Research Imaging Centre who have had to do the same. I would especially like to thank Audrey White for her tireless dedication and friendship.

I would like to acknowledge my friends in the barn who have been a huge support to me both professionally and personally, with particular thanks to Tim Cartlidge, Simon Wilson, William Jenkins and Russell Everett.

Finally I would like to thank my family, without whose support, nothing would have been possible.

ABBREVIATIONS

18F-Fluoride	18F-Sodium fluoride
AS	Aortic Stenosis
AU	Agatston Units
AVA(i)	Aortic Valve Area (index)
AVR	Aortic valve replacement
AVC	Aortic valve calcium
BMI	Body mass index
BMP	Bone morphogenic protein
CT	Computed Tomography
CT-AVC	Computed tomography aortic valve calcium score
EF	Ejection fraction
LDL	Low density lipoprotein
LVOT	Left ventricular outflow tract
MRI	Magnetic resonance imaging
MG	Mean gradient
MDS	Most diseased segment
PET	Positron emission tomography
RA	Right atrium
RANK (L)	Receptor activator of nuclear kappa B (ligand)
ROI	Region of Interest
SV(i)	Stroke volume (index)
SUV	Standard uptake value
TAVI	Trans-catheter aortic valve implantation
TBR	Tissue to background ratio
Vmax	Peak velocity

.

OVERVIEW

Aortic stenosis is a global health concern. Severe stenosis is estimated to affect 3.4% of people above the age of 75 and the prevalence is continuing to increase. The disease process is characterised by progressive fibro-calcific processes within the valve leaflets leading to their restricted mobility and eventually the obstruction of blood flow from the heart. The onset of symptoms heralds a bleak prognosis unless patients undergo either aortic valve replacement surgery or trans-catheter implantation. Echocardiographic measurements of severity are used to distinguish between those patients in whom valve replacement is indicated and those in whom continued watchful waiting is safe. Consequently, clinical uncertainty arises when echocardiographic measurements give different readouts for severity.

Calcification is the central pathological process driving disease progression, therefore even a highly subjective, semi-quantitative, echocardiographic estimation of valvular calcium burden provides prognostic information more powerful than all other variables relied upon to grade disease severity. The poor reproducibility and a lack of confidence in subjective assessments may explain why echocardiographic calcium scoring has largely been overlooked in routine clinical practice. 18F-Fluoride positron emission tomography computed tomography (18F-fluoride PET-CT) and computed tomography calcium scoring (CT-AVC) can more accurately quantify calcification activity and burden respectively, thereby creating an opportunity to profoundly improve patient care. The purpose of this thesis is to study how these techniques should be applied to improve outcomes for patients with aortic stenosis.

Chapter 1: INTRODUCTION

Published by **Pawade TA**, Newby DE, Dweck MR. Calcification in Aortic Stenosis: The Skeleton Key. J Am Coll Cardiol. 2015 Aug 14; 66(5):561-77.

The normal aortic valve consists of three leaflets, each of which is a thin, flexible and mobile structure (1). In aortic stenosis, these leaflets become progressively thickened, fibrosed and calcified thereby restricting their mobility and obstructing the flow of blood from the heart. The onset of symptoms in combination with severe stenosis heralds a bleak prognosis with mortality rates of 26% and 48% at 1 and 2 years respectively (2-4). The only available treatment is an aortic valve replacement (AVR) or a trans-catheter aortic valve implantation (TAVI), however not all patients are suitable candidates for these procedures (5, 6). There are currently no medical therapies capable of modifying disease progression.

1.1 PREVALANCE

Aortic stenosis is common. Previous cross-sectional studies have estimated a population based prevalence of 0.2-0.4 % with a strong age correlation (7, 8). By pooling the data from 7 population-based studies, a recent meta-analysis estimated a prevalence of 12.4% in those aged ≥75 years. Within this age group alone, this corresponded to approximately 4.9 million people in 19 European countries. If only symptomatic severe AS is considered, this translated to 3.4% (1.0 million), a number projected to double by 2050 (9).

1.2 NATURAL HISTORY

There is considerable individual variability with respect to rates of hemodynamic progression and clinical course among adults with aortic stenosis. Collectively, prospective studies have observed annualised increases in peak aortic jet velocities of 0.15-0.3 m/s, mean gradients of 2.7-7 mmHg and decreases in aortic valve area of 0.03-0.1 cm^2 (10-13). Disease progression is largely dictated by baseline severity so there is currently no method of identifying patients who will experience progressive disease amongst those with mild aortic stenosis (12).

Severe aortic stenosis confers an adverse prognosis (14) even in the absence of symptoms (15). However even a diagnosis of mild or moderate aortic stenosis is an adverse prognostic marker. Whilst previous studies have implied that non-severe aortic stenosis is relatively benign, (16) these data were based on catheter-based estimates of disease severity and do not reflect current practice. By contrast, Rosenhek et al demonstrated that mortality in patients with mild to moderate aortic stenosis was 1.8 times higher than that of an age and gender-matched control population and 67 of 171 patients had valve surgery or died within a mean follow-up of 51 months (17). Rapid progression of moderate and even mild stenosis to haemodynamically severe disease was observed in 46% of patients. The strongest predictor of clinical events was the baseline echocardiographic aortic valve calcium score (17). These findings have been corroborated by other studies (12, 18). A method capable of predicting the natural history would therefore represent a significant clinical advance.

1.3 THE NORMAL AORTIC VALVE

The normal aortic valve is a feat of structural engineering, designed to withstand significant forces throughout each cardiac cycle and to last a lifetime. It is composed of three leaflets each of which consists of three layers (Figure 1.1, (19)).

Figure 1.1 The normal aortic valve

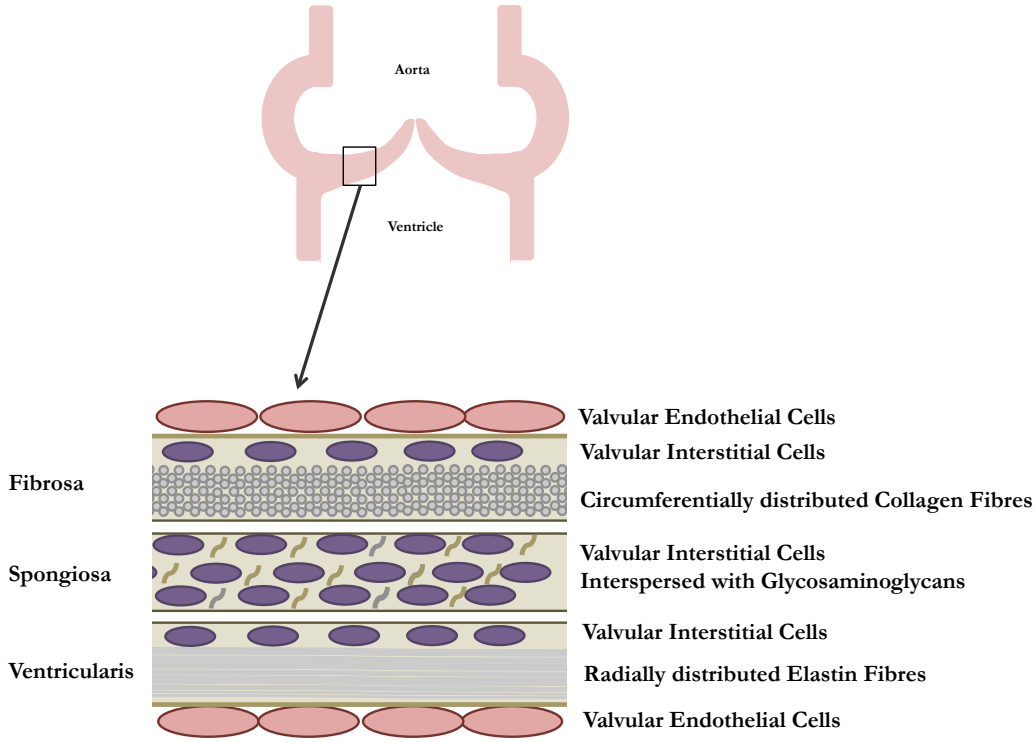

Fibrosa layer. This is sited on the aortic aspect of the valve. It consists of type 1 collagen fibres aligned in a circumferential distribution and is the principle load-bearing layer.

Spongiosa Layer. This functions as a shock-absorber and contains extracellular matrix components including glycosaminoglycans.

Ventricularis Layer. Facing the ventricular aspect, this layer consists of elastin fibres aligned in a radial distribution, which facilitate cusp closure.

The leaflets are lined by valvular endothelial cells. The fibroblast-like valvular interstitial cells are dispersed throughout all three layers.

1.4 PATHOLOGY OF AORTIC STENOSIS

Aortic stenosis was long dismissed as a degenerative condition whereby 'wear and tear' resulted in progressive calcium deposition upon the valve. However emerging evidence has indicated that it develops as part of a highly complex and tightly regulated series of processes each of which may be amenable to medical intervention (1). Aortic stenosis can be thought of as occurring in two phases: an early *initiation phase* dominated by valvular lipid deposition, injury and inflammation with many similarities to atherosclerosis, and a later *propagation phase* where pro-calcific and osteogenic factors take over and ultimately drive disease progression (Figure 1.2) (20).

1.4.1 Initiation Phase: Inflammation

The healthy aortic valve consists of two main cell types; valvular endothelial cells (VECs) and valvular interstitial cells (VICs). It is damage to the lining endothelial cells, which is thought to represent the primary event in the disease process. The mechanism of injury is not fully understood and will almost certainly vary between individuals depending on the primary aetiology. For example in those with bicuspid aortic valves, mechanical stress may provide the initial injurious stimulus as a bileaflet valve is unable to dissipate the haemodynamic stress as effectively as a tri-leaflet valve (21). Evidence for the central role of mechanical stress in the pathology of aortic stenosis can also be found in those with tri-leaflet valves as subsequent calcium distribution often occurs at sites of highest mechanical stress (22). Clearly however all aortic valves are subject to significant haemodynamic stress during the lifetime of an individual and not everyone develops aortic stenosis. Additional pathophysiological insights are provided by the apparent similarities with

atherosclerosis. Age, smoking, hypertension, hyperlipidaemia and diabetes are all associated with an increased likelihood of developing aortic stenosis (23-25) implicating these injurious stimuli as facilitators of endothelial injury. The early stages of aortic stenosis share histological similarities with atherosclerosis however again, not all patients with atherosclerosis develop aortic stenosis and whilst these pathologies undoubtedly overlap, they are not simply different manifestations of the same disease process (26). In the majority of patients, the development of aortic stenosis is likely to require a series of pathological 'hits' reflecting a complex interplay of environmental and genetic factors.

1.4.2 Initiation Phase: Lipids

Lipids: in particular lipoprotein (a) and oxidized low-density lipoprotein (LDL) are postulated to play a key role in the pathogenesis of aortic stenosis. Observational studies have identified cholesterol and its related lipoproteins as independent risk factors for the development of aortic stenosis (23-25, 27). Genetic predisposition to elevated LDL is associated with aortic valve calcification and aortic stenosis (27). Furthermore a strong genome-wide association was recently established between a single nucleotide polymorphism in the locus of lipoprotein (a) and the incidence of aortic valve calcification (28).

Figure 1.2 The pathophysiology of aortic stenosis.

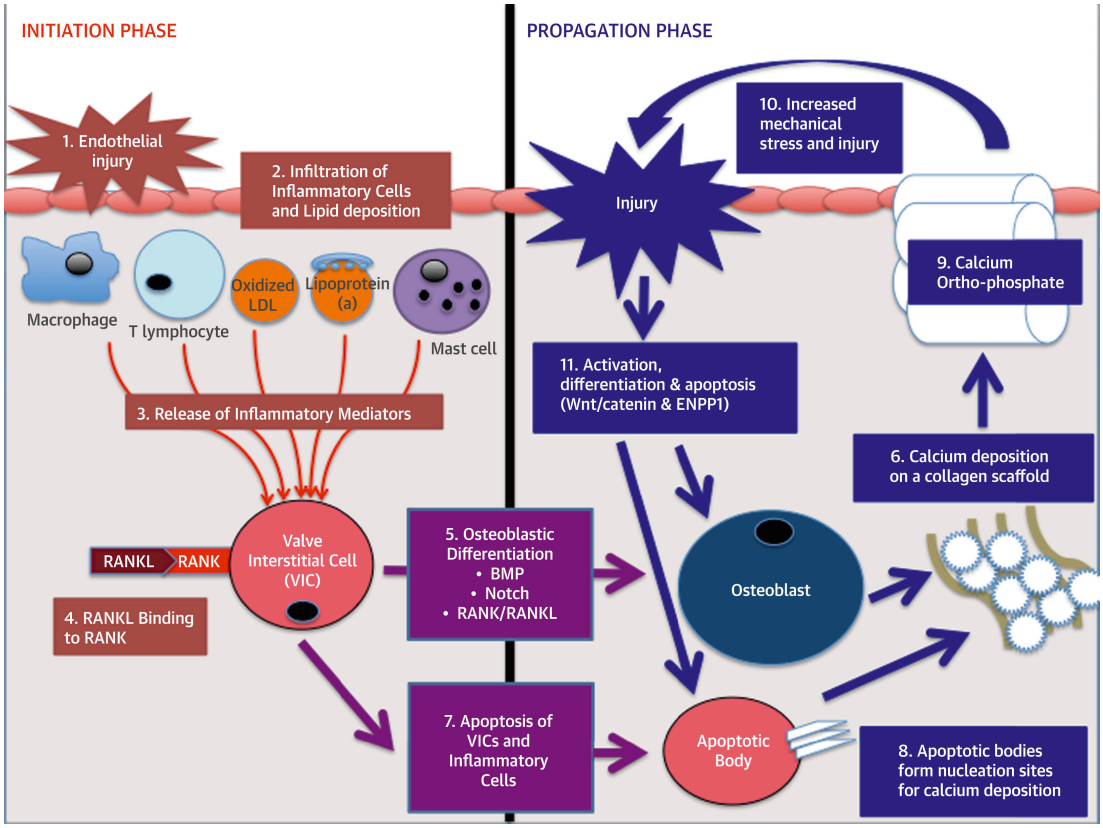

Initiation phase. Endothelial injury (1) facilitates the infiltration of oxidized lipids and inflammatory cells (2) into the valve and the release of pro-inflammatory mediators (3). These trigger the very early stages of valve calcification.

Propagation phase. Pro-inflammatory processes induce valvular interstitial cells to undergo osteogenic differentiation (5) via several different mechanisms, including the binding of RANKL to RANK. Differentiated cells within the aortic valve first lay down a collagen matrix and other bone-related proteins causing valvular thickening and stiffening (6) before producing calcium (7). Apoptotic remnants of some VICs and inflammatory cells (8) create a nidus for apoptosis-mediated calcification (9). Calcification of the valve (10) induces compliance mismatch resulting in increased mechanical stress and injury (11). This results in further calcification via osteogenic differentiation and apoptosis (12). Hence a self-perpetuating cycle of calcification, valve injury, apoptosis and osteogenic activation is established that drives the propagation phase of the disease.

Abbreviations: RANKL, receptor activator of nuclear kappa B ligand; RANK, receptor activator of nuclear kappa B; BMP, bone morphogenic protein; LDL, low density lipoprotein.

Pawade et al. JACC. 2014 (29)

Endothelial injury permits the infiltration of LDL, lipoprotein (a), macrophages and T lymphocytes, thus establishing an inflammatory milieu (22). Another features of aortic stenosis is increased oxidative stress partly due to uncoupling of nitric oxide synthase pathway (30). Whether this is a cause or consequence of endothelial injury is unclear but this perpetuates the oxidation of LDLs and further inflammation. Interestingly in established aortic stenosis, the degree of inflammation is similar in bicuspid and tri-leaflet valves(31)

1.4.3 Inflammation and Calcification

Regions of microcalcification that co-localize with sites of lipid deposition are observed at this early stage. These microscopic deposits of mineralization are more prominent in early valve lesions than would be typical of atherosclerosis suggesting that the pathologies may now be diverging (22). Calcification during the initiation stage may be mediated by cell death and the release of apoptotic bodies in these areas which can form a nidus for subsequent calcium formation (22). Furthermore hydroxyapatite deposition evokes further pro-inflammatory responses from macrophages, creating a positive feedback loop of calcification and inflammation in the early stages of disease (32). Indeed it seems likely that these mechanisms underlie early calcium formation in aortic stenosis and its association with lipid and inflammation.

The apparent link between lipid, inflammation and calcification in these early stages and the pathological similarities with atherosclerosis, led to the hypothesis that statins might be beneficial in patients with aortic stenosis. This was supported by encouraging hypercholesterolemic animal models demonstrating that lipid deposition

and oxidative stress precede the conversion of valvular interstitial cells to those with an osteoblastic phenotype, and that this process is inhibited by atorvastatin (33, 34). However when statins were formally tested in three independent randomised controlled trials of patients with aortic stenosis, each demonstrated a failure of this therapy to halt or retard aortic stenosis progression, despite the serum LDL cholesterol concentrations more than halving (11, 35, 36). This has led investigators to re-examine the pathophysiology underlying aortic stenosis and to the realization that whilst inflammation and lipid deposition may be important in establishing the disease (the initiation phase), the latter stages are instead characterized by an apparently self-perpetuating cycle of calcium formation and valvular injury (the propagation phase, (20). Indeed once this propagation phase has become established, disease progression is dictated neither by inflammation nor lipid deposition but rather by the relentless accumulation of calcium in the valve leaflets. This may explain the failure of statins to modify disease progression in aortic stenosis, which commonly presents once the disease is entrenched within the propagation phase (37, 38).

1.4.4 Propagation Phase: Fibrosis

Skeletal bone formation is characterized by the initial deposition of collagen matrix, that provides a scaffold upon which progressive calcification can develop. Similar structural processes are believed to occur in the aortic valve with many of the same cell mediators and proteins implicated (39). Indeed, in aortic stenosis, collagen is deposited in anticipation of the pro-calcific processes that subsequently dominate. The renin-angiotensin system (RAS) is believed to play a central role in this. Angiotensin converting enzyme (ACE) is up regulated in calcific aortic valve disease

and is likely to be delivered to the valve by LDL, its natural vehicle (40). Here it facilitates the conversion of angiotensin I to angiotensin II which mediates pro-fibrotic effects via the angiotensin II type 1 (AT_1) receptor. Although angiotensin II is also able to mediate anti-fibrotic and anti-inflammatory effects via angiotensin II type 2 (AT_2) receptors, differential expression of these receptors in favour of AT_1 has been demonstrated in calcified aortic valves so that a pro-fibrotic profile dominates. Likewise, whilst angiotensin converting enzyme type 2 (ACE-2) exerts anti-fibrotic and anti-inflammatory influences via the Ang1-7/Mas pathway, this pathway is down regulated in calcified aortic stenosis with reduced expression of both ACE-2 and Mas receptors in calcified valves compared to controls (41). Increased RAS expression is therefore implicated in the development of fibrosis within the valve.

1.4.5 Propagation Phase: Calcification

Beyond this initial fibrosis, valvular calcification in aortic stenosis appears to be predominantly mediated by the development of osteoblast-like cells. In support of this hypothesis, gene profiling studies have demonstrated increased valvular expression of several osteoblast-specific proteins including the Cbfa1/Runx2 transcription factor, essential for osteoblastic differentiation and regulation of osteoblast function (42, 43). A number of other extracellular matrix proteins closely associated with osteoblast function and more commonly associated with skeletal bone formation are also up regulated in calcific aortic valves. These include osteopontin and bone sialoprotein: facilitators of the attachment of osteoblasts to the bone matrix, which demonstrate up to a 7-fold elevation in gene expression at sites of developing calcification (44) (45). Importantly valvular ossification also appears

to be dependent upon angiogenesis, supporting the hypothesis that this is an active highly-regulated pathological process (39).

The source of osteoblast-like cells within the aortic valve remains controversial. *In vitro* multiple cell types present in the vasculature are capable of undergoing differentiation into those with an osteoblast-like phenotype. The most likely candidate appears to be the highly plastic valvular interstitial cell (46). The differentiation of this cell into an osteoblast phenotype is not fully characterized but appears to be a central step in the development of aortic stenosis and regulated by a rapidly growing list of molecules and complex pathways. In vivo molecular imaging has demonstrated that in the early stages of aortic stenosis, this differentiation appears co-ordinated by macrophages (47, 48) via the action of pro-inflammatory cytokines (IL-1β, IL-6, IL-8, tumour necrosis factor-α, insulin-like growth factor-1, and transforming growth factor-β) (20, 49, 50). Pro-calcific pathways including the Notch, Wnt/catenin and receptor activator of nuclear kappa B (RANK) /RANK ligand (RANKL)/ osteoprotegerin (OPG) pathways are also implicated.

Notch belongs to a family of cell surface receptors (Notch 1-4) that are highly expressed in the aortic valve, playing an important role in its morphological development (51). Individuals with loss of function mutations in Notch-1 have higher rates of cardiovascular calcification and aortic stenosis. Indeed, in two unrelated families with a high incidence of congenital aortic valve disease, genome-wide linkage analysis identified loss of function Notch-1 mutations as the cause (51). In particular Notch-1 appears important in establishing osteogenic cells in the valve via the action of bone morphogenic protein-2 (BMP-2) (52). BMP-2 is a potent

osteogenic differentiation factor and part of a family of multifunctional cytokines belonging to the transforming growth factor (TGF)-G superfamily. Expression of BMP-2 is increased in calcified atherosclerotic lesions and aortic valves (43, 53), and it appears to have a central role in the differentiation of plastic cell populations towards an osteogenic phenotype. Indeed exposure of normal human VICs to BMP-2 induces osteoblastic features in these cells (54, 55).

Binding of Wnt to low-density lipoprotein receptor-related protein 5 receptors may also activate the canonical Wnt/catenin pathway that is also implicated in osteogenic cell differentiation (56). Additionally, TGF-β1 is able to induce nuclear translocation of β-catenin, and increased Wnt signalling, stimulating the osteogenic differentiation of mesenchymal progenitor cells (57). The latter process can increase in response to mechanical stress and may therefore explain in part, the self-perpetuating and exponential increase in calcification activity observed once osteogenic differentiation has occurred and the propagation phase is established (Figure 1) (57, 58).

1.4.6 The calcification paradox

Calcium homeostasis is tightly controlled by systemic regulators that govern calcification activity both in the bone and the vasculature, consequently there is an inverse correlation between bone mineral density and vascular calcification. Osteoporosis is associated with age-independent increase in vascular calcification and even cardiovascular mortality (59). Indeed a prospective study of 25,639 men and women demonstrated an inverse correlation between bone mineral density and incident aortic stenosis in older women (60). Moreover, other disorders of bone

turnover including chronic kidney disease and Paget's disease also manifest changes in the vasculature (61-64). This dichotomy has been termed the calcification paradox and is likely to be explained by common pathological pathways having reciprocal effects on the bone and vasculature simultaneously.

1.4.7 The RANK/RANKL/OPG axis

One potential mechanism for this association lies in the activity of the RANK/RANKL/OPG pathway. In bone RANKL (a member of the tumour necrosis factor cytokine family) binds to RANK (a transmembrane protein expressed on marrow stromal cells and pre-osteoclasts) acting as a potent inducer of osteoclast differentiation and activity. This drives demineralization of bone, but is policed by osteoprotegerin (OPG), a soluble decoy receptor, which binds RANKL and prevents it from activating RANK (Figure 2). By contrast, RANKL appears to have the opposite effect on cells in the vasculature, inducing an osteoblastic phenotype in human VIC cells that results in increased matrix calcification, the formation of calcific nodules and increased expression of alkaline phosphatase and osteocalcin (Figure 2a) (65). RANKL also promotes the osteogenic properties of vascular smooth muscle cells, once again via the up regulation of BMP-2. In a sophisticated model attempting to replicate a capillary Davenport et al demonstrated that exposure of human arterial endothelial cells to RANKL promoted the osteoblastic activity of vascular smooth muscle cells in a paracrine fashion, possibly via the release of BMP2 and BMP4 (66). As a consequence whilst OPG-deficient mice develop osteoporosis, they simultaneously accelerate vascular calcification in association with increased expression of RANKL in both regions (67). A potential explanation

for the differential effects of RANK/RANKL/OPG in these two tissues is that in bone there is an abundance of pre-osteoclasts that favours the pro-osteoclastic properties of RANKL (50). By contrast in the vasculature, this pool is reduced such that the pro-osteoblastic effects of this ligand on myofibroblast and smooth muscle cells predominate.

Imbalances in RANKL/OPG signalling have been demonstrated in calcific aortic valves. In human valve tissue taken from patients with aortic stenosis, immunochemistry revealed less OPG positive cells in areas of focal calcification, whilst western blotting demonstrated that OPG was not expressed at relevant levels in aortic stenosis but was detectable in controls. The converse is true of RANKL with increased levels observed in stenotic aortic valves (65). In combination, these data support the hypothesis that the RANK/RANKL/OPG axis is implicated in the development of aortic valve calcification and provide one explanation for the link between this and bone mineral density.

Other investigators have suggested that the differential effects of oxidized LDL might also be of importance, with this molecule appearing to promote calcification and the osteoblastic differentiation of vascular cells *in vitro*, whilst inhibiting these processes in a bone-derived pre-osteoblast cell line (20) (68, 69). Fetuin A is a circulating protein, which can exist in isolation or as a complex with matrix γ-carboxyglutamic acid protein (MGP). Both are powerful guardians against ectopic calcification and simultaneously inhibit many of the procalcific processes discussed above (70). MGP needs to be both carboxylated and phosphorylated to be activated:

a process dependent on vitamin K. Their actions include inhibition of BMP2 and TGF-β, reduction of apoptosis-mediated calcification and direct prevention of calcification by binding to calcium crystals. Indeed there is speculation that use of the vitamin K antagonists such as coumarins, may be associated with increased vascular calcification (71). Additionally, reduced circulating levels of Fetuin-A and MGP are thought to explain the vascular calcification seen with end stage renal failure. Moreover plasma Fetuin-A concentrations are decreased in aortic stenosis and inversely associated with rate of disease progression (72, 73). Interestingly this association was seen only in older patients (>70 years) (74). Conversely, increased plasma dephosphorylated (inactive) MGP was a strong independent predictor of faster stenosis progression, but only in younger patients (≤ 57 years old) (75).

1.4.8 Why does calcium beget calcium?

Once calcification is established in the valve it would appear to initiate further calcium formation. Indeed it is this self-perpetuating cycle of calcification and valve injury that appears to the central driver of *disease progression* and the propagation phase of aortic stenosis. The mechanism for this may in part relate to the compliance mismatch caused by calcific deposits in the leaflets that result in increased mechanical stress, injury-induced activation of the Wnt/catenin pathway and further osteoblast differentiation.

In bone, the mineralization process is regulated by matrix vesicles which are small membranous structures (30-300 nm in diameter). They are formed as blebs off osteoblasts and chondrocytes and contain the prerequisite components for calcium crystal deposition. They facilitate the formation of needle-like crystals of

hydroxyapatite (20, 76) and as these hydroxyapatite crystals expand, they pierce the outer membrane of the vesicle and become exposed to the extracellular environment, thereby forming nucleation sites for further calcium deposition. Structures with a similar morphology to matrix vesicles, termed extra-cellular vesicles, have been identified at sites of ectopic calcification in the vasculature including calcified valves (77, 78). They were initially considered to propagate pro-calcific processes in an analogous manner to that seen in bone however this is now recognized to be an oversimplification of their diverse roles. (77). In atherosclerotic plaques they are thought to originate from osteogenic-transformed vascular smooth muscles cells and macrophages. Under normal circumstances they have an important physiological role as intercellular communicators and are loaded with calcification inhibitors including anti-calcific microRNA and Fetuin A (79, 80). Under pro-calcifying conditions however it is possible that they become trapped in the extracellular matrix thus propagating calcification by direct nucleation in a manner similar to that seen with apopotic bodies. Failure to reach target cells may cause dysregulated gene expression patterns promoting osteogenic differentiation (80). Conversely under pathological states they may become loaded with pro-calcific agents and induce further osteogenesis (81).

Membrane- bound ectonucleotidases are produced by VICs and regulate the extracellular production of inorganic phosphate (a promoter of calcification) and inorganic pyrophosphate (PPi) an inhibitor of pyrophosphate. Ectonucleotide pyrophosphate 1 (ENPP1) is highly up regulated in calcific aortic valve disease, with a polymorphism associated with increased transcripts of ENPP1 identified in stenotic

valves (82). Hydrolysis of extracellular ATP by ENPP1 produces a net increase in inorganic phosphate thus favouring calcification and promoting the production of further ENPP1 in a positive feedback loop (82). Moreover because ATP acts as a cell survival signal for VICs via the $P2Y_2$ receptor, its depletion also triggers apoptosis of these cells, providing a further key stimulus to calcification (82). Finally loss of $P2Y_2$ signalling increases the secretion of interleukin-6 (IL-6), a cytokine that promotes further osteogenic differentiation of VICs via the actions of BMP (83). Thus, via these multiple mechanisms, the ectonucleotidase pathway appears to have a central role in amplifying pro-calcific processes within the valve during the propagation phase of aortic stenosis.

In summary the pathophysiology of aortic stenosis is far more sophisticated than originally perceived. It is likely to be initiated by valvular endothelial injury and in the early stages, is similar to atherosclerosis (initiation phase). Valvular inflammation creates a pro-calcific environment via several potential pathways including the osteogenic differentiation of valvular interstitial cells. Once the process of active calcification has become established within the valve, this becomes a self-perpetuating cycle driving disease progression (propagation phase). For reasons that are not understood, the natural history of this disease is extremely variable between individual patients, with some experiencing a rapid clinical course and others never progressing beyond aortic sclerosis.

1.5 BICUSPID AORTIC VALVES

The bicuspid valve is the commonest congenital heart defect in which the aortic valve consists of 2 leaflets instead of 3. With a male preponderance it is estimated to affect 0.9-1.3% of live births (84-87). These patients are predisposed to a variety of pathologies of which aortic stenosis is the most common and presents approximately 5-10 years earlier than in tri-leaflet valves. Whilst this implies an accelerated clinical course, there is no longitudinal data to confirm this (89). Despite representing a relatively small proportion of the total aortic stenosis population, bicuspid patients constitute approximately 30% of those undergoing surgical aortic valve replacement (85). One study, which included patients with no complications related to bicuspid valves at baseline, showed that over 15 years of follow-up, 26 out of 212 patients (12.3%) underwent surgical aortic valve replacement for severe aortic stenosis (88).

Bicuspid valves occur within a wide range of clinical phenotypes from complex congenital heart disease (89), to normally functioning valves, a heterogeneity which is further reflected in the variability of valvular morphology. The majority of bicuspid valves retain the crown-like structure characteristic of the tri-leaflet valves with incomplete separation of the commisures producing two leaflets of differing size (Figure 1.3 (90). Less commonly, these valves can also manifest as a truly bileaflet structure consisting of two equally sized leaflets with no visible raphe. There is currently no agreement as to how valvular morphology influences the clinical sequelae in these patients.

Figure 1.3 Computed tomography angiography (CTA) images of aortic valves

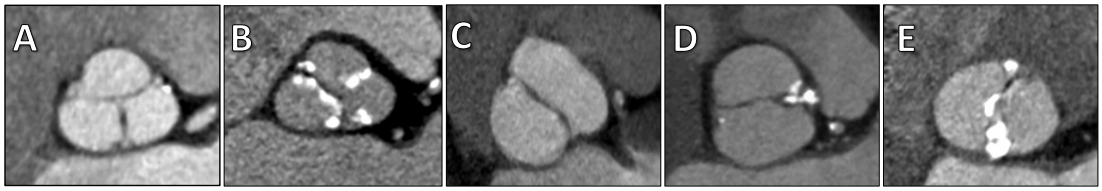

CTA images of bicuspid aortic valves (B, C, D and E) are shown in addition to tri-leaflet valve (A) for comparison. In examples B and C, the right and left coronary cusps are fused with (B) and without (C) a visible raphe. Examples D and E exhibit more distorted geometry, these valves are elliptical in shape with equally sized leaflets. Calcification can be seen affecting the leaflet tips (B and E), commissures (D) and the raphe (B).

The pathobiology of aortic stenosis of the bicuspid valve is likely to share many common pathways with that of the tri-leaflet valve, again representing a complex interplay of environmental and genetic factors. However the evidence for a genetic basis is more compelling. Approximately 30% of first-degree relatives of subjects with a bicuspid valve will themselves have a bicuspid valve or a thoracic aortic aneurysm (a commonly associated pathology, (91, 92). The underlying genetic basis for this is under continued investigation however mutations in the genes encoding the NOTCH1 receptor (93) and fibrillin 1 (94) have been identified in association with bicuspid aortic valves. Fibrillin mutations are thought to increase signalling through TGFβ pathway and in support of this, bicuspid valves have reduced fibrillin expression in association with higher levels of TGFβ (95, 96). Mutations involving constituents of the extracellular matrix such as matrix metalloprotein 12 have been associated with aortic stenosis, although not bicuspid valves specifically (7). However excised bicuspid valves from paediatric patients were characterised by excessive extracellular matrix production, disorganization and VIC disarray (97).

The abnormal valve morphology increases the mechanical stress imposed on the valve tissues and creates turbulent blood flow patterns, which may represent the initiating mechanism by which endothelial cell damage occurs (98, 99). Interestingly the subsequent inflammatory response in bicuspid valves is more aggressive, with increased macrophage infiltration and neovascularization compared with that seen in tri-leaflet valves (100). Additionally altered mechanical forces can directly induce VICs to increase collagen synthesis and upregulate both TGF-β and BMP-4, offering a mechanistic link between the enhanced mechanical stress and calcification (101-103).

In summary therefore, the bicuspid population is a heterogenous subgroup in whom the predilection to aortic stenosis is likely to reflect the consequence of genetic susceptibility in combination with increased mechanical stress.

1.6 CLINICAL IMAGING OF AORTIC VALVE CALCIFICATION

The burden and activity of aortic valve calcification can be measured using non-invasive imaging. In particular positron emission tomography PET, computed tomography (CT) and echocardiography can all be employed to provide assessments of the calcific processes occurring at different stages of the disease process (Figure 1.4). Indeed these techniques have not only informed our understanding as to the importance of calcification in aortic stenosis but have also aided our ability to assess disease severity, and to predict progression and adverse cardiovascular outcomes. The latter is of particular importance. As discussed aortic stenosis progression frequently does not occur in a linear or predictable manner making estimation as to when valve replacement will be required challenging. Annual or biannual clinical review is generally required with serial echocardiography performed in order to track progressive valve narrowing. The development of a non-invasive method capable of predicting the future natural history of aortic stenosis and the likely timing of valve surgery would represent a major advance and help streamline patient care. Given the central role that mineralization plays in disease progression, it is perhaps not surprising that assessments of aortic valve calcification have to date provided the best prediction (15, 17).

Figure 1.4. Multimodality calcification imaging in aortic stenosis.

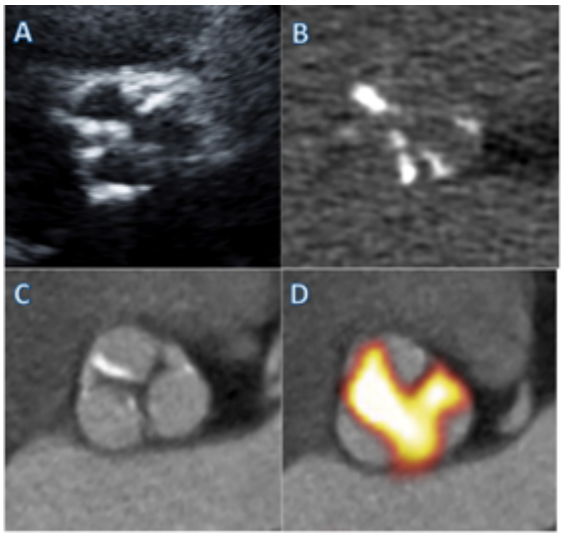

Short axis of a calcified aortic valve from the same subject imaged using two-dimensional echocardiography (A), computed tomography calcium scoring (B) Computed Tomography Angiography (C) and 18F-fluoride positron emission tomography – computed tomography (C).

Pawade et al. JACC. 2014 (29)

1.7 MICROCALCIFICATION

1.7.1 18F-Fluoride Positron Emission Tomography

Positron emission tomography (PET) is a non-invasive imaging technique that allows the activity of specific biological processes to be measured *in vivo* within specific structures including the aortic valve. In principle, any disease process can be evaluated dependent on the availability of a suitable tracer. To date studies in aortic stenosis have largely investigated tracers targeted to inflammation (18F-fluorodeoxyglucose) and calcification (18F-fluoride), aiming to establish the relative contributions of these processes to disease development and progression (104-106).

1.7.2 Inflammation

The PET radiotracer 18F-fluorodeoxyglucose (18F-FDG) is a glucose analogue taken up by metabolically active cells. Because it is unable to proceed through the glycolytic pathway, it accumulates within these cells without further metabolism. Vascular macrophages have higher metabolic requirements than surrounding tissue so that 18F-FDG has emerged as a useful tool for the identification of vascular inflammation, demonstrating that uptake in regions of carotid atheroma correlates well with macrophage density (mean percentage staining of CD68 positive cells, $r = 0.85$; $P<0.0001$) (107, 108) and is modifiable with statin therapy (109).

In order to determine the contribution of inflammation to the pathogenesis of calcific aortic stenosis, PET imaging of the aortic valve was performed of the aortic valve using 18F-FDG in a prospective cohort of 121 patients with the full spectrum of calcific aortic valve disease (including 20 patients with aortic sclerosis and 20

control subjects) (104). 18F-FDG activity was increased in patients with aortic stenosis compared to controls (1.58±0.21 versus 1.30±0.13; P<0.001) and this correlated with disease severity (104). However unlike previous work on carotid atheroma, the 18F-FDG signal did not correlate with macrophage (CD68) staining raising the possibility that in the calcifying aortic valve, 18F-FDG may not be acting as a marker of macrophage driven inflammation, but instead might reflect glucose utilization by other metabolically active cells such as valvular interstitial cells, myofibroblasts, or differentiated osteogenic cells (110).

1.7.3 Calcification

18F-Fluoride has been used as a bone tracer for more than 40 years, exchanging with hydroxyl groups in hydroxyapatite to form fluoroapatite. Similar hydroxyl bonds are also present in the different forms of calcium in the vasculature (including hydroxyapatite and amorphous calcium) so that 18F-fluoride binding acts as a marker of vascular calcification. In particular the binding of 18-fluoride to calcium appears critically dependent upon the surface area of calcium orthophosphate available for incorporation. 18F-fluoride therefore preferentially binds regions of newly developing microcalcification (beyond the resolution of CT), which have a nano-crystalline structure and very high surface area rather than large, established, macroscopic deposits where much of the calcium is internalized and therefore not available for binding (111). On this basis, increased 18F-fluoride uptake is observed in regions of actively developing calcification, demonstrating a close association with alkaline phosphatase staining (r=0.65, P=0.04) on excised aortic valve tissue removed at the time of surgery (110).

When the same cohort of 121 patients was imaged with 18F-fluoride, the observed PET signal in the aortic valve was stronger and more clearly demarcated than was seen with 18F-fluorodeoxyglucose (Figure 1.5). Moreover the spatial distribution of the 18F-fluoride signal was often discrete from the macroscopic calcium deposits identified by CT, indicating that 18F-fluoride uptake does indeed provide distinct but complementary information to CT alone. Uptake was increased in patients with aortic stenosis compared to healthy controls (2.87±0.82 *versus* 1.55±0.17, P<0.001) and correlated with disease severity (r=0.73, P<0.001) (104). Indeed the highest calcification activity, as measured using this tracer, was observed in patients with the most advanced disease (Figure 1.5). Again this supports the hypothesis that calcification begets calcification in aortic stenosis and would explain the rapid rates of disease progression in those at the severe end of the spectrum.

When patients were recalled for repeat CT calcium scoring of the valve at 1 and 2 years, new calcium could be observed in the areas of increased 18F-fluoride activity seen on the baseline scan (Figure 1.5). As a consequence, a close correlation was observed between the baseline valvular 18F-fluoride uptake and the progression of the aortic valve CT calcium score (r=0.80 [0.69-0.87]; P<0.001), with PET appearing to offer some additional predictive information over and above the baseline calcium score. Moreover this translated into an ability to predict valve hemodynamic progression with moderate correlations also observed between 18F-fluoride activity and the mean (r=0.32 [0.13-0.50], P=0.001) and peak (r=0.32 [0.12-0.49], P=0.002) aortic valve gradients. (112). Finally after a median of 1526 days of follow up, 18F-fluoride emerged as a prognostic marker serving as an independent predictor of the

combined end-point of aortic valve replacement and cardiovascular mortality (HR (hazard ratio):1.55 [95% confidence interval, 1.33-1.81], after adjusting for age and sex; P<0.001)

In summary, these data highlight the potential application for 18F-fluoride as an immediate, non-invasive measure of disease activity in aortic stenosis with the ability to predict its natural history. Identifying patients with mild aortic stenosis who will progress to clinically severe stenosis would represent a major clinical advance. Additionally, the instantaneous rapid read-out of disease activity holds particular promise in assessing the early efficacy of novel therapeutic agents, in which treatment effects are likely to be discernible over a much shorter time period than could be resolved using clinical end-points or indeed echocardiography or CT.

Figure 1.5. Relationship between baseline disease severity and PET activity.

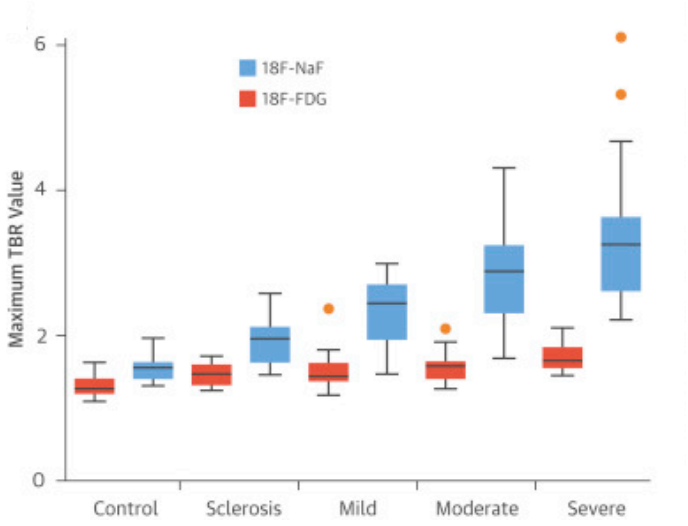

Studies using Positron Emission Tomography have demonstrated that calcification activity in the valve (as measured using 18F-Fluoride) steadily increases with disease severity. As a consequence activity is highest in those with the most advanced disease and a good correlation exists between 18F-Fluoride activity and the baseline CT calcium score (104).

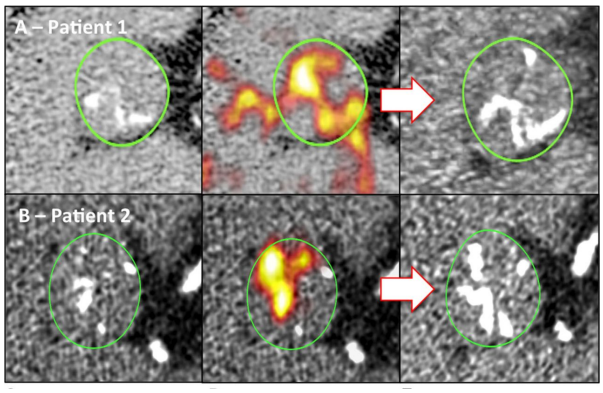

Dweck M R et al. Circ Cardiovasc Imaging. 2014;7:371-378

Baseline Computed Tomography Calcium Scores (left) for patients 1 and 2 (top and bottom). Fused co-axial 18F-Fluoride PET CT Scans (middle) shows Fluoride uptake in red and yellow. One year follow up (right) suggests that baseline PET signal predicts spatial distribution of subsequent macrocalcification (110).

Pawade et al. JACC. 2014 (29)

1.8 MACROCALCIFICATION

1.8.1 Echocardiography

Echocardiography is a cheap, safe and widely used method of assessing aortic stenosis severity in the clinical setting. Indeed international guidelines recommend grading aortic stenosis severity using the following hemodynamic echocardiographic assessments: the peak velocity, the mean gradient and the aortic valve area (113). However echocardiography can also be used to categorize valves according to their degree of valvular calcification into those with none, mild, moderate and severe calcification. Indeed in a series of 128 patients with severe, asymptomatic aortic stenosis, this semi-quantitative assessment provided powerful prognostic information, acting as a strong independent predictor of death or aortic valve replacement that out performed the more conventional hemodynamic measures (114). Whilst this observation has been confirmed in another study of 141 asymptomatic patients (115), the clinical utility of this approach has been limited by disappointing inter-observer agreement in grading the calcification (112, 116).

1.8.2 Computed Tomography Calcium Scoring

Computed tomography (CT) provides detailed, reproducible and accurate assessment of the calcific burden in the aortic valve (116). Using the same protocols employed for coronary calcium scoring, electrocardiography-gated non-contrast CT can provide information with respect to the density, volume and mass of macroscopic calcium deposits within the valve (116). However as in the coronary arteries, the aortic valve calcium burden is generally described using Agatston Units (AU), which takes account of both the radiodensity and volume of calcium. In a series of

explanted aortic valves, a score of 500, 1100 and 2000 AU approximated to 300, 1100 and 1200 mg of aortic valve calcium respectively (116).

Early studies demonstrated that CT calcium scoring of the aortic valve can be used as an alternative marker of stenosis severity, demonstrating a good relationship with hemodynamic echocardiographic assessments (116-118). However until recently we lacked appropriate thresholds that might differentiate patients with and without severe aortic stenosis thereby limiting its utility (Table 1.1, (119) . Thresholds have been proposed as a consequence of a landmark series of papers published by Clavel and colleagues. Across three sites in Europe and North America they performed both echocardiography and CT calcium scoring in 646 patients with moderate or severe aortic stenosis and good left ventricular function. In those subjects in whom the severity of stenosis was not in doubt on echocardiography (n=460), the authors examined the optimal CT calcium score for differentiating moderate from severe aortic stenosis. Interestingly females required less calcium to develop severe hemodynamic stenosis than males (even after correcting for body surface area and the LVOT area calculated by echocardiography), so that the optimal thresholds were found to be 1275 AU in women and 2065 AU in men. These thresholds then appeared to serve as an ‘umpire test’ by independently adjudicating the severity of the stenosis when echocardiographic markers were discordant (42).

Table 1.1. Studies attempting to define computed tomography calcium scoring thresholds for the diagnosis of severe aortic stenosis

Study	Number	Criteria Severe AS	CT-AVC Threshold (AU)	Sens (%)	Spec (%)	PPV (%)	NPV (%)
Cowell et al 2003	157	Vmax >4 m/s	>3700	100	50	39	100
Messika-Zeitoun et al	100	AVA <1 cm^2	>500	100	69	57	100
Clavel et al 2013	460	AVAi ≤0.6 cm^2/m^2 & MG ≥40 mmHg	>1274 (women) >2065 (men)	86 89	89 80	93 88	79 82
Cueff et al 2011	179	AVA <1 cm^2	>1651	82	80	70	88
Cueff et al 2011	20	AVA <1 cm & EF ≤40 % & MG ≤40 mmHg	>1651	95	89	97	80

Abbreviations; CT-AVC, computed tomography aortic valve calcium score; Vmax, peak velocity; AVA, aortic valve area; MG, mean gradient; Sens, sensitivity; Spec, specificity; PPV, positive predictive value; NPV, negative predictive value

Pawade et al. JACC. 2014 (29)

Table 1.2 Studies using aortic valve computed tomography calcium scoring to predict outcomes.

Study	No. Patients	Follow up	Primary Endpoint	Key Findings
Messika-Zeitoune et al 2004	100	2.0±2.3 Years	Survival without dyspnea, angina, syncope, heart failure, or need for surgery	• AVC independently predicted event-free survival, adjusted relative risk (RR) of 1.06 (95% CI 1.02 to 1.10) per 100-AU increment (P<0.001). • 5-year event free survival rate of 90±4% if AVC <500 AU versus 29±14% if AVC ≥500 AU (P<0.0001).
Feuchtner et al 2006	34	18-24 months	Symptoms due to haemodynamic progression or cardiac death	• AVC strongest predictor of a major adverse clinical event (p < 0.001) among all parameters assessed (1,928 +/- 789 versus 5,111 +/- 2,409 Agatston units).
Utsunomiya et al 2013	64	29 months	Cardiac death, AVR, nonfatal MI, and heart failure requiring urgent hospitalization.	• AVC predicted cardiac events (HR: 1.09, 95% CI: 1.04-1.15) per 100-AU increment • AVC Score ≥ median value of 723 AU had associated with worse outcomes (p<0.0001).
Clavel et al 2014	794	3.1± 2.6 years	Mortality	• Severe AVC defined as ≥1,274 AU in women and ≥2,065 AU in men) was independent predictor of overall mortality (HR: ≥1.58; p ≤ 0.04) p,0.0001)

Abbreviations: AVR, aortic valve replacement; MI, myocardial infarction; AVC, aortic valve calcium; CI, confidence interval; AU, Agatston Units; AVCS, aortic valve calcium score

Pawade et al. JACC. 2014 (29)

More importantly the authors went on to demonstrate that, in a population of 794 patients, these thresholds predicted all-cause mortality independent of all other markers of an adverse prognosis (120, 121). This included the standard haemodynamic parameters on echocardiography suggesting that CT can provide additional, complementary information to that obtained during routine clinical care, as had previously been hinted at by earlier studies (Table 1.2) (116, 122-124). An expanding body of literature has also demonstrated the ability of CT calcium scoring to predict disease progression in aortic stenosis. Initial studies indicated that the aortic valve CT calcium score progresses fastest in patients with the highest baseline calcium burden (Figure 1.6) (125). Whilst the employment of CT calcium scoring in this way, holds great promise as a clinical tool, an important consideration is that these thresholds were derived from 3 expert aortic stenosis centres. Therefore their generalizability to a more heterogeneous population remains to be established.

Figure 1.6. Disease progression in aortic stenosis

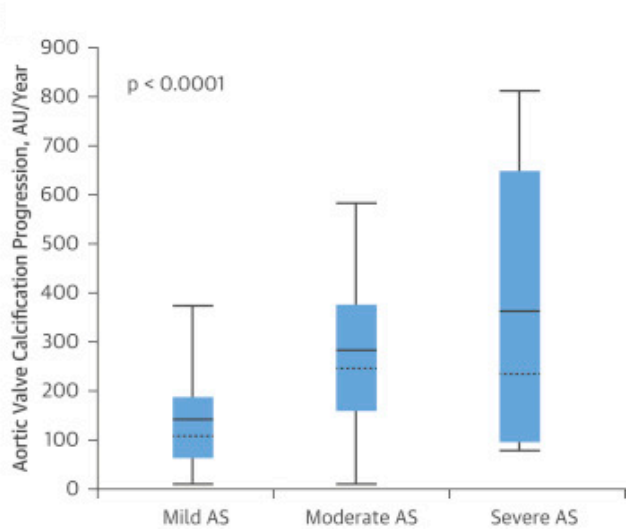

Increased calcium burden appears to translate in to more rapid disease progression as measured using computed tomography calcium scoring in patients with the most advanced forms of aortic stenosis (126).

1.8.3 Bicuspid Aortic Valves

Before CT calcium scoring can be adopted into widespread clinical use, it is essential that its applicability within aortic stenosis subpopulations is understood. Shen et al demonstrated that whilst good correlations between CT calcium scores and mean aortic gradient were observed in patients with tricuspid valves ($r=0.61$, $p<0.0001$) this observed correlations were weaker in those aged ≥51 years with bicuspid aortic valves ($r=0.55$, $p=0.009$) and non-existant in those aged <51 with a bicuspid valve (127). Potential explanations for this are speculative and related to altered pathobiology. These findings warrant further investigation (128).

In summary CT calcium scoring would appear to be a useful method for grading disease severity in aortic stenosis, offering powerful prediction of both disease progression and adverse clinical events. It is potentially complementary to standard echocardiographic assessments and may have some advantages, most notably that it is not dependent on cardiac loading conditions, geometric assumptions nor the presence of other cardiovascular conditions such as mitral regurgitation and hypertension. This technique needs to be validated prior to clinical application, with a better understanding of its utility in aortic subpopulations.

1.9 POTENTIAL NOVEL DISEASE MODIFYING THERAPIES

As our understanding of the pathophysiology of aortic stenosis has improved, the key role that calcification plays in driving disease progression has led us away from targeting inflammation and lipid deposition, and towards therapies capable of directly halting valve calcification (129). How might this be achieved? The close association between disorders of skeletal bone metabolism and increased calcification in the vasculature offers a potential starting point. Indeed a growing body of pre-clinical and clinical data indicates that treatments for osteoporosis, such as bisphosphonates and denosumab, can reduce vascular calcification and that these agents hold considerable promise as novel therapies for aortic stenosis (130).

1.9.1 Bisphosphonates

Bisphosphonates are inhibitors of osteoclast-mediated bone resorption, are well tolerated in the elderly and have been widely used for the treatment of osteoporosis (131). Interestingly bisphosphonates also have important cardiovascular effects, demonstrating a consistent reduction in calcification of the vasculature and the aortic valve (130, 132, 133). This in part appears to be a consequence of their inhibition of bone resorption, which results in reduced release of calcium and phosphate into the circulation and therefore the systemic availability of these pro-calcific substances (130). However bisphosphonates also appear to exert direct anti-calcific effects on the aortic valve tissue itself. For example, they reduce the production of interleukin-1β, interleukin-6 and tumour necrosis factor-α (key inflammatory cytokines implicated in the early stages of aortic stenosis (134)) and inhibit the secretion of matrix metalloproteinases 2 and 9, which remodel the valve as aortic stenosis progresses (135, 136). Moreover nitrogen containing bisphosphonates act as inorganic pyrophosphate (PPi) analogues (62), which as discussed have powerful anti-calcific properties in the vasculature. Finally bisphosphonates attenuate the differentiation of aortic valve myofibroblasts into cells with an osteogenic phenotype (137), the key step in triggering the propagation phase of

aortic stenosis (129). In combination, these data offer support for bisphosphonates as a treatment strategy for aortic stenosis that is increasingly being supported by observational clinical data. A recent analysis of 3,710 women in the Multi-Ethnic Study of Atherosclerosis (MESA) indicated that bisphosphonate use was associated with less valvular and vascular calcification in older women (users versus non-users: aortic valve ring calcium 38 versus 59%, P<0.0001) (138). Other studies appear to support these findings with a direct beneficial effect of these drugs on echocardiographic measures of aortic stenosis progression (139-141) as well as reducing valvular calcification in patients with renal failure and amongst those with bioprosthetic valves (130, 142). Whilst encouraging, such retrospective, observational studies are prone to bias, cannot assess cause-and-effect, have provided conflicting results (143) and are confounded by the underlying effects of the osteoporosis for which these agents were prescribed. Indeed the true impact of bisphosphonates in aortic stenosis will only become clear within the context of a randomised controlled trial (144).

1.9.2 Denosumab

As discussed the OPG/RANK/RANKL axis appears to play a pivotal role in aortic valve calcification and may provide an explanation for the link between osteoporosis and increased vascular calcification. It therefore represents an attractive therapeutic target for reducing vascular calcification. Denosumab is a human monoclonal antibody to RANKL that prevents its binding to RANK thereby recapitulating the actions of OPG. In a trial of 7,868 post-menopausal women with osteoporosis, denosumab increased bone mineral density and reduced vertebral fracture rates by 68% over a 3-year period (145). Importantly, denosumab was extremely well tolerated with very few adverse side effects and no major excess in adverse events. Given the central regulatory role that the OPG/RANK/RANKL system has in vascular and aortic valve calcification, denosumab also holds considerable promise as a novel treatment for aortic stenosis. Again this is supported by pre-clinical data, with denosumab halving the aortic calcification observed in a murine model of osteoporosis

(146). Interestingly in the same study, this reduction was closely associated with inhibited bone resorption from the skeleton, indicating that the cardiovascular effects of denosumab are, like bisphosphonates, in part related to reduced calcium and phosphate release from bone into the circulation.

1.10 CONCLUSION

Aortic stenosis is a common condition that is set to become an increasing health care burden. We lack effective medical therapies capable of slowing its relentless progression towards major surgery or adverse events. Recent insights into the pathophysiology of aortic stenosis have indicated that whilst lipid and inflammation may be important in establishing the disease (initiation phase), it is the self-perpetuating processes of calcification that are predominantly responsible for driving disease progression (propagation phase). On this basis, imaging modalities capable of quantifying aortic valve calcification will be best placed to predict its natural history, whilst novel anti-calcific therapies hold major promise as methods of treatment. Randomised controlled trials of such agents, perhaps using imaging end-points such as CT calcium scoring and 18F-fluoride PET activity, are required to establish their early efficacy.

Figure 1.7. Summary Figure

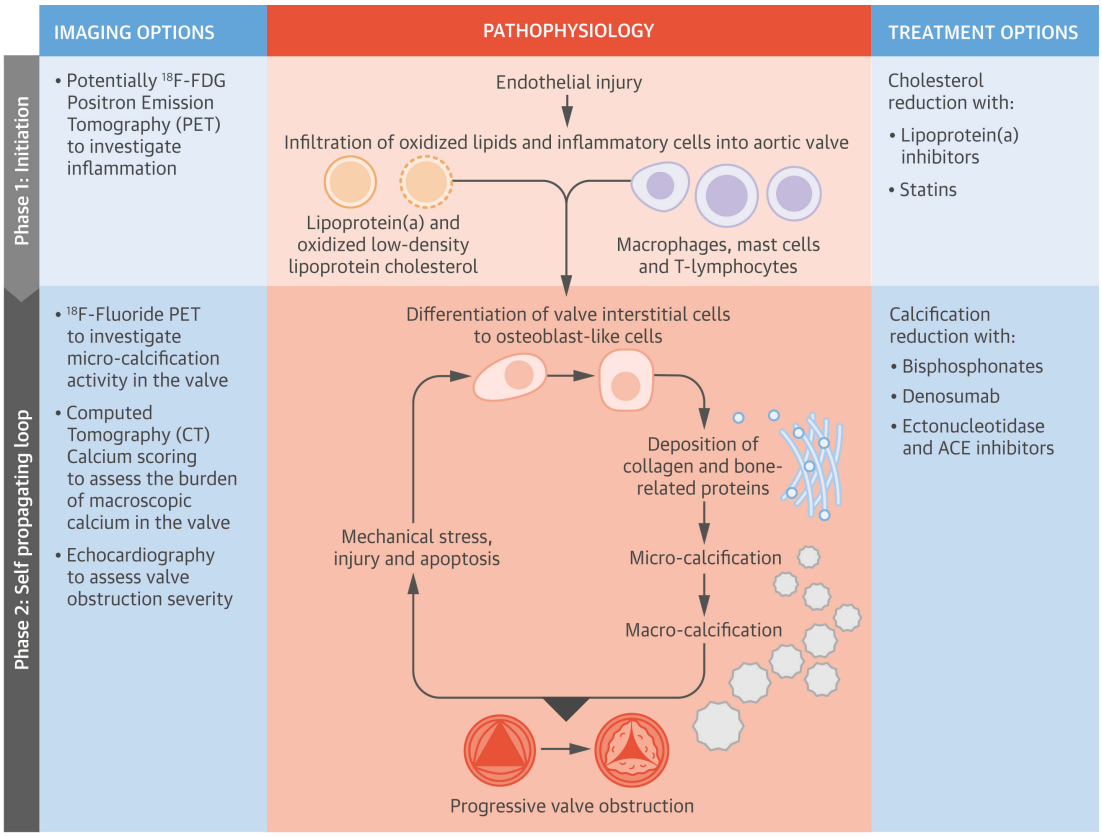

Pawade, T.A. et al. J Am Coll Cardiol. 2015; 66(5):561–77.

The pathogenesis of aortic stenosis can be thought of in two stages: initiation and propagation. These can be imaged using 18F-Fluoride PET (newly developing micro-calcification) and CT calcium scoring (macroscopic calcific deposits). Given the central role of calcification in the propagation phase of aortic stenosis it is perhaps unsurprising that these provide important information with respect to prognosis and disease progression. Moreover calcification represents an important potential therapeutic target using drugs such as denosumab and bisphosphonates to interrupt the vicious cycle of calcification that drives progressive narrowing of the valve.

Pawade et al. JACC. 2014 (29)

1.11 AIMS AND OBJECTIVES

The overarching aim of this thesis was to evaluate and optimise the use of complementary calcification imaging techniques for the study and management of aortic stenosis.

In particular I sought to achieve the following aims:

1. Refine current methods of 18F-fluoride PET-CT image acquisition and analysis in the study of aortic stenosis to improve image quality and scan reproducibility.
   Chapter 3
2. Determine the reproducibility of CT calcium scoring of the aortic valve.
   Chapter 4
3. Describe the relationship between CT-AVC measurements and echocardiographic measurements of disease severity.
   Chapters 4 and 5
4. Determine the ability of CT-AVC measurements to predict disease progression.
   Chapter 4
5. Derive our own optimum sex-specific CT-AVC thresholds and examine their clinical performance in comparison to those previously published.
   Chapter 5
6. Determine the accuracy and clinical significance of CT-AVC measurements and continuity equation-derived estimates of disease severity in patients with bicuspid aortic valves.
   Chapter 6

1.12 HYPOTHESES

I sought to address the following hypotheses

1. Current techniques of 18F-fluoride PET imaging of the calcific aortic valve can be modified to enhance image quality whilst improving scan reproducibility.

2. The scan reproducibility of CT calcium scoring will be within acceptable limits for clinical application.

3. Baseline CT-AVC measurements will correlate with disease severity, predict disease progression and clinical events.

4. Sex-specific CT-AVC thresholds can be used as an umpire test to arbitrate disease severity in patients with discordant echocardiographic measurements.

5. In patients with bicuspid aortic valves, CT-AVC scoring may not be a suitable umpire test.

Chapter 2: METHODS

2. 1 STUDY POPULATIONS

Study populations are described in detail in their respective chapters but predominantly consisted of patients recruited into two aortic stenosis clinical studies conducted at the Edinburgh heart centre; Saltire 2 and the Ring of Fire.

Saltire 2 is a prospective, double-blinded, randomised, placebo-controlled clinical trial investigating the ability of the calcium modulators denosumab and alendronic acid to modify disease progression in aortic stenosis (Appendix 1). I am the principle investigator and was therefore responsible for writing the protocol, acquiring appropriate authorisations, recruiting patients, organising and conducting study visits, collecting data and performing image analysis (with the exception of the echocardiograms). The primary endpoint is the computed tomography aortic valve calcium score (CT-AVC) at 2 years and an exploratory secondary endpoint is 18F-Fluoride positron emission tomography CT (PET-CT) uptake of the aortic valve at 1 year. Before 18F-Fluoride PET could be reliably employed as an imaging endpoint, a substudy was first performed to optimise and assess scan reproducibility in aortic stenosis (chapter 3).

The Ring of Fire is a prospective clinical study which was conducted by Dr Marc Dweck and Dr William Jenkins. It investigated the ability of 18F-Fluoride PET-CT and CT-AVC scoring to measure disease severity, predict disease progression and adverse clinical events. The data on 18F-Fluoride PET has been published and is

therefore not explored further (147, 148). Instead however, within chapter 4 of this thesis, the calcium scoring data is examined in detail. Baseline data from both trials (subject to inclusion criteria) were pooled with that from other international centres to create the aortic stenosis registries used for chapters 5 and 6. The conduct of the baseline visits for both studies are identical and detailed below.

2.1.1 Ethical Considerations

Both studies were approved by the research and development department at the University of Edinburgh, the South-East Scotland ethics committee and the Administration of Radioactive Substances Advisory Committee (ARSAC). Saltire 2 is a clinical trial of an investigative medicinal product (CTIMP) and was therefore also approved by the Medicines Healthcare products and Regulatory Authority (MHRA). Both studies are also registered on the clinicaltrials.gov website (Saltire 2, NCT01358513; Ring of Fire, NCT02132026). Study conduct was overseen by the sponsors at the university of Edinburgh.

2.1.2 Recruitment

Patients with aortic stenosis who attended the cardiology outpatients at the Edinburgh Royal Infirmary were first approached by their usual care team. Those who agreed to be contacted by the research team were issued with an approved patient information sheet prior to their first study visit.

2.1.3 Study Visits

All visits were performed at the clinical research facility (CRF) at the University of Edinburgh. Patients were first required to sign a consent form. Anonymised patient data was entered into case record forms and study visits were also documented in the

clinical notes. Demographics, specifically the date of birth, gender and ethnicity were first recorded. Patients were then asked about symptoms of breathlessness, exertional chest pains and syncope. Breathlessness and angina were graded using the New York Heart Association (NYHA) and Canadian Cardiovascular Society scores respectively. The past medical history was documented using a combination of patient interview, electronic records and clinical notes. Comorbidities of particular interest included a confirmed diagnosis of hypertension, hypercholesterolaemia, diabetes, renal disease, angina, previous coronary artery bypass grafting, previous percutaneous coronary intervention, smoking status, cerebrovascular disease and current or past malignancies. All of the current medications including indication, dose, method of administration and start dates were also recorded.

2.1.4 Clinical Examination

The height and weight were recorded for each patient, from which the body mass index and body surface area were calculated. Sphygmanometry was used to determine the blood pressure and heart rate. All patients underwent a standardized cardiovascular examination in a semi-recumbent position, with the torso at 45 degrees. Specific examination was made of the pulse rate and rhythm, the jugular venous pressure and fluid status. The heart sounds were auscultated for murmurs and lung fields for inspiratory crackles.

2.1.5 Electrocardiogram

All patients underwent a 12-lead electrocardiogram (ECG) which was examined immediately for features of ischaemia, arrhythmia, conduction disease, left ventricular hypertrophy and strain. Left ventricular hypertrophy was diagnosed using

two criteria; the Sokolow-Lyon criteria (the sum of the S wave in V1 and R wave in V5 or V6 ≥35mm) or the Modified Cornell Criteria (R wave in aVL ≥12 mm). Left ventricular strain was defined as asymmetric T wave inversion and ST segment depression in the anterolateral leads (149).

2.1.6 Venesection

At each visit, a cannula was inserted if required and up to 40 mL of blood was subsequently withdrawn. These were routinely tested for full blood count, renal and liver function, electrolytes, glucose and cholesterol. Serum and plasma samples were also spun and stored for future use.

2.2 ECHOCARDIOGRAPHY

Echocardiography employs ultrasound technology to obtain detailed information about cardiac structure and function. It was first pioneered by the Swedish physician Dr Edler in 1953 and after substantial refinement, is now the cornerstone of cardiac imaging and the gold-standard clinical tool for the diagnosis, grading and monitoring of aortic stenosis (150, 151).

2.2.1 Image acquisition and Analysis

Echocardiography was performed by a single experienced echocardiographer (Audrey White) using a pre-specified protocol according to European Society of Echocardiography guidelines (151). For each study the same machine (Phillips Affinity 70 Ultrasound System), room and bed were used to ensure consistency of approach. Patients were asked to undress from the waist up and issued with a gown if necessary. Scans were performed with patients in the left lateral and supine positions.

For each patient, images were acquired in the parasternal long and short-axis views, apical 4 and 5-chamber views, subcostal and suprasternal views. Measurements were made of left and right ventricular dimensions, atrial size, left ventricular outflow tract diameter and aortic root dimensions. Right ventricular size was assessed visually in respect to the left ventricle and function was assessed using tricuspid annular plane systolic excursion (TAPSE). Left ventricular function was estimated using a combination of visual assessment and where possible confirmed using Simpson's biplane measurements. Detailed diastolic assessments were also performed using mitral valve pulsed wave and tissue doppler. All valves were examined by using a combination of visual assessment, colour flow, continuous wave and pulsed wave Doppler. If possible an assessment was made of pulmonary artery systolic pressure and any additional abnormalities including pericardial effusions.

Aortic stenosis severity was assessed based on the European Society of Echocardiography Guidelines (152)Figure 2.1). A semi-quantitative calcification score was assigned as previously published by Rosenhek at al; 1, no calcification; 2, mildly calcified with small isolated spots; 3, moderate calcified with multiple larger spots and 4, heavily calcified with extensive thickening and calcification of all cusps (15). Pulsed wave and continuous wave doppler were used to determine aortic stenosis severity with measurements taken of the peak transvalvular velocity and mean gradient. The aortic valve area was calculated using the continuity equation. The continuous wave doppler measurements were then subsequently repeated using the pencil probe at the apex, suprasternal notch and right sternal edge. For patients in

sinus rhythm the average of 3 measurements were then used, this was increased to 5 for those in atrial fibrillation.

With respect to discerning aortic valve severity, echocardiography was previously shown to have good scan-rescan reproducibility (153) in 20 patients (mean peak velocity 3.47±0.78 m/s) who underwent repeated echocardiography at 3 weeks (mean difference = 0±0.28 m/s, reproducibility coefficient = 0.56, (153).

Figure 2.1 Echocardiographic assessment of aortic stenosis severity

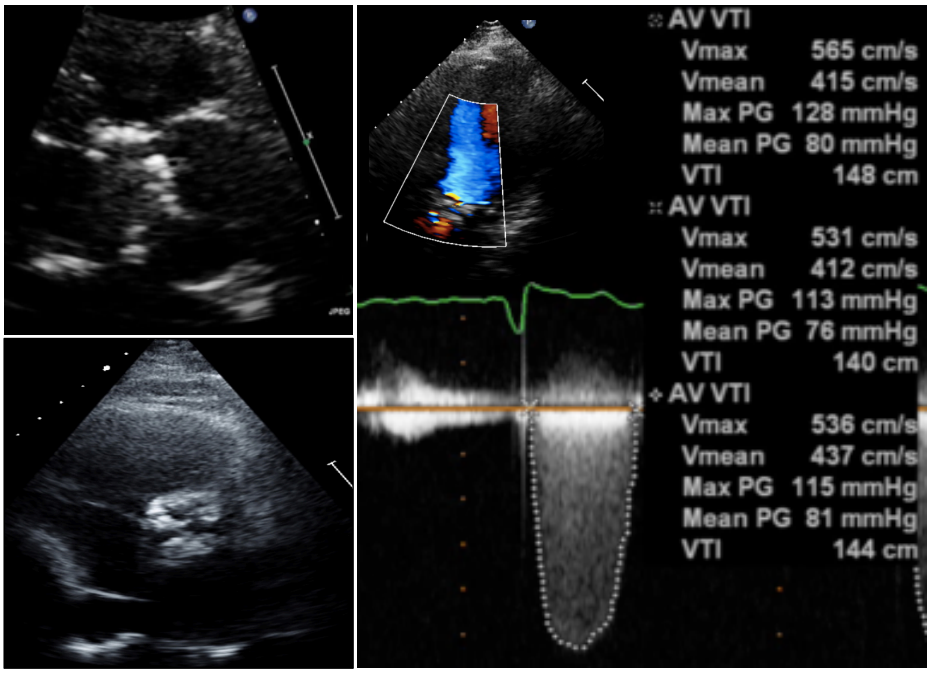

Aortic valve structure, function and calcification score were assessed in the parasternal long (top left) and short axis (bottom left) views. Doppler studies (right) facilitate automated calculation of the peak velocity (Vmax), mean pressure gradient (Mean PG) and peak pressure gradient (Max PG).

2.3 POSITRON EMISSION TOMOGRAPHY

Positron emission tomography (PET) refers to the creation of digital images that depict the bodily distribution of a positron emitting radiotracer. PET is used to study the activity of biological processes and is usually performed in combination with imaging modalities capable of providing anatomical detail. Subject to the availability of a suitable radiotracer, any biological process can theoretically be studied *in vivo* using this technique. All patients recruited into Saltire 2 or the Ring of Fire studies underwent 18F-fluoride PET-CT scanning.

18F-Fluoride is a bone-seeking radionuclide with a half-life of 110 minutes, which is created within a cyclotron by the bombardment of 18-Oxygen enriched water with protons. After coming into contact with the calcifying aortic valve, 18F-fluoride rapidly exchanges for OH on the surface of the hydroxyapatite matrix (Ca10(PO4)6OH2) to form fluoroapatite (Ca10(PO4)6F2) (154). In this way it can be use to target and identify areas of novel microcalcification (Figure 2.2)

Figure 2.2. 18F-Fluoride positron emission tomography

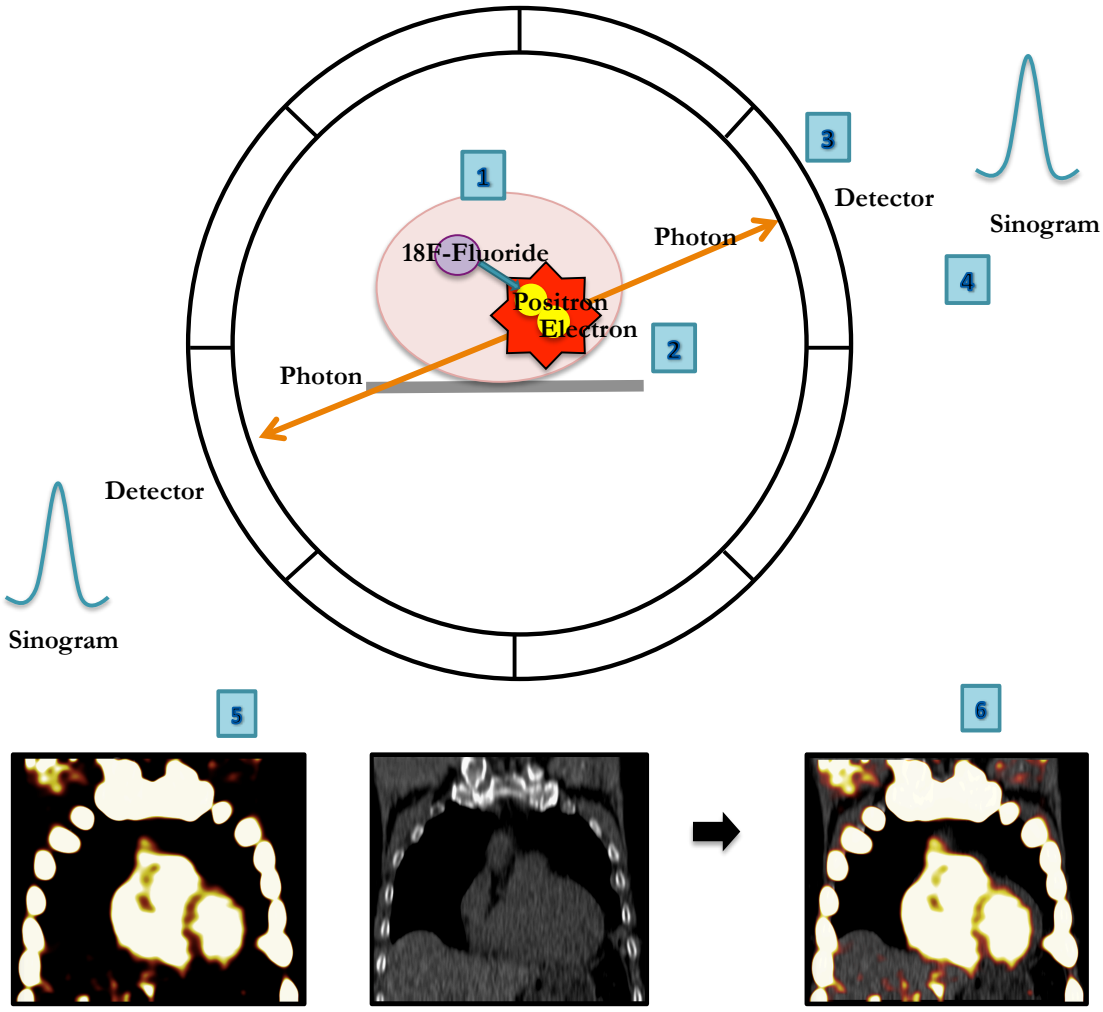

The nucleus of the fluoride ion decays by emitting a positron (1), a subatomic particle which has the same mass as an electron but an opposite charge. Within tissues, an emitted positron collides with an electron resulting in an annihilation reaction (2), the by-product of which is two photons. These emitted photons then travel with an energy of 511 keV at exactly 180 degrees of each other (3). This coincident activity is sensed by pair of PET detectors which convert the light signal into an electronic signal. Two electronic pulses detected in coincidence confirms the presence of an annihilation signal somewhere along the line of response. This data is converted into a series of sinograms for each projection angle (4). Iterative reconstruction algorithms are then applied, to reduce the signal to noise ratio and facilitate the calculation of standardised uptake values for each voxel as follows standardized uptake value = radioactivity concentration/(injected dose/body mass). Digital PET images are created (5) which are subsequently fused with the co-acquired computer tomography (CT) images to create a fused PET-CT (6) containing both biological and anatomical information.

2.3.1 Image acquisition

The radiotracer 18F-Fluoride was synthesised by the radiochemistry department at the Clinical Research Imaging Centre (CRIC) at the University of Edinburgh on the morning of scan days and underwent immediate quality assurance checks. Patients were transferred to lead lined uptake rooms and given 25-50 mg of oral metoprolol if their resting heart rate was >65 beats/min provided there were no contra-indications. Patients were administered 125 MBq of 18F-fluoride flushed with 10 mL of normal saline intravenously, before being required to rest for 60 minutes. Dynamic imaging has previously confirmed that 60 minutes after injection is time point at which optimal contrast between plasma and vascular tissues is observed (155). Prior to the scan all patients were requested to empty their bladder.

Imaging was performed using a hybrid PET and CT scanner (128-multidetector scanner (Biograph mCT Siemens). Images were acquired with patients lying supine and where possible with arms raised. ECG electrodes were attached to the patients to facilitate gating. Attenuation-correction CT scans were first performed (non-enhanced, 120 kV and 50 mA, slice thickness 5mm, increment 3mm). Acquisition of PET data was then performed with in list mode using a single 30-min bed position centred on the valve in three-dimensional mode.

2.3.2 Image analysis

PET-CT analysis was performed using an OsiriX workstation (OsiriX version 3.5.1 64-bit; OsiriX Imaging Software, Geneva, Switzerland). Non-contrast CT images of the aortic valve were first re-orientated and reconstructed to create planar images of the valve at 3 mm slice thickness (Figure 2.3).

Figure 2.3 Creation of planar images of the aortic valve using non-contrast computed tomography.

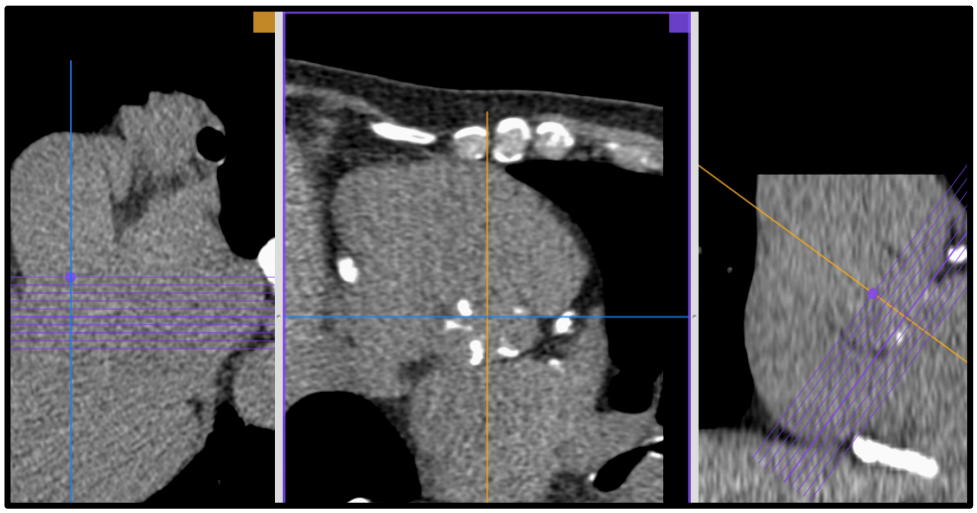

Non-contrast computer tomography images were reoriented in the coronal (far left) and sagittal (far right) planes to create planar view of the aortic valve (centre). These were then reconstructed at 3 mm slice thickness.

Regions of interest were drawn around the perimeter of the valve on the fused non-gated PET and non-contrast CT images (104) Figure 2.4). These generated mean and maximum standard uptake values (SUV) for each slice. Averaging these values across the entire valve produced whole-valve SUV_{mean} and SUV_{max} values respectively. These SUV values were then corrected for blood pool activity to generate respective tissue-to-background ratios (TBR): whole-valve TBR_{mean} and whole-vale TBR_{max}. The blood pool uptake was determined using SUV_{mean} values averaged from across ROIs drawn on 5 contiguous slices in the brachiocephalic vein. For consistency the most caudal ROI was positioned at the point where the innominate vein joined the brachiocephalic vein (104). The scan-rescan reproducibility of 18F-fluoride PET in the aortic forms the subject matter of chapter 3. 18F-Fluorodeoxyglucose in the study of macrophage driven inflammation of carotid plaques has been shown to have excellent scan-rescan reproducibility with intraclass correlation coefficients of 0.9 (0.7-0.97) (156).

Figure 2.4 18F-Fluoride positron emission tomography computed tomography analysis.

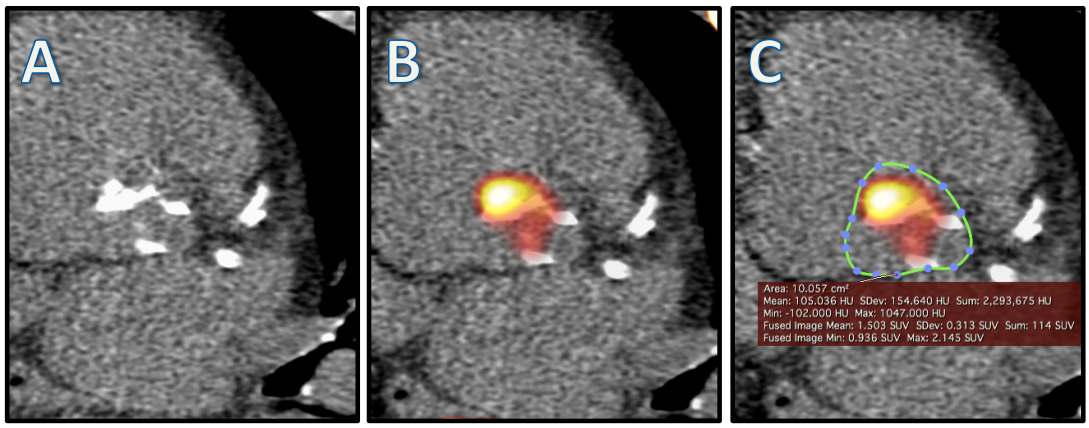

Reconstructed, planar non-contrast images of aortic valve (A) were fused with the ungated PET (B). Regions of interest were drawn around the perimeter of the valve (C), which automatically generated mean and maximum standard uptake values (SUV). This was repeated for each slice for the length of the valve.

2.4 COMPUTER TOMOGRAPHY AORTIC VALVE CALCIUM SCORING

CT creates cross-sectional images of the body and works on the principle that different tissues can be distinguished by their relative ability to absorb photons (attenuation coefficients). Typical CT images are composed of 512 rows, each of 512 pixels, which are multiplied by the slice width to create voxels. Calculating the attenuation coefficient for each voxel facilitates the creation of digital images. Attenuation coefficients are converted to the Hounsfield scale, expressed in Hounsfield units (HU). Calcification is defined on this scale as a hyperattenuated lesion of ≥130 HU with an area of 3-4 adjacent pixels. This can be quantified by applying an arbitrary weighted density score to calcification as follows; 1 = 130 to 199 HU; 2 = 200 to 299 HU; 3 = 300 to 399 HU and 4 ≥ 400 HU. The density factor is multiplied by the area (mm^3) to generate a calcium score in Agatston units (AU).

2.4.1 Image acquisition

All patients underwent an ECG-gated, non-contrast CT scans gated from 75% to 80% of the R-R during held expiration using a, 40 mA/rot [CareDose], 120 kV). Images were reconstructed in the axial plane with 3 mm slice width and 1.5 mm increment. In the Saltire 2 study, ECG-gated contrast-enhanced CT angiography were also performed in diastole and in held expiration. Patients were then observed for 5 minutes to ensure that there were no contrast reactions before their cannula was removed and they were shown out of the department.

2.4.2 Image analysis

Valvular calcification was quantified using dedicated analysis software (Vitrea Advanced, Vital Images, Minnetonka, USA, Supplementary) in the axial plane starting at the base of the valve (Figure 2.5). Care was taken to exclude calcium from extra-valvular structures such as the mitral valve annulus and coronary arteries. When confluent calcium extended into the ascending aorta, the origin of the left coronary artery was set as the most rostral slice beyond which further calcium was excluded. The aortic valve calcium burden was expressed as the CT-AVC (Agatston Units, AU), corrected for the LVOT area (as measured using echocardiography) to generate the CT-AVC density (CT AVCd, AU/cm^2) and the body surface area to create the CT-AVC index (CT AVCi, AU/m^2). The CT calcium volume was also recorded.

The scan-rescan reproducibility of CT-AVC measurement using the Agatston score is unknown, however reproducibility of the calcium volume technique is excellent (correlation coefficient r=0.99, median interscan variability 7.9%, repeatability coefficient 237.8 mm3, limits of agreement −393 to 559 mm^3). Proportional bias is evident whereby higher calcium scores have worse rescan differences (157).

Figure 2.5 Computed tomography aortic valve calcium scoring.

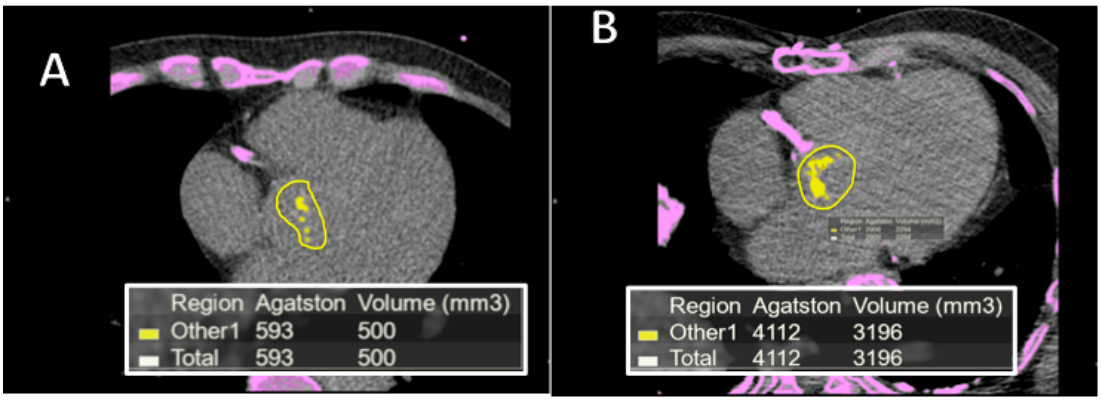

Computed Tomography calcium scoring performed on contiguous slices of the aortic valve in the axial plane. Examples from patients with mild (A) and severe (B) aortic stenosis are shown. All calcium is highlighted in pink. Contours are then drawn around calcium in the aortic valve, which then turns yellow once selected. Automated software calculates the density factor for each pixel before multiplying by the area (mm^3) to generate an overall score in Agatston Units. A calcium volume (mm^3) is also given.

2.4.3. Safety issues.

All CT scans were supervised by a medical practitioner. Where possible, CT angiography images were acquired with prospective gating to minimise radiation exposure. The total dose received by a patient for a given scan (including injected doses, and dose-length product) were recorded and reviewed periodically by the medical physics department. All scans were reported by a consultant radiologist and incidental findings were acted upon as appropriate.

2.5 STATISTICAL ANALYSIS.

The majority of the statistical analyses within this thesis was performed by myself, using SPSS statistics (IBM, version 21) and graphpad Prism (Graphpad Software). Continuous variables were expressed as mean ± standard deviation or median [interquartile range (IQR)] as appropriate. CT-AVC data underwent square-root transformation to achieve normality ($\sqrt{}$AU). Categorical data were presented as number and percentage. Correlations between continuous variables were assessed with linear regression analysis and either Pearson's r or Spearman's Rho subject to the normality of the variables tested. Parametric (unpaired Student's *t*-test) and non-parametric (Mann-Whitney U) tests were used as appropriate. Reproducibility studies were performed using Bland-Altman analyses. Outcome variables were assessed using Kaplan-Meier curves and cox proportional hazards regression analyses. Two-sided significance was taken as $p<0.05$. Statistical support was also provided by Dr Anoop Shah and the dedicated trial statisticians for Saltire 2, Dr Sharon Tuck and Dr Catriona Graham.

Chapter 3

Optimization and Reproducibility of 18F-Fluoride Positron Emission Tomography in Patients with Aortic Stenosis

Published by **Pawade TA**, Cartlidge TRG, Jenkins WSA et al. Optimization and reproducibility of aortic valve 18F-fluoride positron emission tomography in patients with aortic stenosis. *Circ Cardiovasc Imaging*. 2016;9(10):e005131.

Objective

18F-Fluoride positron emission tomography (PET) and computed tomography (CT) can measure disease activity and progression in aortic stenosis. Our objectives were to optimize the methodology, analysis and scan-rescan reproducibility of aortic valve 18F-fluoride PET-CT imaging.

Methods and Results

Fifteen patients with aortic stenosis underwent repeated 18F-fluoride PET-CT. We compared non-gated PET and non-contrast CT, with a modified approach that incorporated contrast CT and ECG-gated PET. We explored a range of image analysis techniques including estimation of blood-pool activity at differing vascular sites and a most-diseased segment (MDS) approach.

Contrast-enhanced ECG-gated PET-CT permitted localization of 18F-fluoride uptake to individual valve leaflets. Uptake was most commonly observed at sites of maximal mechanical stress: the leaflet tips and the commissures. Scan-rescan reproducibility was markedly improved using enhanced analysis techniques leading to a reduction in percentage error from ±63% to ±10% (tissue-to-background ratio MDS mean of 1.55, bias -0.05, limits of agreement -0·20 to +0·11).

Conclusion

Optimized 18F-fluoride PET-CT allows reproducible localization of calcification activity to different regions of the aortic valve leaflet and commonly to areas of increased mechanical stress. This technique holds major promise in improving our understanding of the pathophysiology of aortic stenosis and as a biomarker end-point in clinical trials of novel therapies.

3.1 INTRODUCTION

Aortic stenosis is the most common form of valve disease in the western world and a major health care burden that is set to treble by 2050. However we currently lack any disease-modifying therapies. Calcification appears to be the predominant pathological process driving disease progression leading to major interest in novel treatment strategies aimed at reducing calcification activity in the valve (29). However assessing the efficacy of new therapies requires large trials with prolonged follow-up to demonstrate an impact on disease progression and clinical end-points (11). A non-invasive imaging technique capable of measuring calcification activity in the valve would be highly desirable to assess treatment efficacy in phase 2 clinical trials.

18F-Fluoride is a positron-emitting radiotracer that binds to regions of newly developing microcalcification beyond the resolution of computed tomography (155). 18F-Fluoride is readily taken up by the valves of patients with aortic stenosis and on histology, correlates with markers of calcification activity (147). Importantly this technique predicts disease progression both with respect to echocardiography and CT calcium scoring as well as adverse cardiovascular events (104, 110, 112). 18F-Fluoride positron emission tomography (PET) imaging therefore holds major promise as a marker of calcification activity in aortic stenosis and is an exploratory secondary end-point in the on-going Saltire 2 clinical trial.

Here, we sought to optimize 18F-fluoride PET scanning of the aortic valve, reduce the effects of cardiac motion and assess the scan-rescan reproducibility of this technique to assess its future application as a novel biomarker of calcification activity in clinical trials.

3.2 METHODS

3.2.1 Study Population

Patients aged over 50 years with mild, moderate and severe calcific aortic stenosis were recruited prospectively from outpatient clinics at the Edinburgh Heart Centre. Aortic stenosis severity was determined by clinical echocardiograms and graded according to according to European Society of Cardiology guidelines (152). Since this is a sub-study of the ongoing Saltire 2 clinical trial, patients were required to fulfil the same inclusion and exclusion criteria as those entering the main trial. These included renal failure and women of childbearing potential (full list in Appendix 1).

3.2.3 Initial Image acquisition

Each patient underwent 18F-fluoride positron emission tomography (PET) and computed tomography (CT) scanning on two occasions. The imaging protocol is described in chapter 2.

3.2.4 Initial image analysis

This was performed as described in Chapter 2. To optimize the spatial localization and scan-rescan reproducibility of 18F-fluoride PET-CT imaging, we assessed different approaches to both image acquisition and image analysis.

3.2.5 Optimisation of 18F-Fluoride PET image acquisition: Contrast CT

Our original technique required the reorientation and co-registration of non-contrast CT images of the aortic valve (Figures 2.3 and 2.4). This technique posed several challenges, particularly with respect to aligning with the true plane of the valve and accurately defining its perimeter. Moreover the structure of individual leaflets was not visible on these scans precluding more detailed localization of 18F-fluoride uptake. Contrast CT offered potential solutions to these challenges given its superior anatomical detail and the well-established methodology for finding the true plane of the valve (158) Figure 3.1).

3.2.6 Optimisation of 18F-Fluoride PET image acquisition: ECG-Gated PET Data

PET is susceptible to motion, limiting accurate co-registration and the spatial assessment of PET activity within the valve. As a solution, we employed electrocardiogram (ECG) gating of list mode PET data. These data were reconstructed into 4 gates at 25% intervals of the cardiac cycle. Only data acquired between 50 and 75% of the RR interval were assessed because this period corresponds with diastole when cardiac motion is at a minimum. Given that three quarters of the PET data are therefore discarded, the bedtime was increased to 30 min in order to preserve signal-to-noise.

Figure 3.1 Creation of co-registered planar images of the aortic valve

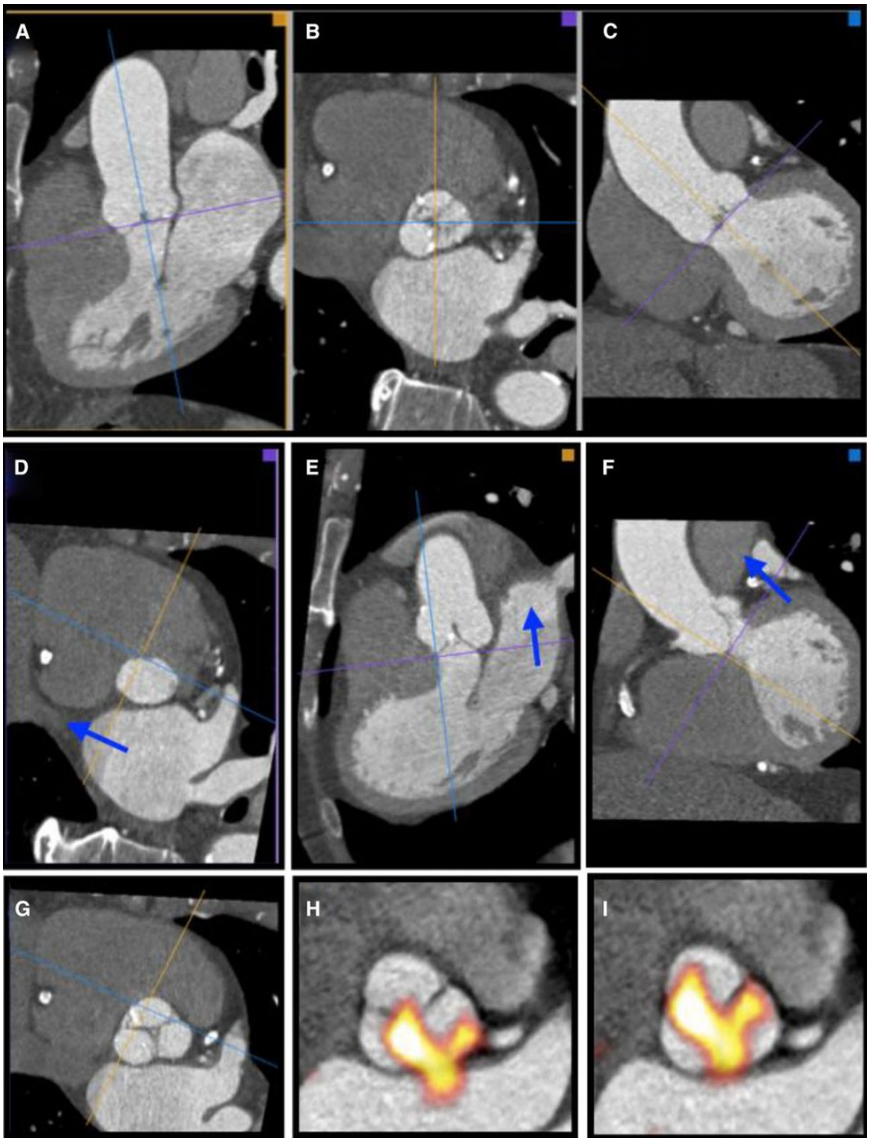

Creation of planar en-face valve images using CT angiography was achieved as follows. First, the CT angiogram is re-orientated to get into the approximate plane of the aortic valve by lining up the axial cross hair (purple in this example) using the images in the coronal (a) and sagittal planes (c). This creates an approximate cross sectional image of the aortic valve in the axial frame (b). Scrolling down in the axial frame, the centre of the crosshairs is then placed over the exact point at which the right coronary cusp disappears, identifying the base of that leaflet (d). Similarly the base of the non-coronary cusp is identified and orthogonal planes adjusted so that the purple plane goes through the base of both these two cusps (d). Finally the base of the left coronary cusp is found by rotation of the axial cross hairs so that first the cusp comes into view. The image is then slowly rotated in the opposite direction until the point where the leaflet first disappears (the base) is again found (f). This produces an en face image of the valve aligned with the base of all three leaflets (g). Adjacent 3-mm slices are then created in that plane and used for subsequent assessment. These slices are fused with the 18F-Fluoride PET images (h) and careful co-registration performed in 3-dimensions to ensure accurate alignment between the PET and CT images (i).

Pawade et al.Circ Cardiovas Imaging. 2016 (159)

3.2.7 Optimisation of 18F-fluoride PET image analysis: Measurement Of Blood Pool Activity

The stability of blood pool measurements in the SVC for 18F-fluoride based tracers has recently been questioned (160) and we were concerned about variation in the measured blood-pool activity at different levels of the brachiocephalic vein. We reasoned that this may be explained by the relatively small diameter of this vein rendering it susceptible to partial volume effects, amplified by the very low PET signal in surrounding lung tissue (especially in the cranial aspects of the brachocephalic vein). We hypothesized that sampling blood-pool activity from the center of the right atrium (a much larger structure) may improve the ease and accuracy with which these measurements could be made and the consequent scan-rescan reproducibility. Using the same co-registered PET and CT images of the heart, re-orientated to the plane of the valve, a 2-cm^2 ROI was drawn in the center of the right atrium at the level of the right coronary ostium and again in the same position one slice superiorly. Averaging the mean SUV for these two slices gave an alternative measure of blood-pool activity, which was used to correct valvular uptake measurements using two different approaches. First we used the conventional method of dividing aortic valve SUV measurements by the blood-pool to generate TBR values. Secondly we subtracted the blood-pool value from the valvular uptake, to generate the corrected aortic valve SUV (cSUV) as described recently (160).

3.2.8 Optimisation of 18F-fluoride PET image analysis: Most -diseased Segment and Whole Valve Approach

One of the biggest difficulties in quantifying uptake in the valve is defining its limits in the z-plane. To overcome this challenge, our original whole valve technique was compared to a 'most-diseased segment' (MDS) approach where the two contiguous slices with the highest SUV values (frequently in the center of the valve) were averaged to generate $SUV_{MDSmean,}$ SUV_{MDSmax} and corresponding TBR values. This is similar to the approach previously used for quantifying 18F-fluorodoexyglucose uptake in carotid and aortic atheroma (161)

3.2.9 Scan-rescan reproducibility

Scan-rescan repeatability and intra-and inter-observer reproducibility of valvular 18F-fluoride PET quantification was assessed for each of the established and novel image analysis approaches described above. Two experienced operators (Tania Pawade and Timothy Cartlidge) quantified uptake values on each of the scan-pairs, on two occasions separated by a 2-week interval to avoid recall bias. Observers were blinded to both their own previous measurements and those of the other operator.

3.2.10 Spatial localisation

The effect of our modifications on spatial resolution and scan-rescan reproducibility were then assessed in comparison with the original approach. First we assessed the ability of the technique to localize increased 18F-fluoride activity to individual valve leaflets and their different regions. Windowing of the fused PET/CT images was performed largely visually although a standardized method incorporated using 2

standard deviations of the blood pool activity in RA as the minimum. Scan-rescan and observer agreements were assessed.

3.2.11 Statistical Analysis

Continuous variables were expressed as mean ± standard deviation and categorical variables were expressed as total and percentage. Kappa statistics (with 95% confidence intervals) were used to measure the intra-observer and scan-rescan agreement in presence or absence of 18F-fluoride uptake across coronary cusps. The kappa values were interpreted as follows: poor <0.20, fair 0.21-0.4, moderate 0.41-0.60, good 0.61-0.80 and very good >0.81.

Intra-observer, inter-observer and scan-rescan reproducibility of several 18F-fluoride PET uptake approaches were analysed and presented using Bland-Altman analysis and percentage error (162). Variability in the different techniques was expressed using the width of the 95% limits of agreement (LOA) from Bland-Altman analyses. For the final approach, we considered the scan re-scan reproducibility to be good and acceptable for use in our future trial if the width of the 95% LOA were within ±0.2 for the $TBR_{MDSmean}$ measurements. Percentage errors for the mean bias were calculated using twice the standard deviation of the difference divided by the overall mean measurements. The intraclass correlation coefficient (ICC) was used to examine the reliability for both intra and inter-observer variability. Statistical analysis was performed using SAS for Windows version 9.4. Graphs were produced using PRISM version 6.0 for Mac.

3.3 RESULTS

3.3.1 Patient Characteristics

Fifteen patients (73±7 years, 67% male) had 2 scans (Table 3.1), 3.9 ±3.3 weeks apart between November 2014 and May 2015. Seven patients had mild aortic stenosis, 4 had moderate and 4 had severe aortic stenosis. In three participants, the between scan interval exceeded 4 weeks (5 weeks, 8 weeks and 14 weeks). The dose of 18F-fluoride was similar on each visit (123±8 and 125±4 MBq, P=0·49). The mean total dose was 29 mSv (range of 12.4 – 47.6 mSv).

Table 3.1 Patient Characteristics

DEMOGRAPHICS	Age (years)	73.3 ± 7.4
	Male	10 (67 %)
VITAL SIGNS	Body Mass Index (kg/m^2)*	29.7 ± 5.6
	Pulse (beats/min)*	67.7 ± 15.5
	Body Surface Area (m^2)*	1.9 ± 0.2
	Mean Arterial Pressure (mmHg)*	100.1 ± 9.3
	Current Smoker	1 (7%)
	Ex smoker	5 (33%)
SYMPTOMS	Chest Pain	4 (27%)
	Breathlessness	7 (47%)
	Syncope	2 (13%)
RELEVANT MEDICAL HISTORY	Hypertension	11 (73%)
	Previous CABG	2 (13%)
	Previous PCI	4 (27%)
	Liver Disease	1 (7%)
	Rheumatic Fever	0 (0%)
	Previous myocardial infarction	3 (20%)
	Hypercholesterolemia	10 (67%)
	Diabetes	4 (27%)
	Renal Disease	0 (0%)
	Cerebrovascular disease	2 (13%)
CONCOMITANT MEDICATIONS	Angiotensin Converting Enzyme	6 (40%)
	ARIIB	3 (20%)
	Beta Blocker	7 (47%)
	Statin	9 (60%)
SCAN INTERVAL	Weeks	3.9 ± 3.3

Abbreviations: CABG, coronary artery bypass grafting; PCI, percutaneous coronary intervention; eGFR, estimated glomerular filtration rate; ARIIB, Angiotensin two receptor blocker.

Pawade et al.Circ Cardiovas Imaging. 2016 (159)

3.3.2 Altered PET acquisition and Image Quality.

Good image quality allowing complete image analysis was achieved on all 15 scan-pairs. The prolonged bed-times of 30 min did not result in increased patient motion during the 18F-Fluoride PET scans. The impact of each stepwise change in the acquisition and analysis protocol on scan-rescan reproducibility is summarized in Table 3.2.

On visual assessment contrast CT imaging of the valve provided much clearer anatomical detail of the leaflets and valve structure compared to non-contrast CT This made it technically easier to get into the true plane of the valve and allowed more accurate regions of interest to be drawn around its perimeter. Co-registration with ECG-gated PET data then allowed localization of 18F-fluoride uptake to individual leaflets and their different regions. This was previously impossible using non-contrast CT and non-gated PET (Figure 3.3).

Activity was most frequently observed at the valve commissures: the point where the valve cusps meet the aortic ring [n=10] and at the tips where the leaflets coapt during diastole (n=8). When examining intra-observer reproducibility for detecting the presence or absence of 18F-fluoride uptake on individual valve leaflets, this was ‘very good’ for the right coronary cusp (kappa=1.00), ‘good’ for the non coronary cusp (kappa=0.63) and ‘moderate’ for the left (kappa=0.58) coronary cusps. The scan-rescan agreement was ‘good’ for the right (kappa=0.76), ‘good’ for the non (kappa=0.63) and ‘very good’ for the left (kappa=0.81) coronary cusps (Tables 3.3 and 3.4).

Table 3.2. Bland-Altman values and percentage errors for each stepwise change to the image acquisition and analysis technique

	MEAN VALUES				MAXIMUM VALUES			
	Ave. Value	**Mean Diff**	**LOA**	**Error (%)**	**Ave. Value**	**Mean Diff**	**LOA**	**Error (%)**
ORIGINAL APPROACH								
Whole Valve, ungated PET, non-contrast CT								
SUV	1.52±0.19	0.01	-0.37, 0.39	26	1.96±0.26	0.09	-0.42, 0.61	27
TBR (brachiocephalic)	1.44±0.45	0.05	-0.84, 0.93	63	1.87±0.61	0.15	-1.05, 1.35	65
RA blood pool correction								
Corrected SUV (subtracting RA)	0.43±0.09	0.01	-0.17, 0.19	43	0.86±0.17	0.09	-0.24, 0.42	39
TBR (dividing RA)	1.42±0.09	0.00	-0.17, 0.17	12	1.84±0.20	0.06	-0.33, 0.46	22
Most Diseased Segment Approach								
SUV	1.65±0.21	0.01	-0.40, 0.41	25	2.13±0.27	0.13	-0.39, 0.65	25
TBR (dividing RA)	1.55±0.08	0.01	-0.15, 0.14	10	2.01±0.15	0.11	-0.17, 0.39	14
FINAL APPROACH								
RA blood pool, most diseased segment, gated PET, contrast CT								
SUV	1.66±0.29	0.04	-0.53, 0.62	35	2.53±0.53	0.28	-0.97, 1.52	50
TBR (dividing RA)	1.55±0.08	0.05	-0.20, 0.11	10	2.39±0.44	0.11	-0.75, 0.97	37

Abbreviations: Ave, average; Diff, difference; Std. Dev, standard deviation; LOA, limits of agreement; SUV, standard uptake value; TBR, tissue to background ratio; PET, positron emission tomography; CT, computed tomography, RA, right atrium.

Pawade et al.Circ Cardiovas Imaging. 2016 (159)

Figure 3.2 Improved localization of PET signal within the aortic valve and its leaflets

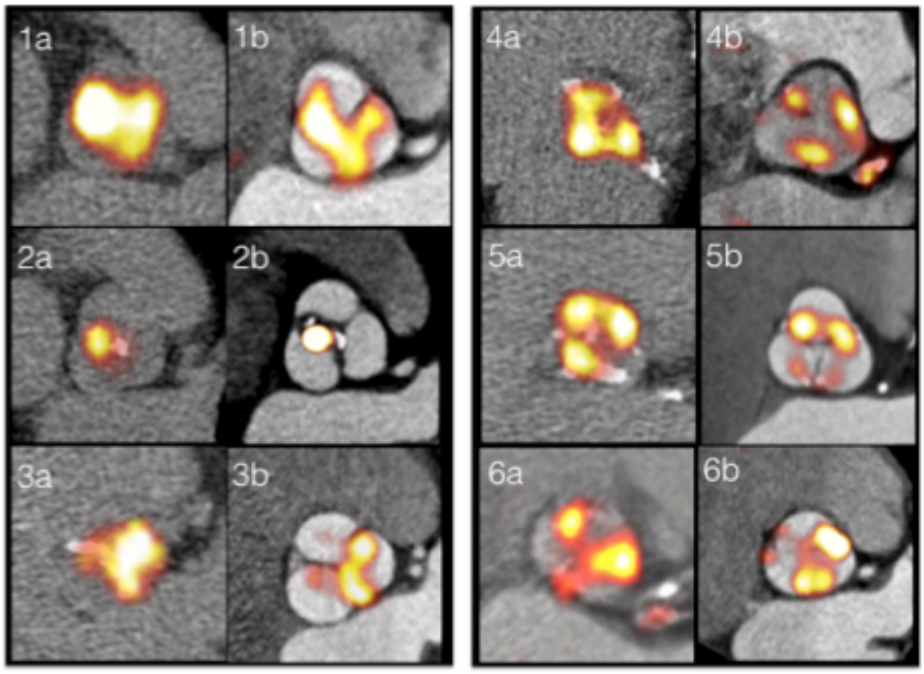

Paired non-gated, non-contrast PET/CT scans (Original approach 1a-6a) and gated, contrast-enhanced PET/CT images (Final approach 1b-6b). Images demonstrate the typical distribution of the tracer uptake within the valve at sites of increased mechanical stress i.e. at the leaflet tips (left: 1,2 and 3) and at the commissures (right: 4,5,6).

Pawade et al.Circ Cardiovas Imaging. 2016 (159)

Table 3.3 Scan-rescan and intraobserver reproducibility for presence or absence of 18F-fluoride uptake.

	Right coronary Cusp			Non Coronary Cusp			Left Coronary Cusps		
Subject	**1a**	**1b**	**2**	**1a**	**1b**	**2**	**1a**	**1b**	**2**
1	+	+	+	+	+	+	+	+	-
2	+	+	+	+	+	+	+	+	+
3	+	+	+	-	+	+	-	+	-
4	+	+	+	+	+	+	+	+	+
5	+	+	+	+	+	+	+	+	+
6	+	+	+	-	-	-	-	-	-
7	+	+	+	+	+	+	+	+	+
8	-	-	-	+	+	+	+	+	+
9	+	+	+	+	+	+	+	+	+
10	+	+	+	+	+	+	+	+	+
11	-	-	-	+	+	+	+	+	+
12	+	+	-	+	+	+	-	-	-
13	+	+	+	+	+	+	+	+	+
14	+	+	+	+	+	+	+	-	+
15	+	+	+	+	+	+	+	+	+

Presence or absence of 18F-Fluoride PET signal is denoted (+ and – respectively) for each individual valve leaflet. The distribution of 18-Fluoride signal on scan 1 images (1a) were reassessed (1b) to assess intraobserver reproducibility and compared to scan 2 (2) to determine scan-rescan reproducibility.

Pawade et al.Circ Cardiovas Imaging. 2016 (159)

Table 3.4 Kappa Statistics for Interobserver and Scan-rescan agreement for 18F-Fluoride PET signal distribution.

a) Right Coronary Cusp

		Scan 1 (Reading 2)	
		Absence	Presence
Scan 1 (1st Reading)	Absence	2	0
	Presence	0	13
Intra-observer agreement		1.00, 95% CI (-, -)	

		Scan 2	
		Absence	Presence
Scan 1 (1st Reading)	Absence	2	0
	Presence	1	12
Scan/Rescan agreement		0.76, 95% CI (0.32, 1.00)	

b) Non Coronary Cusp

		Scan 1 (Reading 2)	
		Absence	Presence
Scan 1 (1st Reading)	Absence	1	1
	Presence	0	13
Intra-observer agreement		0.63, 95% CI (-0.01, 1.00)	

		Scan 2	
		Absence	Presence
Scan 1 (1st Reading)	Absence	1	1
	Presence	0	13
Scan/Rescan agreement		0.63, 95% CI (-0.01, 1.00)	

c) Left Coronary Cusp

		Scan 1 (Reading 2)	
		Absence	Presence
Scan 1 (1st Reading)	Absence	2	1
	Presence	1	11
Intra-observer agreement		0.58, 95% CI (0.07, 1.00)	

		Scan 2	
		Absence	Presence
Scan 1 (1st Reading)	Absence	3	0
	Presence	1	11
Scan/Rescan agreement		0.81, 95% CI (0.47, 1.00)	

The numbers of presence or absence of 18F-Fluoride for right (a), non (b) and left (c) coronary cusps are provided. Kappa statistics and 95% confidence intervals for intra-observer [i.e. Scan 1 (1st Reading) vs. Scan 1 (2nd Reading)] and scan/rescan [i.e. Scan 1 (1st Reading) vs. Scan 2] agreement are also shown.

Pawade et al.Circ Cardiovas Imaging. 2016 (159)

3.3.3 Effect of Altered Image Analysis on PET reproducibility.

Interobserver and intra-observer reproducibility was good using both the original and modified approaches as previously reported. ICC values for intra and inter-observer reproducibility were 0.88 and 0.80 respectively (Table 3.5). However the scan-rescan reproducibility of our original approach produced percentage errors of ±26% and ±27% for the mean and maximum SUV measurements respectively (Table 3.2). Scan re-scan reproducibility for TBR measurements were disappointing with percentage errors of ±63% and ±65%.

3.3.4 Blood pool measurements

The percentage error of our original TBR values was double that of the SUV values suggesting a problem with our blood-pool measurements. Interestingly a step-wise and non-physiological reduction in our original brachio-cephalic vein measurements was observed on moving cranially up the axial slices away from the heart and into the lung. On average a 20% difference in values was observed between the top and bottom slices but this difference could be as high as 66%. By comparison, blood-pool sampling from the right atrium was easier to perform, allowed larger regions of interest to be drawn and was consistent, demonstrating a <1% difference in measurements acquired on adjacent slices (Figure 3.3).

Sampling the blood pool in the right atrium led to a substantial improvement in the scan-rescan reproducibility of all our TBR measurements. Indeed after implementing this approach, the reproducibility of our TBR values consistently outperformed those for SUV values with percentage errors of between ±12% and ±22% for mean and maximum values respectively. In contrast, the approach of subtracting the blood pool

uptake from the tissue SUV to produce cSUV measures did not greatly improve reproducibility resulting in percentage errors of ±43% and ±39% for mean and maximum measurements respectively despite similar limits of agreement. Considerable variation was observed in 18F-fluoride blood pool PET activity across our population (blood pool SUV 1.10±0.35) and even between different scans on the same patients. This is likely to reflect physiological variations in tracer distribution.

Figure 3.3 Measuring blood pool activity

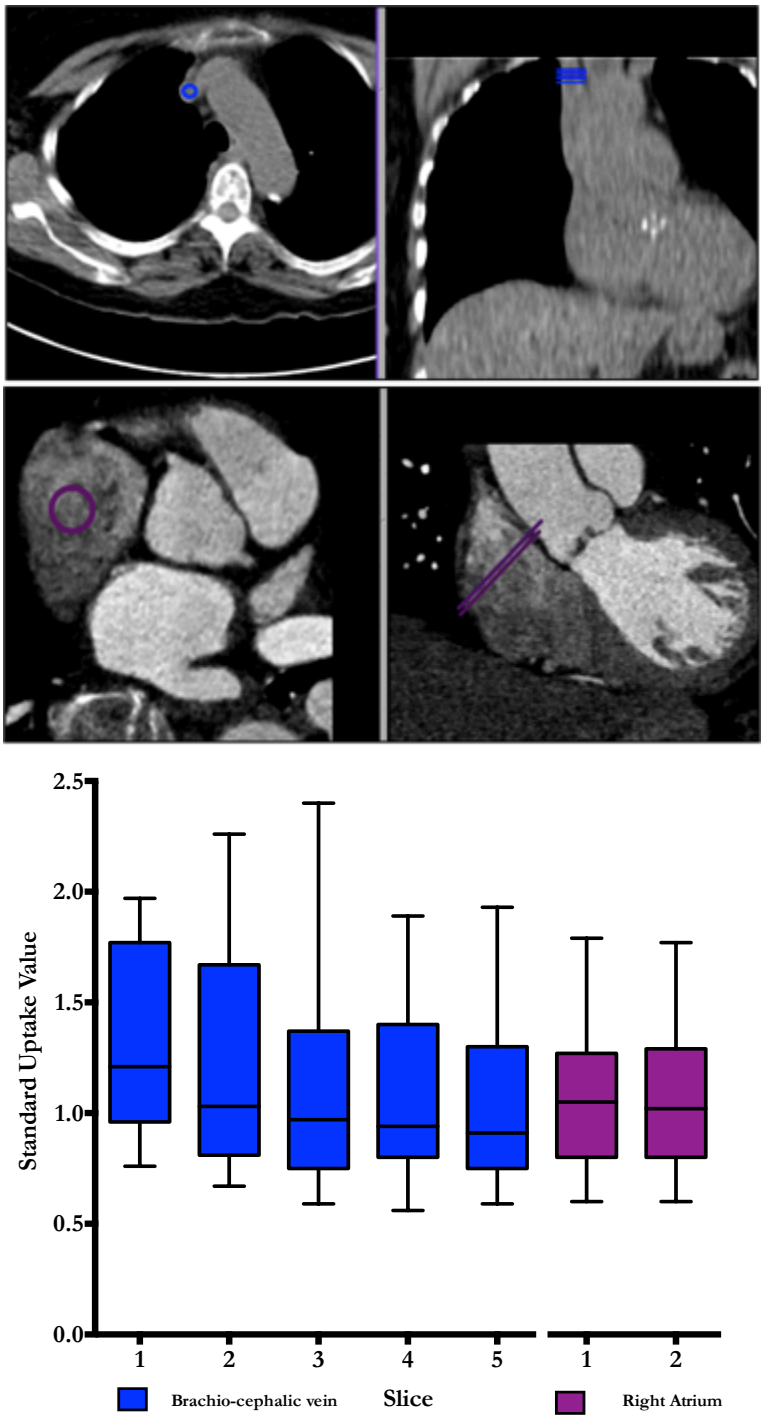

Regions of interest for measuring blood pool activity in the brachiocephalic vein (top) and right atrium (bottom) are shown in the en-face of the valve (left) and coronal (right) planes. Note that the right atrium is a much larger structure allowing for larger regions of interest with less potential for partial volume artifact problems related to poor registration. Tukey plot demonstrates mean SUV values for 5 contiguous slices from brachiocephalic (blue) and 2 from the right atrium (purple). Note the variation in brachocephalic vein measurements between those taken most caudally versus those taken most cranially.

Pawade et al.Circ Cardiovas Imaging. 2016 (159)

3.3.5 MDS Approach

The MDS technique improved the technical ease of image analysis, removing the difficulty in deciding upon the upper and lower limits of the valve in the z-plane. This translated into further improvements in scan-rescan reproducibility for mean TBR values with the percentage error for $TBR_{MDSmean}$ measurements reduced to ±10%. Similarly maximum TBR values were optimized upon addition of the MDS approach (percentage error TBR_{MDSmax} ±14%) as were the SUV measurements (percentage errors: $SUV_{MDSmean}$ ±25%, SUV_{MDSmax} ±25%; Table 3.2).

3.3.6 Final Approach: Addition of Contrast-CT and ECG-gated PET

The addition of contrast CT and ECG-gated PET data, whilst markedly improving image quality as described above, did not have a major affect on scan-rescan reproducibility. Reproducibility of our final approach however, remained good with a percentage error of ±10% for $TBR_{MDSmean}$ measurements (Figure 3.4 and 3.5). This, combined with its ability to localise PET uptake to individual leaflets, made the final approach our preferred strategy. $TBR_{MDSmean}$ values using the final approach did not show any proportional bias with disease severity and were again superior to the equivalent $SUV_{MDSmean}$ values (percentage error ±35%) and to measurements quantifying maximum valvular 18F-fluoride uptake, which were less reproducible after the addition of gated-PET and contrast-CT (percentage errors: SUV_{MDSmax} ±50% and TBR_{MDSmax} ±37% respectively, Table 3.2, Figure 3.4).

Figure 3.4 Final Approach

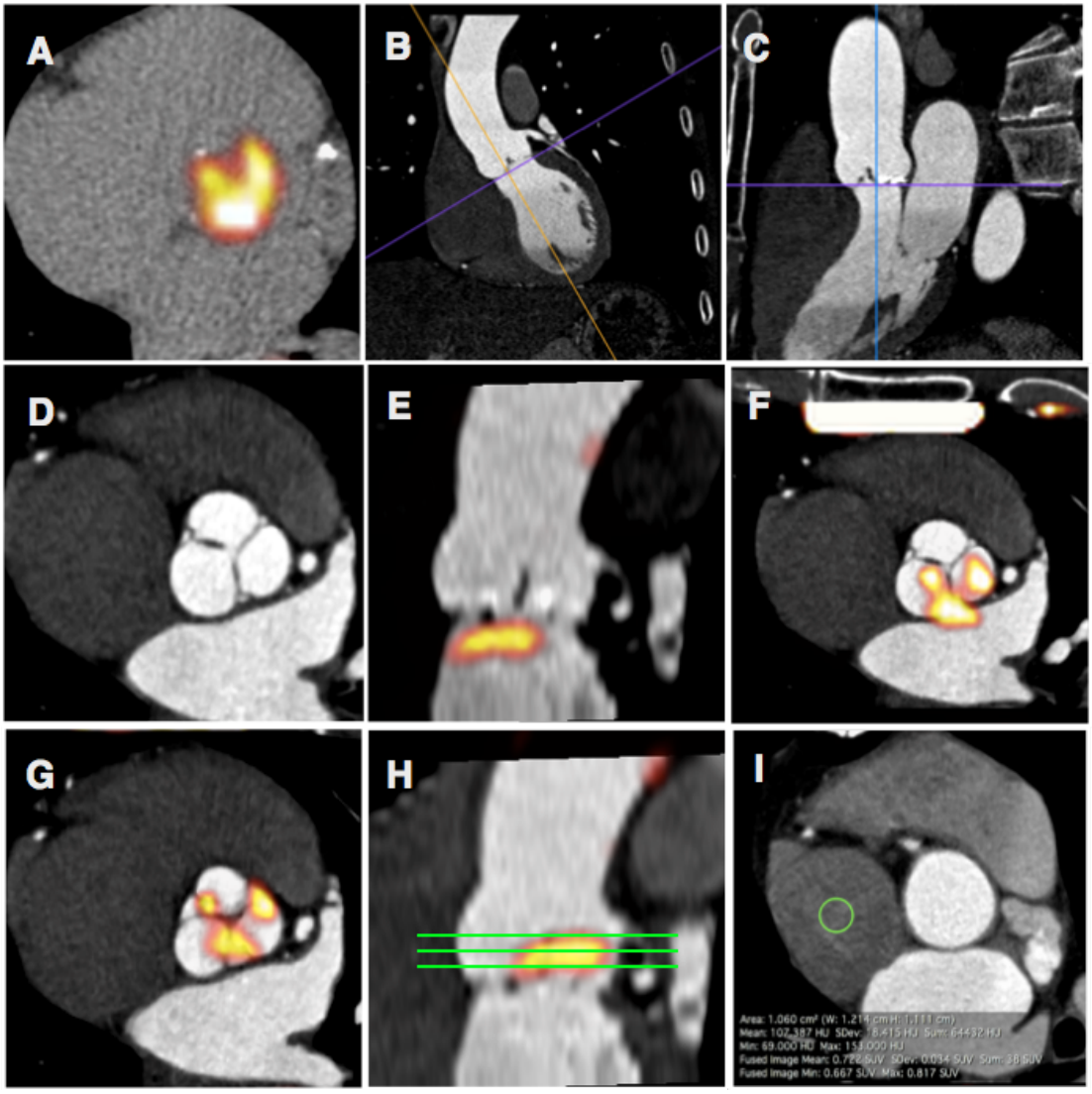

The original technique (A) underwent a series of modifications. Contrast computed tomographic angiographic are reorientated (B and C) to obtain planar views of the aortic valve (D). These are co-registered with the gated PET in multiple views (E and F) to ensure optimal allignment (G). Mean standard uptake values from the most diseased segment (H) are divided by the blood pool which is sampled from the right atrium blood pool (I) to generated the $TBR_{MDSmean}$.

Figure 3.5 Scan-rescan reproducibility for quantification of 18F-Fluoride positron emission tomography activity in the aortic valve

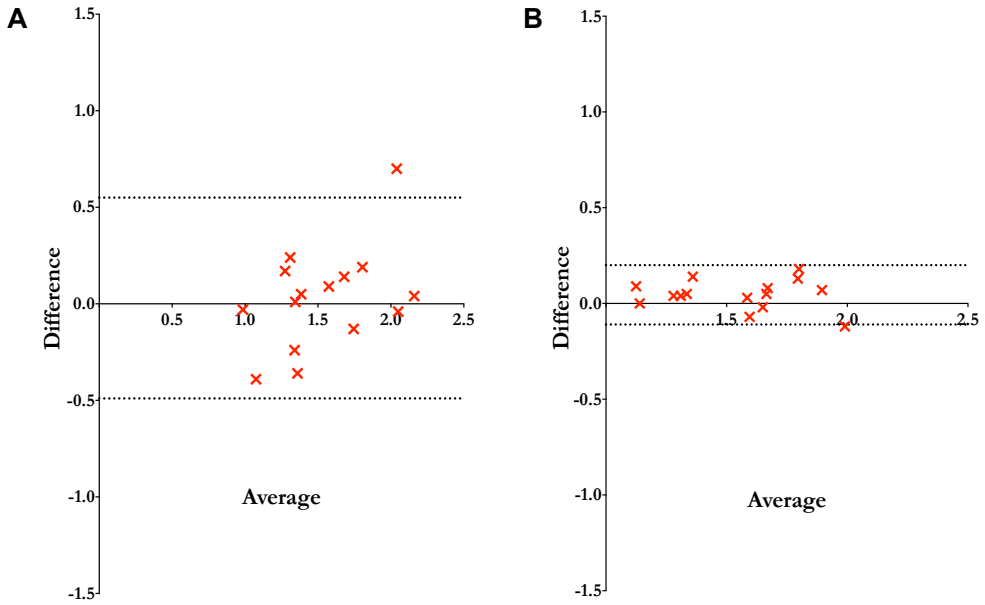

Bland Altman plots of scan-rescan reproducibility for $TBR_{MDSmean}$ measurements using the original image analysis and acquisition methods (left) and then using final method (right). Percentage error for the final method is less than ±10

Table 3.5 Intra/Inter-observer variability of 18F-Fluoride PET Uptake (expressed as a continuous variable)

	Difference		95% limits of agreement	ICC
	Mean	Standard Deviation		
Intra-observer[1]	0.053	0.12	-0.19, 0.30	0.88
Intra-observer[2]	0.028	0.08	-0.13, 0.19	0.98
Inter-observer[3]	-0.092	0.17	-0.42, 0.23	0.80

Abbreviations: ICC, intra class correlation coefficient.

1. Rater 1 Scan 1 (1st Reading) vs. Rater 1 Scan 1 (2nd Reading)
2. Rater 2 Scan 1 (1st Reading) vs Rater 2 Scan 1 (2nd Reading)
3. Rater 1 Scan 1 (1st Reading) vs. Rater 2 Scan 1 (1st Reading)

3.4 DISCUSSION

In this study, we have systematically investigated the acquisition and analysis of 18F-fluoride PET imaging of the aortic valve. First we have improved the spatial localization of tracer uptake using ECG-gated PET data and contrast CT imaging, so that activity can now be localized to individual leaflets and regions within those leaflets. This has demonstrated that calcification activity is most commonly observed at sites of maximal mechanical stress: in particular in regions of leaflet coaptation and at the commissures. Second we have improved the scan-rescan reproducibility ultimately demonstrating good agreement for repeat $TBR_{MDSmean}$ measurements in the valve (percentage error ±10%). This has important implications for application to future clinical trials, indicating that 18F-fluoride might provide a useful imaging end-point of drug efficacy.

In this study we have modified our previous image acquisition protocol to include contrast-enhanced CT imaging of the aortic valve, thereby providing greater definition of the individual valve leaflets and their components. Moreover we have included ECG-gated PET data to reduce the effects of cardiac motion and more accurately localize the pattern of activity on to the valve. The combined effect of these changes has been to improve the spatial localization of PET activity within the valve, which after accurate 3D co-registration, is now possible within specific regions of individual leaflets. This has demonstrated that 18F-fluoride activity predominantly localizes to sites of increased mechanical stress within the valve, supporting mechanical injury as a key driver to the disease process. For example 18F-fluoride activity was observed at the edges of the valve leaflets exactly at the

sites of leaflet impact during valve closure. Additionally uptake was observed at the valve commissures where mechanical stress is concentrated before being transferred to the aortic wall (101, 163). Whilst these findings need to be confirmed in larger studies with further refinement of thresholding techniques, they here provide key insight into the triggers to calcification activity in aortic stenosis and the importance of mechanical injury. Recent data have indicated that the relationship between the valve calcium burden and hemodynamic obstruction is not perfect (121, 164). The ability of PET to accurately localize calcification activity may be useful in trying to understand whether calcium formation at different sites of the valve has different hemodynamic impacts.

We have modified our image analysis protocol, optimizing the scan-rescan reproducibility of 18F-fluoride imaging in the aortic valve using several different approaches. To date, it has been standard practice for 18F-fluorodeoxyglucose PET to measure the blood pool SUV in the brachiocephalic vein (165). This has the benefit of avoiding contamination of myocardial 18F-fluorodeoxyglucose uptake that would overestimate the blood pool activity if measured in the heart. However, this benefit does not exist for 18F-fluoride, which has no background myocardial uptake. We therefore measured blood pool activity in both the right atrium and the brachiocephalic vein. Measurements in the right atrium are easily performed on the en face (short-axis) images of the valve and resulted in much more consistent blood-pool measurements. Moreover this approach led to a dramatic improvement in the scan-rescan reproducibility of our TBR measurements such that they then outperformed equivalent SUV measures. We believe that sampling the blood-pool

activity in the right atrium improved reproducibility because these measurements are less susceptible to the partial volume effects of adjacent lung tissue and because any minor inaccuracies in co-registration with the PET signal will not have a great impact. Furthermore it appears important to correct for variations in background blood pool activity that can occur between scans perhaps due to minor changes in renal function, tracer dose and pharmacokinetic distribution. Chen et al recently surmised that subtracting the blood pool from tissue SUV would improve accuracy (160). However our study findings did not support this and their approach produced lower TBR values thereby increasing the percentage error of our repeat measurements.

Another major improvement in reproducibility was obtained using the most diseased segment (MDS) approach: measuring activity in the two hottest adjacent slices in the valve, rather than attempting to sample the entire valve. The major advantage of this technique is that it removes the considerable difficulty in deciding the limits and boundaries of the valve. Such uncertainty can lead to major differences in valve measurements because uptake is much lower at the extremes of the valve where the volume of tissue is small and inclusion of extraneous tissue will dilute down mean values.

Whilst our stepwise changes to the protocol generally improved the reproducibility of "mean" measures of PET uptake, the effects on "maximum" measures were more variable. This finding is somewhat at odds with experience in oncology where the maximum values are often preferred. This may reflect the use of contrast enhanced

CT (not used in cancer imaging), which allowed accurate and reproducible regions of interest to be drawn around the perimeter of the valve facilitating reproducible measurement of mean PET uptake. In addition it may reflect ECG-gating of the PET data, which discards 75% of the counts, potentially having a greater detrimental impact on maximum values (which rely on counts from only a few pixels and are therefore particularly susceptible to noise) than mean values. It is possible that advanced image analysis approaches that model and correct for cardiac motion without discarding any PET data will improve the reproducibility of TBR_{MDSmax} measurements as has recently been described for coronary 18F-fluoride activity (166).

This is the first study to assess scan-rescan reproducibility for 18F-fluoride uptake in the aortic valve. We acknowledge that scan-rescan reproducibility does not necessary translate to accuracy and sensitivity. The value of 18F-Fluoride as an imaging marker of calcification activity will ultimately be determined by its ability to predict disease progression and to detect changes in calcification activity in response to novel therapies. These aspects are both currently being studied within the Saltire 2 clinical trial. We have already shown that the $TBR_{MDSmean}$ can predict disease progression and clinical events in patients with aortic stenosis (148). We can now report $TBR_{MDSmean}$ measurements, made using our optimized image acquisition and analysis protocols, quantify valvular 18F-fluoride activity with good reproducibility and a 10% error. This translates directly into the requirement for low patient numbers for studies investigating the effects of interventions on 18F-fluoride PET uptake (as a marker of calcification activity), because any true effect will not be swamped by 'noise'

within the measuring technique.

3.4.1 Limitations.

We acknowledge the small sample size, in this study however it is similar to that used in previous studies examining the reproducibility of vascular PET (156)and in part reflects attempts to minimize the radiation exposure associated with repeat PET/CT imaging. Moreover whilst previous studies have indicated that 18F-fluoride uptake correlates with histological markers of calcification activity and accurately predicts the progression in the CT calcium score, we currently lack data to show that 18F-fluoride is modifiable with drug therapy. Largely this is because no drug has yet demonstrated an ability to reduce disease activity in aortic stenosis and we lack reliable animal models of this condition.

3.5 CONCLUSION

In conclusion, we have optimized 18F-fluoride PET-CT imaging in the aortic valve. Excellent localization of the PET signal within the aortic valve is now possible, with uptake observed in regions of maximal mechanical stress. Moreover quantification of valvular 18F-fluoride uptake is also now possible with good scan-rescan reproducibility. 18F-Fluoride PET-CT holds major promise as a method to better understand calcification activity in aortic stenosis and as a surrogate endpoint in clinical trials assessing the efficacy of potential therapeutic interventions.

Chapter 4

Validating Computed Tomography Aortic Valve Calcium Scoring in Aortic Stenosis: A Single Centre Study

Objective

Quantification of aortic valve calcification (AVC) by computed tomography (CT) has major potential for the management of patients with aortic stenosis. We aimed to assess scan-rescan reproducibility, correlation with echocardiography, sex-specific differences and the prediction of disease progression and clinical events.

Methods and Results

Volunteers (72±8 years, 68% men) with and without aortic valve disease (20 controls; 20 aortic sclerosis; 32 mild, 37 moderate, and 27 severe aortic stenosis) underwent CT and echocardiography. Fifteen patients underwent repeat CT scanning to assess CT-AVC reproducibility. Disease progression was assessed at 1 and 2 years using CT-AVC measurements and echocardiography. The primary clinical endpoint was a composite of death and aortic valve replacement (AVR).

Baseline CT-AVC scores were reproducible and correlated strongly with echocardiographic measures of disease severity ($r=0.87$ for peak velocity, $p<0.001$). Women required less calcification than men for the same degree of stenosis (0.061 [95% confidence intervals, 0.052-0.070] versus 0.042 [0.037-0.047] m/sec/√AU respectively, $p<0.001$). Baseline CT AVC predicted disease progression defined either using echocardiography (Δ Vmax $r=0.32$ [0.13–0.49], $p<0.0012$) or CT (Δ CT AVC, $r=0.86$ [0.79-0.91], $p<0.0001$). Sex-specific thresholds for severe CT-AVC independently predicted AVR and death after adjustment for age, sex and echocardiographic measures of disease severity (HR=5.54 [2.37-12.97], $p<0.001$).

Conclusion

CT-AVC scoring exhibits important sex-specific differences, correlates with disease severity and predicts progression. CT-AVC is a major independent determinant of the future risk of AVR and death in patients with aortic stenosis.

4.1 INTRODUCTION

Aortic stenosis represents a major cause of morbidity and mortality that is set to increase with an ageing population. Despite its prevalence, we lack accurate methods of predicting disease progression and clinical events.

Doppler and two-dimensional echocardiography are the principal techniques for assessing disease severity including the peak aortic valve jet velocity, the mean gradient and the aortic valve area (167). However these measures of disease severity are discordant in up to one third of patients with moderate or severe aortic stenosis (121). Diagnostic uncertainty as to the true severity of the disease is therefore common, making decisions regarding timing of surgery challenging. A complementary imaging technique capable of providing independent diagnostic and prognostic information to echocardiography is desirable.

Calcification is thought to represent the central process driving progressive obstruction in aortic stenosis (29). Computed tomography aortic valve calcification (CT-AVC) scoring offers accurate quantification of the valvular calcification burden (116). Recent studies have demonstrated a close association between CT-AVC measurements and hemodynamic assessments of disease severity (121, 168, 169). These studies have also highlighted important sex differences. Compared to men, women develop a greater degree of hemodynamic obstruction for any burden of valvular calcification, even when corrected for body size or the left ventricular outflow tract area. Sex-specific CT-AVC diagnostic thresholds for severe aortic stenosis have subsequently been proposed that predict adverse cardiovascular outcome independently of echocardiography (121, 168).

These early data require rigorous external validation and evaluation before CT calcium scoring is ready for widespread clinical use and potential incorporation into international clinical guidelines. In this study, we aimed to determine whether CT AVC scoring has acceptable scan-rescan reproducibility, demonstrates important sex differences, correlates with echocardiographic measures of disease severity, and predicts aortic stenosis disease progression and clinical outcomes independent of echocardiography.

4.2 METHODS

4.2.1 Study Populations

This chapter utilizes data from 2 cohorts, the Saltire 2 substudy and the Ring of Fire.

4.2.2 Scan reproducibility

The scan-rescan reproducibility of CT-AVC scoring was examined using the same 15 patients described in Chapter 3 (Table 3.1). The scan reproducibility of CT calcium scoring is discussed within this chapter.

4.2.3 Prospective clinical study

The ability of CT-AVC measurements to correlate with disease severity, predict disease progression and clinical events was examined in a prospective clinical study, the Ring of Fire. Patients aged >50 years with aortic sclerosis and mild, moderate or severe aortic stenosis attending the outpatient department of the Edinburgh Heart Centre were recruited in addition to age- and sex-matched control subjects (104, 170, 171).

4.2.4 Baseline Assessment

These participants underwent a full baseline assessment which included history, clinical examination, echocardiography and CT calcium scoring as described in Chapter 2.

4.2.5 Assessment of Disease Progression

Participants were invited to return for repeat clinical assessment and echocardiography 1 and 2 years after enrolment. The same research echocardiographer (Audrey White) performed each echocardiograph. These patients

also underwent repeat ECG-gated CT scanning for calculations of CT-AVC at either the 1 or 2-year time points (147).

4.2.6 Follow-up for Clinical Events

The primary clinical endpoint was a composite of aortic valve replacement (AVR) and all-cause mortality. All deaths were captured from the General Register of Scotland. All events, including AVR (either surgical or transcutaneous), were confirmed by independent review of each patient's healthcare record. Patients were managed in a single tertiary cardiac center, reviewed at a multi-disciplinary meeting and only underwent AVR if they met established indications according to contemporary guidelines (172).

4.2.7 Statistical Methods

Statistical analyses were performed as outlined in Chapter 2. Annualised rates of progression for aortic stenosis were calculated by Dr Anoop Shah either using the mean over two-time points (CT AVC) or regression analysis over three time-points (echocardiography). The effect of clinical, echocardiographic variables, CT-AVC and CT-AVCd upon reaching the primary endpoint were assessed using Cox proportional hazards regression analysis. This included analysis of the CT measurements as both continuous variables and using previously proposed sex-specific thresholds for severe valve calcification (CT AVC, men ≥2,065 AU, women ≥1,274; CT AVCd men 476 AU/cm^2, women 292 AU/cm^2(121). Statistical significance was defined as two-sided $p<0.05$.

4.3 RESULTS: REPRODUCIBILITY STUDY

4.3.1 Patient Characteristics

Fifteen patients (73±7 years, 67% male) received two ECG-gated contrast and non-contrast cardiac scans 3.9 ±3.3 weeks apart between November 2014 and May 2015 (Table 3.1, Chapter 3)

4.3.2 Reproducibility

In three participants, the scan interval exceeded the target of 4 weeks (5 weeks, 8 weeks and 14 weeks). Motion artefact affected 2 scans (7%), which were excluded from the initial analysis. Scan-rescan reproducibility for CT-AVC measurements was very good (median CT-AVC score 1149 AU, mean difference 2% [limits of agreement 16 to -12 %] Figure 4.1). Intra-observer (median CT-AVC score 1178 AU, mean difference 1% [limits of agreement 9 to -11%]) and inter-observer (median CT-AVC score 1207 AU, mean difference 0% [limits of agreement 5 to -6%]) reproducibilities were also excellent.

As a secondary analysis, we next applied the previously published sex-specific CT-AVC thresholds to classify each scan as either severe (n=5) or non-severe (n=10). All scan pairs including those with significant motion artefact were included and demonstrated 100% agreement (kappa statistic=1).

Figure 4.1 Reproducibility of computed tomography aortic valve calcium scoring

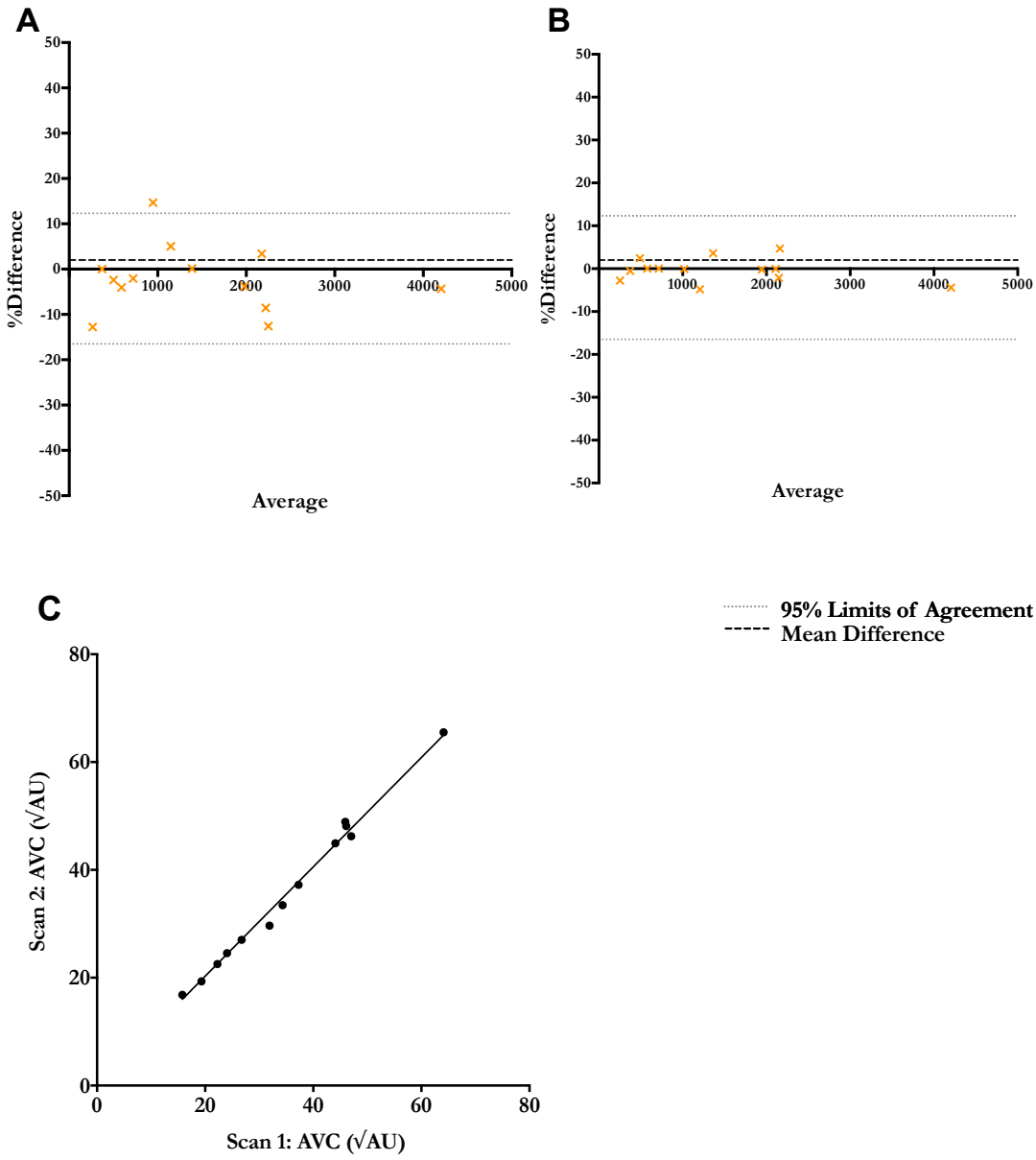

Bland-Altman plots showing scan-rescan reproducibility (A) and inter-observer reproducibility (B). Correlation between scan-pairs (C).

4.4 RESULTS: PROSPECTIVE COHORT STUDY

4.4.1 Patient Characteristics

121 patients (20 controls, 20 with aortic sclerosis, 25 with mild, 33 with moderate and 23 with severe aortic stenosis) were recruited into the prospective cohort study ((104, 170, 171).

4.4.2 CT-AVC and Aortic Stenosis Severity

At baseline, measurements of CT-AVC and CT-AVCd correlated strongly with all echocardiographic measures (Table 4.2). The closest associations were observed with the peak velocity (Vmax), and the weakest with the aortic valve area. Women required less valve calcification to develop the same degree of hemodynamic obstruction as men (linear regression slope of CT AVC vs. Vmax, 0.061 [95% confidence intervals, 0.052-0.070] versus 0.042 [95% confidence intervals, 0.037-0.047] m/s/√AU respectively, $p<0.001$). These sex differences persisted despite correction for LVOT size ($p<0.001$), and body surface area ($p=0.04$) (Figure 4.2).

4.4.3 Patient Follow up

Clinical follow-up and echocardiography was performed in 107 subjects at 1 year and 99 at 2 years (147). During the 2-year follow up period, (median 736 [722–760] days), 97 patients (78%) underwent a repeat cardiac CT (20 at 1 year and a further 77 at 2 years). Scans were not interpretable in 10 subjects (10%) due to motion artifact and were excluded. A total of 87 follow-up ECG-gated cardiac CT scans were therefore available for annualized progression analyses (Figure 4.3).

Table 4.1: Baseline Clinical Characteristics

	ALL	Echo FU	CT FU	AVR/Death
Number	121	99	87	47
CLINICAL				
Age (years)	72±8	72±8.5	72±8	72±10
Male	83 (69)	66 (65)	45 (51)	32 (71)
Body-mass Index (kg/m^2)	27±4	28±4	28±6	28±4
Systolic Blood Pressure	142±18	143±19	144±19	141±20
COMORBIDITY				
Diabetes Mellitus	18 (15)	13 (13)	12 (14)	7(15)
Hypertension	73 (60)	59 (60)	53 (61)	30 (65)
Documented CAD	43 (35)	36 (36)	38 (44)	17 (37)
Current smoker	14 (12)	11 (11)	7 (8)	8 (17)
Serum Creatinine (mg/dL)	1.01±0.29	1.02±0.32	1.00±0.28	0.98±0.33
MEDICATIONS				
ACE inhibitors	47 (39)	36 (36)	36 (41)	18 (39)
AIIRB	13 (11)	11 (11)	10 (11)	4 (9)
Beta Blockers	48 (40)	41 (41)	40 (46)	19 (41)
Statins	65 (54)	54 (54)	54 (62)	28 (60)
ECHOCARDIOGRAPHY				
Peak velocity (m/s)	2.8 [1.7-3.7]	2.6 [1.7-3.6]	2.6 [1.7-3.6]	3.8 (3.5-4.1)
Mean gradient (mmHg)	16 [6-29]	14 [6-27]	14 [6-27]	34 [23-44]
Valve area (cm^2)	1.34 [0.98-2.09]	1.37 [1.06-2.12]	1.33 [1.06-1.99]	0.91 [0.70-1.16]
Calcium Score	1.6±0.9	1.5±0.9	1.5±0.9	2.3±0.6
ELECTROCARDIOGRAPHY				
LVH	28 (23)	19 (19)	17 (20)	16 (34)
LV Strain	13 (11)	9 (9)	8 (9)	10 (22)
COMPUTED TOMOGRAPHY				
AV Calcium Score (AU)	554 [19-1762]	530 [13-1515]	585 [46-1487]	2680 [716-3847]
TIME IN STUDY				
	1880 [1263-1949]	1491 [1420-1560]	1503 [1434-1566]	809 [359-1455]

Abbreviations: ACE, angiotensin converting enzyme; AIIRB, angiotensin 2 receptor antagonists; AS, aortic stenosis; AV, aortic valve; CAD, coronary artery disease; AU, arbitrary unit; LV, left ventricle; LVH, left ventricular hypertrophy; FU, follow up.

Baseline characteristics are shown for all patients. Subsequent columns show the patient characteristics for those patients who had echocardiography follow up available, computed tomography follow up available and for those who had met the primary endpoint of aortic valve replacement or death. The mean±SD, median [IQR] and number (percentage) are shown.

Table 4.2 Correlation between computed tomography aortic valve scores and echocardiographic indices of severity

	Peak Velocity m/s	**Mean Gradient (mmHg)**	**Aortic Valve Area (cm^2)**	**Echocardiography Calcium score**
Aortic Valve Calcium Score	0.87 p<0.001	0.85 p<0.001	-0.66 p<0.001	0.81 p<0.001
Aortic Valve Calcium Density	0.89 p<0.001	0.87 p<0.001	-0.69 p<0.001	0.82 p<0.001

Pearson's correlation and respective p values are shown.

Figure 4.2 Correlation between computed tomography aortic valve calcium scores and echocardiographic measurements of peak velocity in males and females.

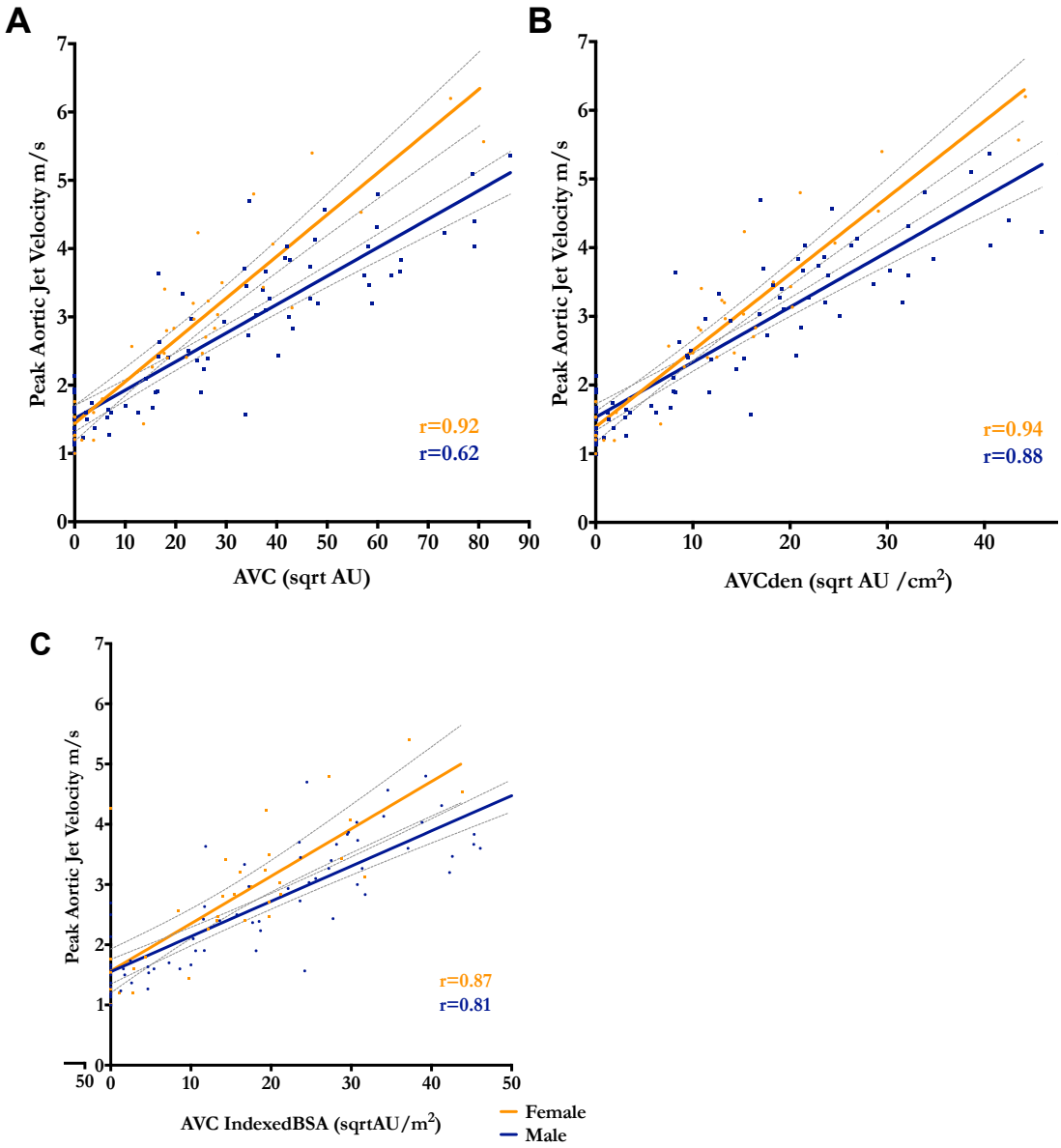

A. Correlation between peak aortic-jet velocity (m/s) with total aortic valve calcium scores (√AU) for males (blue) and females (orange).
B. Corrected for the left ventricular outflow tract area to generate the AVC density (√AU/cm^2)
C. Corrected for body surface area (√AU/m^2)

Abbreviations: AVC, aortic valve calcium; AU, Agatston Units

Figure 4.3. Study protocol and CONSORT diagram.

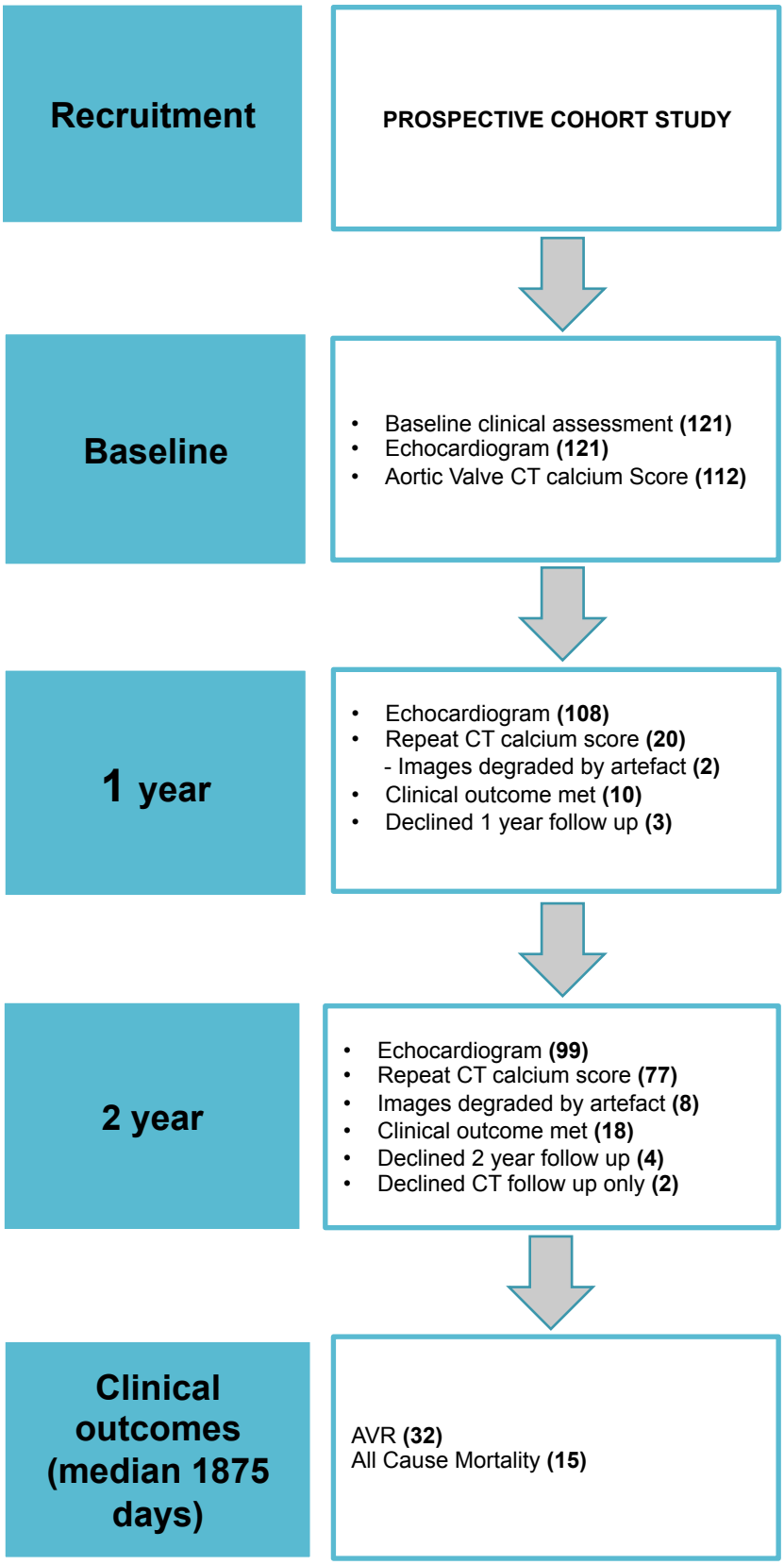

Abbreviations: CT, computed tomography; AVR, aortic valve replacement.

4.4.4. Aortic Stenosis Progression

Across all patients with aortic stenosis, modest progression in each echocardiographic measure of aortic stenosis severity was observed (Table 4.3). However when patients were divided in to mild, moderate and severe aortic stenosis, only those patients in the moderate group demonstrated clear evidence of disease progression on echocardiography (Figure 4.4). For CT, large annual changes in CT AVC score were observed across the whole aortic stenosis cohort with clear evidence of disease progression in all of the subgroups with mild, moderate and severe disease (Table 4.3, Figure 4.4). The most rapid rates of progression were observed in patients with the most severe aortic stenosis.

Prediction of Disease Progression

The baseline CT-AVC predicted disease progression, whether this was measured using CT (Δ CT-AVC, r=0.86 [95% confidence intervals, 0.79-0.91], p<0.0001; Figure 3) or echocardiography (Δ Vmax r=0.32 [95% confidence intervals, 0.13–0.49], p<0.0012, Δ mean gradient , r=0.37 [95% confidence intervals, 0.19–0.53], p=0.0002; Table 4). The rate of progression of AVC score correlated with echocardiographic measures of aortic stenosis progression (Δ Vmax, r=0.40 [95% confidence intervals, 0.22-0.58], Δ mean gradient, r=0.45 [95% confidence intervals, 0.26-0.61], both p<0.0001) (Table 4.4, Figure 4.5).

Table 4.3 Progression and outcome data.

Variable	All patients	Control Subjects	Aortic Sclerosis	Mild Aortic Stenosis	Moderate Aortic Stenosis	Severe Aortic Stenosis
BASELINE ECHOCARDIOGRAPHY						
No. of patients	121	20	20	25	33	23
Peak jet velocity (m/s)	2.8±1.2	1.3±0.2	1.7±0.2	2.5±0.2	3.4±0.3	4.6 ±0.6
Mean gradient (mmHg)	16.2±0.49	3.6±1.0	5.9±1.4	13.2±2.7	25.2±4.1	48.6±15.4
Aortic valve area (cm^2)	1.34±0.40	2.54±0.49	2.27±0.41	1.42±0.30	1.13±0.27	0.76±0.21
FOLLOW-UP ECHOCARDIOGRAPHY						
No. of patients	99	20	17	24	26	12
Change in peak velocity (m/s/year)	0.08 [-0.02-0.18] *p<0.001*	0.05 [-0.03-0.09]	0.03 [-0.08-0.08]	0.08 [-0.01-0.18]	0.17 [0.07-0.30]	0.10 [-0.11-0.19]
Change in mean gradient (mmHg/year)	0.7 [-0.2-2.9] *p<0.001*	0.1 [-0.5-0.3]	0.0 [-0.7-0.6]	1.0 [-0.3-2.2]	3.2 [0.7-5.0]	2.6 [-0.1-5.3]
Change in aortic valve area (cm^2/year)	-0.05 [-0.14-0.02) *p<0.001*	-0.10 [-0.25--0.01]	-0.04 [-0.12-0.07]	-0.09 [-0.16--0.02]	-0.05 [-0.13-0.03]	-0.04 [-0.08--0.02]
BASELINE COMPUTED TOMOGRAPHY						
No. of patients	112	20	20	23	30	19
Aortic valve Calcium score (AU)	554 [19-1762]	0 [0-3]	46 [2-224]	489 [281-693]	1427 [777-2215]	3386 [1770-6211]
FOLLOW-UP COMPUTED TOMOGRAPHY						
No. of patients	87	18	18	21	24	6
Change in aortic valve calcium score (AU / year)	61 [5-226] *p<0.001*	2 [0-8]	19 [0-52]	64 [48-134]	289 [106-443]	342 [163-583]
CLINICAL OUTCOME						
Number of event-free days	1880 [1263-1949]	1893 [1824-1920]	1902 [1850-2002]	1914 [1859-1995]	1864 [798-2002]	752 [336-1497]
All cause mortality	15	2	2	4	2	5
Aortic-valve replacement	32	0	0	1	15	16
Composite outcome (%)	47 (39)	2 (10)	2 (10)	5 (20)	17 (21)	21 (91)

Mean ± (Standard Deviation), Median [Interquartile Range] and Number (Percentages) are shown.

Figure 4.4. Computed tomography calcium scoring and disease progression.

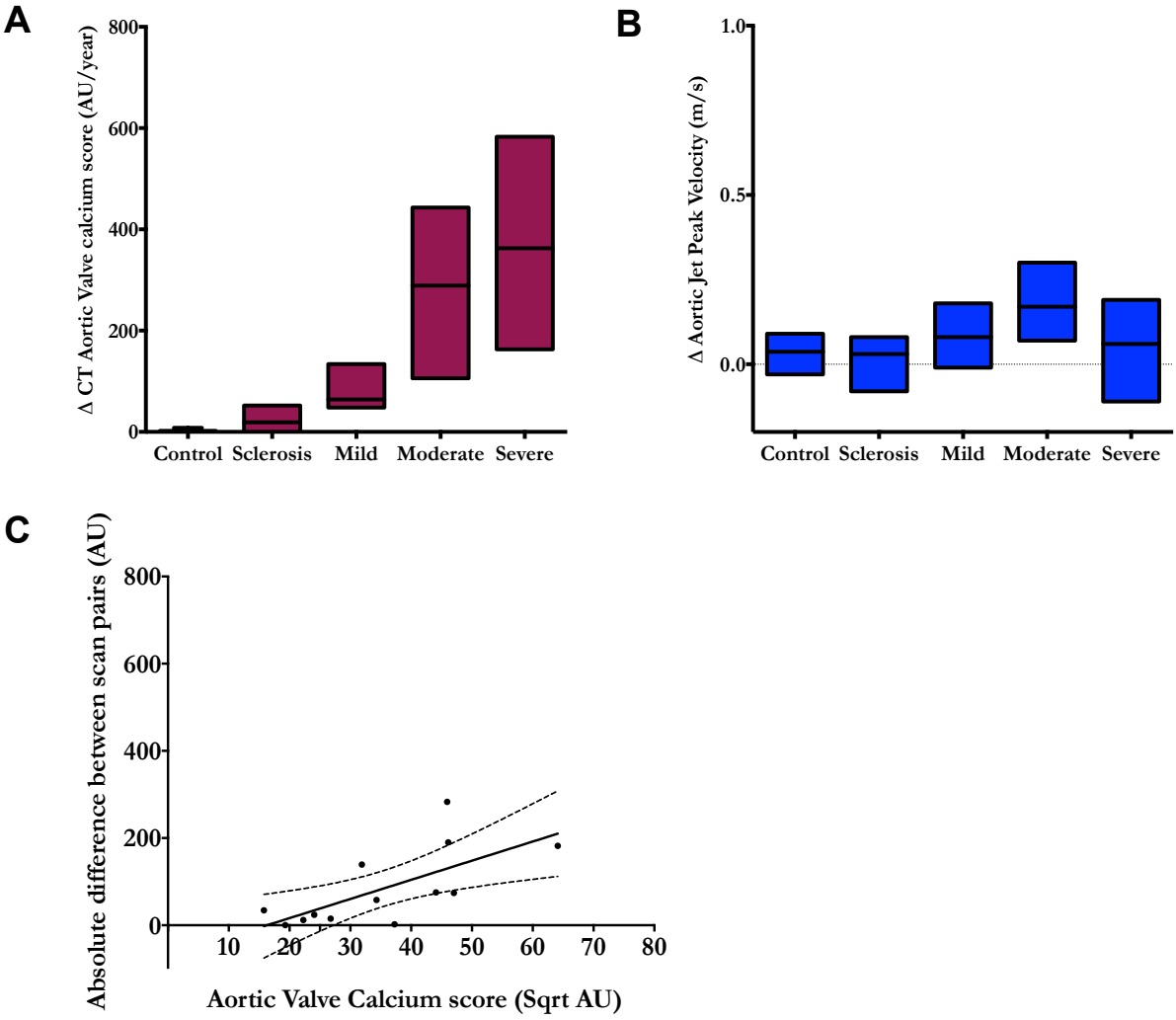

A&B. Annualized disease progression across each cohort using computed tomography (CT) calcium scoring (A) and echocardiography (B). Relatively large annualized changes in the CT calcium score are observed compared to smaller changes and wide overlap in the peak aortic-jet velocity measurements.
C. Absolute difference in aortic valve calcium scores between scan pairs (AU). This demonstrates the proportional bias in scan-rescan reproducibility, but also that this error is less than the annual changes observed in panel A.

Figure 4.5 Computed tomography aortic valve calcium scoring predicts disease progression

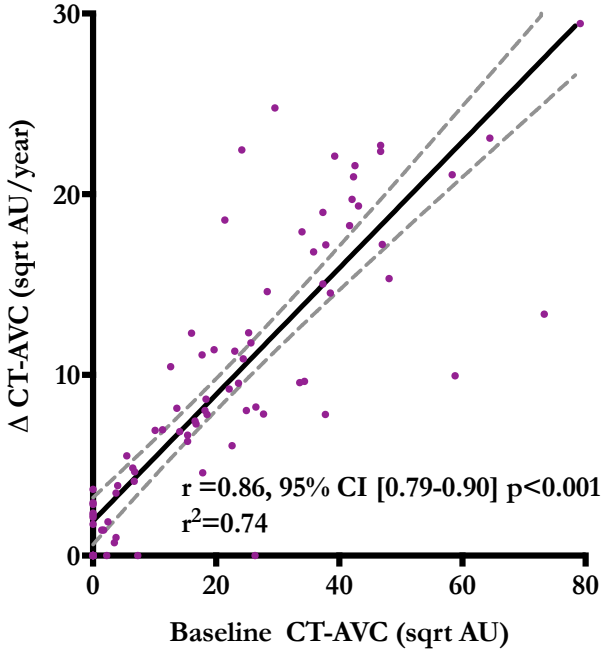

The baseline CT-AVC calcium score offers powerful prediction of disease progression as measured using computed tomography.

Abbreviations; CT-AVC, computed tomography aortic valve calcium score; CI confidence interval

Table 4.4 Baseline imaging and prediction of disease progression

Baseline Imaging Assessment	RATE OF CHANGE			
	CT-AVC (AU/yr)	Peak velocity (m/s/yr)	Mean Gradient (mmHg/yr)	Aortic Valve Area (cm^2/yr)
AV Calcium Score (AU)	*r*=0.86 (0.82-0.92) P<0.001	*r*=0.36 (0.16-0.53) P<0.001	*r*=0.40 (0.21-0.56) P<0.001	*r*=0.06 (-0.15-0.27) P=0.54
Peak Velocity (m/s)	*r*=0.79 (0.70-0.86) P<0.001	*r*=0.28 (0.08-0.45) P=0.006	*r*=0.40 (0.22-0.56) P<0.001	*r*=0.08 (-0.13-0.27) P=0.45

Abbreviations: AV: aortic valve; AU: Agatston unit; CT-AVC, computed tomography aortic valve calcium,

4.4.5 Prediction of Adverse Clinical Outcomes

Clinical outcomes were assessed at a median of 1,875 [1,188-1948] days after enrollment and 32 (26%) patients had received aortic valve replacement (AVR). There were 15 deaths (12%) of which 6 were cardiovascular deaths. Overall, 47/121 (39%) subjects were adjudicated to have reached the primary clinical end-point. Two control subjects died: 1 cardiovascular and 1 non-cardiovascular death.

4.4.6 Echocardiography

On univariate cox-proportional hazards analysis, severe aortic valve calcification as defined by an echocardiographic calcium score (ECS) of 3 was a strong predictor of AVR and death (hazards ratio, 6.00 [95% confidence intervals, 3.21-11.24], $p<0.001$). After adjustment for age and sex, it remained an independent predictor (hazards ratio, 6.07 [95% confidence intervals, 3.21-11.47], $p\leq0.001$). However when peak velocity was included in the model, this effect was no longer significant (hazards ratio, 1.19 [95% confidence intervals, 0.50-2.82], $p=0.690$).

4.4.7 Computed Tomography

When examined as a continuous variable, baseline CT-AVC was a predictor of AVR and death (hazard ratio per unit increase in CT AVC, 1.06 [95% confidence intervals, 1.05-1.08] /√AU, $p<0.001$) and remained an independent predictor after multivariate adjustment for age, sex and peak velocity (hazard ratio, 1.04 [95% confidence intervals, 1.02-1.07], $p<0.001$). Similarly CT-AVCd proved to be an independent predictor of outcome after multivariate adjustment for age, sex and peak velocity (hazard ratio per unit increase in CT-AVCd, 1.07 [95% confidence intervals, 1.02-1.12] /√AU, $p=0.006$).

We next investigated the prognostic utility of the previously proposed sex-specific CT-AVC thresholds for severe aortic stenosis (≥1,274 AU in females and ≥2,065 AU in males) as well as the equivalent CT-AVCd cut-offs (≥292 AU/cm^2 in females and ≥476 AU/cm^2 in males.(121) On univariate analysis, the presence of severe CT-AVC was associated with a 15-fold increase in the likelihood of AVR and death (hazards ratio, 14.85 [95% confidence intervals, 7.49 - 29.42], p<0.001) and remained an independent predictor of AVR and death after adjustment for age, sex (hazards ratio, 14.82 [95% confidence intervals, 7.40 - 29.70], p<0.001) and the peak aortic jet velocity (hazards ratio, 5.54 [95% confidence intervals, 2.37 - 12.97], p<0.001). Similarly, severe CT-AVCd provided independent prediction of death and AVR after adjustment for these same factors (hazards ratio, 3.10 [95% confidence intervals, 1.33 -7.20], p=0.009; Figures 4.6 and 4.7).

Figure 4.6 Event-free survival using sex-specific computed tomography aortic valve calcium scoring thresholds.

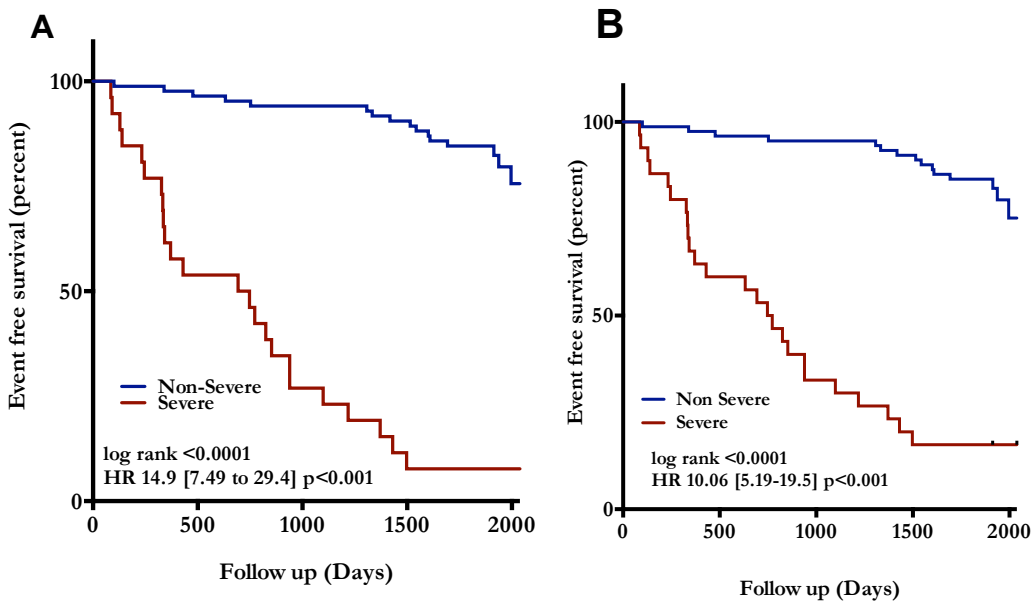

Event free survival using the sex-specific computed tomography (CT) thresholds for CT aortic valve calcium (A) and aortic valve calcium density (B) are shown. Severe calcification as defined by these thresholds was associated with an adverse prognosis

Figure 4.7. Sex-specific computer tomography aortic valve calcium thresholds predict the composite primary endpoint of aortic valve replacement and death.

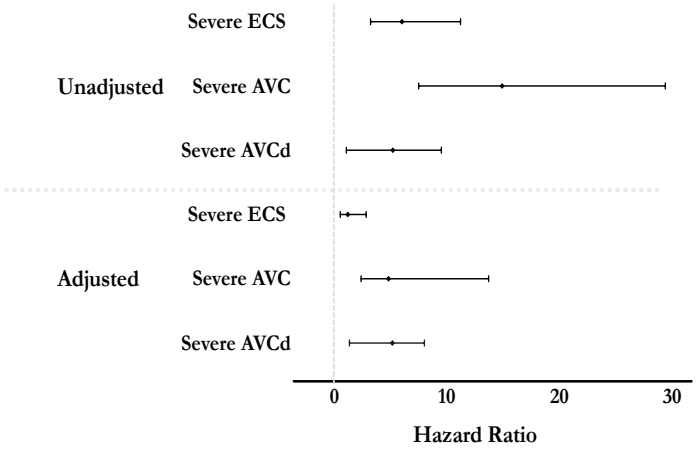

	HR	95% CI	Sig
Severe ECS	6.00	3.21-11.2	<0.001
Unadjusted Severe AVC	14.9	7.49-29.4	<0.001
Severe AVCd	10.06	5.19-19.5	0.001
Severe ECS	1.19	0.50-2.82	0.690
Adjusted Severe AVC	5.54	2.37-13.0	0.001
Severe AVCd	3.10	1.33-7.20	0.009

CT Calcium scoring is an independent predictor of aortic valve replacement (AVR) and death. Hazards ratios (HR) with 95% confidence intervals (CI) are given for severe aortic valve calcification as defined using the echocardiographic calcium score (ECS) and thresholds for AVC and AVCd. Hazard ratio for both the unadjusted analysis and analysis after adjustment for age, sex and peak aortic jet velocity are shown with their respective confidence intervals and p values.

Abbreviations: ECS, echocardiography calcium score; AVC, aortic valve calcium score; AVCd, aortic valve calcium density; HR, hazard ratio; CI, confidence interval

4.5 DISCUSSION

In this comprehensive, prospective, single-centre imaging study, we have confirmed that CT calcium scoring is reproducible, has important sex differences, and predicts disease severity and progression. Moreover, independent of standard risk factors and echocardiographic measures of disease severity, baseline scores for CT-AVC is a major determinant of the future risk of AVR and death in patients with aortic stenosis. These data are supportive of the use of CT calcium scoring in clinical practice as an adjunct to echocardiography, especially where echocardiographic findings are discordant or when attempting to assess future risk.

Standard clinical follow up for patients with aortic stenosis encompasses clinical history, examination and Doppler echocardiography. Whilst echocardiography is a robust and reliable clinical tool that provides accurate assessment in the majority of patients, it does have some limitations. Even in experienced hands, discordant echocardiographic measures of severity are seen in approximately a third of patients, most frequently due to conflicting aortic valve area and peak velocity or mean gradient measurements (173). This common discrepancy can be explained by low-flow states in only a minority of patients, resulting in diagnostic difficulty and problems addressing the need for valve replacement. A complementary technique that can aid in assessing disease severity and improving risk stratification is therefore highly desirable. Given the central role of calcification in the progression of aortic stenosis, direct assessments of aortic valve calcification holds major potential (29) and in particular, CT calcium scoring (116, 168, 169).

Before an imaging technique can be applied to routine clinical practice, clinicians need to be reassured that it is robust and reproducible. Measurement of CT-AVC is technically straightforward although it can be complicated by confluent calcium in the aortic root, left ventricular outflow tract, coronary arteries and mitral valve annulus. In this study, we have demonstrated that excellent reproducibility can be achieved with a consistent approach to dealing with calcium from extra-valvular structures. Unfortunately motion artefact still occurs in approximately 5-10% of cases despite administration of beta-blockade and ECG-gating, hampering image quality and rendering these scans challenging to interpret. However, given that the anticipated clinical application will adopt the employment of sex-specific thresholds, it was reassuring these limitations did not result in reclassification for any patients within our reproducibility cohort.

There is a strong association between CT-AVC measurements and hemodynamic AS severity on echocardiography. We have confirmed the findings of previous studies by demonstrating that, despite correction for anatomical size differences, less valvular calcification is required in women to produce severe haemodynamic obstruction (121). This supports the need for sex-specific thresholds when assessing severity. The discrepancy is unaccounted for but is thought to relate to a higher degree of valvular fibrosis in women (174). These findings warrant further exploration, as different therapeutic strategies may be required in men and women.

CT calcium scoring appeared to be a superior predictor of disease progression as measured by CT or echocardiography. Additionally progression of disease severity was easier to detect using CT calcium scoring compared to echocardiography at all stages of aortic stenosis disease severity. Indeed only CT-AVC scoring was able to measure disease progression in patients with mild, moderate and severe aortic stenosis. This in combination with its excellent reproducibility supports a role for CT-AVC in monitoring disease progression particularly in the context of research trials investigating the effects of novel therapies. We also demonstrated that progression in the CT-AVC score accelerates with progressive disease severity, consistent with a self-perpetuating cycle of injury and calcification (29).

Finally we have confirmed the ability of CT-AVC to predict clinical events. A strong correlation was observed between baseline CT-AVC and disease progression as measured using both CT and echocardiography. Moreover a strong association was observed between baseline AVC and the future incidence of AVR and death independent of age, sex and standard echocardiographic measures of disease severity. This was observed both when CT-AVC measurements were considered as continuous variables or as a dichotomous variable according to the sex-specific thresholds proposed by Clavel et al.(121)

4.5.1 Study Limitations

This was a single centre study and it therefore yet to be determined whether these findings apply to a wider, more heterogenous cohort. We acknowledge that while our prospective cohort represented the full physiological range of calcific aortic valve disease and allowed us to evaluate disease progression at each of these stage, this

resulted in a smaller proportion of patients with moderate or severe stenosis. Consequently only a modest event-rate was observed despite protracted follow up. In addition, those patients with the most severe disease underwent AVR before repeat echocardiography and CT could be performed at 2 years. This will have introduced survival bias in our estimates of disease progression by CT and especially by echocardiography. Therefore, our current estimates are likely to under represent the true extent of disease progression in this severe group of patients and perhaps explains apparent the fall in progression rates with echocardiography.

4.6 CONCLUSION

In combination with previous studies, we have demonstrated that CT-AVC scoring is a robust and reproducible clinical tool that can reliably assess disease severity, and predict disease progression and adverse clinical outcomes. We believe that this technique holds promise as a useful adjunctive investigation in the management of patients with this common and potentially life-threatening condition. This is the first external validation of clinical utility of sex-specific CT calcium scoring thresholds and supports their clinical utility in providing powerful patient risk stratification. We envisage that their primary clinical application would therefore be to assist with decision-making with regards to the confirmation of severe aortic valve disease and the consideration of AVR not only in patients with discordant echocardiographic findings but also those undergoing cardiac surgery for another indication such as coronary artery bypass grafting. Nonetheless, before these thresholds can be incorporated into widespread clinical guidelines, the ability of these thresholds to identify severe aortic stenosis and predict clinical outcomes within a larger, more heterogenous population needs to be examined.

Chapter 5

Validating Computed Tomography Aortic Valve Calcium Scoring in Patients with Aortic Stenosis: A Multi-centre Study.

Objective

To establish the clinical utility of computed tomography aortic valve calcium scoring (CT-AVC) in patients with aortic stenosis.

Methods and Results

Patients with aortic stenosis who had undergone electrocardiogram-gated CT-AVC measurements within 3 months of echocardiography were entered into a collaborative international multicenter observational registry. The identification of sex specific CT-AVC thresholds to diagnose severe aortic stenosis was determined in patients with concordant echocardiographic assessments in whom disease severity was unambiguous. In patients with prospective long-term follow up, we assessed whether these thresholds predict aortic valve replacement (AVR) and death. Finally CT-AVC thresholds were used as an 'umpire test' to arbitrate disease severity in patients with discordant echocardiographic measurements.

In 918 patients recruited from 8 international centers (age 77±10, 60% male, peak aortic-jet velocity 3.88±0.90 m/s), 708 (77%) patients had concordant echocardiographic assessments, in whom optimal sex-specific CT-AVC thresholds (women 1377, men 2062 AU) provided excellent discrimination for severe aortic stenosis (c-statistic: women 0.92, men 0.88; P<0.001 for both) and were nearly identical to those previously reported (women 1274, men 2065 AU).

Clinical outcomes were available in 237 patients over a median of 1029 [100-2,251] days. Sex-specific CT-AVC thresholds were independent predictors of AVR and death (hazards ratio, 3.02 [95% confidence intervals, 1.83-4.99], p<0.001) after adjustment for age, sex, peak aortic-jet velocity and aortic valve area. Among the 210 (23%) patients with discordant echocardiographic assessments, CT-AVC defined 103 (49%) with severe calcification in whom CT-AVC conferred an adverse prognosis.

Conclusions

Sex-specific CT-AVC thresholds for severe aortic stenosis are consistent across different patient populations and provide powerful independent prognostic information. CT-AVC thresholds should be used to guide clinical management especially in those with uncertain disease severity.

5.1 INTRODUCTION

Aortic stenosis is a common and potentially fatal condition in which progressive fibro-calcific changes within the valve leaflets cause outflow tract obstruction. Severe symptomatic stenosis is an indication for aortic valve replacement (AVR) and timely referral is essential to prevent adverse clinical events (2). Stenosis severity is determined using echocardiography and commonly graded using the peak velocity (Vmax), mean gradient (MG) and aortic valve area (AVA) (175). The latter is less flow dependent and can be indexed to body surface area (AVAi) (152). In the majority of patients, these measurements provide concordant assessments and the severity of aortic stenosis is clear. However as previously discussed, in around a quarter of cases, these measures are discordant, creating confusion as to the true severity of aortic stenosis and difficulties in clinical decision-making (121, 164). An independent complementary test that could be used to arbitrate the true severity of aortic stenosis would therefore have major clinical utility and potentially improve patient care (176).

In the previous chapter we confirmed the presence of importance sex differences with respect to the association between computed tomographic aortic valve calcification (CT-AVC) measurements and hemodynamic measures of stenosis severity on echocardiography (177-179). We also confirmed that the recently proposed sex-specific CT-AVC thresholds (women 1274 AU and men 2065 AU) predict adverse clinical events (121, 168). There is currently great interest in using these thresholds as an alternative assessment of aortic stenosis severity and as an "umpire test" in patients with discordant echocardiographic findings (180). However

before thresholds can enter routine clinical use, their widespread clinical applicability needs to be established.

The aim of this study was to investigate the clinical utility and generalizability of sex-specific CT-AVC thresholds in an international multicenter registry incorporating a wide range of patient populations, different scanner vendors, and varied image analysis platforms. Specifically we sought to determine the ability of the thresholds to identify severe aortic stenosis in those with concordant echocardiographic measures, to establish the ability of this technique to predict clinical outcomes, and to arbitrate disease severity in patients with discordant echocardiographic findings.

5.2 METHODS

Eight international centers were invited to contribute clinical, CT and echocardiography data from patients with aortic stenosis into a multicenter registry (Table 5.1). Patients were required to have at least mild aortic stenosis (peak velocity [Vmax] >2.5 m/s or mean gradient [MG] >10 mmHg) and to have undergone electrocardiogram-gated CT calcium scoring within 3 months of the echocardiogram. Patients with other forms of valvular heart disease of at least moderate severity or an estimated glomerular filtration rate <30 mL/min/1.73 m^2 were excluded.

Three centers contributed data from five prospective aortic stenosis clinical research studies: Edinburgh Heart Centre, Edinburgh, UK (NCT01358513 NCT02132026), Hôpital Bichat, Paris, France (NCT00338676 and NCT00647088), and Institut Universitaire de Cardiologie et de Pneumologie, Québec City, Québec, Canada, (NCT01679431). Two centers (Paris and Quebec) had previously published CT-AVC thresholds (121) but here provided separate distinct populations of patients that did not overlap with their original cohort. The remaining 5 centers contributed data from patients in Europe and North America who had undergone these investigations for clinical indications (Table 5.1). The University of Edinburgh co-ordinated the study and its design was approved by the South East Scotland Research Ethics Committee and the Health Research Authority of the United Kingdom. Informed consent was obtained for those patients who had taken part in research studies. In patients who had undergone scans for clinical indications, patients were de-identified and anonymised.

Table 5.1 Centre List

CENTRE	COHORT	CT SCANNER	IMAGE ANALYSIS SOFTWARE
Centre for Cardiovascular Science, University of Edinburgh, United Kingdom	Research: Ring of Fire	Biograph mCT Siemens	Vitrea Advanced, Vital Images,
Hôpital Bichat Paris, France	Research COFRASA GENERAC	Philips scanner (MX 8000 IDT 16, Phillips Medical Systems, Andover, MA, USA) General Electric scanner (Light speed VCTTM, General Electric Company, Fairfield, Connecticut, USA	Philips Medical Systems Aquarius iNtuition
Institut Universitaire de Cardiologie et de Pneumologie Québec City, Québec. Canada	Research	SOMATOM, Siemens Medical Systems, Fordheim, Germany;	TeraRecon
Guy's and St Thomas' NHS Foundation Trust London, United Kingdom	Clinical	Philips Brilliance ICT scanner Siemens Force Dual Source Scanner	Aquarius iNtuition Edition Ver.4.4.11 TeraRecon
Hospital Vall d'Hebron, Barcelona, Spain	Clinical	Siemens Definition AS+ (64*2 detectors)	Syngovia (Siemens clinical station).
Centre Hospitalier Universitaire Amiens- Picardie, France	Clinical	General Electric CT 750 HD Discovery CT750 HD (GE Healthcare). - Optima CT660 (GE Healthcare). - LightSpeed VCT XT (GE Healthcare)	Smartscore 4.0 (GE Healthcare) , work station = Advantage Workstation 4.6 (GE Healthcare).
Vascular Medical Institute, University of Pittsburgh, United States of America	Clinical	GE Discovery 750HD	Vital Images, Vitrea software
Centre, Cardiologique due Nord Saint Denis, France	Clinical	General Electric Revolution	SMARTCORE version 4.0

5.2.1 Computed Tomography Aortic Valve Calcium Scoring

All centres performed non-contrast CT scans gated from 75% to 80% of the R-R interval, with a tube current of 42 to 1312 A and a voltage of 120 kV. Imaging was performed on a range of different scanners (Table 5.1). At the discretion of the attending clinician, some centres administered beta-blockade to achieve a resting heart rate of ≤65 beats per minute (Amiens, France and Edinburgh, United Kingdom).

Image analysis was performed locally using a range of different software packages. At the initiation of the study, consensus was reached regarding the optimum method for calcium scoring and this was then applied at each of the centers, ensuring consistency of approach. In brief, CT-AVC scores were quantified on contiguous 3-mm axial slices as described in Chapter 2, commencing at the base of the valve, with care taken to exclude calcium originating from extra-valvular structures such as the mitral valve annulus, the ascending aorta and coronary arteries. The total AVC in Agatston Units (AU) was calculated and subsequently indexed to the body surface area (AVCi (AU/m^2)) or divided by the left ventricular outflow tract area to estimate calcium density (AVCd (AU/cm^2)). In order to stratify for gender the CT-AVC scores were then divided by the derived sex-specific thresholds to generate a ratio whereby a ratio ≥1 was consistent with severe calcification on CT.

5.2.2 Echocardiography

Echocardiography was performed according to the European Association of Cardiovascular Imaging and American Society of Echocardiography guidelines as described in Chapter 2 (152). Echocardiographic data were defined as concordant when findings from both the Vmax and AVA provided the same assessment of disease severity (severe AS: AVA <1.0 cm^2 Vmax ≥4.0 m/s; non-severe AS: AVA ≥1.0 cm^2 Vmax <4.0 m/s). Patients in whom the Vmax and AVA gave discordant assessments of aortic stenosis severity were sub-categorized as having normal-flow or low-flow. Discordant low-flow patients were further subdivided into those with a low (<50%, classical low-flow severe aortic stenosis) or preserved (≥50%, paradoxical low-flow severe aortic stenosis) ejection fraction (152). Discordant normal-flow patients were further subdivided into those with Vmax ≥4.0 m/s (and AVA ≥1.0 cm^2) versus patients with Vmax <4.0 m/s (and AVA <1.0 cm^2) (175). The sex-specific CT-AVC thresholds were then applied to these discordant patients in order to arbitrate whether they had severe or non-severe disease (Figure 5.1).

Figure 5.1. Echocardiographic classification of aortic stenosis

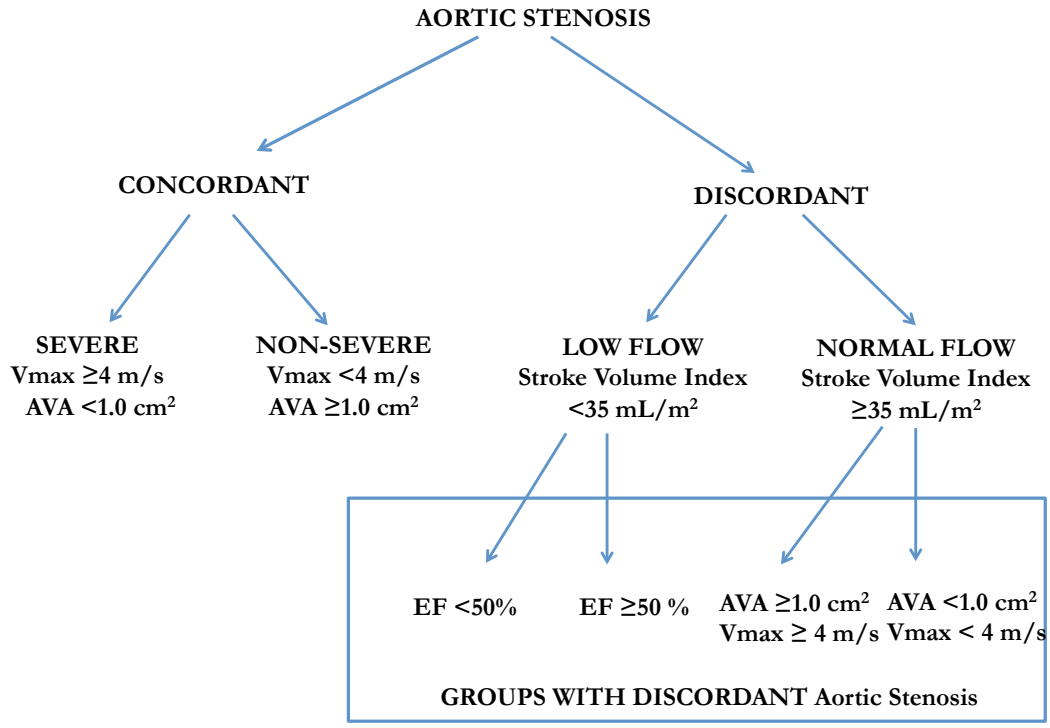

Abbreviations: Vmax, peak aortic jet velocity; AVA, aortic valve area; EF, ejection fraction.

5.2.3 Prediction of Outcomes

The primary outcome was the time to first event of death or aortic valve replacement. Aortic valve replacement included both open surgical procedures and transcatheter aortic valve implantation (TAVI). Patients in whom a decision to refer for aortic valve replacement had already been made at the time of CT calcium scoring or who had CT imaging performed as part of the work up prior to TAVI or surgery were excluded from this analysis.

5.2.4 Statistical Analysis

Statistical analyses were performed as outlined in Chapter 2. Additionally, in patients with concordant echocardiographic data, receiver operator curves were derived to assess CT-AVC thresholds and to identify the optimum thresholds for severe aortic stenosis. Kaplan-Meier curves and cox proportional hazards regression analyses were used to determine the ability of CT-AVC measurements to predict adverse clinical events. Two-sided significance was taken as $p<0.05$.

5.3 RESULTS

Data were collated from 918 patients across 8 international centers (age 77±10 years, 60% male, Vmax 3.88±0.90 m/s; Table 5.2) with 431 patients undergoing imaging within prospective clinical research studies and 487 patients being imaged as part of routine clinical care. The latter group included 366 patients being considered for TAVI.

CT-AVC measurements correlated with the different echocardiographic measures of aortic stenosis severity (Table 5.3). When subdivided by sex, women had lower CT-AVC scores to achieve the same degree of hemodynamic obstruction than men even after indexing for body surface area (AVCi) or the left ventricular outflow tract area (AVCd).

Table 5.2. Patient Characteristics

			CONCORDANT		DISCORDANT LOW FLOW		DISCORDANT NORMAL FLOW	
		ALL	SEVERE	NON-SEVERE	EF<50 %	EF≥50 %	Vmax≥ 4 m/s AVA≥1 cm^2	Vmax<4 m/s AVA<1 cm^2
CLINICAL		918	436	272	7	68	35	96
Age	years ± SD	77±10	80±9	72±10	81±7	77±11	74±11	79±8
Males	%	60	51	78	57	57	80	52
Height	cm ± SD	165±12.0	164±13	169±8	163±7	167±9	171±8	163±9
Weight	cm ± SD	78±17	75±17	82±17	69±12	84±17	84±17	72±16
Body Surface Area	m^2 ± SD	1.88±0.25	1.83±.24	1.94±0.25	1.76±0.19	1.96±0.23	1.99±.0.23	1.79±0.23
Body Mass Index	kg/m^2± SD	28±6	28±6	29±5	26±4	30±5	29±5	27±5
Systolic Blood Pressure	mmHg ± SD	136±20	134±19	139±21	124±28	139±19	137±18	137±20
Diastolic Blood Pressure	mmHg ± SD	72±12	71±12	74±13	76±19	75±10	71±10	71±11
Possible Symptoms	%	70	91	47	100	75	69	58
Hypertension	%	77	77	82	57	81	83	75
Coronary Artery Disease	%	45	49	37	43	50	34	44
Ever smoked	%	32	24	42	29	50	34	39
Diabetes	%	28	30	24	0	28	20	26
Hyperlipidaemia	%	65	64	59	43	68	54	68
Scan Interval	Days [IQR]	5 [1-25]	7 [1-25]	1 [0-10]	8 [2-31]	7 [2-26]	4 [1-27]	3 [0-23]

Table 5.2 continued. Patient Characteristics

			CONCORDANT		DISCORDANT LOW FLOW		DISCORDANT NORMAL FLOW	
		ALL	SEVERE	NON-SEVERE	EF<50 %	EF≥50 %	Vmax≥ 4 m/s AVA≥1 cm^2	Vmax<4 m/s AVA<1 cm^2
ECHOCARDIOGRAPHY		918	436	272	7	68	35	96
Peak velocity	mmHg ± SD	3.88±0.90	4.61±0.50	2.9±0.50	3.21±0.44	3.47±0.36	4.30±0.33	3.51±0.33
Percentage ≥4 m/s	%	51	100	0	0	0	100	0
Mean Gradient	m/s ± SD	38±19	54±14	19±7	26±8	30±7	44±8	30±7
Percentage ≥40 mmHg	%	48	91	5.3	0	12	69	8
Aortic Valve Area	cm^2 ± SD	0.90±0.35	0.66±0.15	1.33±0.28	0.66±0.21	0.72±0.15	1.16±0.17	0.83±0.11
Percentage ≤ 1.0 cm^2	%	67	100	0	100	100	0	100
Aortic Valve Area Index	cm^2/m^2 ± SD	0.48±0.18	0.36±0.08	0.69±0.15	0.37±0.11	0.37±0.08	0.59±0.13	0.47±0.07
Percentage ≤ 0.6 cm^2	%	77	99	0	100	100	66	100
Bicuspid	%	7	4	12	0	3	23	4
Ejection Fraction	% ± SD	61±8.5	61±8	60±9	31±5	58±8	61±10	61±8
COMPUTED TOMOGRAPHY								
Aortic Valve Calcium Score	AU [IQR]	2055 [1054-3339]	2951 [2081-4144]	895 [528-1577]	2237 [1406-2975]	1900 [1127-2772]	2917 [1912-3752]	1310 [763-2068]
Aortic Valve Calcium Index	AU/m^2 [IQR]	1088 [557-1810]	1612 [1133-2330]	468 [276-810]	1210 [773-2263]	989 [584-1406]	1387 [900-1852]	764 [481-1140]
Aortic Valve Calcium Density	AU/cm^2 [IQR]	580 [284-940]	860 [599-1220]	232 [133-282]	588 [448-1729]	588 [397-806]	690 [473-903]	412 [236-630]

Table 5.3. Correlations between Echocardiography measurements and Computed Tomography Aortic Valve Calcium Scores

		Vmax (m/s)	Mean Gradient (mmHg)	AVA (cm^2)	AVAi ($cm^2/m^{2)}$
ALL PATIENTS					
AVC	*Correlation*	0.66	0.64	-0.49	-0.54
	Sig.	p<0.001	p<0.001	p<0.001	p<0.001
	N	918	918	918	915
AVCi	*Correlation*	0.68	0.67	-0.54	-0.54
	Sig.	p<0.001	p<0.001	p<0.001	p<0.001
	N	915	915	915	915
AVCd	*Correlation*	**0.69**	0.66	-0.59	-0.62
	Sig.	p<0.001	p<0.001	p<0.001	p<0.001
	N	916	916	916	913
MEN					
AVC	*Correlation*	0.70	0.67	-0.54	-0.56
	Sig.	p<0.001	p<0.001	p<0.001	p<0.001
	N	548	548	548	547
AVCi	*Correlation*	0.71	0.69	-0.57	-0.55
	Sig.	p<0.001	p<0.001	p<0.001	p<0.001
	N	547	547	547	547
AVCd	*Correlation*	**0.72**	0.69	-0.62	-0.63
	Sig.	p<0.001	p<0.001	p<0.001	p<0.001
	N	547	547	545	547
WOMEN					
AVC	*Correlation*	0.66	0.67	-0.56	-0.58
	Sig.	p<0.001	p<0.001	p<0.001	p<0.001
	N	370	370	370	368
AVCi	*Correlation*	0.67	**0.67**	-0.58	-0.56
	Sig.	<0.001	<0.001	<0.001	<0.001
	N	368	368	368	368
AVCd	*Correlation*	0.65	0.65	-0.63	-0.63
	Sig. (2-	<0.001	<0.001	<0.001	<0.001
	N	369	369	369	367

Abbreviations: Vmax, peak velocity; AVA, aortic valve area; AVAi, indexed aortic valve area; AVC, aortic valve calcium score; AVCi, indexed aortic valve calcium score; AVCd, aortic valve calcium density; sig, significance.

5.4 Patients with Concordant Echocardiography

5.4.1 Performance of CT-AVC Thresholds

Overall 708 (77%) patients had concordant echocardiographic assessments of their disease severity (defined using the Vmax and AVA). Patients with concordant-severe disease (n=436) had AVC scores that were more than double patients with concordant non-severe disease (n=272) ($p<0.0001$). In these concordant patients, we determined that the optimum CT-AVC thresholds for severe aortic stenosis were 1377 AU for women and 2062 AU for men (Figure 5.2). These thresholds had a sensitivity of 87% and specificity 84% in women and a sensitivity of 80% and a specificity of 85% in men with a c-statistic of 0.92 and 0.88 respectively (Table 5.4). This provided a high degree of discrimination for identifying severe aortic stenosis (Figure 5.3). The CT-AVC thresholds performed similarly well when echocardiographic disease severity was defined using MG and AVAi (c-statistic: 0.93 women, 0.92 men; Table 5.5, (121)

Figure 5.2. Receiver operator curves

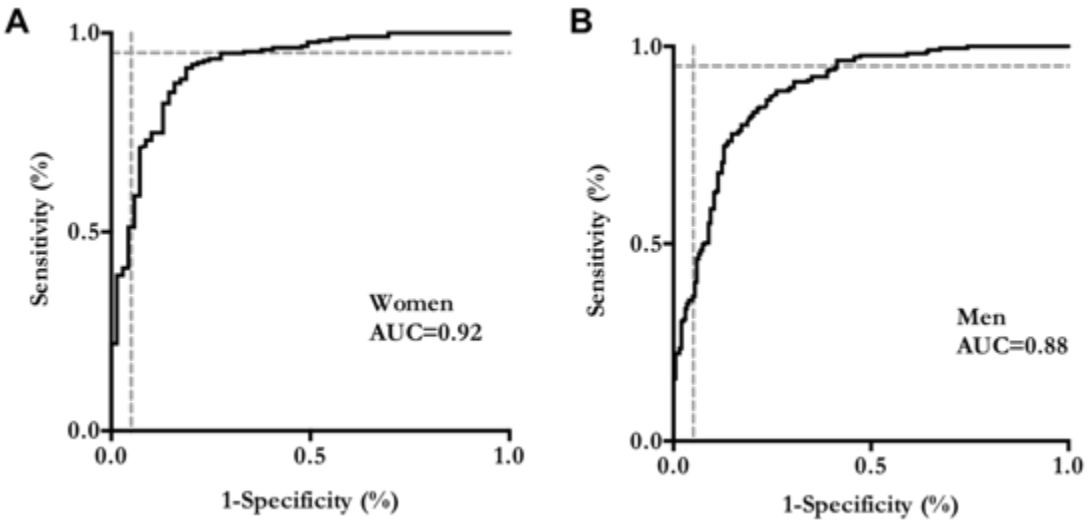

Receiver operator curves for women (left) and men (right) assessing the accuracy of computed tomography aortic valve calcification (CT-AVC) scoring against echocardiography in patients with concordant echocardiographic measures (n=708). The dashed lines represent 95% sensitivity (horizontal) and 95% specificity (vertical).

Abbreviations: AUC, area under the curve.

Table 5.4. Computed tomography aortic valve calcium scoring thresholds for severe aortic stenosis in patients with concordant echocardiographic measures.

The **peak velocity** and **aortic valve area** were used to adjudicate stenosis severity.

		THRESHOLD	SENSITIVITY (%)	SPECIFICITY (%)
AORTIC VALVE CALCIUM (AU)				
WOMEN				
AUC=0.92	Clavel et al	1274	88	81
	Optimum	1377	87	84
	Most Specific	2646	51	96
	Most Sensitive	774	95	62
MEN				
AUC=0.88	Clavel et al	2065	80	82
	Optimum	2062	80	85
	Most Specific	3905	36	95
	Most Sensitive	1196	95	58
AORTIC VALVE CALCIUM INDEX (AU/m^2)				
WOMEN				
AUC=0.92	Clavel et al	637	92	77
	Optimum	784	88	83
	Most Specific	1512	49	95
	Most Sensitive	500	95	68
MEN				
AUC =0.90	Clavel et al	1067	81	85
	Optimum	1058	82	85
	Most Specific	1814	45	95
	Most Sensitive	659	95	69
AORTIC VALVE CALCIUM DENSITY (AU/cm^2)				
WOMEN				
AUC =0.93	Clavel et al	292	96	75
	Optimum	420	88	88
	Most Specific	706	61	96
	Most Sensitive	307	95	77
MEN				
AUC =0.91	Clavel et al	476	88	81
	Optimum	527	83	84
	Most Specific	909	52	95
	Most Sensitive	376	95	73

Abbreviations: AUC, area under curve.

Clavel et al refers to thresholds proposed in reference (121)

Table 5.5. Computed tomography aortic valve calcium scoring (CT-AVC) thresholds for severe aortic stenosis in patients with concordant echocardiographic measures.

The **mean gradient** and **indexed aortic valve area** were used to adjudicate stenosis severity.

		THRESHOLD	SENSITIVITY (%)	SPECIFICITY (%)
AORTIC VALVE CALCIUM (AU)				
WOMEN				
AUC=0.92	Clavel et al	1274	89	81
	Optimum	1377	86	83
MEN				
AUC=0.88	Clavel et al	2065	81	87
	Optimum	2062	81	87
AORTIC VALVE CALCIUM INDEX (AU/m^2)				
WOMEN				
AUC=0.92	Clavel et al	637	93	76
	Optimum	784	89	80
MEN				
AUC =0.90	Clavel et al	1067	82	88
	Optimum	1058	83	88
AORTIC VALVE CALCIUM DENSITY (AU/cm^2)				
WOMEN				
AUC =0.93	Clavel et al	292	96	77
	Optimum	420	90	88
MEN				
AUC =0.91	Clavel et al	476	90	88
	Optimum	527	85	89

Abbreviations: AUC, area under curve.

Clavel et al refers to thresholds proposed in reference (121)

Figure 5.3 Computed tomography aortic valve calcium (CT-AVC) scores in patients with concordant echocardiographic measurements

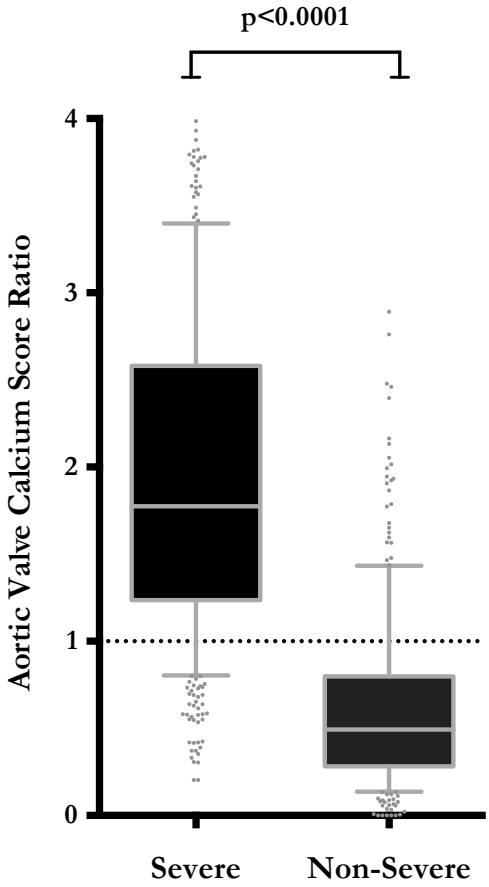

In order to stratify for sex, CT-AVC scores were divided by the respective sex-specific thresholds for severe aortic stenosis (1277 AU in women and 2062 AU in men) to generate AVC ratios. A score above the dotted line represents CT-AVC above the sex-specific threshold and therefore severe aortic valve calcification. A CT-AVC score below the dotted line represents CT-AVC below the sex-specific threshold and non-severe calcification. Patients with concordant-severe aortic stenosis, as defined by echocardiography, had CT-AVC ratios that were more than double those with concordant non-severe disease. Box and Whiskers plot, error bars are from the 10th to 90th centile and the horizontal line represents the median value.

5.4.2 Disagreement between CT calcium scoring and echocardiography

Patients with concordant-severe disease (n=436) had CT-AVC scores that were more than double patients with concordant non-severe disease (n=272) ($p<0.0001$, Figure 5.3). However, overlap between these two groups was observed. Indeed, of the 436 patients with concordant-severe disease on echocardiography, 69 (16%) had a calcium score consistent with non-severe disease on CT. Although a borderline score (defined as AVC ratio ≥ 0.80) was found in 29, 40 patients had clear disagreement between the echocardiographic and CT assessments. These patients appeared to be more likely to have a history of concomitant coronary artery disease, diabetes mellitus and hypertension (Table 5.6). Similarly amongst the patients with concordant non-severe disease on echocardiography (n=272), 47 had severe calcification on CT, 11 of whom had borderline scores (defined as a ratio <1.2). Clear disagreement therefore persisted in 36 of these subjects who had a similar demographic profile to the cohort as a whole.

Table 5.6 Patient characteristics of outliers

		All Patients	Severe AVC Ratio <0.8	Non-Severe AVC Ratio≥1.2
CLINICAL		918	40	36
Age	years ± SD	77±10	78±8	75±9
Males	%	60	65	73
Height	cm ± SD	165±12.0	161±8	171±9
Weight	cm ± SD	78±17	72±15	89±21
Body Surface Area	m^2 ± SD	1.88±0.25	1.78±0.21	2.03±0.29
Body Mass Index	kg/m^2± SD	28±6	28±6	30±6
Systolic Blood Pressure	mmHg ± SD	136±20	135±20	136±14
Diastolic Blood Pressure	mmHg ± SD	72±12	69±14	78±10
Heart Rate	bpm ± SD	69±13	71±12	66±10
Possible Symptoms	%	70	88	42
Hypertension	%	77	73	78
Coronary Artery Disease	%	45	68	36
Ever smoked	%	32	18	53
Diabetes	%	28	43	19
Hyperlipidaemia	%	65	70	53
Scan Interval	Days [IQR]	5 [1-25]	13 [1-26]	2 [0-13]
ECHOCARDIOGRAPHY				
Peak aortic jet velocity	mmHg ± SD	3.88±0.9	4.41±0.48	3.46±0.32
Percentage ≥4m/s	%	51	100	0
Mean Gradient	m/s ± SD	38±19	48±11	28±7
Percentage ≥40	%	48	83	3
Aortic Valve Area	cm^2 ± SD	0.90±0.35	0.71±0.15	1.23±.18
Percentage ≤ 1.0	%	67	100	0
Aortic Valve Area Index	cm^2/m^2 ± SD	0.48±0.18	0.40±0.15	0.60±.10
Percentage ≤ 0.6	%	77	100	0
Bicuspid	%	7	8	11
COMPUTED TOMOGRAPHY				
Aortic Valve Calcium Score	AU [IQR]	2055 [1054-3339]	1024 [735-1340]	3230 [2642-3985]

5.4.3 Prediction of Adverse Outcomes

Clinical outcome data were available in 237 (26%) patients after a median of 1029 [100-2,251] days. In total 100 patients were adjudicated to have reached the primary clinical end-point: with 73 having undergone AVR and 27 patients having died. On univariate analysis when examined as a continuous variable, the CT-AVC measurements ($\sqrt{}$AU) predicted adverse events (HR per square root increase, 1.02 [95% confidence intervals, 1.01-1.04]; p<0.001). Moreover CT-AVC remained the only significant independent predictor of clinical events after adjustment for age, sex, Vmax and AVA (HR per square root increase, 1.03 [95% confidence intervals, 1.00-1.04]; p=0.004).

Similar results were obtained when the sex-specific thresholds were applied and CT-AVC was considered as a categorical variable (severe versus non-severe). On univariate analysis, severe CT-AVC was associated with a 3-fold increase in the likelihood of AVR and death (hazards ratio, 2.73 [95% confidence intervals, 1.79–4.16]; p<0.001). In addition, severe CT-AVC was the only independent predictor of AVR and death on multivariable analysis after adjustment for age, sex, Vmax ≥4 m/s and AVA <1 cm^2 (hazards ratio, 3.02 [95% confidence intervals, 1.83–4.99]; p<0.001; Figure 5.4).

Figure 5.4. Survival analyses

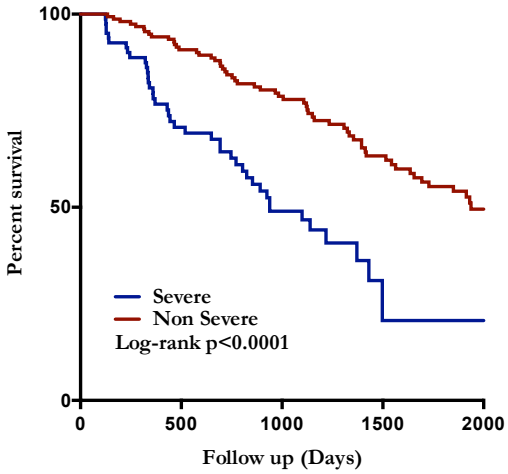

Kaplan-Meier Curves demonstrating event free survival using the sex-specific thresholds for severe CT-AVC. Severe calcification was associated with an adverse prognosis (log-rank p<0.001) compared to patients with non-severe calcification.

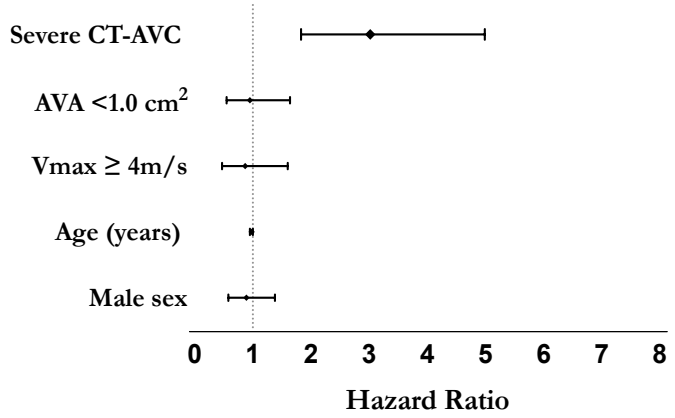

	HR	95% CI	Sig
Severe CT-AVC	3.02	1.83 – 4.99	<0.001
AVA <1.0 cm^2	0.95	0.55 – 1.64	0.843
Vmax ≥ 4m/s	0.87	0.47 – 1.60	0.653
Age (years)	0.98	0.95 – 1.00	0.065
Male sex	0.89	0.58 – 1.38	0.61

Forrest plot for multivariate analysis. Sex-specific CT-AVC thresholds emerged as the only independent predictor of aortic valve replacement (AVR) and death. Patients with a severe CT-AVC had a more than 3-fold increase in these events.

Abbreviations: Severe CT-AVC, computed tomography aortic valve calcium score equal to or above the threshold for severe; AVA, aortic valve area; Vmax, peak aortic jet velocity; HR, hazard ratio; CI, confidence intervals; Sig, significance.

5.5. Patients with Discordant Echocardiography

A total of 210 (23%) patients in this study had discordant echocardiographic assessments of disease severity: 79 with low-flow and 131 with normal-flow. Considerable heterogeneity in CT-AVC scores was observed in these patients with 103 (49%) having severe calcification and 107 (51%) having non-severe calcification. This heterogeneity persisted to differing extents in each of the subgroups examined (Figure 5.5). Within the low-flow category, 4 patients did not have an ejection fraction available. Severe calcification was present in 36 patients (52%) with paradoxical low-flow and 5 (71%) with classical low-flow aortic stenosis. Amongst discordant normal-flow patients, severe calcification was observed in 26 (74%) subjects with a high Vmax >4.0 m/s (AVA >1.0 cm^2) and 33 (34%) patients with a low Vmax <4.0 m/s (AVA <1.0 cm^2).

Within the discordant subgroup, outcomes were available in 44 patients in whom 21 patients were adjudicated to have reached the primary endpoint. On univariate analysis, severe CT-AVC was again associated with a 3-fold increase in the likelihood of AVR and death (hazards ratio, 3.12 [95% confidence intervals, 1.31–7.42]; p<0.010). On multivariate analysis, severe CT-AVC was once more an independent predictor of adverse outcomes (hazards ratio, 2.96 [95% confidence intervals, 1.12–7.80]; p=0.028) as a continuous variable after adjustment for age, sex, Vmax and AVA.

Figure 5.5. Computed tomography aortic valve calcium scores (CT-AVC) in discordant patients.

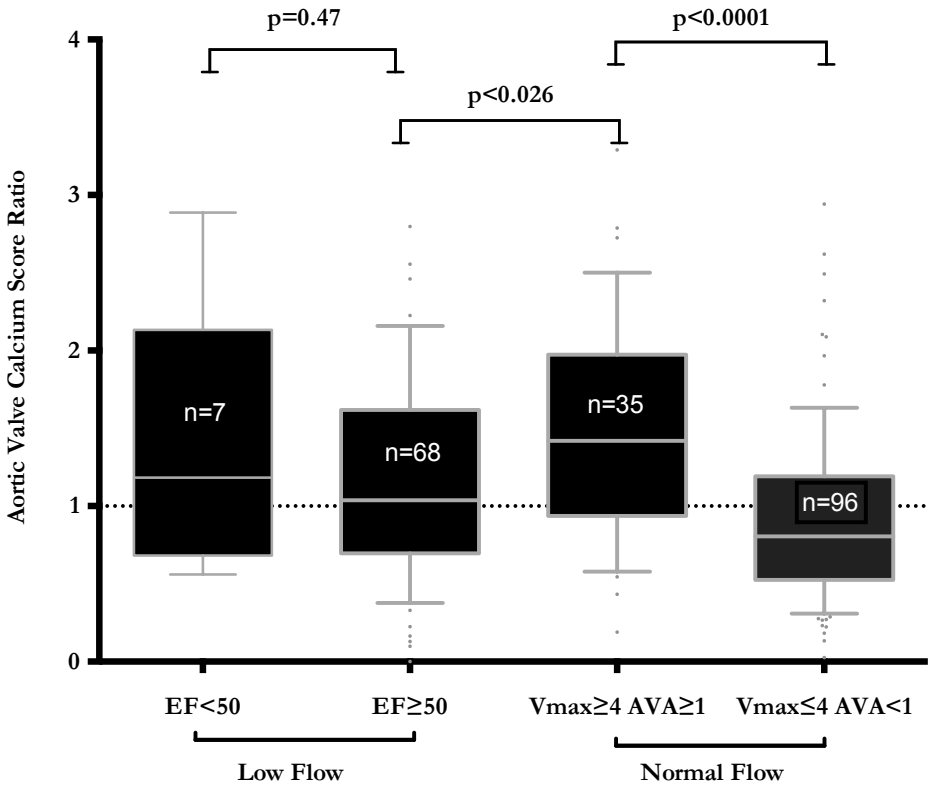

In order to stratify for sex, CT-AVC scores were divided by the respective sex-specific thresholds for severe aortic stenosis (1277 AU in women and 2062 AU in men). A score above the dotted line represents CT-AVC above the sex-specific threshold and therefore severe aortic valve calcification. A CT-AVC score below the dotted line represents CT-AVC below the sex-specific threshold and non-severe calcification. Considerable heterogeneity in disease severity as assessed by CT-AVC was observed in all 4 sub-groups of patients with discordant echocardiographic findings. Box and Whiskers plot, error bars are from the 10th to 90th centile and the horizontal line represents the median value.

Abbreviations. EF, ejection fraction; Vmax, peak aortic jet velocity; AVA, aortic valve area.

5.6 Performance of Previously Published CT-AVC thresholds

We repeated our analyses using the previously published CT-AVC thresholds, (women, 1274 AU and men, 2065 AU) which were nearly identical to the present thresholds (121). In women, the threshold of 1274 AU had a sensitivity of 88% and specificity 81%. Similarly, in men the threshold of 2065 AU had a sensitivity of 80% and a specificity of 82% (Table 5.4).

These thresholds conferred very similar risk-prediction. On univariate analysis, severe calcification predicted AVR and death (hazards ratio, 2.69 [95% confidence intervals, 1.77– 4.11]; p<0.001) and was the only independent predictor of AVR and death on multivariable analysis after adjustment for age, sex, peak velocity ≥4 m/s and AVA <1 cm^2 (hazards ratio, 2.97 [95% confidence intervals, 1.80–4.90]; p<0.001).

When applied to the discordant population, the published thresholds reclassified 4 patients so that numbers with severe calcification within each subgroup were as follows; 37 patients (54%) with paradoxical low-flow; 5 (71%) with classical low-flow aortic stenosis; 27 (77%) with a high Vmax >4.0 m/s (AVA >1.0 cm^2) and 35 (36%) patients with a low Vmax <4.0 m/s (AVA <1.0 cm^2). For those with available clinical outcomes, severe calcification was again associated with a 2-3-fold increase in the likelihood of AVR and death on univariate analysis (hazards ratio, 2.90 [95% confidence intervals, 1.21–6.91]; p=0.016) and multivariate analysis (hazards ratio, 2.70 [95% confidence intervals, 1.02-7.16]; p=0.046) after adjustment for Vmax ≥4 m/s, age and sex.

5.7 DISCUSSION

In a multicenter international registry, we present the largest study to date, simultaneously investigating both CT-AVC and echocardiography in patients with aortic stenosis. We have demonstrated that sex-specific thresholds for CT-AVC are highly reproducible across different patient populations and demonstrate excellent discrimination for detecting severe aortic stenosis. Moreover we have reaffirmed that CT-AVC thresholds are a powerful predictor of adverse clinical events independent of standard echocardiographic indices. On this basis, we believe that CT-AVC should be used as a complementary imaging test alongside echocardiography, particularly in the high proportion of aortic stenosis patients with discordant echocardiographic measurements and uncertain disease severity.

The identification of severe aortic stenosis is essential, because in those patients with symptoms, this diagnosis often triggers major cardiac surgery and aortic valve replacement. CT-AVC holds promise as an alternative assessment of disease severity to complement echocardiography with the advantage that it is independent of loading conditions and hemodynamic influences. CT-AVC thresholds for severe aortic stenosis have recently been proposed from a derivation cohort comprising 451 patients (3), demonstrating good agreement with echocardiography and the prediction of clinical events in the same population (168, 181). However these thresholds had not previously been validated in an independent multicentre cohort and it was unclear if they were reproducible or generalizable in different patient populations or influenced by variations in imaging technology and analysis software. The primary objective of this study was to validate CT-AVC in aortic stenosis in an

independent international multi-center cohort and to investigate its widespread clinical applicability. We included patients from a variety of clinical settings, across five countries, imaged on an array of different scanners and analysed locally using a spectrum of different analysis software. Moreover we tested CT-AVC against all four of the recommended echocardiographic measurements of disease severity in widespread clinical practice.

Despite the heterogeneity present in our patient population, our thresholds (women 1377 men 2062 AU) for severe disease were nearly identical to those originally proposed (women 1274 AU and men 2065 AU) and performed similarly well. Our data therefore confirm both the reproducibility of these CT-AVC thresholds for severe disease and their clinical utility as an alternative assessment of disease severity. Whilst sex-specific thresholds for AVCi and AVCd also performed well compared to echocardiography, they appeared to offer little additional benefit especially given the added complexity of their derivation.

Of primary importance is the ability of CT-AVC to predict clinical outcomes. Indeed assessing how quickly patients with aortic stenosis are likely to proceed to AVR and whether they are at risk of death are two major objectives in clinical practice. Echocardiographic estimation of valvular calcification has been overlooked as a measure of disease severity, despite conferring more powerful risk-prediction than all other variables currently in routine use (15). CT-AVC facilitates accurate, reproducible calcium quantification (116) and in a large subgroup of our population in whom prospective outcome data were available, we have confirmed the powerful

prognostic information that CT-AVC provides independent of standard echocardiographic and clinical variables. Indeed CT-AVC was associated with a three-fold increase in AVR or death, and emerged as the sole predictor of these events on multivariable analysis. This is despite the fact that decisions to refer for AVR would have been based largely on echocardiographic assessments not CT-AVC scores, the results of which were unavailable to clinicians.

How then might CT-AVC be used in clinical practice? Consistent with previous studies, almost a quarter of our patients (n=210, 23%) had discordant echocardiographic measurements. In these patients, the severity of stenosis remained in question and we explored whether CT-AVC might act as an arbitrator or umpire test. Our results suggest that there is substantial heterogeneity in disease severity in these discordant patients that persisted within each of the different sub-groups examined. Given the lack of a gold-standard assessment of disease severity in discordant patients, it is important to note that CT-AVC provided similarly powerful prognostic information in these subjects as it did across the wider aortic stenosis population (hazard ratio of ~3 for AVR or death). CT AVC would therefore appear to hold particular value as both an arbitrator of disease severity and as a prognostic marker in this challenging and common cohort of patients. We believe that where diagnostic and prognostic uncertainty exists, CT-AVC appears to be a much more robust and powerful guide to patient management than the currently proposed arbiter of dobutamine stress echocardiography (15). The simplicity, generalizability and reproducibility of CT-AVC also lends itself to rapid application in the clinic and is

not reliant on advanced echocardiographic techniques that are more dependent on operator technique and expertise.

Figure 5.6 Clinical application of computed tomography aortic valve calcium scoring

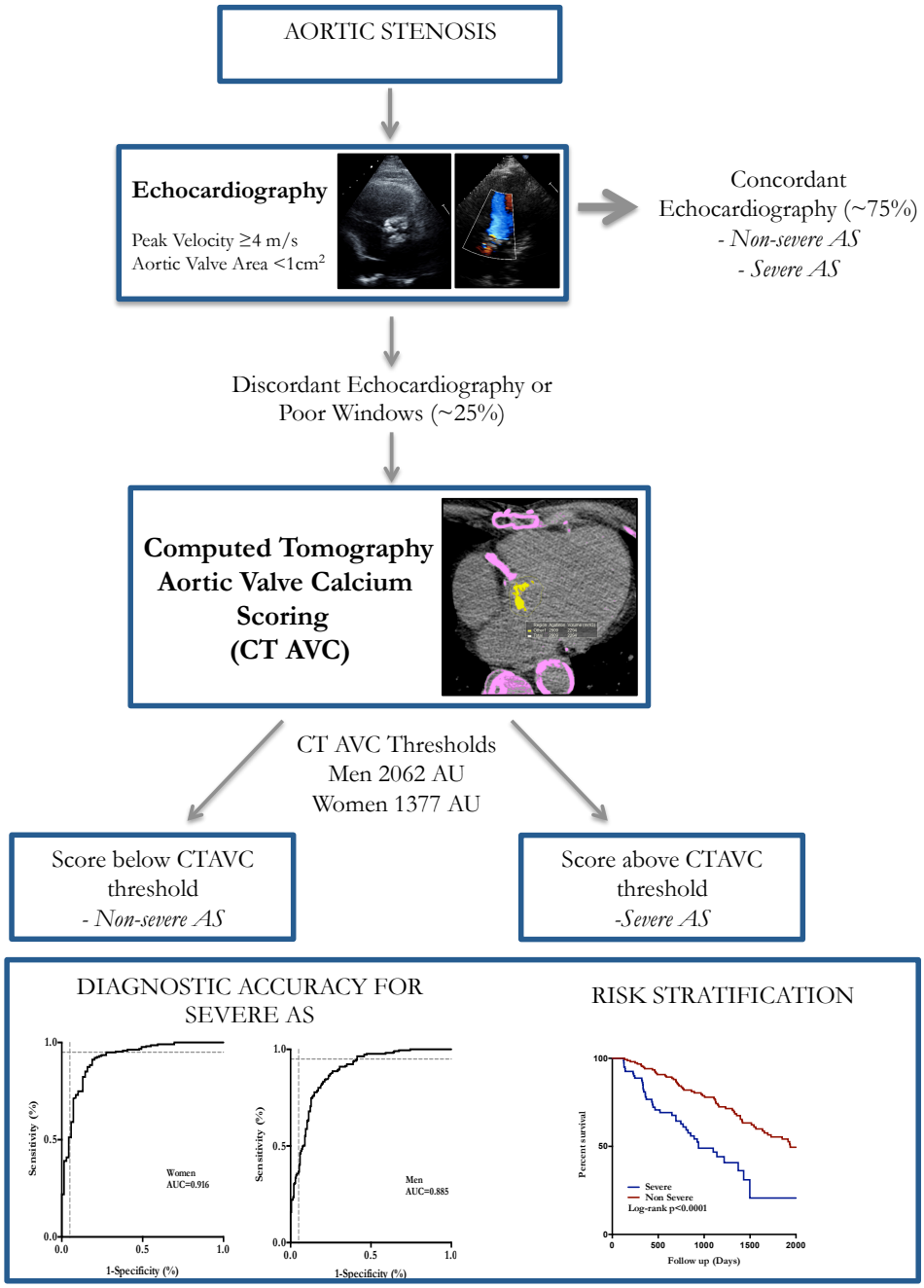

Patients with aortic stenosis (AS) should initially be assessed with echocardiography. In a quarter of patients there is discordance in echocardiographic assessments of disease severity, causing diagnostic uncertainty. CT-AVC provides an alternative and complementary assessment of disease severity. Sex-specific thresholds (men 2062 AU, women 1377 AU) are highly reproducible across different patient populations and provide excellent discrimination for severe AS versus echocardiography (c-statistic: women 0.92, men 0.88). CT-AVC also provides powerful prognostic information and risk stratification. Patients with severe calcification have a 3-fold increase in AVR and death compared to those with non-severe calcification (hazards ratio, 3.02 [95% confidence intervals, 1.83–4.99]; p<0.001 after adjustment for age, sex, peak aortic-jet velocity and aortic valve area).

5.7.1 Limitations of CT-AVC scoring in aortic stenosis

In patients with concordant measures, echocardiography is the gold-standard technique for defining disease severity. We therefore first examined the diagnostic accuracy of the AVC thresholds in those patients with concordant measures only. The thresholds mostly agreed with echocardiography, however in approximately 10% of cases there was clear disagreement. These apparent mismatches could be accounted for by a number of factors relating to both the disease process and the scanning techniques.

Individual variations in pathobiology may affect the relationship between calcium burden and echocardiographic measurements (Figure 5.6). For example it is becoming increasingly appreciated that the contribution of valvular fibrosis to haemodynamic obstruction may have been underestimated, particularly in women and younger patients. Fibrosis is thought to be visible as non-calcific thickening on contrast CT angiography and efforts are currently underway to obtain volumetric measurements of this to determine whether a composite 'fibro-calcific' score improves the correlation with echocardiographic findings. Disparate findings may equally by explained by the pattern of calcium distribution. It is conceivable that, for the same volume of calcium, a diffuse pattern of calcification would restrict the motion of all three leaflets and have a greater impact upon the effective orifice area than would a focal pattern. Again, this can be visualised using CT angiography which, for patients undergoing work up for TAVI, is already within the imaging protocol.

Figure 5.6. Comparison of Echocardiographic and Computed Tomography Findings in Patients with Aortic Stenosis.

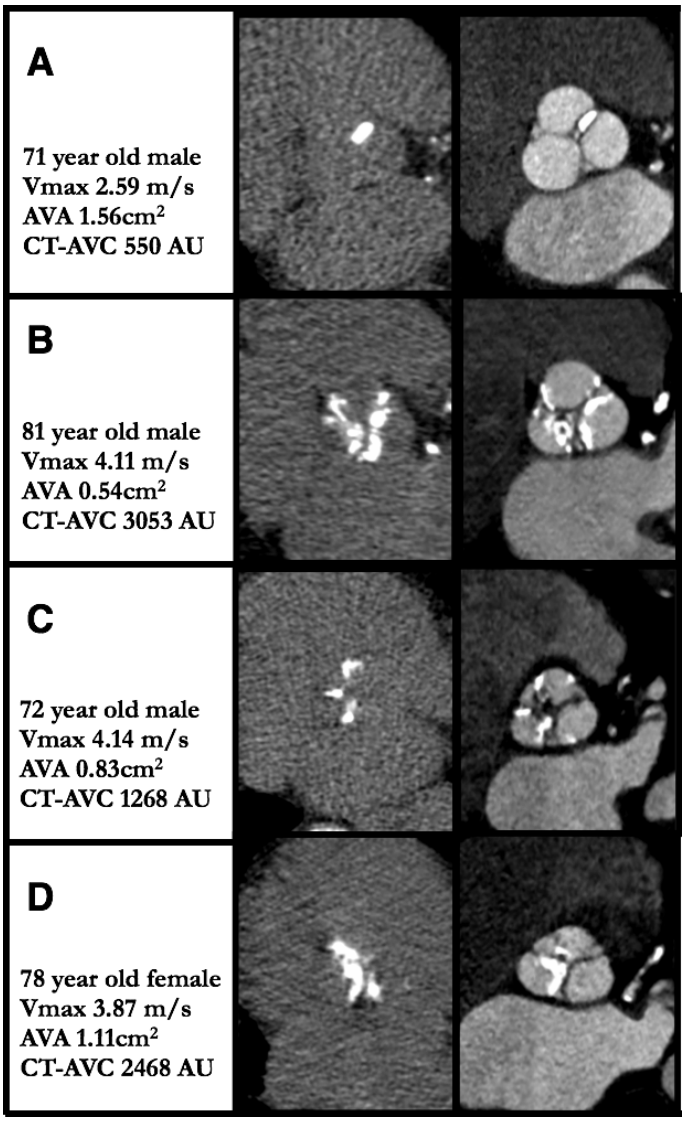

In ~90% of patients echocardiography assessments of disease severity agreed with CT AVC. **A.** 71 year old male in whom both the Vmax and AVA suggested non-severe aortic stenosis by echocardiography. The CT AVC of 550 AU (non-severe) also indicated non-severe disease, with no evidence of non-calcific valve thickening on CT angiography. **B.** 71 year old male in whom the Vmax and AVA both indicated severe haemodynamic aortic stenosis. CT AVC confirmed severe calcification affecting all three cusps.
In ~10% there was clear disagreement between the CT AVC and echocardiographic assessments of disease severity. **C.** A 72-year-old man where the Vmax and AVA confirmed severe aortic stenosis. However CT AVC was in the non-severe range. Contrast CT demonstrated non-calcific valve thickening, contributing to valve stiffening alongside the calcification and potentially explaining this discrepancy. **D.** A 78 year old female where the Vmax and AVA both indicated non-severe aortic stenosis, yet the CT AVC suggested severe calcification. CT angiography demonstrated that this calcification was not evenly distributed but instead concentrated in the non-coronary cusp.

Abbreviations: Vmax, peak aortic jet velocity, AVA aortic valve area; CTAVC, computed tomography aortic valve calcium score.

5.7.2 Inter-centre Variability

In chapter 4, CT aortic valve calcium scoring was validated against echocardiography in a single-centre study which employed identical acquisition, reconstruction and analysis protocols for all the non-contrast CT scans. In addition, a single echocardiographer performed all of the echocardiograms. By contrast, within this multi-centre study, multiple different scanners and protocols were employed which would have inevitably introduced interscan variability. Before considering how this may have impacted the observed relationship between the CT calcium scores and echocardiographic measurements, it is important to note that the density factor applied in the Agatston method is arbitrary and was not validated histologically at the time of conception. Additionally the technique was developed utilising electron-beam CT, 3 mm slice thickness and increments, with a filtered back projection (FBR) reconstruction algorithm (182). In the intervening years, scanner models, acquisition methodology and imaging post-processing have advanced considerably.

It is well recognised that image quality is inversely correlated with heart rate (183). Whilst CT imaging of the coronary arteries routinely utilises administration of beta-blockers, there appears to be a perceived risk associated with their administration in aortic stenosis patients (with only 2 centres routinely administering beta-blockade in this study). Yet our experience (Chapter 4) has been that motion artefacts can have large effects on image quality and the final CT-AVC score. (184). Interestingly, variability in Agatston scores is also influenced by reconstruction intervals with larger scores observed at the 60% and 65% intervals (184) and optimal interscan

variability at the 70% interval (185). The choice of slice thickness and increment is also important as thinner slices are better able to detect smaller calcifications. Indeed almost half of small calcifications detectable on 1.5 mm scans are missed on 3.0 mm scans (186, 187). Lower slice thickness also minimises the effects of partial voluming by reducing voxel size (188, 189). The non linear weighting factor of the Agatston scoring means that even small artefacts can produce relatively large changes in the final score.

Agatston scores also vary according to the scanner type (e.g. electron beam versus multi-detector CT) and vendor (190, 191). This may be partly related to the algorithms utilised to transform the X-ray data into digital images. Whilst CT-calcium scoring images at the University of Edinburgh utilised filtered back projection, many vendors have moved to iterative reconstruction. This is thought to reduce noise and radiation dose without compromising image quality and has been associated with a trend for lower Agatston scores (190).

Finally, this study has been designed on the basis that echocardiography is the gold-standard imaging technique. It is well acknowledged however that it is subject to patient and operator dependent factors. Misalignment of the Doppler signal with aortic blood flow can result in underestimation of the peak velocity and therefore disease severity. Considered together, the cumulative impact of each of these variables may affect the observed relationship between measured CT aortic valve calcium scores and echocardiographic measurements (which was weaker than that observed in Chapter 4) and thereby explain some of the outliers. Reassuringly,

despite all of these difficulties, the optimal sex-specific CT-AVC thresholds were still nearly identical to those previously published. However, if CT calcium scoring thresholds are indeed considered for incorporation into international guidelines, they may need to be accompanied by guidance on an optimal and unified approach to acquisition and reconstruction.

5.8 CONCLUSIONS

In this large multi-centre international registry of nearly a thousand patients with aortic stenosis, we have established the excellent accuracy of the sex-specific AVC thresholds for severe aortic stenosis and confirmed their independent prognostic capability. On this basis, we believe that CT-AVC is now ready for widespread clinical use as a complementary imaging test alongside echocardiography in patients with aortic stenosis.

Chapter 6

Severe Aortic Stenosis and Aortic Valve Calcification in the Bicuspid Aortic Valve.

Objectives
To discern the utility of CT calcium scoring and the clinical accuracy of the continuity-derived estimations of the aortic valve area (AVA_{CE}) in patients with bicuspid aortic valves.

Methods and Results
This was an international, multicenter, multimodality observational imaging study. The study population consisted of 3 cohorts. In cohort 1, different measures of aortic stenosis severity were compared between bicuspid and tri-leaflet valves in patients who had undergone echocardiography and CT aortic valve calcium scoring (CT-AVC). In cohort 2, the relationship between different measures of valve stenosis severity and the magnitude of left ventricular hypertrophy and myocardial fibrosis using cardiac magnetic resonance imaging (CMR) was examined. Finally the ability of continuity derived estimates of aortic valve area measurements to predict the primary endpoint of aortic valve replacement (AVR)/death was examined in those patients from cohorts 1 and 2 for whom outcomes were available (cohort 3).

A total of 1099 patients (76±10 years, 59% male) were studied, of whom 125 had a bicuspid valve. Within cohort 1 (n=933), higher continuity derived estimates of aortic valve area (AVA_{CE}) were observed in those with bicuspid valves (n=68, 1.07±0.35 cm) compared to those with tri-leaflet valves (0.89±0.36 cm $p<0.001$,). This was despite no differences in peak velocity (Vmax) measurements (p=0.152), or CT-AVC scores (p=0.313). Amongst the bicuspid population, weak correlations were observed between the CT-AVC scores and the AVA_{CE} r=-0.28, $p<0.022$ when compared to the Vmax, r =0.50, $p<0.001$. CT-AVC thresholds (women 1377, men 2062 AU) provided excellent discrimination for severe stenosis in this population.

Within cohort 2 (n=166), AVA_{CE} measurements in bicuspid valves (n=57) failed to correlate with either the MRI mass index (r = -0.14, p=0.310) or fibrosis volume (r= -0.12, p=0.376). This was not improved by substituting MRI planimetered AVA measurements. By contrast, in these patients, the Vmax correlated with both measurements: mass index, r=0.49, $p=<0.001$ and fibrosis volume, r=0.41, p=0.002. Finally within cohort 3 (n=365), AVA_{CE} measurements from patients with bicuspid valves (n=58) failed to independently predict AVR/death after adjustment for Vmax ≥4 m/s, age and gender. By contrast in patients with tri-leaflet valves, an AVA_{CE} <1 cm^2 emerged as an independent predictor of AVR/death after adjustment for the same variables (hazard ratio =1.68, 95% confidence intervals 1.07 to 2.66, p=0.025).

Conclusions
In patients with bicuspid aortic valves, estimations of aortic valve area are larger and fail to correlate with objective markers of disease severity or predict clinical outcomes. AVA measurements in this population should therefore be interpreted with caution, and in low-flow states, CT-AVC thresholds could be used to arbitrate disease severity.

6.1 INTRODUCTION

The bicuspid aortic valve was first described by Leonardo Da Vinci over 500 years ago (192) It is the commonest congenital heart defect and with a male preponderance, it is estimated to affect 0.9-1.3% of live births (84-87). Bicuspid valves are associated with different haemodynamic profiles to tri-leaflet valves and increased mechanical stresses (98, 99). This, in combination with increased genetic susceptibility, (93, 94) is thought to account for accelerated valvular degeneration. As a consequence, aortic stenosis is the commonest associated complication, occurring on average 5-10 years earlier than in patients with tri-leaflet valves (85). The predilection for aortic stenosis amongst bicuspid valves is further highlighted by their relatively high representation (30-50 %) amongst those undergoing surgical aortic valve replacement (85).

Current guidelines recommend assessing bicuspid valves stenosis using echocardiography in the same way as for tri-leaflet valves with standard thresholds in the mean gradient, peak velocity and aortic valve area (175), From the previous chapter, it was noted that patients with bicuspid valves comprised 23% of those in whom the peak velocity was within the severe range (≥4 m/s), but the aortic valve area measurements were non-severe (≥1 cm^2, Table 5.2). We hypothesized that differences may exist in how the different echocardiographic parameters of stenosis severity perform in bicuspid valves given their altered haemodynamics and opening profiles (127, 193, 194). Our aim was to investigate this hypothesis in an international, multicenter, multi-modality imaging registry incorporating detailed

echocardiographic, magnetic resonance and computed tomography (CT) assessments as well as clinical outcomes.

6.2 METHODS

6.2.1 Study Populations

The study involved three separate cohorts of patients with at least mild aortic stenosis (peak aortic jet velocity >2.5 m/s or mean gradient >10 mmHg, Figure 6.1). *Cohort 1* compared the different measures of aortic stenosis severity on echocardiography and CT aortic valve calcium (AVC) scoring in bicuspid and tri-leaflet valves within a large international aortic stenosis registry (as described in chapter 5). *Cohort 2* examined the relationship between the different echocardiographic assessments of bicuspid valve stenosis and the magnitude of left ventricular hypertrophy and myocardial fibrosis on magnetic resonance. These patients had been recruited to a prospective cohort study conducted by Dr Calvin Chin at the Edinburgh Heart Centre, investigating the Role of Myocardial Fibrosis in Aortic Stenosis (NCT01755936, (195). *Cohort 3* examined the relationship between echocardiographic measures of bicuspid aortic stenosis severity and clinical outcomes. It comprised patients from cohorts 1 and 2, in whom prospective outcome data were available. The presence or absence of a bicuspid valve was determined in each patient on the basis of all the available imaging data.

6.2.3 Echocardiography

Echocardiography was performed in all study patients according to the European Society of Echocardiography guidelines and used to classify patients into those with

bicuspid or tri-leaflet aortic valves. Measurements of aortic valve disease severity were performed as outlined in Chapter 2.

6.2.4 CT Calcium Scoring

Patients in cohort 1 were recruited as part of a large multicenter registry of patients with aortic stenosis. All these patients underwent CT-AVC scoring alongside echocardiography as an alternative assessment of aortic stenosis severity as previously described in Chapter 2.

6.2.5 Cardiac Magnetic Resonance

Patients in Cohort 2 were recruited from the Edinburgh Heart Centre as previously described (195). CMR was performed alongside echocardiography using a 3-T scanner (MAGNETOM Verio, Siemens AG, Erlangen, Germany). Aortic valve area was planimetered in systole on short-axis cine images of the aortic valve acquired at the tips of the leaflets (AVA_{planim}) by an observer who was blinded to echocardiographic measurements (Dr Russell Everett). Short-axis cine images were acquired and used to calculate ventricular volumes, mass, and function. Myocardial fibrosis was assessed in all patients using late gadolinium enhancement (LGE) and the T1 mapping-derived indexed extracellular volume (iECV) as a marker of the diffuse myocardial fibrosis volume (ECV multiplied by LV end-diastolic myocardial volume (195).

6.2.6 Outcomes

Patients in cohorts 1 and 2 in whom prospective clinical outcome data were available formed cohort 3. In these patients the ability of the different echocardiographic

measures of severity to predict the time to the first event in the primary composite endpoint of aortic valve replacement (AVR) or death were examined.

6.2.7 Statistical Analysis

This was performed as described in Chapter 2.

Figure 6.1 Study Cohorts

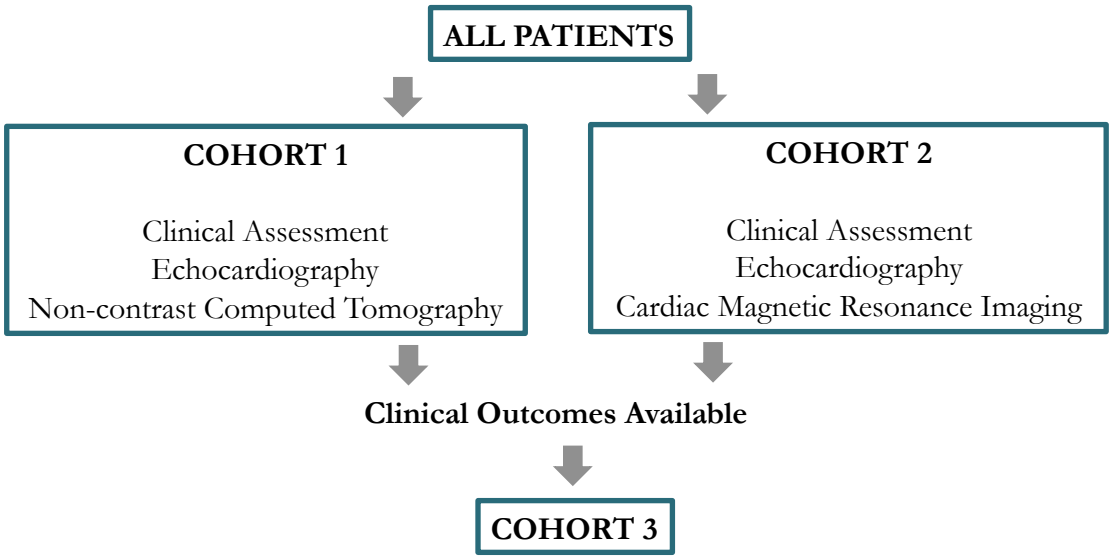

6.3 RESULTS

In total, we examined data from 1099 patients (mean age 76±10 years, 59% male, with aortic stenosis, 125 of whom had a bicuspid aortic valve. CT-AVC was available in 933 patients in *Cohort 1* (Table 6.1). *Cohort 2* comprised of 166 patients who underwent CMR alongside echocardiography (Table 2). Prospective clinical outcome data were available from 365 patients who comprised *Cohort 3*.

Table 6.1. Patient characteristics COHORT 1

		TRI-LEAFLET	BICUSPID	*P value*
CLINICAL		865	68	
Age	years ± SD	78±9	64±14	*<0.001* **
Males	%	59	72	*0.039* *
Height	cm ± SD	165±11	169±8	*0.009* *
Weight	cm ± SD	77±17	81±19	*0.167*
Body Surface Area	m^2 ± SD	1.87±0.24	1.94±0.20	*0.016**
Body Mass Index	kg/m^2± SD	28±6	28±6.5	*0.978*
Systolic Blood Pressure	mmHg ± SD	137±20	131±17	*0.05* *
Diastolic Blood Pressure	mmHg ± SD	72±13	75±9	*0.0251**
Possible Symptoms	%	70	44	*<0.001* **
Hypertension	%	78	62	*0.004* *
Coronary Artery Disease	%	46	27	*0.001* *
Ever smoked	%	31	38	*0.223*
Diabetes	%	28	16	*0.034* *
Hyperlipidaemia	%	67	43	*<0.001* **
ECHOCARDIOGRAPHY				
Peak aortic jet velocity	mmHg ± SD	3.88±0.88	3.72±0.95	*0.152*
Percentage ≥4m/s	%	51	44	
Mean Gradient	m/s ± SD	39±19	36±19	*0.191*
Percentage ≥40	%	48	43	
Aortic Valve Area	cm^2 ± SD	0.89±0.36	1.07±0.35	*<0.001** *
Percentage ≤ 1.0	%	68	43	
Aortic Valve Area Index	cm^2/m^2 ± SD	0.48±0.17	0.55±0.18	*0.001**
Percentage ≤ 0.6	%	77	60	
LVOT Diameter	cm ± SD	2.12±0.21	2.29±0.94	*<0.001* **
Valsalva Diameter	cm ± SD	3.29±0.44	3.64±0.65	*<0.001** *
Tubular Diameter	cm ± SD	2.92±0.71	3.48±0.94	*<0.001* **
Ejection Fraction	% ± SD	59±12	60±15	*0.634*
COMPUTED TOMOGRAPHY				
Aortic Valve Calcium Score	AU [IQR]	2072 [1050-3281]	1856 [969-3668]	*0.313*

Abbreviations; LVOT, left ventricular outflow tract

6.4 COHORT 1

6.4.1 Assessment of valve stenosis and calcification

In Cohort 1, 865 patients had a tri-leaflet valve and 68 had a bicuspid valve. The latter were younger and had fewer co-morbidities. The severity of aortic stenosis was similar in the patients with bicuspid versus tri-leaflet valves according to the peak velocity, mean gradient, peak gradient and the CT calcium score. The only echocardiographic parameter that differed between the groups was the AVA_{CE}, which was higher in patients with bicuspid versus tri-leaflet valves (Table 6.1). This difference in AVA persisted after indexing for body surface area.

Similar findings were observed when analysis was restricted to those patients with severe aortic stenosis (peak velocity of ≥4 m/s). Once again those with bicuspid aortic valves had values for AVA_{CE} that were more than 20% higher than patients with tri-leaflet valves (0.84 cm^2 versus 0.69 cm^2 respectively <0.001) despite having similar peak aortic jet velocities (p=0.994), mean gradients (p=0.821) and aortic valve calcium scores (p=0.773).

6.4.2 Computed Tomographic Calcium Scores.

In bicuspid valves, whilst the correlations between CT-AVC and both Vmax and mean gradient were good, the association with AVA_{CE} was extremely weak (r^2=0.08, p=0.022). By contrast, in tri-leaflet valves CT-AVC correlated well with all echocardiographic measurements of severity (Table 6.2, Figures 6.2 and 6.3). The observed association between CT-AVC and Vmax was stronger in younger patients (age ≤60 years; n= 22, r=0.67, p=0.001).

To discern the ability of CT-AVC to act as an arbitrator of disease severity amongst patients with bicuspid valves and concordant echocardiographic measurements, an umpire test was performed using the validated sex-specific CT-AVC thresholds (1377 in women and 2062 in men). There was excellent agreement between the CT-AVC scores and echocardiographic measurements. Patients with concordant severe disease had CT-AVC scores over double those with concordant-non severe disease (median CT-AVC of 3359 versus 1180 AU respectively, p<0.001, Figure 6.4).

Table 6.2. Correlation between computed tomography aortic valve calcium scores (CT-AVC) and echocardiography.

	Vmax (m/s)	Mean Gradient (mmHg)	AVA_{CE} (cm^2)	AVAi ($cm^2/m^{2)}$
BICUSPID CT-AVC				
Correlation	0.50	0.46	-0.28	-0.38
95% CI	0.26 to 0.70	0.22 to 0.66	-0.48 to -0.08	-0.58 to - 0.17
Sig.	p<0.001	p=0.001	p=0.022	P=0.002
N	68	68	68	68
TRI-LEAFLET CT-AVC				
Correlation	0.67	0.62	-0.50	-0.49
95% CI	0.64 to 0.70	0.62 to 0.69	-0.54 to -0.45	-0.58 to -0.50
Sig.	p<0.001	p<0.001	p<0.001	p<0.001
N	865	865	865	861

Abbreviations; Vmax, peak aortic jet velocity; $AVA_{CE,}$ continuity equation-derived aortic valve area; AVAi, indexed aortic valve area; CI, confidence intervals, CT-AVC; computed tomography aortic valve calcium scores.

Correlations are shown between individual echocardiographic measures of severity (Vmax, mean gradient, aortic valve area and indexed aortic valve area) and the computed tomography aortic valve calcium scores for bicuspid valves (top) and tri-leaflet (bottom)

Figure 6.2 Peak velocity versus computed tomography aortic valve calcium (CT-AVC) scores in bicuspid and tricuspid valves.

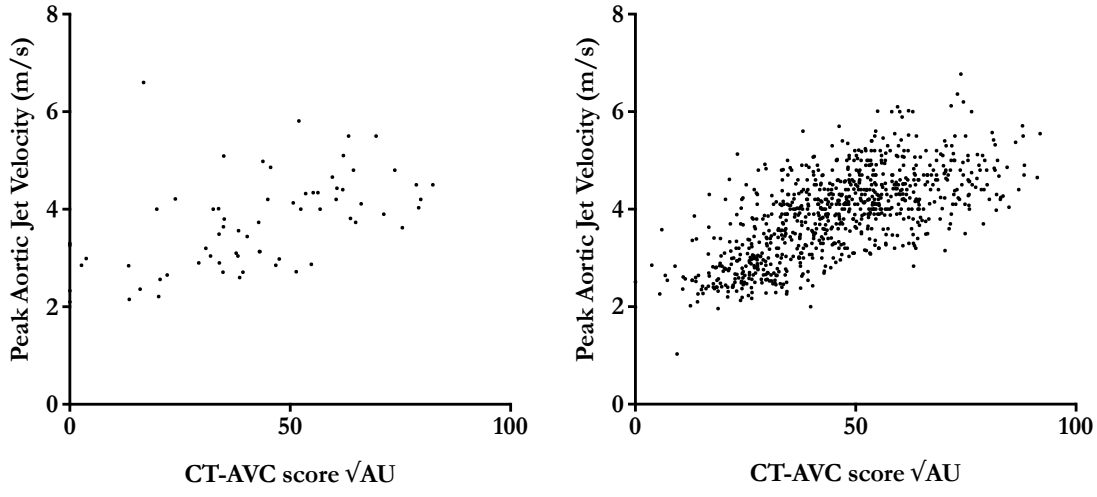

Figure 6.3. Linear regression curve for the computed tomographic aortic valve calcium score (CT-AVC) and the continuity-derived aortic valve area (AVA).

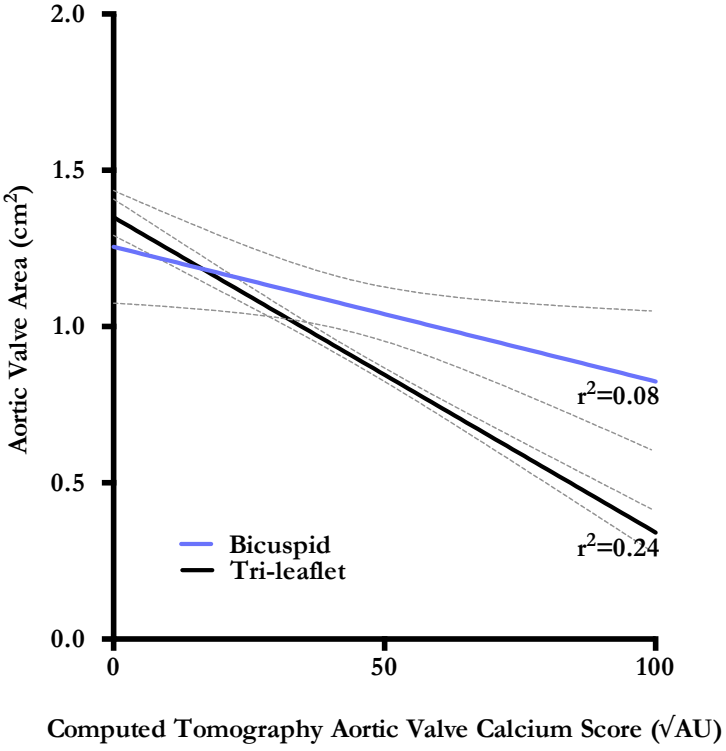

Associations between the (CT-AVC) scores and the aortic valve area for bicuspid valves (blue) compared to tri-leaflet valves (black). The dotted grey lines indicate the 95% confidence intervals.

Figure 6.4 Computed tomography aortic valve calcium (CT-AVC) scores in patients with bicuspid aortic valves and concordant echocardiographic measurements.

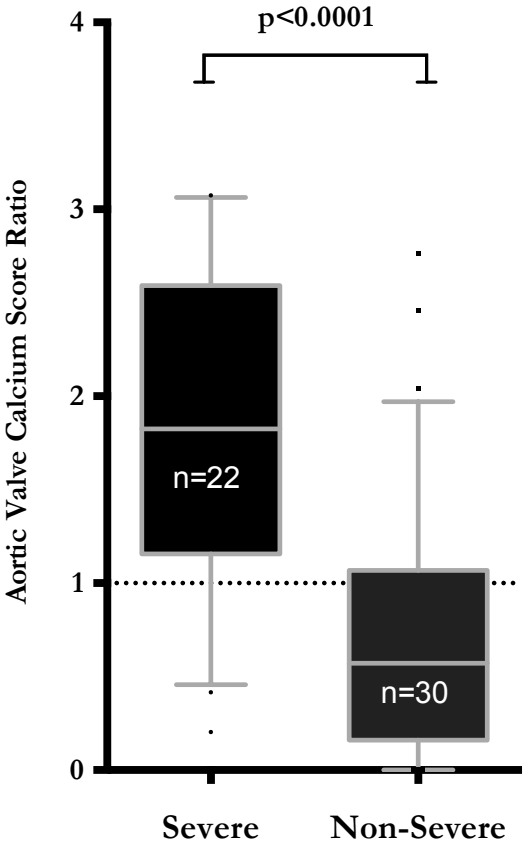

Box and Whiskers plot. A score above the dotted line represents CT-AVC above the sex-specific threshold and therefore severe aortic valve calcification. A CT-AVC score below the dotted line represents CT-AVC below the sex-specific threshold and non-severe calcification. Patients with concordant-severe aortic stenosis, as defined by echocardiography, had CT-AVC ratios that were more than double those with concordant non-severe disease. Error bars are from the 10^{th} to 90^{th} centile and the horizontal line represents the median value.

6.5 COHORT 2

6.5.1 Assessments of left ventricular remodelling

In Cohort 2, 109 patients had a tri-leaflet and 57 a bicuspid valve. In all patients, planimetered measurements from the MR were available for comparison with AVA measurements derived using the continuity equation. A strong correlation was observed between values for AVA_{planim} and the echocardiographic AVA_{CE} ($r=0.75$ $p<0.001$). However measurements for AVA_{planim} were 50% higher than AVA_{CE} regardless of valvular morphology (mean AVA value 1.53 ± 0.55 cm^2 versus 0.95 ± 0.028 cm^2 respectively, $p<0.001$, average bias=0.49 ± 0.40 cm^2, 95% limits of agreement = -0.29 to 1.28 cm^2). When patients with a peak velocity of ≥4 m/s were selected, there appeared to be a trend for lower mean values for AVA_{planim} in bicuspid valves compared to tri-leaflet valves although this fell just short of statistical significance (mean AVA_{planim} value 1.20 ± 0.35 cm^2 versus 1.36 ± 0.32 cm^2 respectively, $p=0.053$). A stronger correlation was seen between the peak velocity and the AVA_{CE} compared to the AVA_{planim} (-0.667 95% CI [-0.64 to -0.80] and $r=-0.551$ 95% CI [-0.19 to -0.68], respectively, both $p<0.001$). CMR measurements again confirmed that the bicuspid patients had larger LVOT diameters.

Data on the hypertrophic response and myocardial fibrosis were available in all the patients with a bicuspid aortic valve (Tables 6.3 and 6.4). Moderate but significant correlations were observed between these two markers of left ventricular remodelling and both the peak velocity and the mean gradient. By contrast the AVA whether assessed using planimetry or the continuity equation did not demonstrate any

association with either the LV mass index nor the fibrosis volume (Table 6.4). Amongst patients with tri-leaflet valves a significant correlation was observed between the AVA_{CE} and the LV mass index but not the fibrosis volume.

Table 6.3 Patient characteristics COHORT 2

		TRI-LEAFLET	BICUSPID	*P value*
CLINICAL		109	57	
Age	years ± SD	73±7	59±12	*<0.001* **
Males	%	59	72	*0.054*
Height	cm ± SD	165±8	170±7	*<0.001* **
Weight	cm ± SD	79±15	82±14	*0.222*
Body Surface Area	m^2 ± SD	1.85±0.18	1.93±0.18	*0.015**
Body Mass Index	kg/m^2± SD	29±5	28±4	*0.291*
Systolic Blood Pressure	mmHg ± SD	154±20	144±21	*0.003* *
Diastolic Blood Pressure	mmHg ± SD	83±11	86±12	*0.107*
ECHOCARDIOGRAPHY				
Peak aortic jet velocity	mmHg ± SD	3.73±0.77	4.02±1.09	*0.048**
Percentage ≥4m/s	%	40	53	
Mean Gradient	m/s ± SD	32±14	40±25	*0.009**
Percentage ≥40	%	27	46	
Aortic Valve Area	cm^2 ± SD	0.95±0.35	0.94±0.36	*0.751*
Percentage ≤ 1.0	%	65	65	
Aortic Valve Area Index	cm^2/m^2 ± SD	0.51±0.18	0.49±0.19	*0.441*
Percentage ≤ 0.6	%	74	82	
LVOT Diameter	cm ± SD	2.17±0.19	2.054±0.23	*<0.001***
Valsalva Diameter	cm ± SD	3.33±0.63	3.76±0.85	*<0.001* **
Tubular Diameter	cm ± SD	2.97±0.71	3.01±0.94	*<0.001* **
Ejection Fraction	% ± SD	59±12	60±15	*0.634*
CARDIAC MRI				
Planimetered AVA	cm^2 ± SD	1.60±0.50	1.39±0.62	*0.018*
Mass Index	mL/m^2	87±19	92±25	*0.129*
Fibrosis Volume	mL/m^2	23±8	24±9	*0.438*
LVOT diameter	cm ± SD	1.94±0.7	2.36±0.4	*<0.001* **
Valsalva Diameter	cm ± SD	2.59±1.2	3.14±0.9	*0.002**
Tubular Diameter	cm ± SD	3.15±0.92	3.72±0.68	*<0.001* **

Abbreviations; LVOT, left ventricular outflow tract

Table 6.4 Correlations between cardiac magnetic resonance (CMR) and echocardiography.

	MASS INDEX	FIBROSIS VOLUME
BICUSPID		
AVA_{CE} (cm^2)		
Correlation	-0.14	-0.12
Significance	p=0.310	p=0.376
Number	56	56
VMAX (m/s)		
Correlation	0.49	0.41
Significance	p<0.001	p-0.002
Number	57	57
MEAN GRADIENT (mmHg)		
Correlation	0.50	0.40
Significance	p<0.001	p<0.001
Number	57	57
TRI-LEAFLET		
AVA_{CE} (cm^2)		
Correlation	-0.21	-0.10
Significance	p=0.028	p=0.286
Number	108	108
VMAX (m/s)		
Correlation	0.46	0.29
Significance	p<0.001	p=0.003
Number	109	109
MEAN GRADIENT (mmHg)		
Correlation	-0.44	0.25
Significance	p<0.001	p=0.008
Number	109	109
PLANIMETERED AVA (cm^2)		
BICUSPID VALVE		
Correlation	-0.02	-0.06
Significance	p=0.873	P=0.695
Number	56	56
TRI-LEAFLET VALVE		
Correlation	-0.07	-0.04
Significance	p=0.477	P=0.658
Number	165	165

Abbreviations; AVA, aortic valve area, AVA_{CE}; continuity equation derived aortic valve area; Vmax, peak aortic jet velocity;

Correlations are shown between cardiac magnetic resonance imaging measurements of mass index and fibrosis volume with echocardiographic measurements of severity; aortic valve area; peak aortic jet velocity; mean aortic gradient and CMR planimetered aortic valve measurements.

6.6 COHORT 3.

6.6.1 Outcomes

Clinical outcomes of AVR and death were available for 58 of the patients with bicuspid aortic valves. Of these 29 reached the primary endpoint of AVR/death (28 AVR, 1 died). On multivariate cox regression analysis, AVA did not emerge as an independent predictor of AVR or death after adjustment for age, gender and peak velocity >4 m/s, By contrast, both the peak velocity and mean gradient were independent predictor of these events after similar adjustment (hazard ratio 4.93 for Vmax ≥4 m/s, 95% confidence intervals 1.86 to 13.09, p=0.001; hazard ratio 4.32 for mean gradient ≥ 40mmHg, 95% confidence intervals 2.09 to 8.97, p<0.001). In patients with tri-leaflet aortic valves, outcomes were available for 307 patients of whom 40 reached the primary endpoint (28 AVR, 12 deaths). In this cohort, AVA provided powerful prognostic information. Indeed, an AVA <1 cm^2 emerged as the sole independent predictor of AVR/death on multivariate analysis (hazard ratio 1.68, 95% confidence intervals 1.07 to 2.66, p=0.025, Figure 6.5)

Figure 6.5 Prediction of adverse clinical events.

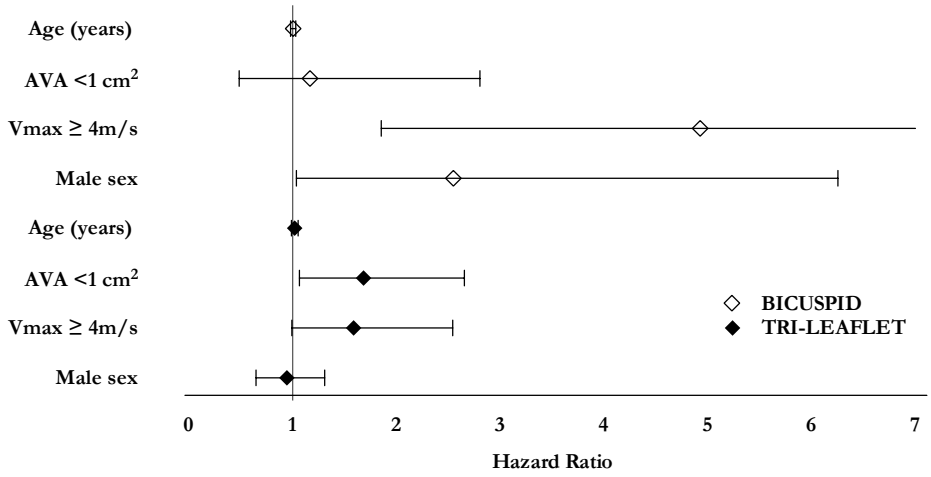

Multivariate cox regression analysis for prediction of the primary composite endpoint of aortic valve replacement or death. Hazard ratios are plotted with 95% confidence intervals for patients with bicuspid (white diamond) and tri-leaflet (black diamond) valves. Within the bicuspid population an AVA < 1cm^2 fails to independently predict clinical events once entered into the multivariate model.

Abbreviations: AVA; aortic valve area; Vmax, peak aortic jet velocity.

6.7 DISCUSSION

The results of this large multimodality imaging study demonstrate that AVA measurements do not provide an accurate assessment of aortic stenosis severity in patients with a bicuspid valve. Specifically, in bicuspid valves, AVA_{CE} measurements tend to underestimate the severity of stenosis, demonstrate poor correlation with other markers of valve stenosis severity and markers of left ventricular remodeling, and do not predict the development of future clinical events. By contrast, and in line with clinical guidelines, AVA_{CE} measurements demonstrated good association with each of these parameters in patients with tri-leaflet valves.

Our data suggest that in the bicuspid population continuity equation derived estimates of the AVA are higher than expected and therefore tend to underestimate aortic stenosis severity. This could either by explained by differences in valve geometry and flow-dynamics that exist between bicuspid and tri-leaflet valves or measurement errors in the continuity equation (possibly related to larger LVOT diameters) when applied to these patients. Further work is required to better understand this important issue, however it appears that irrespective of the method of calculation, AVA values underestimate stenosis severity in bicuspid valves.

Having proposed a clinical role for computed tomography calcium scoring of the aortic valve in the previous 2 chapters, we next examined whether this technique could be applied to those with bicuspid aortic valves. There were no overall differences in CT-AVC scores between the bicuspid and tri-leaflet populations in our cohort and in contrast to the findings of a previous study (127), we observed higher

correlations between CT-AVC scores and peak velocity measurements in the younger bicuspid patients. The extremely weak association between the AVA_{CE} and CT-AVC in the bicuspid population is likely to again reflect inaccuracies in continuity equation derived AVA estimates when applied to this population rather than problems with CT-AVC. Indeed, amongst those with bicuspid valves and concordant echocardiography, the new sex-specific CT-AVC thresholds provided excellent discrimination for severe stenosis supporting its utility as an umpire test in all discordant patients irrespective of whether the valve is bicuspid or trileaflet.

AVA_{CE} measurements in patients with bicuspid valve disease also failed to correlate with alternative markers of stenosis severity as assessed using both echocardiography and CT calcium scoring. This was despite these markers correlating closely with each other. Moreover, AVA measurments failed to correlate with markers of LV remodeling including the magnitude of the hypertrophic response and the degree of myocardial fibrosis (as a maker of LV decompensation). These processes develop in response to the increased afterload associated with progressive valvular stenosis. The lack of association therefore adds to concerns regarding the ability of AVA_{CE} to assess bicuspid valve stenosis.

Finally we assessed whether AVA_{CE} measurements might predict clinical events in patients with bicuspid valves. Once again whilst the Vmax and mean gradient both provided independent prediction of adverse clinical events AVA_{CE} failed to do so. Such events are closely related to the severity of valve narrowing providing a final

line of evidence that AVA_{CE} does not provide a clinically useful assessment of this parameter.

Are the problems with AVA generic or simply confined to patients with bicuspid aortic valve disease? We were able to answer this question by investigating AVA in over 900 patients with tri-leaflet aortic valves. In these patients AVA performed well providing agreement with the other markers of aortic stenosis severity, assessments of LV remodeling and providing independent prediction of clinical events. Our data would therefore support continuing use of this parameter in the majority of patients with aortic stenosis whilst urging considerable caution in use of AVA in patients with bicuspid valves.

6.7.1 Limitations

As advanced imaging was not performed in all patients, the true incidence of bicuspid valves in patients undergoing echocardiographic assessment alone is likely to be underestimated. However any underestimation would dilute any differences between the two groups and reduce the likelihood of significant differences.

6.8 CONCLUSION

In summary, in patients with a bicuspid valve, the continuity equation estimates of the aortic valve area are larger and exhibit weaker associations with upstream and downstream markers of disease severity and clinical outcome. Considerable caution should be taken in interpreting AVA measurements in patients with bicuspid valves. This is of particular relevance in patients with discordant measurements in whom an AVA_{CE} value outwith the severe range could create false reassurance or clinical uncertainty thereby delaying referrals for aortic valve implantation. We would

therefore advocate that in patients with bicuspid aortic valves and normal flow, the values for peak aortic jet velocity should supercede all others. In those with low-flow states, the sex-specific CT-AVC could provide an alternative technique for identifying those with severe stenosis.

Conclusions and Future Directions

8.1 18-F-FLUORIDE POSITRON EMISSION TOMOGRAPHY

18F-Fluoride PET-CT detects and quantifies novel microcalcification beyond the resolution of CT, making this the earliest biological process in aortic stenosis which we are currently able to image. On this basis, it is anticipated that detectable changes in the PET signal will long precede those identified using CT calcium scoring or echocardiography. Additionally, 18F-fluoride PET activity correlates with aortic stenosis disease severity, predicts disease progression and adverse clinical events (104, 147, 196). On the basis of these findings, it is hoped that 18F-fluoride may be able to predict the natural history of patients with aortic stenosis. Additionally these properties inform its future promise as surrogate clinical endpoint in aortic stenosis clinical trials testing the efficacy of novel therapeutic agents. If this potential is realised, this would transform the design of these trials by obviating the requirement for very large sample sizes and protracted follow up.

8.1.1 Optimised 18F-Fluoride Reproducibility.

The revised methodology of right atrial blood pool sampling and calculation of the mean standard uptake value for the most diseased segment of the valve has improved scan-rescan reproducibility to an error of only 10%. Given that a novel agent with a clinically relevant impact is likely to have an efficacy exceeding this (~>20%), meaningful drug effects should be detectable. However enhanced reproducibility does not necessarily translate to enhanced accuracy, and the sensitivity of 18F-fluoride PET to the effects of disease modifying therapies is yet to be established. Furthermore, it is not yet known whether this technique is able to track disease

progression in aortic stenosis, nor whether it truly offers incremental information over and above the far simpler technique of CT calcium scoring. In order to truly discern and validate the application of 18F-fluoride in this context, these outstanding issues are currently being addressed in the Saltire 2 randomised controlled trial in which 18F-fluoride PET uptake of the valve at 12 months is an exploratory secondary endpoint.

8.1.2 Optimised Methods for Spatial Localisation of Radiotracer Uptake

Previous work has suggested that the baseline valvular 18F-fluoride PET predicts the subsequent spatial distribution of macrocalcification on CT (Figure 1.4, (147). Modified techniques have sufficiently improved image quality so that calcification activity can be now localized more accurately. Therefore this key hypothesis, which is central to the utility of 18F-fluoride PET as a calcification biomarker, can also now be verified prospectively. Further work first needs to be done to achieve a more consistent and robust approach to windowing, which currently relies mostly on visual assessment.

8.2 COMPUTED TOMOGRAPHY AORTIC VALVE CALCIUM SCORING

Computed tomography calcium scoring (CT-AVC) is cheap, widely accessible, has an acquisition time of seconds, requires no contrast and is associated with low radiation doses. Additionally, the process of assigning a calcium score using commercially available software is relatively quick and straightforward. On this basis, the technique holds appeal for patients and practitioners alike. In a series of studies, we sought to determine how this tool may be harnessed to improve clinical care for patients with aortic stenosis.

8.2.3 Reproducibility of Aortic Valve Computed Tomography Calcium Scoring

Within the context of a single-centre study we established that the reproducibility of CT calcium scoring is within acceptable limits for clinical application. Inter and intra observer reproducibility were excellent and scan-rescan reproducibility was associated with an error of approximately 14%. The two challenges with the greatest impact on reproducibility were motion artefact and confluent calcium, both of which produce falsely elevated calcium scores. The presence and degree of motion artefact can be minimised by judicious use of rate-limiting medication. A subjective judgement on the scan quality then needs to be made before analysis. Deciding how to exclude calcium extending into extra-valvular structures is a commonly encountered challenge and can only be overcome by operator experience and consistent methodology. This may explain some of the proportional bias seen with the technique whereby higher scores were associated with worse reproducibility. Reassuringly the impact of this is minimal beyond a certain threshold. Indeed the clinical application of CT-AVC is expected to involve the categorical classification of patients using sex-specific thresholds for severe calcification. On this basis, the

absolute score is less significant and the aforementioned limitations are only likely to influence patients with borderline scores. Indeed when scan-rescan agreement for CT calcium scoring as a categorical variable was tested in the substudy, agreement was 100%.

8.2.4 Aortic Valve Calcium and Disease Severity

In the Ring of Fire study (Chapter 4), strong linear correlations were observed between the CT calcium scores and the echocardiographic measurements. This was in contrast to the more moderate relationship observed in the multicenter study (Chapter 5). Some of this discrepancy will relate to the different sample populations. Whilst a full spectrum of disease (from controls to very severe) were examined in the Ring of Fire study, the multicentre study consisted mainly of a cluster of patients with moderate or severe aortic stenosis. Other factors likely to have influenced the observed correlation between these two variables within the multicentre study were explored in detail in chapter 5. These included scanner type, scanner vendor, acquisition protocols, reconstruction algorithms and observer expertise. The correlation coefficients derived from the research cohorts were generally higher than those observed in clinical cohorts. This is perhaps unsurprising and to ensure a more seamless transition into the clinical arena, guidelines describing the clinical application of CT calcium scoring in aortic stenosis should be accompanied by guidance on image acquisition, reconstruction and analysis to ensure a unified approach.

8.2.5 Sex Differences in Aortic Valve Calcification

CT calcium scoring needs to be interpreted in light of patient demographics. A consistent finding in this thesis and in previous studies was that women need less calcium than men to achieve the same degree of obstruction, even after correction for smaller body size (121). Whilst generally accepted, this observation remains unexplained. The current working hypothesis is that it relates to a greater degree of valvular fibrosis in women. This has not yet been conclusively substantiated although it is supported by anecdotal evidence (Figure 7.1). Similarly, whilst biological differences are likely to be explained by androgen-receptor pathways, this is not confirmed and available data examining the effect of sex hormones on inflammation, fibrosis and calcification is conflicting (197, 198). Volumetric analysis of non-calcific thickening using contrast CT scans is currently being performed in the Saltire 2 cohort to discern whether its inclusion improves the correlation between echocardiography and CT-AVC scores. Ultimately the development of a composite fibro-calcific score which may better reflect the disease process and facilitate tailored treatment plans is envisaged. It is conceivable that a predominantly fibrotic disease process may follow a more indolent course and respond better to antifibrotic therapies, such as Angiotensin Converting Enzyme inhibitors. Regardless of the aetiology, these findings confirm that sex-specific CT diagnostic thresholds are mandatory.

Figure 7.1. Fibrotic aortic valve disease in a woman

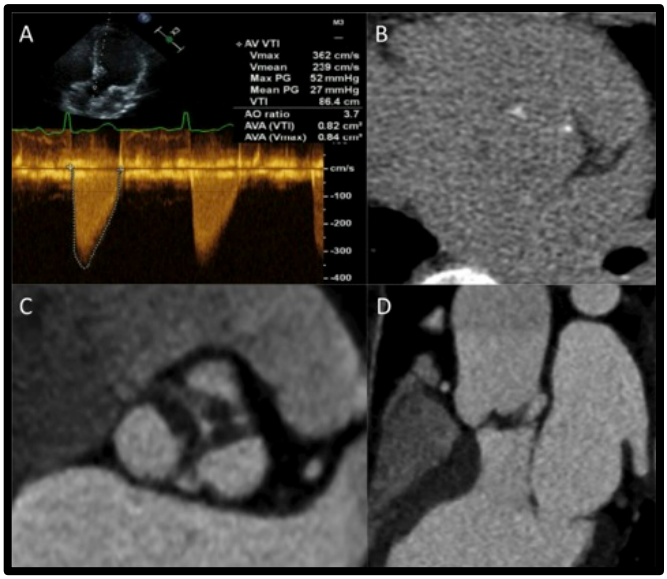

A 58-year-old woman with aortic stenosis investigated by echocardiography and CT. (A) Doppler echocardiography demonstrating a peak aortic valve (AV) velocity of 3.6 m/s, a mean gradient of 27 mm Hg and an aortic valve area (AVA) of 0.8 cm^2 based upon the continuity equation. (B) Non-contrast calcium scoring CT in the axial plane showing minimal aortic valve calcification (AV calcium score 37 AU). (C) Images from contrast-enhanced CT in the en face plane and (D) coronal plane revealing marked leaflet thickening with low attenuation signal suggestive of valve fibrosis. AO, aorta; AV, aortic valve; AVA, aortic valve areas; PG, pressure gradient; VTI, velocity time integral.

Timothy R G Cartlidge et al. Heart 2017;103:8-9

8.2.7 Sex-specific CT-AVC thresholds

On the basis of observed gender differences, sex-specific CT thresholds (women 1274 AU and men 2065 AU) have previously been proposed from a derivation cohort comprising 451 patients (121, 168). This cohort only consisted of patients recruited into prospective clinical studies being conducted in expert centres (121). To determine how these thresholds performed in a 'real-world' scenario, we determined our own thresholds for severe calcification in an international, multicenter, multivendor registry. Despite the intentional heterogeneity present in our patient population, our thresholds (women 1377 men 2062 AU) for severe disease were nearly identical to those originally proposed and demonstrated excellent discrimination for detecting severe aortic stenosis. Indeed CT calcium scoring agreed with echocardiography in approximately 90% of cases and patients with concordant-severe disease had AVC scores that were more than double those in patients with concordant non-severe disease.

8.2.7 Bicuspid aortic valves

When applied to the bicuspid population, these sex-specific CT thresholds again provided excellent discrimination for identifying those with severe aortic stenosis. This is of particular importance in these patients as we also identified that both continuity-derived and MRI planimetered assessments of aortic valve area were inaccurate. Indeed the peak velocity measurements provided the best assessment of disease severity when compared to downstream markers of disease severity and clinical outcomes. Sex-specific CT-AVC thresholds could provide a complementary technique for the assessment of disease severity, particularly in patients with suspected low-flow states or poor echocardiographic windows.

Previously published data has advised caution when applying CT-AVC scoring in younger patients with bicuspid aortic valves (127). These authors observed weaker correlations between CT calcification and echocardiographic measurements in this subgroup and speculated whether this could be explained by valvular fibrosis. By contrast, within our cohort, the highest correlations between peak velocity and CT calcification were actually observed in the youngest bicuspid valve patients. The reasons for this discrepency are unclear although our sample size was considerably larger and where possible, a multimodality approach to the identification of bicuspid valves was adopted. Nonetheless to examine this further, volumetric analysis of non-calcific thickening is being performed within bicuspid subgroups in an attempt to determine the fibrotic burden in these patients.

8.2.8 CT Aortic Valve Calcium and Clinical Course.

In comparison to echocardiography, the baseline calcium score appeared to offer the best prediction of disease progression whether this was measured using annualised changes in calcium score or peak velocity. In addition, annualised changes were more easily detectable using CT calcium scoring than echocardiography. Of primary importance, CT aortic valve calcium scoring was the most powerful predictor of the primary composite endpoint of death and aortic valve replacement. Furthermore sex-specific CT thresholds predicted aortic valve replacement and death independently of all the variables used to guide clinical decision-making (age, peak velocity and aortic valve area). This was despite clinicians being blinded to the calcium scores.

Vascular calcification is a recognised marker of adverse cardiovascular prognosis. Aortic arch calcification, abdominal aortic calcification and aortic sclerosis have all been shown to provide powerful risk prediction of coronary heart disease (199-201) and as previously discussed, even a crude, subjective echocardiographic assessment of valvular calcium burden provides more powerful risk prediction than all other echocardiographic variables (15). Vascular calcification is likely to be a marker of endothelial dysfunction, inflammation, altered calcium metabolism, lipid accumulations and genetic polymorphisms, all processes which contribute to adverse cardiovascular events (26). On this basis it was reassuring that the adverse events observed in this thesis were primarily driven by aortic valve replacements. This indicates that the thresholds predict clinical decompensation in patients who are candidates for invasive treatments as opposed to simply those who are at high risk of cardiovascular mortality.

8.2.9 Clinical Application of sex-specific CT-AVC thresholds

On the basis of the above findings, we believe that sex-specific CT-AVC thresholds should enter routine clinical practice to arbitrate disease severity in patients for whom clinical decision making is being hampered by inconclusive echocardiographic findings. The current ESC guideines recommend dobutamine stress echo as the first line investigation for patients with suspected low-flow, low gradient aortic stenosis (152). CT-AVC scoring is advised as a last resort only, however it is a far simpler technique and would be of particular value in those patients suboptimal echocardiographic windows or in centres where there is insufficient technical expertise.

It is important to note however that there was clear disagreement between CT and echocardiography in approximately 10% of patients with concordant echocardiography. This raises an interesting conundrum. Given that the calcium score is the more powerful predictor of adverse events, which is of more clinical significance for the patient; an echocardiographic diagnosis of severe aortic stenosis or a CT diagnosis? Current data suggest the latter, in which case should all patients with symptoms and a calcium score above the threshold be referred for surgery. To take this a step further should asymptomatic patients with severe CT calcification also be referred for surgery? These questions can only be definitively addressed in prospective studies. Although it is first important to note that, to date, CT-AVC thresholds have been derived from patients recruited from Europe and North America. The Multi-Ethnic study of atherosclerosis has demonstrated that coronary artery calcium scores need to be interpreted in light of age, gender and ethnicity (202). It is plausible that in future a similar approach will be adopted for aortic valve calcification.

8.3 CLINICAL PERSPECTIVE

Aortic stenosis is a significant and growing public health burden. Whilst the prevalence is undoubtedly higher in older patients, there is considerable heterogeneity within this population with respect to age, co-morbidity, clinical course and pathophysiology. Despite this, there is a failure to individualise strategies for defining disease severity, surveillance and intervention. Echocardiography is the gold-standard investigation for guiding clinical decision however the emergence and refinement of complementary calcification imaging techniques in tandem with advancements in deciphering the pathophysiology will facilitate a clinical approach tailored to individual patients. This could avoid protracted and potentially unnecessary follow-up for the large proportion of patients in whom aortic stenosis never progresses beyond the mild stage whilst appropriately diverting resources to those who are at risk of adverse clinical events. This will translate to improved care and better clinical outcomes for patients with aortic stenosis.

8.4 FUTURE PERSPECTIVES

This thesis has examined at length how the measurement of valvular calcification can be applied to improve patient care. However it remains to be established whether calcium metabolism can also be targeted by drug therapies. A medical treatment capable of modifying the clinical course of aortic stenosis is highly desirable yet remains elusive and as the complexity of aortic stenosis pathophysiology is being gradually unmasked, so too are attractive novel therapeutic targets. This is likely to form the cornerstone of future research in aortic stenosis.

8.4.1 Medical Treatment of Aortic Stenosis

Saltire 2 is a proof of concept clinical trial exploring whether currently available osteoporosis medications can be repurposed to modify disease progression in aortic stenosis (Appendix 1). Patients have been randomised to alendronic acid (n=50), denosumab (n=50) or their respective matched placebos (n=50). The primary endpoint is the aortic valve calcium score at 2 years. 18F-Fluoride PET uptake at 1 year is a major exploratory secondary endpoint. Other secondary endpoints include the change in thoracic aortic and coronary 18F-fluoride uptake at 1 year and the CT calcium score at 2 years. In an attempt to futher understand the calcification paradox, nested mechanistic studies will explore associations between serum and imaging biomarkers and relate these to histological findings when possible. The study design also provides a unique platform upon which to further optimise and validate the current calcification and fibrosis imaging techniques within the context of a longitudunal study. If a positive outcome was subsequently confirmed in a larger phase 3 trial powered for clinical endpoints, this would represent a major clinical breakthrough.

Even if these therapies prove ineffective, it is likely that that future treatments should still be directed at breaking the self-perpetuating cycle of valvular injury, osteogenic differentiation and calcium deposition. A rapidly expanding list of signaling pathways and molecular processes governing the pathogenesis of aortic stenosis have been elucidated uncovering many additional targets at different phases of the disease. Ultimately many of the pro-calcific pathways in the valve appear to converge on the up regulation of osteogenic differentiation factors (e.g. BMP-2, Wnt-catenin) that establish osteoblast-like function within the valve. These factors therefore provide an attractive therapeutic strategy although given the overlap in factors governing calcification in the bone and the valve, the major challenge will be to slow aortic stenosis progression without compromising bone health. One potential approach would be to target the upstream cytokines that activate BMP such as using inhibitors of IL-6 or TNF-α (as already used in rheumatoid arthritis). However, once again it remains unclear whether targeting inflammation will be effective in the propagation phase once the pro-calcific processes have become established. Targeting ectonucleotidases may be more effective given their apparently central role in establishing the positive feedback loop by which calcium begets calcium. Indeed ectonucleotidase inhibitors have already been tested in the warfarin rat model and have been shown to prevent the development of calcific aortic valve disease (203), whilst interest also surrounds $P2Y_2$ receptor antagonists as a means of reducing VIC apoptosis and the calcification that this induces. Therapeutic administration of Fetuin-A, or a mimetic of MGP could simultaneously target multiple pathways thought to drive valvular calcification. In addition further investigation is warranted

to assess whether potentially pro-calcific drugs, including calcium supplements and coumarins, should be avoided in patients with aortic stenosis.

Therapies targeting non-calcific pathways may also be of importance. The ability of Lipoprotein (a) lowering therapies to modify aortic stenosis disease progression, is likely to form the basis of a future clinical trial. Given the failure of the statin trials, it will be of great interest to determine whether a more targeted lipid intervention will have greater success in reducing disease progression in the propagation phase (204).

Based on the apparent contribution of the renin-angiotensin system (RAS) to the initiation of aortic stenosis, it is also not unreasonable to consider the therapeutic potential of angiotensin-converting enzyme inhibitors, selective angiotensin 1 receptor antagonists or novel renin inhibitors as treatments particular in patients assumed to have a higher susceptibility to valvular fibrosis (205). Indeed, these agents are also likely to have a beneficial effect with respect to hypertension and left ventricular remodelling in aortic stenosis, given the role that the RAS system also plays in driving myocardial hypertrophy, fibrosis and the transition to heart failure. If CT angiography is confirmed as being capable of quantifying non-calcific valvular thickening and fibrosis, this could be employed in combination with calcification imaging techniques to better direct therapeutic strategies, although it is likely that most patients will require simultaneous targeting of calcification and fibrosis pathways.

8.4.2 Early surgical intervention

There has been much debate on the role of early surgical intervention in patients with asymptomatic severe aortic stensosis. The landmark paper by Ross and Braunwald which continues to guide current clinical practice, (14) was published in 1968, long before the advent of advanced cardiac imaging. Whilst many patients with truly asymptomatic severe stenosis do enjoy a good prognosis, it is not unreasonable to question whether those with high risk features should undergo aortic valve replacement prior to clinical decompensation. Indeed this forms the basis of the early surgical intervention trial EVOLVED-AS (NCT03094143) in which patients with asymptomatic, severe aortic stenosis and myocardial fibrosis are being randomised to either continued watchful waiting or early surgery. This important question is therefore being addressed. However, given the overwhelmingly powerful risk prediction afforded by CT calcium scoring, another potentially exciting approach would be to investigate whether severe calcification on CT should be a criterion for aortic valve replacement in the context of a similar prospective randomised controlled trial.

8.4.3 Conclusion

To conclude, in recent years there has been a paradigm shift with respect to the perceived role of calcification in aortic stenosis. Formerly considered a passive process, it is now appreciated to be complex, potentially modifiable and the principle factor dictating both disease progression and clinical outcomes. Calcification should therefore take centre stage with respect to the development of complementary imaging modalities and future therapies.

REFERENCES

1. Rajamannan NM, Evans FJ, Aikawa E, Grande-Allen KJ, Demer LL, Heistad DD, et al. Calcific Aortic Valve Disease: Not Simply a Degenerative Process: A Review and Agenda for Research From the National Heart and Lung and Blood Institute Aortic Stenosis Working GroupExecutive Summary: Calcific Aortic Valve Disease – 2011 Update. Circulation. 2011;124(16):1783-91.
2. Braunwald E. On the natural history of severe aortic stenosis. Journal of the American College of Cardiology. 1990;15(5):1018-20.
3. Chizner MA, Pearle DL, deLeon AC. The natural history of aortic stenosis in adults. Am Heart J. 1980;99(4):419-24.
4. Turina J, Hess O, Sepulcri F, Krayenbuehl HP. Spontaneous course of aortic valve disease. European heart journal. 1987;8(5):471-83.
5. Lassnigg A, Hiesmayr M, Frantal S, Brannath W, Mouhieddine M, Presterl E, et al. Long-term absolute and relative survival after aortic valve replacement: a prospective cohort study. Eur J Anaesthesiol. 2013;30(11):695-703.
6. Gaede L, Kim WK, Blumenstein J, Liebetrau C, Dorr O, Nef H, et al. Temporal trends in transcatheter and surgical aortic valve replacement : An analysis of aortic valve replacements in Germany during 2012-2014. Herz. 2016.
7. Nkomo VT, Gardin JM, Skelton TN, Gottdiener JS, Scott CG, Enriquez-Sarano M. Burden of valvular heart diseases: a population-based study. Lancet (London, England). 2006;368(9540):1005-11.
8. Melton LJ, 3rd. History of the Rochester Epidemiology Project. Mayo Clinic proceedings. 1996;71(3):266-74.
9. Osnabrugge RL, Mylotte D, Head SJ, Van Mieghem NM, Nkomo VT, LeReun CM, et al. Aortic stenosis in the elderly: disease prevalence and number of candidates for transcatheter aortic valve replacement: a meta-analysis and modeling study. Journal of the American College of Cardiology. 2013;62(11):1002-12.
10. Cowell SJ, Newby DE, Prescott RJ, Bloomfield P, Reid J, Northridge DB, et al. A randomized trial of intensive lipid-lowering therapy in calcific aortic stenosis. The New England journal of medicine. 2005;352(23):2389-97.
11. Rossebo AB, Pedersen TR, Boman K, Brudi P, Chambers JB, Egstrup K, et al. Intensive lipid lowering with simvastatin and ezetimibe in aortic stenosis. The New England journal of medicine. 2008;359(13):1343-56.
12. Otto CM, Burwash IG, Legget ME, Munt BI, Fujioka M, Healy NL, et al. Prospective study of asymptomatic valvular aortic stenosis. Clinical, echocardiographic, and exercise predictors of outcome. Circulation. 1997;95(9):2262-70.
13. Eveborn GW, Schirmer H, Heggelund G, Lunde P, Rasmussen K. The evolving epidemiology of valvular aortic stenosis. the Tromso study. Heart (British Cardiac Society). 2013;99(6):396-400.
14. Ross J, Jr., Braunwald E. Aortic stenosis. Circulation. 1968;38(1 Suppl):61-7.

15. Rosenhek R, Binder T, Porenta G, Lang I, Christ G, Schemper M, et al. Predictors of outcome in severe, asymptomatic aortic stenosis. The New England journal of medicine. 2000;343(9):611-7.
16. Horstkotte D, Loogen F. The natural history of aortic valve stenosis. European heart journal. 1988;9 Suppl E:57-64.
17. Rosenhek R, Klaar U, Schemper M, Scholten C, Heger M, Gabriel H, et al. Mild and moderate aortic stenosis. Natural history and risk stratification by echocardiography. European heart journal. 2004;25(3):199-205.
18. Gohlke-Barwolf C, Minners J, Jander N, Gerdts E, Wachtell K, Ray S, et al. Natural history of mild and of moderate aortic stenosis-new insights from a large prospective European study. Curr Probl Cardiol. 2013;38(9):365-409.
19. David Merryman W. Mechano-potential etiologies of aortic valve disease. Journal of biomechanics. 2010;43(1):87-92.
20. New SE, Aikawa E. Molecular imaging insights into early inflammatory stages of arterial and aortic valve calcification. Circulation research. 2011;108(11):1381-91.
21. Pachulski RT, Chan KL. Progression of aortic valve dysfunction in 51 adult patients with congenital bicuspid aortic valve: assessment and follow up by Doppler echocardiography. British heart journal. 1993;69(3):237-40.
22. Otto CM, Kuusisto J, Reichenbach DD, Gown AM, O'Brien KD. Characterization of the early lesion of 'degenerative' valvular aortic stenosis. Histological and immunohistochemical studies. Circulation. 1994;90(2):844-53.
23. Thanassoulis G, Massaro JM, Cury R, Manders E, Benjamin EJ, Vasan RS, et al. Associations of long-term and early adult atherosclerosis risk factors with aortic and mitral valve calcium. Journal of the American College of Cardiology. 2010;55(22):2491-8.
24. Stewart BF, Siscovick D, Lind BK, Gardin JM, Gottdiener JS, Smith VE, et al. Clinical factors associated with calcific aortic valve disease. Cardiovascular Health Study. Journal of the American College of Cardiology. 1997;29(3):630-4.
25. Stritzke J, Linsel-Nitschke P, Markus MR, Mayer B, Lieb W, Luchner A, et al. Association between degenerative aortic valve disease and long-term exposure to cardiovascular risk factors: results of the longitudinal population-based KORA/MONICA survey. European heart journal. 2009;30(16):2044-53.
26. Otto CM. Why is aortic sclerosis associated with adverse clinical outcomes? Journal of the American College of Cardiology. 2004;43(2):176-8.
27. Smith JG, Luk K, Schulz CA, Engert JC, Do R, Hindy G, et al. Association of low-density lipoprotein cholesterol-related genetic variants with aortic valve calcium and incident aortic stenosis. Jama. 2014;312(17):1764-71.
28. Thanassoulis G, Campbell CY, Owens DS, Smith JG, Smith AV, Peloso GM, et al. Genetic associations with valvular calcification and aortic stenosis. The New England journal of medicine. 2013;368(6):503-12.
29. Pawade TA, Newby DE, Dweck MR. Calcification in Aortic Stenosis: The Skeleton Key. Journal of the American College of Cardiology. 2015;66(5):561-77.
30. Miller JD, Chu Y, Brooks RM, Richenbacher WE, Pena-Silva R, Heistad DD. Dysregulation of antioxidant mechanisms contributes to increased oxidative stress in calcific aortic valvular stenosis in humans. Journal of the American College of Cardiology. 2008;52(10):843-50.

31. Hamatani Y, Ishibashi-Ueda H, Nagai T, Sugano Y, Kanzaki H, Yasuda S, et al. Pathological Investigation of Congenital Bicuspid Aortic Valve Stenosis, Compared with Atherosclerotic Tricuspid Aortic Valve Stenosis and Congenital Bicuspid Aortic Valve Regurgitation. PloS one. 2016;11(8):e0160208.
32. Nadra I, Mason JC, Philippidis P, Florey O, Smythe CD, McCarthy GM, et al. Proinflammatory activation of macrophages by basic calcium phosphate crystals via protein kinase C and MAP kinase pathways: a vicious cycle of inflammation and arterial calcification? Circulation research. 2005;96(12):1248-56.
33. Rajamannan NM, Subramaniam M, Springett M, Sebo TC, Niekrasz M, McConnell JP, et al. Atorvastatin inhibits hypercholesterolemia-induced cellular proliferation and bone matrix production in the rabbit aortic valve. Circulation. 2002;105(22):2660-5.
34. Weiss RM, Ohashi M, Miller JD, Young SG, Heistad DD. Calcific aortic valve stenosis in old hypercholesterolemic mice. Circulation. 2006;114(19):2065-9.
35. Cowell SJ, Newby DE, Prescott RJ, Bloomfield P, Reid J, Northridge DB, et al. A randomized trial of intensive lipid-lowering therapy in calcific aortic stenosis. The New England journal of medicine. 2005;352(23):2389-97.
36. Chan KL, Teo K, Dumesnil JG, Ni A, Tam J, Investigators A. Effect of Lipid lowering with rosuvastatin on progression of aortic stenosis: results of the aortic stenosis progression observation: measuring effects of rosuvastatin (ASTRONOMER) trial. Circulation. 2010;121(2):306-14.
37. Puri R, Nicholls SJ, Shao M, Kataoka Y, Uno K, Kapadia SR, et al. Impact of Statins on Serial Coronary Calcification During Atheroma Progression and Regression. Journal of the American College of Cardiology. 2015;65(13):1273-82.
38. Capoulade R, Clavel MA, Dumesnil JG, Chan KL, Teo KK, Tam JW, et al. Impact of metabolic syndrome on progression of aortic stenosis: influence of age and statin therapy. Journal of the American College of Cardiology. 2012;60(3):216-23.
39. Mohler ER, 3rd, Gannon F, Reynolds C, Zimmerman R, Keane MG, Kaplan FS. Bone formation and inflammation in cardiac valves. Circulation. 2001;103(11):1522-8.
40. O'Brien KD, Shavelle DM, Caulfield MT, McDonald TO, Olin-Lewis K, Otto CM, et al. Association of angiotensin-converting enzyme with low-density lipoprotein in aortic valvular lesions and in human plasma. Circulation. 2002;106(17):2224-30.
41. Peltonen T, Napankangas J, Ohtonen P, Aro J, Peltonen J, Soini Y, et al. (Pro)renin receptors and angiotensin converting enzyme 2/angiotensin-(1-7)/Mas receptor axis in human aortic valve stenosis. Atherosclerosis. 2011;216(1):35-43.
42. Ducy P. Cbfa1: a molecular switch in osteoblast biology. Developmental dynamics : an official publication of the American Association of Anatomists. 2000;219(4):461-71.
43. Rajamannan NM, Subramaniam M, Rickard D, Stock SR, Donovan J, Springett M, et al. Human Aortic Valve Calcification Is Associated With an Osteoblast Phenotype. Circulation. 2003;107(17):2181-4.

44. Pohjolainen V, Taskinen P, Soini Y, Rysä J, Ilves M, Juvonen T, et al. Noncollagenous bone matrix proteins as a part of calcific aortic valve disease regulation. Human Pathology. 2008;39(11):1695-701.
45. Ganss B, Kim RH, Sodek J. Bone sialoprotein. Critical reviews in oral biology and medicine : an official publication of the American Association of Oral Biologists. 1999;10(1):79-98.
46. Liu AC, Joag VR, Gotlieb AI. The emerging role of valve interstitial cell phenotypes in regulating heart valve pathobiology. The American journal of pathology. 2007;171(5):1407-18.
47. Aikawa E, Nahrendorf M, Figueiredo JL, Swirski FK, Shtatland T, Kohler RH, et al. Osteogenesis associates with inflammation in early-stage atherosclerosis evaluated by molecular imaging in vivo. Circulation. 2007;116(24):2841-50.
48. Aikawa E, Otto CM. Look more closely at the valve: imaging calcific aortic valve disease. Circulation. 2012;125(1):9-11.
49. Watson KE, Bostrom K, Ravindranath R, Lam T, Norton B, Demer LL. TGF-beta 1 and 25-hydroxycholesterol stimulate osteoblast-like vascular cells to calcify. The Journal of clinical investigation. 1994;93(5):2106-13.
50. Tintut Y, Demer L. Role of osteoprotegerin and its ligands and competing receptors in atherosclerotic calcification. Journal of investigative medicine : the official publication of the American Federation for Clinical Research. 2006;54(7):395-401.
51. Garg V, Muth AN, Ransom JF, Schluterman MK, Barnes R, King IN, et al. Mutations in NOTCH1 cause aortic valve disease. Nature. 2005;437(7056):270-4.
52. Nigam V, Srivastava D. Notch1 represses osteogenic pathways in aortic valve cells. Journal of molecular and cellular cardiology. 2009;47(6):828-34.
53. Bostrom K, Watson KE, Stanford WP, Demer LL. Atherosclerotic calcification: relation to developmental osteogenesis. The American journal of cardiology. 1995;75(6):88B-91B.
54. Yang X, Meng X, Su X, Mauchley DC, Ao L, Cleveland JC, Jr., et al. Bone morphogenic protein 2 induces Runx2 and osteopontin expression in human aortic valve interstitial cells: role of Smad1 and extracellular signal-regulated kinase 1/2. J Thorac Cardiovasc Surg. 2009;138(4):1008-15.
55. Yang X, Fullerton DA, Su X, Ao L, Cleveland Jr JC, Meng X. Pro-Osteogenic Phenotype of Human Aortic Valve Interstitial Cells Is Associated With Higher Levels of Toll-Like Receptors 2 and 4 and Enhanced Expression of Bone Morphogenetic Protein 2. Journal of the American College of Cardiology. 2009;53(6):491-500.
56. Caira FC, Stock SR, Gleason TG, McGee EC, Huang J, Bonow RO, et al. Human degenerative valve disease is associated with up-regulation of low-density lipoprotein receptor-related protein 5 receptor-mediated bone formation. Journal of the American College of Cardiology. 2006;47(8):1707-12.
57. Chen JH, Chen WL, Sider KL, Yip CY, Simmons CA. beta-catenin mediates mechanically regulated, transforming growth factor-beta1-induced myofibroblast differentiation of aortic valve interstitial cells. Arteriosclerosis, thrombosis, and vascular biology. 2011;31(3):590-7.

58. Rajamannan NM. Oxidative-mechanical stress signals stem cell niche mediated Lrp5 osteogenesis in eNOS(-/-) null mice. Journal of cellular biochemistry. 2012;113(5):1623-34.
59. Kado DM, Browner WS, Blackwell T, Gore R, Cummings SR. Rate of bone loss is associated with mortality in older women: a prospective study. Journal Of Bone And Mineral Research: The Official Journal Of The American Society For Bone And Mineral Research. 2000;15(10):1974-80.
60. Pfister R, Michels G, Sharp SJ, Luben R, Wareham NJ, Khaw KT. Inverse association between bone mineral density and risk of aortic stenosis in men and women in EPIC-Norfolk prospective study. International journal of cardiology. 2015;178:29-30.
61. Aksoy Y, Yagmur C, Tekin GO, Yagmur J, Topal E, Kekilli E, et al. Aortic valve calcification: association with bone mineral density and cardiovascular risk factors. Coronary artery disease. 2005;16(6):379-83.
62. Demer LL, Tintut Y. Vascular calcification: pathobiology of a multifaceted disease. Circulation. 2008;117(22):2938-48.
63. Persy V, D'Haese P. Vascular calcification and bone disease: the calcification paradox. Trends in molecular medicine. 2009;15(9):405-16.
64. Hultgren HN. Osteitis deformans (Paget's disease) and calcific disease of the heart valves. The American journal of cardiology. 1998;81(12):1461-4.
65. Kaden JJ, Bickelhaupt S, Grobholz R, Haase KK, Sarikoc A, Kilic R, et al. Receptor activator of nuclear factor kappaB ligand and osteoprotegerin regulate aortic valve calcification. Journal of molecular and cellular cardiology. 2004;36(1):57-66.
66. Davenport C, Harper E, Forde H, Rochfort KD, Murphy RP, Smith D, et al. RANKL promotes osteoblastic activity in vascular smooth muscle cells by upregulating endothelial BMP-2 release. Int J Biochem Cell Biol. 2016;77(Pt A):171-80.
67. Bucay N, Sarosi I, Dunstan CR, Morony S, Tarpley J, Capparelli C, et al. osteoprotegerin-deficient mice develop early onset osteoporosis and arterial calcification. Genes & development. 1998;12(9):1260-8.
68. Parhami F, Morrow AD, Balucan J, Leitinger N, Watson AD, Tintut Y, et al. Lipid oxidation products have opposite effects on calcifying vascular cell and bone cell differentiation. A possible explanation for the paradox of arterial calcification in osteoporotic patients. Arteriosclerosis, thrombosis, and vascular biology. 1997;17(4):680-7.
69. Demer LL. Vascular calcification and osteoporosis: inflammatory responses to oxidized lipids. International journal of epidemiology. 2002;31(4):737-41.
70. Schurgers LJ, Uitto J, Reutelingsperger CP. Vitamin K-dependent carboxylation of matrix Gla-protein: a crucial switch to control ectopic mineralization. Trends in molecular medicine. 2013;19(4):217-26.
71. Tantisattamo E, Han KH, O'Neill WC. Increased vascular calcification in patients receiving warfarin. Arteriosclerosis, thrombosis, and vascular biology. 2015;35(1):237-42.

72. Kaden JJ, Reinohl JO, Blesch B, Brueckmann M, Haghi D, Borggrefe M, et al. Systemic and local levels of fetuin-A in calcific aortic valve stenosis. International journal of molecular medicine. 2007;20(2):193-7.
73. Koos R, Brandenburg V, Mahnken AH, Muhlenbruch G, Stanzel S, Gunther RW, et al. Association of fetuin-A levels with the progression of aortic valve calcification in non-dialyzed patients. European heart journal. 2009;30(16):2054-61.
74. Mohty D CN, Pibarot P, Fournier D, Pépin A, Audet A, Després JP, Mathieu P. Reduced fetuin a serum level is associated with faster progression and increased valvular calcification in elderly patients with aortic stenosis. J Clin and Exp Cardiol. 2011;2(8):147.
75. Capoulade R, Cote N, Mathieu P, Chan KL, Clavel MA, Dumesnil JG, et al. Circulating levels of matrix gla protein and progression of aortic stenosis: a substudy of the Aortic Stenosis Progression Observation: Measuring Effects of rosuvastatin (ASTRONOMER) trial. Can J Cardiol. 2014;30(9):1088-95.
76. Proudfoot D, Skepper JN, Hegyi L, Bennett MR, Shanahan CM, Weissberg PL. Apoptosis regulates human vascular calcification in vitro: evidence for initiation of vascular calcification by apoptotic bodies. Circulation research. 2000;87(11):1055-62.
77. Osteikoetxea X, Nemeth A, Sodar BW, Vukman KV, Buzas EI. Extracellular vesicles in cardiovascular disease: are they Jedi or Sith? J Physiol. 2016;594(11):2881-94.
78. Kim KM. Calcification of matrix vesicles in human aortic valve and aortic media. Federation proceedings. 1976;35(2):156-62.
79. Aikawa E. Extracellular vesicles in cardiovascular disease: focus on vascular calcification. J Physiol. 2016;594(11):2877-80.
80. Krohn JB, Hutcheson JD, Martinez-Martinez E, Aikawa E. Extracellular vesicles in cardiovascular calcification: expanding current paradigms. J Physiol. 2016;594(11):2895-903.
81. Goettsch C, Hutcheson JD, Aikawa M, Iwata H, Pham T, Nykjaer A, et al. Sortilin mediates vascular calcification via its recruitment into extracellular vesicles. The Journal of clinical investigation. 2016;126(4):1323-36.
82. Cote N, El Husseini D, Pepin A, Guauque-Olarte S, Ducharme V, Bouchard-Cannon P, et al. ATP acts as a survival signal and prevents the mineralization of aortic valve. Journal of molecular and cellular cardiology. 2012;52(5):1191-202.
83. El Husseini D, Boulanger MC, Mahmut A, Bouchareb R, Laflamme MH, Fournier D, et al. P2Y2 receptor represses IL-6 expression by valve interstitial cells through Akt: implication for calcific aortic valve disease. Journal of molecular and cellular cardiology. 2014;72:146-56.
84. Roberts WC. Anatomically isolated aortic valvular disease. The case against its being of rheumatic etiology. The American journal of medicine. 1970;49(2):151-9.
85. Roberts WC, Ko JM. Frequency by decades of unicuspid, bicuspid, and tricuspid aortic valves in adults having isolated aortic valve replacement for aortic stenosis, with or without associated aortic regurgitation. Circulation. 2005;111(7):920-5.

86. Larson EW, Edwards WD. Risk factors for aortic dissection: a necropsy study of 161 cases. The American journal of cardiology. 1984;53(6):849-55.
87. Gray GW, Salisbury DA, Gulino AM. Echocardiographic and color flow Doppler findings in military pilot applicants. Aviation, space, and environmental medicine. 1995;66(1):32-4.
88. Michelena HI, Desjardins VA, Avierinos JF, Russo A, Nkomo VT, Sundt TM, et al. Natural history of asymptomatic patients with normally functioning or minimally dysfunctional bicuspid aortic valve in the community. Circulation. 2008;117(21):2776-84.
89. Shone JD, Sellers RD, Anderson RC, Adams P, Jr., Lillehei CW, Edwards JE. The developmental complex of "parachute mitral valve," supravalvular ring of left atrium, subaortic stenosis, and coarctation of aorta. The American journal of cardiology. 1963;11:714-25.
90. Bosse Y, Miqdad A, Fournier D, Pepin A, Pibarot P, Mathieu P. Refining molecular pathways leading to calcific aortic valve stenosis by studying gene expression profile of normal and calcified stenotic human aortic valves. Circulation Cardiovascular genetics. 2009;2(5):489-98.
91. Huntington K, Hunter AG, Chan KL. A prospective study to assess the frequency of familial clustering of congenital bicuspid aortic valve. Journal of the American College of Cardiology. 1997;30(7):1809-12.
92. Kerstjens-Frederikse WS, Du Marchie Sarvaas GJ, Ruiter JS, Van Den Akker PC, Temmerman AM, Van Melle JP, et al. Left ventricular outflow tract obstruction: should cardiac screening be offered to first-degree relatives? Heart. 2011;97(15):1228-32.
93. McKellar SH, Tester DJ, Yagubyan M, Majumdar R, Ackerman MJ, Sundt TM, 3rd. Novel NOTCH1 mutations in patients with bicuspid aortic valve disease and thoracic aortic aneurysms. J Thorac Cardiovasc Surg. 2007;134(2):290-6.
94. Pepe G, Nistri S, Giusti B, Sticchi E, Attanasio M, Porciani C, et al. Identification of fibrillin 1 gene mutations in patients with bicuspid aortic valve (BAV) without Marfan syndrome. BMC medical genetics. 2014;15:23.
95. Nataatmadja M, West J, Prabowo S, West M. Angiotensin II Receptor Antagonism Reduces Transforming Growth Factor Beta and Smad Signaling in Thoracic Aortic Aneurysm. The Ochsner journal. 2013;13(1):42-8.
96. Nataatmadja M, West M, West J, Summers K, Walker P, Nagata M, et al. Abnormal extracellular matrix protein transport associated with increased apoptosis of vascular smooth muscle cells in marfan syndrome and bicuspid aortic valve thoracic aortic aneurysm. Circulation. 2003;108 Suppl 1:II329-34.
97. Hinton RB, Jr., Lincoln J, Deutsch GH, Osinska H, Manning PB, Benson DW, et al. Extracellular matrix remodeling and organization in developing and diseased aortic valves. Circulation research. 2006;98(11):1431-8.
98. Garcia J, Barker AJ, Murphy I, Jarvis K, Schnell S, Collins JD, et al. Four-dimensional flow magnetic resonance imaging-based characterization of aortic morphometry and haemodynamics: impact of age, aortic diameter, and valve morphology. Eur Heart J Cardiovasc Imaging. 2016;17(8):877-84.
99. Hope MD, Hope TA, Meadows AK, Ordovas KG, Urbania TH, Alley MT, et al. Bicuspid aortic valve: four-dimensional MR evaluation of ascending aortic systolic flow patterns. Radiology. 2010;255(1):53-61.

100. Moreno PR, Astudillo L, Elmariah S, Purushothaman KR, Purushothaman M, Lento PA, et al. Increased macrophage infiltration and neovascularization in congenital bicuspid aortic valve stenosis. J Thorac Cardiovasc Surg. 2011;142(4):895-901.
101. Deck JD, Thubrikar MJ, Schneider PJ, Nolan SP. Structure, stress, and tissue repair in aortic valve leaflets. Cardiovasc Res. 1988;22(1):7-16.
102. Smith KE, Metzler SA, Warnock JN. Cyclic strain inhibits acute pro-inflammatory gene expression in aortic valve interstitial cells. Biomechanics and modeling in mechanobiology. 2010;9(1):117-25.
103. Merryman WD, Schoen FJ. Mechanisms of calcification in aortic valve disease: role of mechanokinetics and mechanodynamics. Current cardiology reports. 2013;15(5):355.
104. Dweck MR, Jones C, Joshi NV, Fletcher AM, Richardson H, White A, et al. Assessment of valvular calcification and inflammation by positron emission tomography in patients with aortic stenosis. Circulation. 2012;125(1):76-86.
105. Marincheva-Savcheva G, Subramanian S, Qadir S, Figueroa A, Truong Q, Vijayakumar J, et al. Imaging of the Aortic Valve Using Fluorodeoxyglucose Positron Emission Tomography: Increased Valvular Fluorodeoxyglucose Uptake in Aortic Stenosis. Journal of the American College of Cardiology. 2011;57(25):2507-15.
106. Dweck MR, Khaw HJ, Sng GK, Luo EL, Baird A, Williams MC, et al. Aortic stenosis, atherosclerosis, and skeletal bone: is there a common link with calcification and inflammation? European heart journal. 2013;34(21):1567-74.
107. Tahara N, Kai H, Nakaura H, Mizoguchi M, Ishibashi M, Kaida H, et al. The prevalence of inflammation in carotid atherosclerosis: analysis with fluorodeoxyglucose-positron emission tomography. European heart journal. 2007;28(18):2243-8.
108. Tawakol A, Migrino RQ, Bashian GG, Bedri S, Vermylen D, Cury RC, et al. In vivo 18F-fluorodeoxyglucose positron emission tomography imaging provides a noninvasive measure of carotid plaque inflammation in patients. Journal of the American College of Cardiology. 2006;48(9):1818-24.
109. Tahara N, Kai H, Ishibashi M, Nakaura H, Kaida H, Baba K, et al. Simvastatin attenuates plaque inflammation: evaluation by fluorodeoxyglucose positron emission tomography. Journal of the American College of Cardiology. 2006;48(9):1825-31.
110. Dweck MR, Jenkins WS, Vesey AT, Pringle MA, Chin CW, Malley TS, et al. 18F-NaF Uptake Is a Marker of Active Calcification and Disease Progression in Patients with Aortic Stenosis. Circulation Cardiovascular imaging. 2014.
111. Irkle A VA, Lewis DY, Bird JLE, Dweck MR, Joshi FR, Gallagher FA, Warburton EA, Bennett MR, Brindle KM, Newby DE, Rudd JH, Davenport AP. . Identifying active vascular micro-calcification by 18F-sodium fluoride positron emission tomography. . Nature Comms. 2015.
112. WSA Jenkins AS, MAH Pringle, WJA Cowie, H Richardson, A Fletcher, R Pessotto, NA Boon, JHF Rudd, DE Newby, MR Dweck. 18F-NaF is a predictor of progression and outcome in Aortic Valve Disease. J Am Coll Cardiol 2014;63(12_S): doi:101016/S0735-1097(14)60995-5. 2014.

113. Baumgartner H, Hung J, Bermejo J, Chambers JB, Evangelista A, Griffin BP, et al. Echocardiographic assessment of valve stenosis: EAE/ASE recommendations for clinical practice. Journal of the American Society of Echocardiography : official publication of the American Society of Echocardiography. 2009;22(1):1-23; quiz 101-2.
114. Rosenhek R, Binder T, Porenta G, Lang I, Christ G, Schemper M, et al. Predictors of outcome in severe, asymptomatic aortic stenosis. The New England journal of medicine. 2000;343(9):611-7.
115. Cioffi G, Mazzone C, Faggiano P, Tarantini L, Di Lenarda A, Russo TE, et al. Prognostic stratification by conventional echocardiography of patients with aortic stenosis: the "CAIMAN-ECHO score". Echocardiography. 2013;30(4):367-77.
116. Messika-Zeitoun D, Aubry MC, Detaint D, Bielak LF, Peyser PA, Sheedy PF, et al. Evaluation and clinical implications of aortic valve calcification measured by electron-beam computed tomography. Circulation. 2004;110(3):356-62.
117. Liu F, Coursey CA, Grahame-Clarke C, Sciacca RR, Rozenshtein A, Homma S, et al. Aortic valve calcification as an incidental finding at CT of the elderly: severity and location as predictors of aortic stenosis. AJR American journal of roentgenology. 2006;186(2):342-9.
118. Koos R, Kuhl HP, Muhlenbruch G, Wildberger JE, Gunther RW, Mahnken AH. Prevalence and clinical importance of aortic valve calcification detected incidentally on CT scans: comparison with echocardiography. Radiology. 2006;241(1):76-82.
119. Aggarwal SR, Clavel MA, Messika-Zeitoun D, Cueff C, Malouf J, Araoz PA, et al. Sex differences in aortic valve calcification measured by multidetector computed tomography in aortic stenosis. Circulation Cardiovascular imaging. 2013;6(1):40-7.
120. Chin CWL, Khaw HJ, Luo E, Tan S, White AC, Newby DE, et al. Echocardiography Underestimates Stroke Volume And Aortic Valve Area: Implications For Patients With Small-Area Low-Gradient Aortic Stenosis. Canadian Journal of Cardiology. (0).
121. Clavel MA, Messika-Zeitoun D, Pibarot P, Aggarwal SR, Malouf J, Araoz PA, et al. The complex nature of discordant severe calcified aortic valve disease grading: new insights from combined Doppler echocardiographic and computed tomographic study. Journal of the American College of Cardiology. 2013;62(24):2329-38.
122. Feuchtner GM, Muller S, Grander W, Alber HF, Bartel T, Friedrich GJ, et al. Aortic valve calcification as quantified with multislice computed tomography predicts short-term clinical outcome in patients with asymptomatic aortic stenosis. The Journal of heart valve disease. 2006;15(4):494-8.
123. Koos R, Mahnken AH, Sinha AM, Wildberger JE, Hoffmann R, Kuhl HP. Aortic valve calcification as a marker for aortic stenosis severity: assessment on 16-MDCT. AJR American journal of roentgenology. 2004;183(6):1813-8.
124. Clavel MA, Pibarot P, Messika-Zeitoun D, Capoulade R, Malouf J, Aggarval S, et al. Impact of Aortic Valve Calcification, as Measured by MDCT, on Survival in Patients With Aortic Stenosis: Results of an International Registry Study. Journal of the American College of Cardiology. 2014;64(12):1202-13.

125. Messika-Zeitoun D, Bielak LF, Peyser PA, Sheedy PF, Turner ST, Nkomo VT, et al. Aortic valve calcification: determinants and progression in the population. Arteriosclerosis, thrombosis, and vascular biology. 2007;27(3):642-8.
126. Virginia Nguyen CCM, Candice Estellat MD, Isabelle Codogno MS, Virginie Huart PhD, Joelle Benessiano PharmD, Xavier Duval MD, Philippe Pibarot DVM, PhD g, Marie Annick Clavel ME-S, Alec Vahanian MD a, e, f, Messika-Zeitoun D. Hemodynamic and Anatomic Progression of Aortic Stenosis Heart. 2015.
127. Shen M, Tastet L, Capoulade R, Larose E, Bedard E, Arsenault M, et al. Effect of age and aortic valve anatomy on calcification and haemodynamic severity of aortic stenosis. Heart (British Cardiac Society). 2016.
128. Cartlidge TR, Pawade TA, Dweck MR. Aortic stenosis and CT calcium scoring: is it for everyone? Heart (British Cardiac Society). 2017;103(1):8-9.
129. Otto CM. Calcific aortic stenosis--time to look more closely at the valve. The New England journal of medicine. 2008;359(13):1395-8.
130. Price PA, Faus SA, Williamson MK. Bisphosphonates alendronate and ibandronate inhibit artery calcification at doses comparable to those that inhibit bone resorption. Arteriosclerosis, thrombosis, and vascular biology. 2001;21(5):817-24.
131. Fleisch H, Russell RG, Francis MD. Diphosphonates inhibit hydroxyapatite dissolution in vitro and bone resorption in tissue culture and in vivo. Science. 1969;165(3899):1262-4.
132. Rosenblum IY, Flora L, Eisenstein R. The effect of disodium ethane-1-hydroxy-1,1-diphosphonate (EHDP) on a rabbit model of athero-arteriosclerosis. Atherosclerosis. 1975;22(3):411-24.
133. Kramsch DM, Chan CT. The effect of agents interfering with soft tissue calcification and cell proliferation on calcific fibrous-fatty plaques in rabbits. Circulation research. 1978;42(4):562-71.
134. Sansoni P, Passeri G, Fagnoni F, Mohagheghpour N, Snelli G, Brianti V, et al. Inhibition of antigen-presenting cell function by alendronate in vitro. J Bone Miner Res. 1995;10(11):1719-25.
135. Giraudo E, Inoue M, Hanahan D. An amino-bisphosphonate targets MMP-9-expressing macrophages and angiogenesis to impair cervical carcinogenesis. The Journal of clinical investigation. 2004;114(5):623-33.
136. Lai TJ, Hsu SF, Li TM, Hsu HC, Lin JG, Hsu CJ, et al. Alendronate inhibits cell invasion and MMP-2 secretion in human chondrosarcoma cell line. Acta pharmacologica Sinica. 2007;28(8):1231-5.
137. Elmariah S CG, Fuster V, Badimon JJ. Bisphosphonates prevent oxidized low- density lipoprotein-induced expression of osteogenic markers in aortic valve myofibro- blasts. J Am Coll Cardiol. 2010;55(10 suppl 1):E1398.
138. Elmariah S, Delaney JA, O'Brien KD, Budoff MJ, Vogel-Claussen J, Fuster V, et al. Bisphosphonate Use and Prevalence of Valvular and Vascular Calcification in Women MESA (The Multi-Ethnic Study of Atherosclerosis). Journal of the American College of Cardiology. 2010;56(21):1752-9.
139. Innasimuthu AL, Katz WE. Effect of bisphosphonates on the progression of degenerative aortic stenosis. Echocardiography. 2011;28(1):1-7.

140. Skolnick AH, Osranek M, Formica P, Kronzon I. Osteoporosis treatment and progression of aortic stenosis. The American journal of cardiology. 2009;104(1):122-4.
141. Sterbakova G, Vyskocil V, Linhartova K. Bisphosphonates in calcific aortic stenosis: association with slower progression in mild disease--a pilot retrospective study. Cardiology. 2010;117(3):184-9.
142. Rapoport HS, Connolly JM, Fulmer J, Dai N, Murti BH, Gorman RC, et al. Mechanisms of the in vivo inhibition of calcification of bioprosthetic porcine aortic valve cusps and aortic wall with triglycidylamine/mercapto bisphosphonate. Biomaterials. 2007;28(4):690-9.
143. Aksoy O, Cam A, Goel SS, Houghtaling PL, Williams S, Ruiz-Rodriguez E, et al. Do bisphosphonates slow the progression of aortic stenosis? Journal of the American College of Cardiology. 2012;59(16):1452-9.
144. Dweck MR, Newby DE. Osteoporosis is a major confounder in observational studies investigating bisphosphonate therapy in aortic stenosis. Journal of the American College of Cardiology. 2012;60(11):1027; author reply
145. Cummings SR, San Martin J, McClung MR, Siris ES, Eastell R, Reid IR, et al. Denosumab for prevention of fractures in postmenopausal women with osteoporosis. The New England journal of medicine. 2009;361(8):756-65.
146. Helas S, Goettsch C, Schoppet M, Zeitz U, Hempel U, Morawietz H, et al. Inhibition of receptor activator of NF-kappaB ligand by denosumab attenuates vascular calcium deposition in mice. The American journal of pathology. 2009;175(2):473-8.
147. Dweck MR, Jenkins WS, Vesey AT, Pringle MA, Chin CW, Malley TS, et al. 18F-sodium fluoride uptake is a marker of active calcification and disease progression in patients with aortic stenosis. Circulation Cardiovascular Imaging. 2014;7(2):371-8.
148. Jenkins WS, Vesey AT, Shah AS, Pawade TA, Chin CW, White AC, et al. Valvular (18)F-Fluoride and (18)F-Fluorodeoxyglucose Uptake Predict Disease Progression and Clinical Outcome in Patients With Aortic Stenosis. Journal of the American College of Cardiology. 2015;66(10):1200-1.
149. Carter WA, Estes EH, Jr. Electrocardiographic Manifestations of Ventricular Hypertrophy; a Computer Study of Ecg-Anatomic Correlations in 319 Cases. Am Heart J. 1964;68:173-82.
150. Singh S, Goyal A. The origin of echocardiography: a tribute to Inge Edler. Texas Heart Institute journal. 2007;34(4):431-8.
151. Baumgartner H, Hung J, Bermejo J, Chambers JB, Edvardsen T, Goldstein S, et al. Recommendations on the Echocardiographic Assessment of Aortic Valve Stenosis: A Focused Update from the European Association of Cardiovascular Imaging and the American Society of Echocardiography. Journal of the American Society of Echocardiography : official publication of the American Society of Echocardiography. 2017;30(4):372-92.
152. Baumgartner H, Hung J, Bermejo J, Chambers JB, Edvardsen T, Goldstein S, et al. Recommendations on the Echocardiographic Assessment of Aortic Valve Stenosis: A Focused Update from the European Association of Cardiovascular Imaging and the American Society of Echocardiography. Journal Of The

American Society Of Echocardiography: Official Publication Of The American Society Of Echocardiography. 2017;30(4):372-92.
153. Smith LA, Cowell SJ, White AC, Boon NA, Newby DE, Northridge DB. Contrast agent increases Doppler velocities and improves reproducibility of aortic valve area measurements in patients with aortic stenosis. Journal of the American Society of Echocardiography : official publication of the American Society of Echocardiography. 2004;17(3):247-52.
154. Hawkins RA, Choi Y, Huang SC, Hoh CK, Dahlbom M, Schiepers C, et al. Evaluation of the skeletal kinetics of fluorine-18-fluoride ion with PET. Journal of nuclear medicine : official publication, Society of Nuclear Medicine. 1992;33(5):633-42.
155. Irkle A, Vesey AT, Lewis DY, Skepper JN, Bird JL, Dweck MR, et al. Identifying active vascular microcalcification by (18)F-sodium fluoride positron emission tomography. Nat Commun. 2015;6:7495.
156. Rudd JH, Myers KS, Bansilal S, Machac J, Rafique A, Farkouh M, et al. (18)Fluorodeoxyglucose positron emission tomography imaging of atherosclerotic plaque inflammation is highly reproducible: implications for atherosclerosis therapy trials. Journal of the American College of Cardiology. 2007;50(9):892-6.
157. Morgan-Hughes GJ, Owens PE, Roobottom CA, Marshall AJ. Three dimensional volume quantification of aortic valve calcification using multislice computed tomography. Heart. 2003;89(10):1191-4.
158. Litmanovich DE, Ghersin E, Burke DA, Popma J, Shahrzad M, Bankier AA. Imaging in Transcatheter Aortic Valve Replacement (TAVR): role of the radiologist. Insights into imaging. 2014;5(1):123-45.
159. Pawade TA, Cartlidge TR, Jenkins WS, Adamson PD, Robson P, Lucatelli C, et al. Optimization and Reproducibility of Aortic Valve 18F-Fluoride Positron Emission Tomography in Patients With Aortic Stenosis. Circulation Cardiovascular imaging. 2016;9(10).
160. Chen W, Dilsizian V. PET assessment of vascular inflammation and atherosclerotic plaques: SUV or TBR? Journal of nuclear medicine : official publication, Society of Nuclear Medicine. 2015;56(4):503-4.
161. Fayad ZA, Mani V, Woodward M, Kallend D, Abt M, Burgess T, et al. Safety and efficacy of dalcetrapib on atherosclerotic disease using novel non-invasive multimodality imaging (dal-PLAQUE): a randomised clinical trial. Lancet (London, England). 2011;378(9802):1547-59.
162. Critchley LA, Critchley JA. A meta-analysis of studies using bias and precision statistics to compare cardiac output measurement techniques. J Clin Monit Comput. 1999;15(2):85-91.
163. Aikawa E, Nahrendorf M, Sosnovik D, Lok VM, Jaffer FA, Aikawa M, et al. Multimodality molecular imaging identifies proteolytic and osteogenic activities in early aortic valve disease. Circulation. 2007;115(3):377-86.
164. Dweck MR, Chin C, Newby DE. Small valve area with low-gradient aortic stenosis: beware the hard hearted. Journal of the American College of Cardiology. 2013;62(24):2339-40.
165. Tawakol A, Migrino RQ, Bashian GG, Bedri S, Vermylen D, Cury RC, et al. In vivo 18F-fluorodeoxyglucose positron emission tomography imaging

provides a noninvasive measure of carotid plaque inflammation in patients. Journal of the American College of Cardiology. 2006;48(9):1818-24.
166. Rubeaux M, Joshi N, Dweck MR, Fletcher A, Motwani M, Thomson LE, et al. Motion correction of 18F-sodium fluoride PET for imaging coronary atherosclerotic plaques. Journal Of Nuclear Medicine: Official Publication, Society Of Nuclear Medicine. 2015.
167. Bonow RO, Carabello BA, Chatterjee K, de Leon AC. 2008 Focused update incorporated into the ACC/AHA 2006 guidelines for the management of patients with valvular heart disease: a report of the American College of Cardiology/American Heart Association Task Force on Practice Guidelines (Writing Committee to Revise the 1998 Guidelines for the Management of Patients With Valvular Heart Disease): endorsed by the Society of Cardiovascular Anesthesiologists, Society for Cardiovascular Angiography and Interventions, and Society of Thoracic Surgeons. Circulation. 2008;118(15):e523-661.
168. Clavel MA, Pibarot P, Messika-Zeitoun D, Capoulade R, Malouf J, Aggarval S, et al. Impact of aortic valve calcification, as measured by MDCT, on survival in patients with aortic stenosis: results of an international registry study. Journal of the American College of Cardiology. 2014;64(12):1202-13.
169. Utsunomiya H, Yamamoto H, Kitagawa T, Kunita E, Urabe Y, Tsushima H, et al. Incremental prognostic value of cardiac computed tomography angiography in asymptomatic aortic stenosis: significance of aortic valve calcium score. International journal of cardiology. 2013;168(6):5205-11.
170. Dweck MR, Chow MW, Joshi NV, Williams MC, Jones C, Fletcher AM, et al. Coronary arterial 18F-sodium fluoride uptake: a novel marker of plaque biology. Journal of the American College of Cardiology. 2012;59(17):1539-48.
171. Dweck MR, Khaw HJ, Sng GK, Luo EL, Baird A, Williams MC, et al. Aortic stenosis, atherosclerosis, and skeletal bone: is there a common link with calcification and inflammation? European heart journal. 2013;34(21):1567-74.
172. Vahanian A, Alfieri O, Andreotti F, Antunes MJ, Baron-Esquivias G, Baumgartner H, et al. [Guidelines on the management of valvular heart disease (version 2012). The Joint Task Force on the Management of Valvular Heart Disease of the European Society of Cardiology (ESC) and the European Association for Cardio-Thoracic Surgery (EACTS)]. G Ital Cardiol (Rome). 2013;14(3):167-214.
173. Minners J, Allgeier M, Gohlke-Baerwolf C, Kienzle RP, Neumann FJ, Jander N. Inconsistencies of echocardiographic criteria for the grading of aortic valve stenosis. European heart journal. 2008;29(8):1043-8.
174. Zhu D, Hadoke PW, Wu J, Vesey AT, Lerman DA, Dweck MR, et al. Ablation of the androgen receptor from vascular smooth muscle cells demonstrates a role for testosterone in vascular calcification. Sci Rep. 2016;6:24807.
175. Baumgartner H, Hung J, Bermejo J, Chambers JB, Evangelista A, Griffin BP, et al. Echocardiographic assessment of valve stenosis: EAE/ASE recommendations for clinical practice. Journal Of The American Society Of Echocardiography: Official Publication Of The American Society Of Echocardiography. 2009;22(1):1-23; quiz 101-2.

176. Chin CW, Pawade TA, Newby DE, Dweck MR. Risk Stratification in Patients With Aortic Stenosis Using Novel Imaging Approaches. Circulation Cardiovascular Imaging. 2015;8(8):e003421.
177. Cowell SJ, Newby DE, Burton J, White A, Northridge DB, Boon NA, et al. Aortic valve calcification on computed tomography predicts the severity of aortic stenosis. Clinical radiology. 2003;58(9):712-6.
178. Koos R, Mahnken AH, Sinha AM, Wildberger JE, Hoffmann R, Kuhl HP. Aortic valve calcification as a marker for aortic stenosis severity: assessment on 16-MDCT. AJR American Journal Of Roentgenology. 2004;183(6):1813-8.
179. Cueff C, Serfaty JM, Cimadevilla C, Laissy JP, Himbert D, Tubach F, et al. Measurement of aortic valve calcification using multislice computed tomography: correlation with haemodynamic severity of aortic stenosis and clinical implication for patients with low ejection fraction. Heart (British Cardiac Society). 2011;97(9):721-6.
180. Glasziou P, Irwig L, Deeks JJ. When should a new test become the current reference standard? Ann Intern Med. 2008;149(11):816-22.
181. Nguyen V, Cimadevilla C, Estellat C, Codogno I, Huart V, Benessiano J, et al. Haemodynamic and anatomic progression of aortic stenosis. Heart (British Cardiac Society). 2015;101(12):943-7.
182. Agatston AS, Janowitz WR, Hildner FJ, Zusmer NR, Viamonte M, Jr., Detrano R. Quantification of coronary artery calcium using ultrafast computed tomography. Journal of the American College of Cardiology. 1990;15(4):827-32.
183. Van Hoe LR, De Meerleer KG, Leyman PP, Vanhoenacker PK. Coronary artery calcium scoring using ECG-gated multidetector CT: effect of individually optimized image-reconstruction windows on image quality and measurement reproducibility. AJR American journal of roentgenology. 2003;181(4):1093-100.
184. Schlosser T, Hunold P, Voigtlander T, Schmermund A, Barkhausen J. Coronary artery calcium scoring: influence of reconstruction interval and reconstruction increment using 64-MDCT. AJR American journal of roentgenology. 2007;188(4):1063-8.
185. Matsuura N, Horiguchi J, Yamamoto H, Hirai N, Tonda T, Kohno N, et al. Optimal cardiac phase for coronary artery calcium scoring on single-source 64-MDCT scanner: least interscan variability and least motion artifacts. AJR American journal of roentgenology. 2008;190(6):1561-8.
186. van der Bijl N, de Bruin PW, Geleijns J, Bax JJ, Schuijf JD, de Roos A, et al. Assessment of coronary artery calcium by using volumetric 320-row multi-detector computed tomography: comparison of 0.5 mm with 3.0 mm slice reconstructions. The international journal of cardiovascular imaging. 2010;26(4):473-82.
187. Vliegenthart R, Song B, Hofman A, Witteman JC, Oudkerk M. Coronary calcification at electron-beam CT: effect of section thickness on calcium scoring in vitro and in vivo. Radiology. 2003;229(2):520-5.
188. Muhlenbruch G, Klotz E, Wildberger JE, Koos R, Das M, Niethammer M, et al. The accuracy of 1- and 3-mm slices in coronary calcium scoring using multi-slice CT in vitro and in vivo. European radiology. 2007;17(2):321-9.

189. Yoon HC, Goldin JG, Greaser LE, 3rd, Sayre J, Fonarow GC. Interscan variation in coronary artery calcium quantification in a large asymptomatic patient population. AJR American journal of roentgenology. 2000;174(3):803-9.
190. Willemink MJ, Takx RA, de Jong PA, Budde RP, Bleys RL, Das M, et al. The impact of CT radiation dose reduction and iterative reconstruction algorithms from four different vendors on coronary calcium scoring. European radiology. 2014;24(9):2201-12.
191. Horiguchi J, Yamamoto H, Akiyama Y, Hirai N, Marukawa K, Fukuda H, et al. Variability of repeated coronary artery calcium measurements by 16-MDCT with retrospective reconstruction. AJR American journal of roentgenology. 2005;184(6):1917-23.
192. Braverman AC, Guven H, Beardslee MA, Makan M, Kates AM, Moon MR. The bicuspid aortic valve. Curr Probl Cardiol. 2005;30(9):470-522.
193. Schnell S, Smith DA, Barker AJ, Entezari P, Honarmand AR, Carr ML, et al. Altered aortic shape in bicuspid aortic valve relatives influences blood flow patterns. Eur Heart J Cardiovasc Imaging. 2016.
194. Richards KE, Deserranno D, Donal E, Greenberg NL, Thomas JD, Garcia MJ. Influence of structural geometry on the severity of bicuspid aortic stenosis. Am J Physiol Heart Circ Physiol. 2004;287(3):H1410-6.
195. Chin CW, Everett RJ, Kwiecinski J, Vesey AT, Yeung E, Esson G, et al. Myocardial Fibrosis and Cardiac Decompensation in Aortic Stenosis. JACC Cardiovascular imaging. 2016.
196. Dweck MR, Joshi NV, Rudd JH, Newby DE. Imaging of inflammation and calcification in aortic stenosis. Current cardiology reports. 2013;15(1):320.
197. Osako MK, Nakagami H, Koibuchi N, Shimizu H, Nakagami F, Koriyama H, et al. Estrogen inhibits vascular calcification via vascular RANKL system: common mechanism of osteoporosis and vascular calcification. Circulation research. 2010;107(4):466-75.
198. Kim RY, Yang HJ, Song YM, Kim IS, Hwang SJ. Estrogen Modulates Bone Morphogenetic Protein-Induced Sclerostin Expression Through the Wnt Signaling Pathway. Tissue engineering Part A. 2015;21(13-14):2076-88.
199. Wilson PW, Kauppila LI, O'Donnell CJ, Kiel DP, Hannan M, Polak JM, et al. Abdominal aortic calcific deposits are an important predictor of vascular morbidity and mortality. Circulation. 2001;103(11):1529-34.
200. Iribarren C, Sidney S, Sternfeld B, Browner WS. Calcification of the aortic arch: risk factors and association with coronary heart disease, stroke, and peripheral vascular disease. Jama. 2000;283(21):2810-5.
201. Otto CM, Lind BK, Kitzman DW, Gersh BJ, Siscovick DS. Association of aortic-valve sclerosis with cardiovascular mortality and morbidity in the elderly. The New England journal of medicine. 1999;341(3):142-7.
202. McClelland RL, Chung H, Detrano R, Post W, Kronmal RA. Distribution of coronary artery calcium by race, gender, and age: results from the Multi-Ethnic Study of Atherosclerosis (MESA). Circulation. 2006;113(1):30-7.
203. Cote N, El Husseini D, Pepin A, Bouvet C, Gilbert LA, Audet A, et al. Inhibition of ectonucleotidase with ARL67156 prevents the development of calcific aortic valve disease in warfarin-treated rats. European journal of pharmacology. 2012;689(1-3):139-46.

204. Hung MY, Tsimikas S. What is the ultimate test that lowering lipoprotein(a) is beneficial for cardiovascular disease and aortic stenosis? Curr Opin Lipidol. 2014;25(6):423-30.
205. Nadir MA, Wei L, Elder DH, Libianto R, Lim TK, Pauriah M, et al. Impact of renin-angiotensin system blockade therapy on outcome in aortic stenosis. Journal of the American College of Cardiology. 2011;58(6):570-6.

APPENDIX 1

Saltire 2 SUMMARY:

Bisphosphonates and RANKL Inhibition in Aortic Stenosis. Study Protocol for Randomized controlled trial

1.0 STUDY DESIGN

Saltire 2 (NCT02132026) will be a prospective, randomized-controlled, double-blinded clinical trial. We have obtained the relevant approvals from the South East Scotland Ethics Committee and the Medicines and Health Regulatory Authority. This trial is being funded by the British Heart Foundation. 150 patients who fulfil the inclusion and exclusion criteria will be recruited from cardiology clinics at the Royal Infirmary of Edinburgh. Recruitment is anticipated to take one year with follow up lasting two years.

1.1 OBJECTIVES

The primary objective of this study is to determine whether denosumab or alendronic acid are able to slow or halt disease progression in aortic stenosis as measured by the computed tomography (CT) calcium score of the valve. Additional major objectives are to measure the impact of these drugs on active calcification in the valve and aortic valve jet velocity as measured by 18F-Fluoride PET and echocardiography respectively. Non-contrast CT will also be used to determine their effects on bone mineral density, aortic and coronary calcification. Finally we will measure parameters such as quality of life and 6 minute walk times.

1.2 ENDPOINTS

The primary endpoint of this study will be the aortic valve calcium score at 2 years.

Secondary endpoints will include i) change in aortic valve 18F-NaF uptake at 6 months determined by positron emission tomography, ii) change in aortic-jet velocity at two years determined by Doppler echocardiography, iii) change in thoracic aortic and coronary artery calcium score at two years determined by computed tomography,

iv) change in thoracic aorta and coronary 18F-Fluoride uptake at 6 months determined by positron emission tomography, v) change in thoracic spine bone mineral density at two years determined by quantitative computed tomography, vi) change in quality of life determined by SF-EQ 36.

1.3 PATIENT POPULATION

Participants attending cardiology clinics at the Royal Infirmary of Edinburgh who meet the inclusion and exclusion criteria will be invited to participate in the study and provided with an information sheet. We anticipate recruiting predominantly patients with mild and moderate aortic stenosis to minimize the number of patients referred for surgery during the course of the study Those who express an interest will then be invited to attend a screening visit where eligibility will be confirmed and written consent will be obtained.

Inclusion criteria

- age >50 years
- peak aortic jet velocity of >2.5 m/s on Doppler echocardiography
- grade 2-4 calcification of the aortic valve on echocardiography

Exclusion Criteria

- Anticipated or planned aortic valve surgery in the next 6 months,
- Life expectancy less than 2 years,
- Treatment for osteoporosis with bisphosphonates or denosumab.
- Known allergy or intolerance to alendronate or denosumab, or any of their excipients

- Abnormalities of the oesophagus or conditions, which delay oesophageal/gastric emptying.
- Inability to sit or stand for at least 30 minutes.
- Hypocalcaemia
- Regular calcium supplementation
- Dental extraction within 6 months
- Long-term corticosteroid use.
- History of osteonecrosis of the jaw
- Poor dental hygiene
- Major or untreated cancers
- Women of child-bearing potential who have experienced menarche, are pre-menopausal, have not been sterilized or who are currently pregnant.
- Women who are breastfeeding
- Renal failure (estimated glomerular filtration rate of <30 mL/min)
- Inability to undergo scanning
- Allergy or contraindication to iodinated contrast
- Inability or unwilling to give informed consent
- Likelihood of non-compliance to treatment allocation or study protocol.

1.4 RANDOMISATION

All recruited patients will first undergo baseline clinical assessment before randomisation. These include routine haematological and biochemical profiling, 12-lead electrocardiography, echocardiography, computed tomography aortic valve

calcium scoring and 18F-NaF positron emission tomography scanning. They will subsequently be randomised using a web-based computer-generated randomisation process with minimisation techniques employed to ensure balancing of key variables age (<73 and ≥73 years), sex, presence or absence of a bicuspid valve and baseline aortic valve calcium scores (‘≤1607, >1607 Agatston Units).

Seventy-five patients will be randomised (2:1) to either subcutaneous denosumab 60 mg (n=50) or matched placebo (n=25) every 6 months; and a further 75 will be randomised (2:1) to oral alendronate 70 mg (n=50) or matched placebo (n=25) once weekly (Figure 1.1). The active alendronate will be overencapsulated with lactose monohydrate in order to appear identical to the matched alendronate placebo which will consist of hard gelatin capsules containing lactose monohydrate. Denosumab is manufactured as a prefilled syringe therefore denosumab placebo will consist a 1mL subcutaneous injection of 0.9% saline solution. Both syringes will be covered in foil and administered only by a selected team of unblinded nurses.

Figure 1.1 Randomisation of study drugs

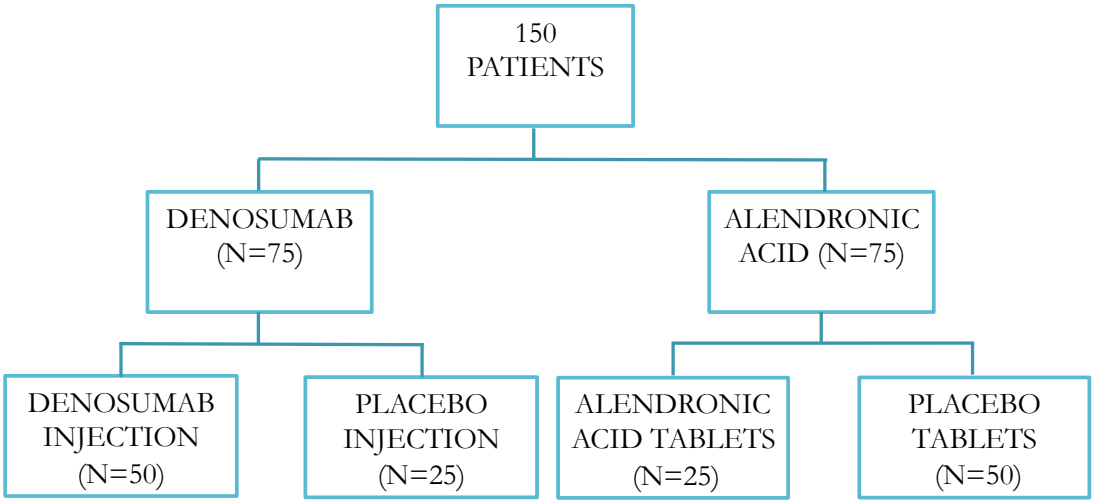

1.5 FOLLOW UP

Patients will then undergo 6 monthly assessments for 2 years.

1.5.1 Clinical Assessment: At 6, 12, 18 and 24 months, participants will undergo repeat clinical assessment which includes a clinical examination and assessment of their symptoms. Blood sampling and 12-lead electrocardiogram will also be performed. For those randomized to the tablet arm, compliance will be recorded by patient history and tablet count. At baseline and 24 months, patients will also be asked to complete a 6 minute walk test and a SF-36 Questionnaire.

1.5.2 Echocardiography: Aortic stenosis severity will be assessed at baseline and every 6 months by a single, dedicated research ultrasonographer to assess aortic stenosis severity using the peak aortic valve velocity, the mean gradient, aortic valve area and aortic valve calcification score.

1.5.3 Computed Tomography Calcium Scoring: Non-contrast CT calcium scoring of the aortic valve will be assessed at baseline, 12 months and 2 years. It will be performed using the same protocol and scanner (Biograph 128, Siemens) at each time point.

1.5.4 18F-Fluoride PET CT Imaging: Study scans will be performed at baseline and at 12 months.

1.5.5 Blood samples: These will be collected at baseline and 6, 12, 18 and 24 months. Blood samples will be used for routine clinical biochemistry and haematology. Blood will also be used for cardiac and bone biomarker measurements including troponin, galectin, brain natriuretic and C-Telopeptide. A single blood sample will also be taken for genotyping studies.

Table 1.1 Study Follow up

Test	Baseline	Rand-omisation	6 months	12 months	18 months	24 months
History & Examination	✔		✔	✔	✔	✔
18F-Fluoride PET-CT	✔			✔		
CT-AVC	✔		✔			✔
Echo	✔		✔	✔	✔	✔
12 lead ECG	✔		✔	✔	✔	✔
Biomarkers	✔		✔	✔	✔	✔
Biochemistry and Haematology	✔	✔	✔	✔	✔	✔
Blood for Genetic Analysis	✔					
SF-36 Questionnaire	✔					✔
6 minute Walk Test	✔					✔
Denosumab Administration		✔	✔	✔	✔	
Alendronate Dispensed		✔	✔	✔	✔	

Abbreviations: PET-CT, positron emission tomography- computed tomography; CT-AVC, computed tomography aortic valve calcium scoring; Echo, echocardiography; ECG, electrocardiography; SF, short form.

Figure 1.2 Study Design

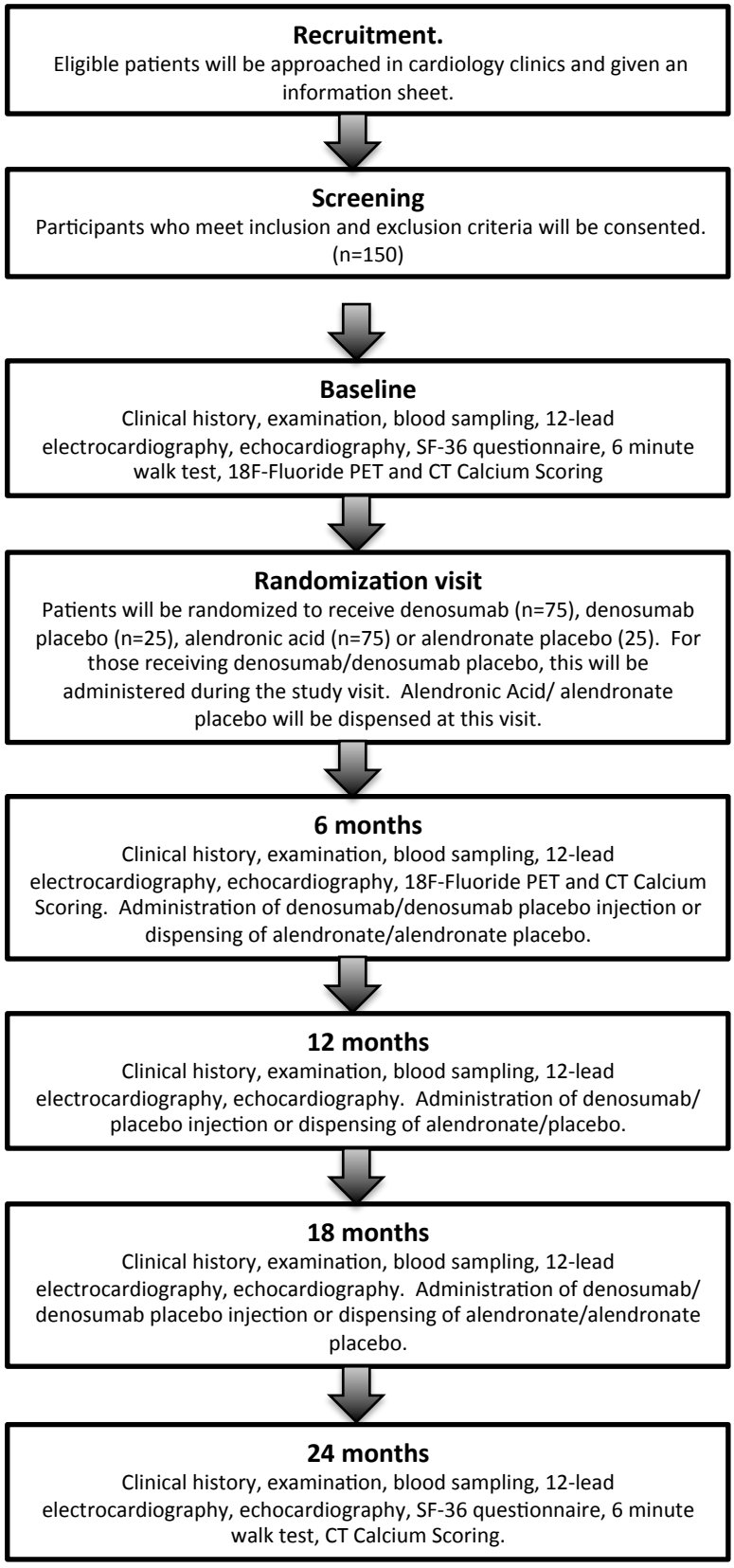

1.6 POWER CALCULATIONS

In the absence of pilot data, we powered the study based on what we considered to be a clinically relevant treatment effect of 40%. Using baseline and 2-year aortic valve calcium scores from patients with aortic stenosis from our previous studies. The change in aortic valve calcium score was skewed [median (interquartile range) 565 (190.5, 910.0)] so a log-transformation was applied to the data resulting in a mean (standard deviation) of 6.103 (0.867). To detect a difference of 40% in the back transformed mean aortic valve calcium score (i.e. 447.2 to 268.3) would need a sample size of 47 participants per group assuming a two-sided, two-sample test with 5% level of significance and 80% power. This calculation assumes that it is appropriate to combine both of the placebo arms to compare against denosumab and also alendronate. It also does not take into account multiple comparisons and to account for potential drop-outs we have increased the total sample size to 150.

1.7 DISCUSSION

Severe Aortic Stenosis is a major cause of morbidity and mortality. (9) Identification of an efficacious medical therapy for aortic stenosis would therefore potentially solve a global health issue and spare patients from the risks associated with aortic valve replacement or implantation. Even in the event of a negative result, an important outstanding question will have been addressed. Furthermore refinement and validation of 18F-Fluoride PET CT as an imaging modality capable of generating real time readouts of calcification activity could facilitate its application in future clinical studies on aortic stenosis which have previously relied on echocardiographic parameters.

Appendix 2

PUBLICATIONS ARISING FROM THIS THESIS

- Doris MK, Rubeaux M, **Pawade T** et al. Motion-corrected imaging of the aortic valve with $_{18}$F-NaF PET/CT and PET/MR: a feasibility study. *J Nucl Med*. 2017 May 25. (Epub ahead of print).
- Cartlidge TR, **Pawade TA**, Dweck MR. Aortic stenosis and CT calcium scoring: is it for everyone? *Heart*. 2017 Jan 1;103(1):8-9.
- **Pawade TA**, Cartlidge TRG, Jenkins WSA et al. Optimization and Reproducibility of Aortic Valve 18F-Fluoride Positron Emission Tomography in Patients with Aortic Stenosis. *Circ Cardiovasc Imaging*. 2016 Oct; 9(10).
- Chin CW, **Pawade TA**, Newby DE, Dweck MR.Risk Stratification in Patients With Aortic Stenosis Using Novel Imaging Approaches. *Circ Cardiovasc Imaging*. 2015 Aug;8(8):e003421.
- **Pawade TA**, Newby DE, Dweck MR. Calcification in Aortic Stenosis: The Skeleton Key. *J Am Coll Cardiol.* 2015 Aug 4;66(5):561-77.
- **Pawade TA**, Newby DE. Treating aortic stenosis: arresting the snowball effect. *Expert Rev Cardiovasc Ther*. 2015 May;13(5):461-3.

GRANTS RELATING TO THIS THESIS

2013 British Heart Foundation Scholarship, SS/CH/09/002/26360, £70 093.
2016 British Heart Foundation Clinical Research Training Fellowship, FS/16/19/31982, £204, 540.

JOURNAL OF THE AMERICAN COLLEGE OF CARDIOLOGY
© 2015 BY THE AMERICAN COLLEGE OF CARDIOLOGY FOUNDATION
PUBLISHED BY ELSEVIER INC.

VOL. 66, NO. 5, 2015
ISSN 0735-1097/$36.00
http://dx.doi.org/10.1016/j.jacc.2015.05.066

THE PRESENT AND FUTURE

STATE-OF-THE-ART REVIEW

Calcification in Aortic Stenosis

The Skeleton Key

Tania A. Pawade, MD,*† David E. Newby, MD, PhD,*† Marc R. Dweck, MD, PhD*†‡

ABSTRACT

Aortic stenosis is a common, potentially fatal condition that is set to become an increasing public health burden. Once symptoms develop, there is an inexorable deterioration with a poor prognosis. Despite this, there are no medical therapies capable of modifying disease progression, and the only available treatment is aortic valve replacement, to which not all patients are suited. Conventional teaching suggests that aortic stenosis is a degenerative condition whereby "wear and tear" leads to calcium deposition within the valve. Although mechanical stress and injury are important factors, it is becoming increasingly appreciated that aortic stenosis is instead governed by a highly complex, regulated pathological process with similarities to skeletal bone formation. This review discusses the pathophysiology of aortic stenosis with an emphasis on the emerging importance of calcification, how this can be visualized and monitored using noninvasive imaging, and how our improved knowledge may ultimately translate into novel disease-modifying treatments.
(J Am Coll Cardiol 2015;66:561–77) © 2015 by the American College of Cardiology Foundation.

Aortic stenosis is the most common form of valve disease in the Western world and is set to become an ever-increasing public health burden (1,2). Despite this, there are no medical therapies to halt or delay disease progression, and the only available treatment is aortic valve replacement or implantation, to which not all patients are suited. There is, therefore, a major unmet clinical need to identify pharmacological treatments capable of modifying this disease process.

Aortic stenosis was long considered to be a degenerative condition whereby "wear and tear" resulted in progressive calcium formation within the valve. Although mechanical stress and injury remain central to its pathophysiology, emerging evidence has indicated that aortic stenosis develops as part of a highly complex and tightly regulated series of processes, each of which may be amenable to medical intervention (3). In particular, aortic stenosis can be divided into 2 distinct phases: an early *initiation phase* dominated by valvular lipid deposition, injury, and inflammation, with many similarities to atherosclerosis, and a later *propagation phase* where pro-calcific and pro-osteogenic factors take over and ultimately drive disease progression (**Figure 1**) (4). This review discusses the pathophysiology of aortic stenosis, with an emphasis on the emerging importance of calcification, how this can be imaged with modern noninvasive techniques, and how our improved knowledge might ultimately lead to the development of novel therapies.

PATHOLOGY OF AORTIC STENOSIS

INFLAMMATION, LIPIDS, AND THE INITIATION PHASE OF AORTIC STENOSIS. Under normal circumstances, the aortic valve is composed of 3 leaflets, each of which is a thin (<1 mm), smooth, flexible, and

From the *British Heart Foundation/University of Edinburgh Centre for Cardiovascular Science, Edinburgh, United Kingdom; †Edinburgh Heart Centre, NHS Lothian, Edinburgh, United Kingdom; and the ‡Translational and Molecular Imaging Institute, Icahn School of Medicine at Mount Sinai, New York, New York. Drs. Pawade and Dweck and Prof. Newby are supported by the British Heart Foundation (SS/CH/09/002, FS/14/78, and CH/09/002); and are the Principal Investigators of the randomized controlled trial Saltire 2: Bisphosphonates and RANKL Inhibition in Aortic Stenosis (NCT02132026). Prof. Newby is also supported by a Wellcome Trust Senior Investigator Award (WT103782AIA).
Listen to this manuscript's audio summary by *JACC* Editor-in-Chief Dr. Valentin Fuster.

Manuscript received February 4, 2015; revised manuscript received May 26, 2015, accepted May 26, 2015.

ABBREVIATIONS AND ACRONYMS

BMP = bone morphogenetic protein

CT = computed tomography

FDG = fluorodeoxyglucose

LDL = low-density lipoprotein

OPG = osteoprotegerin

PET = positron emission tomography

RANK = receptor activator of nuclear factor kappa B

RANKL = receptor activator of nuclear kappa B ligand

TGF = transforming growth factor

VIC = valvular interstitial cell

mobile structure (3). In aortic stenosis, these leaflets become thickened, fibrosed, and calcified, resulting in reduced leaflet mobility and progressive valvular obstruction.

The early stages of aortic stenosis are in many ways similar to atherosclerosis. Indeed, the 2 conditions share many common risk factors, with large longitudinal studies consistently demonstrating that the *incidence* of aortic stenosis is linked to factors such as smoking, age, and hypertension (5–7). As in atherosclerosis, endothelial damage due to increased mechanical stress and reduced shear stress is believed to be the initiating injury, perhaps best illustrated by bicuspid valve disease. The characteristic 2-leaflet structure of these valves results in less efficient dissipation of mechanical stress and accelerated endothelial damage, so that patients almost universally develop aortic stenosis and display more rapid disease progression (8).

Following endothelial damage, the same lipids implicated in atherosclerosis infiltrate the valve, in particular, lipoprotein(a) and oxidized low-density lipoprotein (LDL) cholesterol. Consequently, observational studies have identified cholesterol and its related lipoproteins as independent risk factors for the development of aortic stenosis (5–7,9). Indeed, a strong genome-wide association was recently established between a single-nucleotide polymorphism in the locus of lipoprotein(a) and the incidence of aortic valve calcification (10). Progressive endothelial injury and lipid oxidization then establishes an inflammatory response within the valve that is characterized predominantly by infiltration of macrophages, but also involves T lymphocytes and mast cells (11). At this early stage, regions of stippled microcalcification that colocalize with sites of lipid deposition are observed (11). The formation of these microcalcifications may be mediated by cell death and the release of apoptotic bodies in these areas. Such apoptotic bodies are similar to the matrix vesicles found in bone, which contain the prerequisite components for calcium crystal deposition (including calcium and inorganic phosphate ions) and facilitate the formation of needle-like crystals of hydroxyapatite (4,12). In bone, as these hydroxyapatite crystals expand, they pierce the outer membrane of the vesicle and become exposed to the extracellular environment, thereby forming nucleation sites for further calcium deposition. It is probable that similar processes also occur within the valve (13). Furthermore, hydroxyapatite deposition evokes further proinflammatory responses from macrophages, creating a positive feedback loop of calcification and inflammation in the early stages of disease (14). It seems likely that these mechanisms underlie early calcium formation in aortic stenosis and its association with lipid and inflammation.

The apparent link between lipid, inflammation, and calcification in these early stages and the pathological similarities with atherosclerosis led to the hypothesis that statins might be beneficial in patients with aortic stenosis. This was supported by encouraging nonrandomized human data (15) and studies in hypercholesterolemic animal models demonstrating that lipid deposition and oxidative stress precede the conversion of valvular interstitial cells to those with an osteoblastic phenotype, and that this process is inhibited by atorvastatin (16,17). However, when statins were formally tested in 3 independent randomized controlled trials of patients with aortic stenosis, each demonstrated a failure of this therapy to halt or retard aortic stenosis progression, despite reducing the serum LDL cholesterol concentrations by more than one-half (18–20). This has led investigators to re-examine the pathophysiology underlying aortic stenosis and to the realization that although inflammation and lipid deposition may be important in establishing the disease (the initiation phase), the later stages are instead characterized by an apparently self-perpetuating cycle of calcium formation and valvular injury (the propagation phase) (4). Indeed, once this propagation phase has become established, disease progression is dictated neither by inflammation nor by lipid deposition, but rather by the relentless accumulation of calcium in the valve leaflets. This may explain the failure of statins to modify disease progression in aortic stenosis, which commonly presents beyond the initiation phase. Moreover, there is some data that statins may even be procalcific in the vasculature (21,22).

CALCIFICATION AND THE PROPAGATION PHASE. Skeletal bone formation is characterized by the initial deposition of collagen matrix, which provides a scaffold upon which progressive calcification can develop. With time, this calcium acquires a more ordered crystalline structure until the characteristic features of lamellar bone are finally observed. Similar structural processes are believed to occur in the aortic valve, with many of the same cell mediators and proteins implicated (23). Indeed, in aortic stenosis, collagen is deposited in anticipation of the procalcific processes that subsequently dominate. This fibrotic process within the valve may be mediated, in part, by reduced nitric oxide expression following endothelial injury (24); however, the renin-angiotensin system (RAS) is also believed to play a central

FIGURE 1 The Pathophysiology of Aortic Stenosis

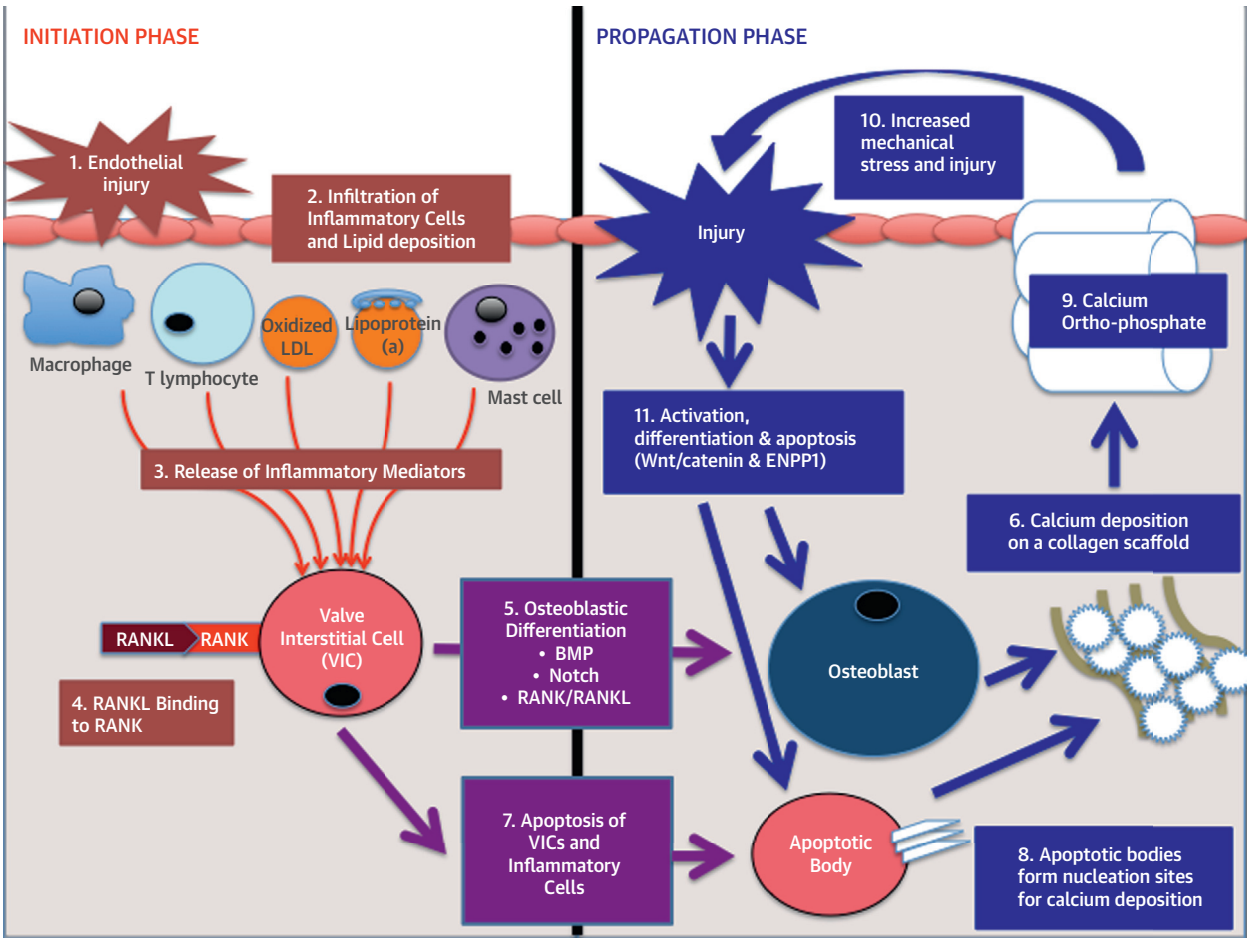

Initiation phase: endothelial injury **(1)** facilitates the infiltration of oxidized lipids and inflammatory cells **(2)** into the valve and the release of proinflammatory mediators **(3)**. These trigger the very early stages of valve calcification. The propagation phase: these proinflammatory processes subsequently induce VICs to undergo osteogenic differentiation **(5)** via several different mechanisms, including the binding of RANKL to RANK **(4)**. Differentiated cells within the aortic valve first lay down a collagen matrix and other bone-related proteins causing valvular thickening and stiffening before producing calcium **(6)**. Additionally, apoptotic remnants of some VICs and inflammatory cells **(7)** create a nidus for apoptosis-mediated calcification **(8)**. Calcification of the valve **(9)** induces compliance mismatch, resulting in increased mechanical stress and injury **(10)**. This results in further calcification via osteogenic differentiation and apoptosis **(11)**. Hence, a self-perpetuating cycle of calcification, valve injury, apoptosis, and osteogenic activation is established that drives the propagation phase of the disease. BMP = bone morphogenetic protein; ENPP1 = ectonucleotide pyrophosphate 1; LDL = low-density lipoprotein; RANK = receptor activator of nuclear kappa B; RANKL = receptor activator of nuclear kappa B ligand; RAS = renin-angiotensin system; VIC = valvular interstitial cell.

role. Angiotensin-converting enzyme (ACE) is up-regulated in calcific aortic valve disease and is likely to be delivered to the valve by LDL, its natural vehicle (25). Here it facilitates the conversion of angiotensin I to II, which mediates profibrotic effects via the angiotensin II type 1 (AT_1) receptor. Although angiotensin II is also able to mediate antifibrotic and anti-inflammatory effects via angiotensin II type 2 (AT_2) receptors, differential expression of these receptors in favor of AT_1 has been demonstrated in calcified aortic valves, so that a profibrotic profile dominates. Likewise, although angiotensin-converting enzyme type 2 (ACE-2) exerts antifibrotic and anti-inflammatory influences via the Ang1-7/Mas pathway, this pathway is down-regulated in calcified aortic stenosis, with reduced expression of both ACE-2 and Mas receptors in calcified valves compared with control subjects (26). Increased RAS expression is, therefore, implicated in the development of fibrosis within the valve. On a systemic level, RAS is implicated in the development of hypertension, which often accompanies aortic stenosis and

may accelerate its progression given the increased mechanical stress it imposes upon the valve (27).

Beyond this initial fibrosis, valvular calcification in aortic stenosis ultimately dominates and appears dependent upon the presence of osteoblast-like cells that develop an osteogenic phenotype. In support of this hypothesis, gene-profiling studies have demonstrated increased valvular expression of several osteoblast-specific proteins, including the Cbfa1/Runx2 transcription factor, essential for osteoblastic differentiation and regulation of osteoblast function (28,29). A number of other extracellular matrix proteins closely associated with osteoblast function and more commonly associated with skeletal bone formation are also up-regulated in calcific aortic valves. These include osteopontin and bone sialoprotein, which are facilitators of the attachment of osteoblasts to the bone matrix, and demonstrate up to a 7-fold elevation in gene expression at sites of developing calcification (30,31). Importantly, valvular ossification also appears to be dependent upon angiogenesis, supporting the hypothesis that this is an active, highly regulated, pathological process (23).

The source of osteoblast-like cells within the aortic valve remains controversial. In vitro, multiple cell types present in the vasculature are capable of undergoing differentiation into those with an osteoblast-like phenotype. The most likely candidate appears to be the myofibroblast, a highly plastic cell that is also commonly referred to as the valve interstitial cell (VIC) (32). The differentiation of this cell into an osteoblast phenotype is not fully characterized, but appears to be a central step in the development of aortic stenosis and is regulated by a rapidly growing list of molecules and complex pathways. In vivo molecular imaging has demonstrated that in the early stages of aortic stenosis, this differentiation appears coordinated by macrophages (33,34) via the action of proinflammatory cytokines (interleukin [IL]-1β, IL-6, IL-8, tumor necrosis factor [TNF]-α, insulin-like growth factor-1, and transforming growth factor [TGF]-β) (4,35,36). However, in the later stages, this differentiation again appears to be dominated by calcific pathways, including the Notch, Wnt/β-catenin, and receptor activator of nuclear factor kappa B (RANK)/receptor activator of nuclear factor kappa B ligand (RANKL)/osteoprotegerin (OPG) pathways, which we discuss here.

Notch belongs to a family of cell surface receptors (Notch 1 to 4) that are highly expressed in the aortic valve, playing an important role in its morphological development (37). Individuals with loss-of-function mutations in Notch-1 have higher rates of cardiovascular calcification and aortic stenosis. In 2 unrelated families with a high incidence of congenital aortic valve disease, genome-wide linkage analysis identified loss-of-function Notch-1 mutations as the cause (37). In particular, Notch-1 appears to be important in establishing osteogenic cells in the valve via the action of bone morphogenetic protein (BMP)-2 (38). BMP-2 is a potent osteogenic differentiation factor and part of a family of multifunctional cytokines belonging to the TGF-β superfamily. Expression of BMP-2 is increased in calcified atherosclerotic lesions and aortic valves (29,39), and it appears to have a central role in the differentiation of plastic cell populations toward an osteogenic phenotype. Indeed, exposure of normal human VICs to BMP-2 induces osteoblastic features in these cells (40,41). In addition, binding of Wnt to LDL receptor-related protein 5 receptors may activate the canonical Wnt/β-catenin pathway that is also implicated in osteogenic cell differentiation (42). Similarly, TGF-β1 is able to induce nuclear translocation of β-catenin and increased Wnt signaling, stimulating the osteogenic differentiation of mesenchymal progenitor cells (43). The latter process can increase in response to mechanical stress and may therefore explain, in part, the self-perpetuating and exponential increase in calcification activity observed once osteogenic differentiation has occurred and the propagation phase is established (**Figure 1**) (43,44).

Systemic regulators that govern calcification activity, both in the bone and in the vasculature, tightly control calcium homeostasis; consequently, there is an inverse correlation between bone mineral density and vascular calcification. Osteoporosis is associated with age-independent increases in vascular calcification and even cardiovascular mortality (45). A prospective study of 25,639 men and women demonstrated an inverse correlation between bone mineral density and incident aortic stenosis in older women (46). Moreover, other disorders of bone turnover, including chronic kidney disease and Paget's disease, also manifest changes in the vasculature (47–50). This dichotomy has been termed the "calcification paradox" and is likely to be explained by common pathological pathways having reciprocal effects on the bone and vasculature simultaneously.

A potential mechanism for this association lies in the activity of the RANK/RANKL/OPG pathway (**Figure 2A**). In bone, RANKL (a member of the TNF cytokine family) binds to RANK (a transmembrane protein expressed on marrow stromal cells and pre-osteoclasts), acting as a potent inducer of osteoclast

differentiation and activity. This drives demineralization of bone, but is policed by osteoprotegerin (OPG), a soluble decoy receptor, which binds RANKL and prevents it from activating RANK (**Figure 2**). In contrast, RANKL appears to have the opposite effect on cells in the vasculature, inducing an osteoblastic phenotype in human VIC cells that results in increased matrix calcification, the formation of calcific nodules, and increased expression of alkaline phosphatase and osteocalcin (**Figure 2A**) (51). RANKL also promotes the osteogenic properties of vascular smooth muscle cells, once again via the up-regulation of BMP-2. As a consequence, whilst OPG-deficient mice develop osteoporosis, they simultaneously accelerate vascular calcification in association with increased expression of RANKL in both regions (52). A potential explanation for the differential effects of RANK/RANKL/OPG in these 2 tissues is that in bone there is an abundance of pre-osteoclasts that favors the pro-osteoclastic properties of RANKL (36). In contrast, this pool is absent in the vasculature so that RANKL's pro-osteoblastic effects on myofibroblast and smooth muscle cells predominate.

Imbalances in RANKL/OPG signaling have been demonstrated in calcific aortic valves. In human valve tissue taken from patients with aortic stenosis, immunochemistry revealed less OPG-positive cells in areas of focal calcification, whereas western blotting demonstrated that OPG was not expressed at relevant levels in aortic stenosis, but was detectable in control subjects. The converse is true of RANKL, with increased levels observed in stenotic aortic valves (51). In combination, these data support the hypothesis that the RANK/RANKL/OPG axis is implicated in the development of aortic valve calcification and provide 1 explanation for the link between aortic valve calcification and bone mineral density. Other investigators have suggested that the differential effects of oxidized LDL might also be of importance, with this molecule appearing to promote calcification and the osteoblastic differentiation of vascular cells in vitro, whilst inhibiting these processes in a bone-derived pre-osteoblast cell line (4,53,54).

Fetuin-A is a circulating protein that can exist in isolation or as a complex with matrix γ-carboxyglutamic acid protein (MGP). Both are powerful guardians against ectopic calcification and simultaneously inhibit many of the procalcific processes discussed earlier (55). MGP needs to be both carboxylated and phosphorylated to be activated, a process dependent on vitamin K. There is speculation that use of the vitamin K antagonists, such as coumarins, may be associated with increased vascular calcification (56). The actions of fetuin-A and MGP include inhibition of BMP2 and TGF-β, reduction of apoptosis-mediated calcification, and direct prevention of calcification by binding to calcium crystals. Reduced circulating levels of Fetuin-A and MGP are thought to explain the vascular calcification seen with end-stage renal failure. Moreover, plasma fetuin-A concentrations are decreased in aortic stenosis and inversely associated with the rate of disease progression (57,58). Interestingly, this association was seen only in older patients (>70 years of age) (59). Conversely, increased plasma dephosphorylated (inactive) MGP was a strong independent predictor of faster stenosis progression, but only in younger patients (≤57 years of age) (60).

WHY DOES CALCIUM BEGET CALCIUM? Once calcification is established in the valve, it would appear to initiate further calcium formation. This self-perpetuating cycle of calcification and valve injury appears to be the central driver of *disease progression* and the propagation phase of aortic stenosis (**Figure 1**).

The mechanism for this may, in part, relate to the compliance mismatch caused by calcific deposits in the leaflets that results in increased mechanical stress, injury-induced activation of the Wnt/β-catenin pathway, and further osteoblast differentiation. However, it may also be explained by the actions of membrane-bound ectonucleotidases. These are produced by VICs and regulate the extracellular production of inorganic phosphate (a promoter of calcification) and inorganic pyrophosphate, an inhibitor of pyrophosphate. Ectonucleotide pyrophosphatase 1 (ENPP1) is highly up-regulated in calcific aortic valve disease, with a polymorphism associated with increased transcripts of ENPP1 identified in stenotic valves (61). Hydrolysis of extracellular adenosine triphosphate (ATP) by ENPP1 produces a net increase in inorganic phosphate, thus favoring calcification and promoting the production of further ENPP1 in a positive feedback loop (61). Moreover, because ATP acts as a cell survival signal for VICs via the $P2Y_2$ receptor, its depletion also triggers apoptosis of these cells, providing a further key stimulus to calcification (61). Finally, loss of $P2Y_2$ signaling increases the secretion of IL-6, a cytokine that promotes further osteogenic differentiation of VICs via the actions of BMP (62). Thus, via these multiple mechanisms, the ectonucleotidase pathway appears to have a central role in amplifying procalcific processes within the valve during the propagation phase of aortic stenosis.

Given that the pathophysiology and the progression of aortic stenosis are dominated by calcification,

FIGURE 2 Mechanisms Underlying the Relationship Between Bone Mineral Density and Valvular Calcification and Potential Mechanisms of Action for Denosumab and Bisphosphonates

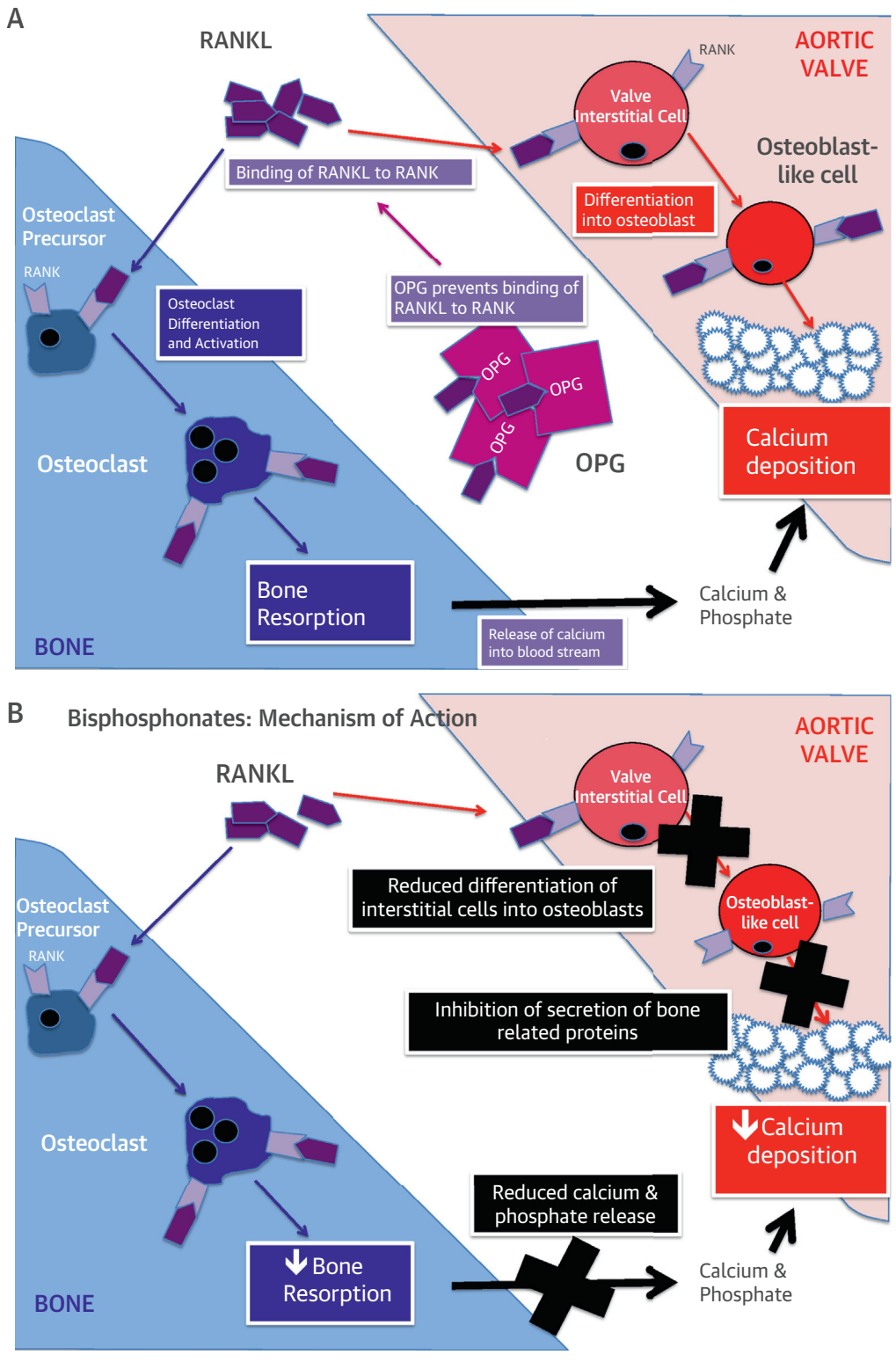

Continued on the next page

FIGURE 2 Continued

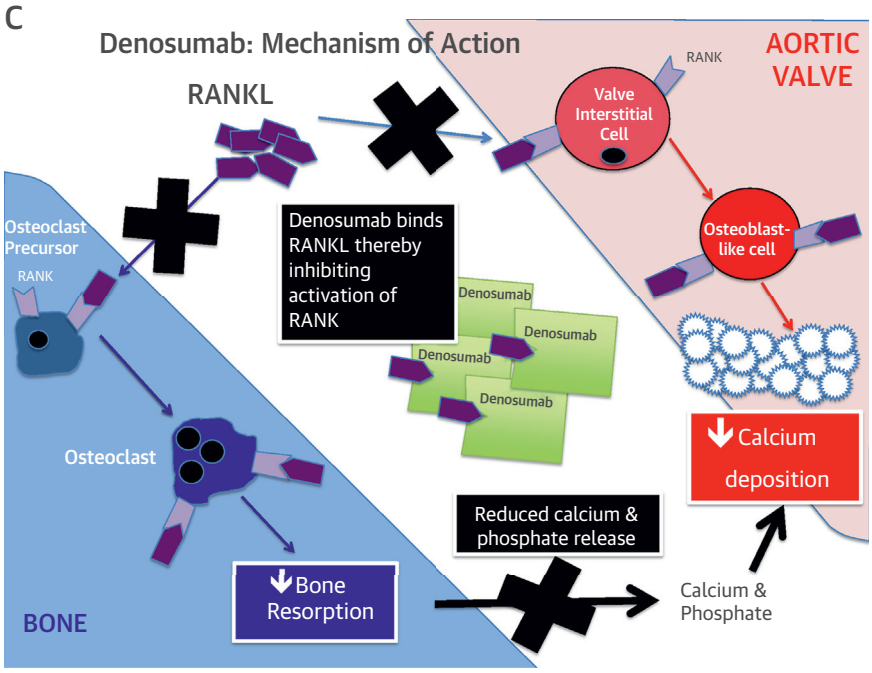

(A) Schematic representation of the differential effects of the RANK/RANKL/OPG axis upon skeletal bone and the calcifying aortic valve. Aortic valve: binding of RANKL to RANK on valvular interstitial cells induces osteogenic differentiation and calcium deposition. Bone: binding of RANKL to RANK on osteoclast precursors induces osteoclastic maturation and differentiation, resulting in bone resorption and increased availability of calcium and phosphate. Osteoprotegerin binds to RANKL, preventing it from binding to RANK, thus reducing both bone resorption and calcium deposition within the valve. **(B)** Proposed mechanism of action of bisphosphonates in the treatment of aortic stenosis. Bisphosphonates reduce the production of inflammatory cytokines, thereby reducing osteogenic differentiation of VICs. They also inhibit the production of matrix metalloproteinases and regulate extracellular mineralization within the vasculature. Simultaneously, the prevention of bone resorption by bisphosphonates also reduces the availability of procalcific substances. In combination, this is likely to result in reduced calcium deposition in the valve, along with reduced bone resorption. **(C)** Proposed mechanism of action of denosumab in the treatment of aortic stenosis. Binding of denosumab to RANKL prevents its binding to RANK, which inhibits the osteogenic differentiation of valvular interstitial cells. It simultaneously prevents osteoclast differentiation in the bone, and inhibits bone resorption and availability of procalcific substances. In combination, this is likely to result in reduced calcium deposition in the valve and reduced bone resorption. OPG = osteoprotegerin; other abbreviations as in Figure 1.

we will next discuss how this process can be imaged to better understand the pathophysiology of aortic stenosis, to predict disease progression and clinical outcomes, and to help develop novel treatments strategies for this common and potentially fatal condition.

CLINICAL IMAGING OF AORTIC VALVE CALCIFICATION

The burden and activity of aortic valve calcification can be measured using noninvasive imaging. In particular, echocardiography, computed tomography (CT), and positron emission tomography (PET) can all be used to provide progressively more detailed assessments of the calcific processes occurring within the valve (Figure 3). These techniques have not only informed our understanding as to the importance of calcification in aortic stenosis, but have also aided our ability to assess disease severity and to predict progression and adverse cardiovascular outcomes. The latter is of particular importance. Aortic stenosis progression frequently does not occur in a linear or predictable manner, making estimation as to when valve replacement will be required challenging. Annual or biannual clinical review is generally required, with serial echocardiography performed to track progressive valve narrowing. The development of a noninvasive method capable of predicting the future natural history of aortic stenosis and the likely timing of valve surgery would represent a major advance and help streamline patient care. Given

FIGURE 3 Different Methods for Imaging Calcification in a Single Subject With Aortic Stenosis

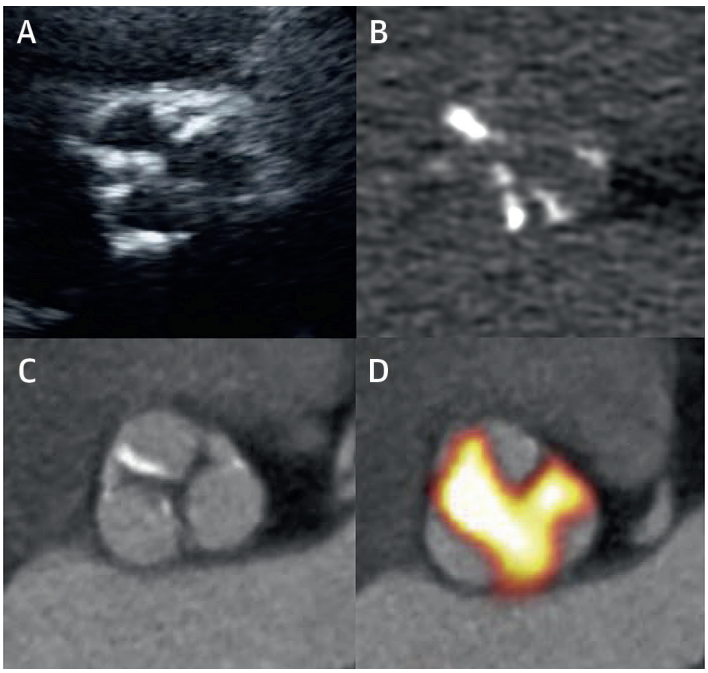

(A) 2-dimensional echocardiography. **(B)** CT calcium scoring. **(C)** CT angiography. **(D)** 18F-fluoride PET-CT. CT = computed tomography; PET = positron emission tomography.

the central role that mineralization plays in disease progression, it is, perhaps, not surprising that assessments of aortic valve calcification have, to date, provided the best prediction.

ECHOCARDIOGRAPHY

Echocardiography is a cheap, safe, and widely used method of assessing aortic stenosis severity in the clinical setting. International guidelines recommend grading aortic stenosis severity using the following hemodynamic echocardiographic assessments: the peak velocity, the mean gradient, and the aortic valve area (63). However, echocardiography can also be used to categorize valves according to their degree of valvular calcification into those with no, mild, moderate, and severe calcification. Indeed, in a series of 128 patients with severe, asymptomatic aortic stenosis, this semiquantitative assessment provided powerful prognostic information, acting as a strong independent predictor of death or aortic valve replacement that outperformed the more conventional hemodynamic measures (64). Although this observation has been confirmed in another study of 141 asymptomatic patients (65), the clinical utility of this approach has been limited by disappointing interobserver agreement in grading the calcification (66,67).

CT CALCIUM SCORING

CT provides a much more detailed, reproducible, and accurate assessment of the calcific burden in the aortic valve than echocardiography (66). Using the same protocols used for coronary calcium scoring, electrocardiography-gated noncontrast CT can provide information with respect to the density, volume, and mass of macroscopic calcium deposits within the valve (66). However, as in the coronary arteries, the aortic valve calcium burden is generally described using Agatston units (AU), which take both the radiodensity and volume of calcium into account. In a series of explanted aortic valves, scores of 500, 1,100, and 2,000 AU approximated to 300, 1,100, and 1,200 mg of aortic valve calcium, respectively (66).

Early studies demonstrated that CT calcium scoring of the aortic valve could be used as an alternative marker of stenosis severity, demonstrating a good relationship with hemodynamic echocardiographic assessments (66,68,69). However, until recently, we lacked appropriate thresholds that might differentiate patients with and without severe aortic stenosis, thereby limiting its utility (**Table 1**) (70). These thresholds are now available as a consequence of a landmark series of papers published by Clavel et al. (71–73). Across 3 sites in Europe and North America, they performed both echocardiography and CT calcium scoring in 646 patients with moderate or severe aortic stenosis and good left ventricular function. In those subjects whose severity of stenosis was not in doubt on echocardiography (n = 460), the authors examined the optimal CT calcium score for differentiating moderate from severe aortic stenosis. Interestingly, female subjects required less calcium to develop severe hemodynamic stenosis than male subjects (even after correcting for body surface area and the left ventricular outflow tract area calculated by echocardiography), so that the optimal thresholds were found to be 1,275 AU in women and 2,065 AU in men. These thresholds then appeared to be of use in adjudicating the severity of the stenosis when echocardiographic markers were discordant. More importantly, the authors went on to demonstrate that, in a population of 794 patients, these thresholds predicted all-cause mortality independent of all other markers of an adverse prognosis (73). Standard hemodynamic parameters on echocardiography were included in this analysis, suggesting that CT can provide additional, complementary information to

TABLE 1 Studies Attempting to Define Computed Tomography Calcium Scoring Thresholds for the Diagnosis of Aortic Stenosis

First Author (Ref. #)	Year	n	Method and Criteria for Defining Severe Aortic Stenosis	Calcium Score Threshold (AU)	Sensitivity	Specificity	Positive Predictive Value	Negative Predictive Value
Cowell et al. (107)	2003	157	Echocardiography aortic valve velocity >4 m/s	>3,700	100	50	39	100
Messika-Zeitoun et al. (66)	2004	100	Echocardiography aortic valve area <1 cm^2	>500	100	69	57	100
Koos et al. (74)	2004	72	Cardiac catheter aortic valve area <1 cm^2	>563	85	92	95	77
Clavel et al. (72)	2013	460	Echocardiography aortic valve area index ≤0.6 cm^2/m^2, mean gradient ≥40 mm Hg	>1,274 (women) >2,065 (men)	86 89	89 80	93 88	79 82
Cueff et al. (108)	2011	179	Echocardiography aortic valve area <1 cm^2	>1,651	82	80	70	88
Cueff et al. (108)	2011	20	Echocardiography low flow/low gradient severe AS Aortic valve area <1 cm *and* ejection fraction ≤40% *and* mean pressure gradient ≤40 mm Hg[2]	>1,651	95	89	97	80

Values are % unless otherwise indicated.
AS = aortic stenosis; AU = Agatston units.

that obtained during routine clinical care, as had previously been hinted at by earlier studies (**Table 2**) (66,73-75).

An expanding body of published data has also demonstrated the ability of CT calcium scoring to predict disease progression in aortic stenosis. Initial studies indicated that the aortic valve CT calcium score progresses fastest in patients with the highest baseline calcium burden (76). We have recently confirmed this predictive ability in a large prospective study of patients with the full range of calcific aortic valve disease. The fastest rates of progression were again observed in subjects with the most advanced disease. Indeed, a good correlation was observed between the baseline calcium score and disease progression at 1 year ($r = 0.58$; 95% confidence interval [CI]: 0.15 to 0.82; $p = 0.01$) (77), which strengthened further after 2 years of follow-up ($r = 0.90$; 95% CI: 0.84 to 0.93; $p < 0.001$) (67). Moderate associations between the baseline CT calcium score and echocardiographic measures of disease progression were also observed (e.g., change in mean gradient; $r = 0.40$; 95% CI: 0.21 to 0.56; $p < 0.001$) (67), and very similar observations were recently reported in a different patient population (**Figure 4**) (78).

In summary, CT calcium would, therefore, appear to be a useful alternative method for grading disease severity in aortic stenosis, offering powerful

TABLE 2 Studies Using Aortic Valve Computed Tomography Calcium Scoring to Predict Outcomes

First Author (Ref. #)	Year	n	Duration of Follow-Up	Outcomes	Key Findings
Messika-Zeitoun et al. (66)	2004	100	2.0 ± 2.3 yrs	Event-free survival Survival without dyspnea, angina, syncope, heart failure, or need for surgery	AVC independently predicted event-free survival, with an adjusted relative risk of 1.06 (95% CI: 1.02–1.10) per 100-AU increment ($p < 0.001$). 5-year event free survival rate was 90 ± 4% for those with AVC <500 AU vs. 29 ± 14% for those with AVC ≥500 AU ($p < 0.0001$).
Feuchtner et al. (73)	2006	34	18–24 months	Major adverse clinical event Symptoms due to hemodynamic progression Cardiac death	AVC strongest predictor of a major adverse clinical event ($p < 0.001$) among all parameters assessed (1,928 ± 789 AU vs. 5,111 ± 2,409 AU).
Utsunomiya et al. (109)	2013	64	29 months	Cardiac events Cardiac death, AVR, nonfatal MI, and heart failure requiring urgent hospitalization	AVC predictor of cardiac events (HR: 1.09; 95% CI: 1.04–1.15) per 100-AU increment AVCS ≥723 (the median value) had significantly worse outcomes than those with AVCS <723 ($p < 0.0001$)
Clavel et al. (75)	2014	794	3.1 ± 2.6 yrs	Mortality	Severe AVC (defined as ≥1,274 AU in women and ≥2,065 AU in men) was an independent predictor of overall mortality (HR: 1.71; 95% CI: 1.12 to 2.62; $p = 0.01$)

AU = Agatston units; AVC = aortic valve calcium; AVCS = aortic valve calcium score; AVR = aortic valve replacement; CI = confidence interval; HR = hazard ratio; MI = myocardial infarction.

FIGURE 4 Relationship Among Baseline Disease Severity, Disease Activity, and Disease Progression

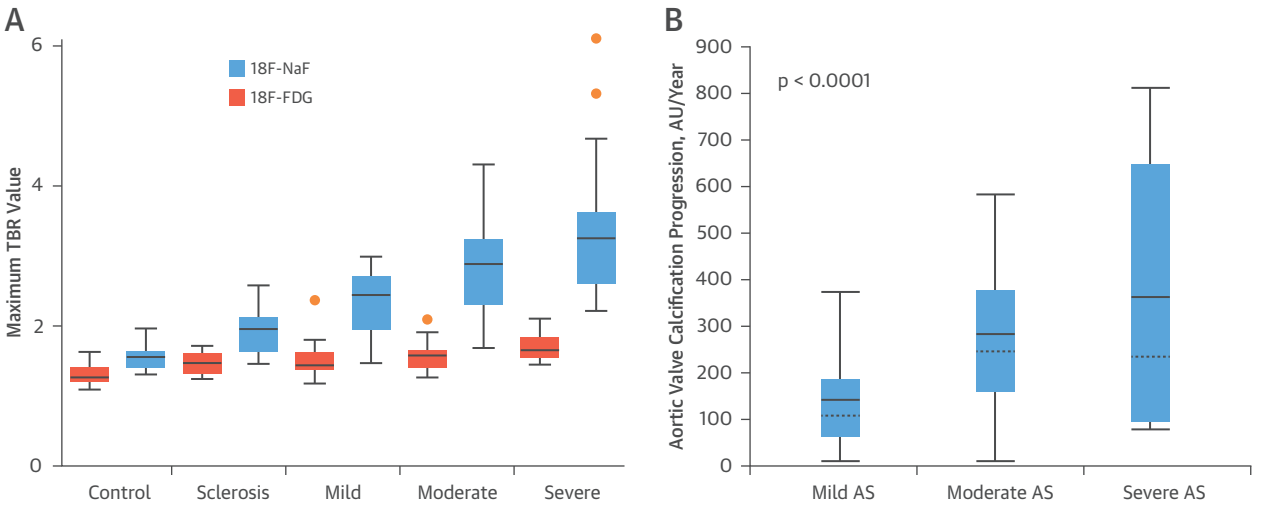

(A) Studies using PET have demonstrated that calcification activity in the valve (as measured using ^{18}F-fluoride) steadily increases with disease severity. As a consequence, activity is highest in those with the most advanced disease, and a good correlation exists between ^{18}F-fluoride activity and the baseline CT calcium score (79). **(B)** Subsequently, this increased calcification activity appears to translate to more rapid disease progression (as measured by both echocardiography and CT calcium scoring) in patients with the most advanced forms of aortic stenosis (78). Reproduced with permission from Nguyen V, et al. (78). AS = aortic stenosis; AU = Agatston units; CT = computed tomography.

prediction of both disease progression and adverse clinical events. It is potentially complementary to standard echocardiographic assessments and may have some advantages, most notably that it is not dependent on cardiac loading conditions, geometric assumptions, or on the presence of other cardiovascular conditions, such as mitral regurgitation and hypertension. Further work is now required to validate the proposed thresholds in other patient populations and to explain the observed sex differences.

POSITRON EMISSION TOMOGRAPHY

PET is a noninvasive imaging technique that allows the activity of specific biological processes to be measured in vivo within specific structures, including the aortic valve. In principle, any disease process can be evaluated dependent on the availability of a suitable tracer. To date, studies in aortic stenosis have largely investigated tracers targeted to inflammation (^{18}F-fluorodeoxyglucose [FDG]) and calcification (^{18}F-fluoride), aiming to establish the relative contributions of these processes to disease development and progression (79–81).

INFLAMMATION. The PET radiotracer ^{18}F- FDG is a glucose analog taken up by metabolically active cells. Because it is unable to proceed through the glycolytic pathway, it accumulates within these cells without further metabolism. Because vascular macrophages have higher metabolic requirements than the surrounding tissue, ^{18}F-FDG has emerged as a useful tool for the identification of vascular inflammation. Uptake in regions of carotid atheroma correlates well with macrophage density (mean percent staining of CD68-positive cells, $r = 0.85$; $p < 0.0001$) (82,83) and is modifiable with statin therapy (84).

To determine the contribution of inflammation to the pathogenesis of calcific aortic stenosis, we performed PET imaging of the aortic valve using ^{18}F-FDG in a prospective cohort of 121 patients with the full spectrum of calcific aortic valve disease (including 20 patients with aortic sclerosis and 20 control subjects) (79). ^{18}F-FDG activity was increased in patients with aortic stenosis compared with control subjects (1.58 ± 0.21 vs. 1.30 ± 0.13; $p < 0.001$), and this correlated with disease severity (79). However, unlike previous work on carotid atheroma, the ^{18}F-FDG signal did not correlate with macrophage (CD68) staining, raising the possibility that ^{18}F-FDG may not be acting as a marker of inflammation in the calcifying aortic valve, but instead might reflect glucose utilization by other metabolically-active cells, such as myofibroblasts or differentiated osteogenic cells (77).

CALCIFICATION. ^{18}F-fluoride has been used safely as a bone tracer for more than 40 years, exchanging with hydroxyl groups in hydroxyapatite to form fluoroapatite. Similar hydroxyl bonds are also present in the different forms of calcium in the vasculature (including hydroxyapatite and amorphous calcium) so that ^{18}F-fluoride binding acts as a marker of vascular calcification. In particular, the binding of ^{18}F-fluoride to calcium appears to be critically dependent upon the surface area of calcium orthophosphate available for incorporation. ^{18}F-fluoride, therefore, preferentially binds regions of newly developing microcalcification (beyond the resolution of CT), which have a nanocrystalline structure and very high surface area, rather than to large, established, macroscopic deposits, where much of the calcium is internalized and, therefore, not available for binding (85). On this basis, increased ^{18}F-fluoride uptake is observed in regions of actively developing calcification, demonstrating a close association with alkaline phosphatase staining ($r = 0.65$; $p = 0.04$) on excised aortic valve tissue removed at the time of surgery (77).

When the same cohort of 121 patients was imaged with ^{18}F-fluoride, the observed PET signal in the aortic valve was stronger and more clearly demarcated than was seen with ^{18}F-FDG (**Figure 3**). Moreover, the spatial distribution of the ^{18}F-fluoride signal was often discrete from the macroscopic calcium deposits identified by CT, indicating that ^{18}F-fluoride uptake provides distinct, but complementary information to CT alone. Uptake was increased in patients with aortic stenosis compared with healthy control subjects (2.87 ± 0.82 vs. 1.55 ± 0.17; $p < 0.001$) and correlated with disease severity ($r = 0.73$; $p < 0.001$) (79). Indeed, the highest calcification activity, as measured using this tracer, was observed in patients with the most advanced disease (**Figure 4A**). Again, this supports the hypothesis that calcification begets calcification activity in aortic stenosis and would explain the rapid rates of disease progression in those at the severe end of the spectrum.

When patients were recalled for repeat CT calcium scoring of the valve at 1 and 2 years, new calcium could be observed in the areas of increased ^{18}F-fluoride activity seen on the baseline scan (**Figure 5**). As a consequence, a close correlation was observed between the baseline valvular ^{18}F-fluoride uptake and the progression of the aortic valve CT calcium score ($r = 0.80$; 95% CI: 0.69 to 0.87; $p < 0.001$), with PET appearing to offer some additional predictive information over and above the baseline calcium score. Moreover, this translated into an ability to predict valve hemodynamic progression, with moderate correlations also observed between ^{18}F-fluoride activity and the mean ($r = 0.32$; 95% CI: 0.13 to 0.50; $p = 0.001$) and peak ($r = 0.32$; 95% CI: 0.12 to 0.49; $p = 0.002$) aortic valve gradients (67). Finally, after a median of 1,526 days of follow-up, ^{18}F-fluoride emerged as a prognostic marker serving as an independent predictor of the combined endpoint of aortic valve replacement and cardiovascular mortality (hazard ratio: 1.55; 95% CI: 1.33 to 1.81, after adjusting for age and sex; $p < 0.001$).

In summary, these data highlight the potential application of ^{18}F-fluoride as an immediate, noninvasive measure of disease activity in aortic stenosis with the ability to predict its natural history. The instantaneous readout of disease activity holds particular promise in assessing the early efficacy of novel therapeutic agents, in which treatment effects are likely to be discernible over a much shorter time period than could be resolved using clinical endpoints, echocardiography, or CT.

Should ^{18}F-fluoride PET be used as a clinical tool? Although PET performed well in predicting the natural history of aortic stenosis, the far simpler technique of CT calcium scoring appeared to provide almost equivalent prediction of disease progression. Moreover, in agreement with the work by Clavel et al. (72,73), CT again provided incremental prediction of clinical outcomes to even echocardiographic assessments of hemodynamic severity. Whilst supporting a greater role for CT, this would argue against the use of PET in the routine clinical arena. It also raises the question as to why an anatomic measure of calcium burden can provide such effective prediction of future disease progression? We believe that this reflects the close association between calcification activity in the valve (as assessed by ^{18}F-fluoride) and the baseline calcium score ($r = 0.80$; $p < 0.001$), and provides further evidence for the model of calcium begetting further calcium formation in the propagation phase of the disease (**Figure 1**). Regardless of the mechanism, the close link between calcium burden and calcification activity in the valve ensures that even the simplest methods of aortic valve calcium burden provide a surrogate of disease activity and effective prediction of disease progression.

The imaging techniques described previously allow us to image calcification in the valve in progressive detail. They have helped to confirm the important role that calcification plays in driving aortic stenosis and have allowed us to both characterize the severity of disease and to better predict disease progression. We anticipate that CT calcium scoring will assume a greater clinical role, whereas PET will prove a powerful research tool, in particular as an endpoint

FIGURE 5 Change in Aortic Valve CT Calcium Score and ^{18}F-Sodium Fluoride PET Activity After 1 Year

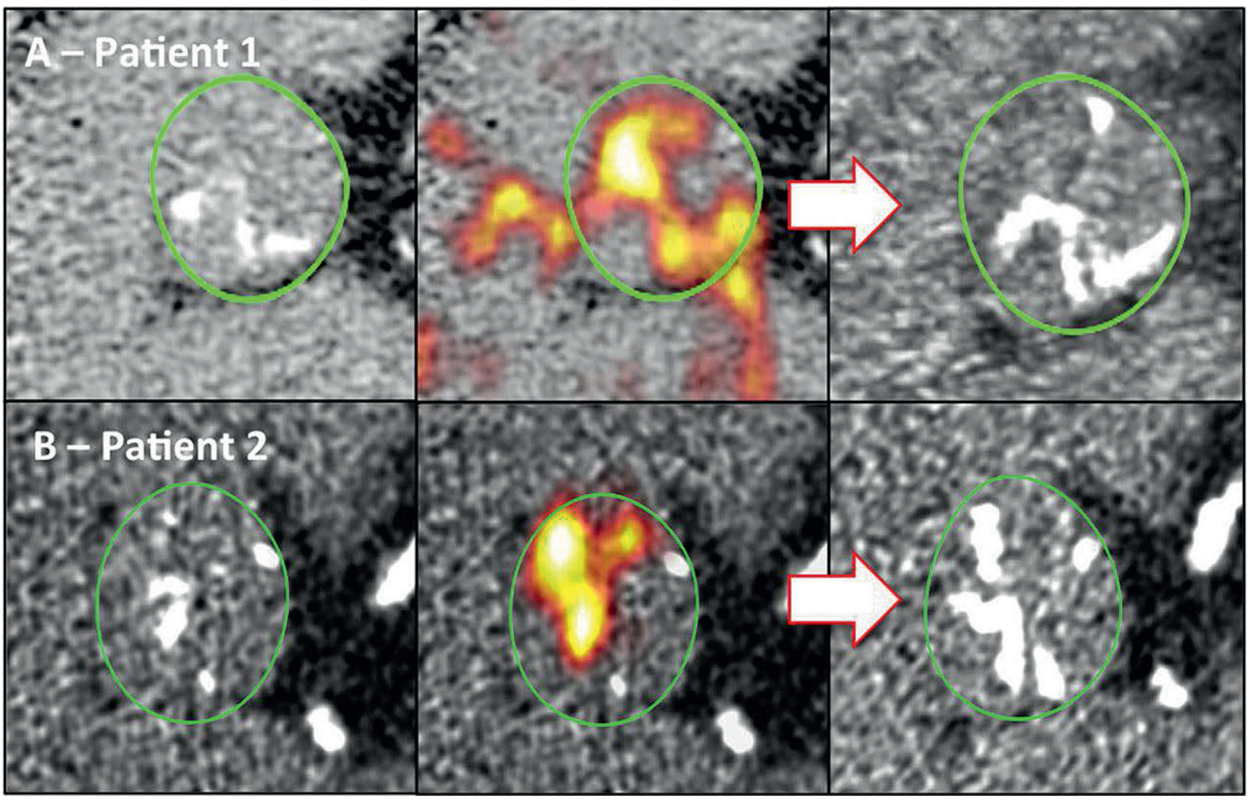

Baseline CT calcium scores **(left)** for patients 1 and 2 **(top and bottom)**. Fused coaxial ^{18}F-fluoride PET-CT scans **(middle)** show fluoride uptake in **red** and **yellow**. The 1-year follow-up **(right)** suggests that the baseline PET signal predicts the spatial distribution of subsequent macrocalcification (77). Abbreviations as in **Figure 3**.

in clinical trials assessing the efficacy of novel, potentially disease-modifying therapies. Indeed, ^{18}F-fluoride PET has the potential to provide both mechanistic insights and a far more rapid readout of efficacy than CT calcium scoring or echocardiographic parameters.

POTENTIAL NOVEL DISEASE-MODIFYING THERAPIES

As our understanding of the pathophysiology of aortic stenosis has improved, the key role that calcification plays in driving disease progression has led us away from targeting inflammation and lipid deposition and toward therapies capable of directly halting valve calcification (86). How might this be achieved? The close association between disorders of skeletal bone metabolism and increased calcification in the vasculature offers a potential starting point. A growing body of pre-clinical and clinical data indicates that treatments for osteoporosis, such as bisphosphonates and denosumab, can reduce vascular calcification and that these agents hold considerable promise as novel therapies for aortic stenosis (87).

BISPHOSPHONATES. Bisphosphonates are inhibitors of osteoclast-mediated bone resorption, are well tolerated in elderly patients, and have been widely used for the treatment of osteoporosis (88). Interestingly, bisphosphonates also have important cardiovascular effects, demonstrating a consistent reduction in calcification of the vasculature and the aortic valve (87,89,90). This, in part, appears to be a consequence of their inhibition of bone resorption, which results in reduced release of calcium and phosphate into the circulation and, therefore, in the reduced systemic availability of these procalcific substances (**Figure 2B**) (87). However, bisphosphonates also appear to exert direct anticalcific effects on the aortic valve tissue itself. They reduce the production of IL-1β, IL-6, and TNF-α (key inflammatory cytokines implicated in the early stages of aortic stenosis [91]) and inhibit the secretion of matrix

metalloproteinases 2 and 9, which remodel the valve as aortic stenosis progresses (**Figure 1**) (92,93). Moreover, nitrogen-containing bisphosphonates act as inorganic pyrophosphate analogs (48), which, as discussed, have powerful anticalcific properties in the vasculature. Finally, bisphosphonates attenuate the differentiation of aortic valve myofibroblasts into cells with an osteogenic phenotype (94), the key step in triggering the propagation phase of aortic stenosis (86). In combination, these data offer support for bisphosphonates as a treatment strategy for aortic stenosis that is increasingly being supported by observational clinical data. A recent analysis of 3,710 women in the MESA (Multi-Ethnic Study of Atherosclerosis) indicated that bisphosphonate use was associated with less valvular and vascular calcification in older women (users vs. nonusers: aortic valve ring calcium 38% vs. 59%; $p < 0.0001$) (95). Other studies appear to support these findings with a direct beneficial effect of these drugs on echocardiographic measures of aortic stenosis progression (96–98), as well as reducing valvular calcification in patients with renal failure and amongst those with bioprosthetic valves (87,99). Although encouraging, such retrospective, observational studies are prone to bias, cannot assess cause-and-effect, have provided conflicting results (100), and are confounded by the underlying effects of the osteoporosis for which these agents were prescribed. Indeed, the true effect of bisphosphonates in aortic stenosis will only become clear within the context of a randomized controlled trial (101).

DENOSUMAB. As discussed, the OPG/RANK/RANKL axis appears to play a pivotal role in aortic valve calcification and may provide an explanation for the link between osteoporosis and increased vascular calcification. It, therefore, represents an attractive therapeutic target for reducing vascular calcification (**Figure 2C**). Denosumab is a human monoclonal antibody to RANKL that prevents its binding to RANK, thereby recapitulating the actions of OPG. In a trial of 7,868 post-menopausal women with osteoporosis, denosumab increased bone mineral density and reduced vertebral fracture rates by 68% over a 3-year period (102). Importantly, denosumab was extremely well tolerated, with very few adverse side effects and no major excess of adverse events. Given the central regulatory role of the OPG/RANK/RANKL system in vascular and aortic valve calcification, denosumab also holds considerable promise as a novel treatment for aortic stenosis. Again, this is supported by preclinical data, with denosumab halving the aortic calcification observed in a murine model of osteoporosis (103). Interestingly, in the same study, this reduction was closely associated with inhibited bone resorption from the skeleton, indicating that the cardiovascular effects of denosumab are, like bisphosphonates, in part related to reduced calcium and phosphate release from bone into the circulation.

FUTURE PERSPECTIVES

Bisphosphonates and denosumab hold promise as novel treatments for aortic stenosis and are currently being investigated as part of an ongoing randomized control trial (NCT02132026) (104). However, even if these prove ineffective, we believe that future treatments should still be directed at the propagation phase and at breaking the self-perpetuating cycle of valvular injury, osteogenic differentiation, and calcium deposition. As discussed, a rapidly expanding list of signaling pathways and molecular processes governing the pathogenesis of aortic stenosis have been elucidated, uncovering many additional targets at different phases of the disease; these are discussed in the following paragraphs. In addition, further investigation is warranted to assess whether potentially pro-calcific drugs, including calcium supplements and coumarins, should be avoided in patients with aortic stenosis.

Ultimately, many of the procalcific pathways in the valve appear to converge on the up-regulation of osteogenic differentiation factors (e.g., BMP-2, Wnt-β-catenin) that establish osteoblast-like function within the valve. These factors therefore provide an attractive therapeutic strategy, although, given the overlap in factors governing calcification in the bone and the valve, the major challenge will be to slow aortic stenosis progression without compromising bone health. One potential approach would be to target the upstream cytokines that activate BMP, such as using inhibitors of IL-6 or TNF-α (as already used in rheumatoid arthritis). However, once again, it remains unclear whether targeting inflammation will be effective in the propagation phase once the procalcific processes have become established. Targeting ectonucleotidases may be more effective, given their apparently central role in establishing the positive feedback loop by which calcium begets calcium. Ectonucleotidase inhibitors have already been tested in the warfarin rat model and have been shown to prevent the development of calcific aortic valve disease (105). Interest also surrounds $P2Y_2$ receptor antagonists as a means of reducing VIC apoptosis and the calcification that this induces. Therapeutic administration of fetuin-A, or a mimetic of MGP, could

CENTRAL ILLUSTRATION **The Pathogenesis of Aortic Stenosis in 2 Stages**

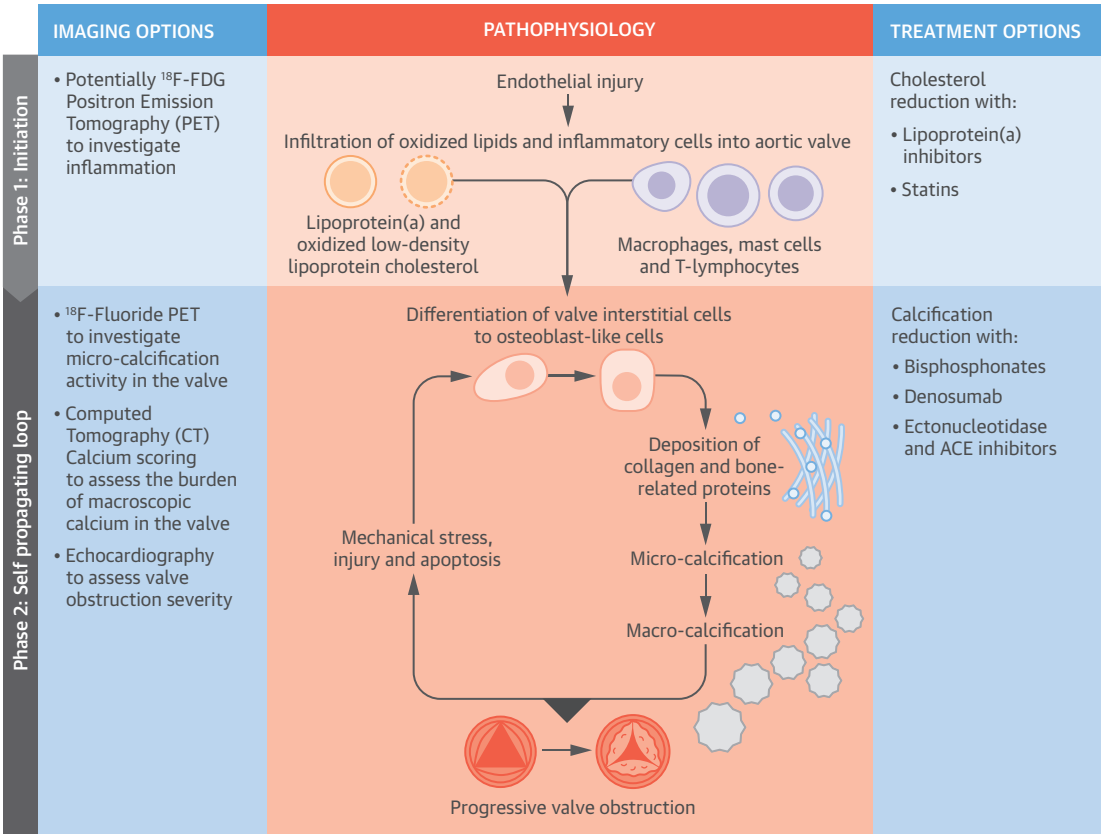

Pawade, T.A. et al. J Am Coll Cardiol. 2015; 66(5):561–77.

Initiation phase: similar to the early stages of atherosclerosis, endothelial injury facilitates the infiltration of oxidized lipids and inflammatory cells into the valve and the release of proinflammatory mediators. These trigger the very early stages of valve calcification so that the incidence of aortic stenosis closely relates to traditional cardiovascular risk factors for atherosclerosis. Propagation phase: these proinflammatory processes subsequently induce VICs to undergo osteogenic differentiation. The VICs first lay down a collagen matrix and other bone-related proteins before producing calcium (7,8). Calcification of the valve induces compliance mismatch, resulting in increased mechanical stress, injury, and apoptosis (9), which triggers further calcification (10). Hence, a self-perpetuating cycle of calcification, valve injury, and osteogenic activation is established that drives the propagation phase of the disease. As a consequence, disease progression in aortic stenosis more closely relates to procalcific factors, rather than lipid infiltration or inflammation. The different stages of calcification in the valve can be imaged using ^{18}F-Fluoride PET (newly developing microcalcification) and CT calcium scoring (macroscopic calcific deposits). Given the central role of calcification in the propagation phase of aortic stenosis, it is perhaps unsurprising that these imaging techniques provide important information with respect to prognosis and disease progression. Moreover, calcification represents an important potential therapeutic target, with the use of drugs, such as denosumab and bisphosphonates, to interrupt the vicious cycle of calcification that drives progressive narrowing of the valve.
ACE = angiotensin-converting enzyme; CT = computed tomography; FDG = fluorodeoxyglucose; PET = positron emission tomography; VIC = valvular interstitial cell.

simultaneously target multiple pathways thought to drive valvular calcification.

The ability of lipoprotein(a)-lowering therapies to modify aortic stenosis disease progression is likely to form the basis of a future clinical trial. Given the failure of the statin trials, it will be of great interest to determine whether a more targeted lipid intervention will have greater success in reducing disease progression in the propagation phase (106). On the basis of the apparent contribution of the RAS to the initiation of aortic stenosis, it is also not unreasonable to consider ACE inhibitors, or even selective AT_1 receptor antagonists or novel renin inhibitors, as novel treatments. Indeed, these agents are also likely to have a beneficial effect with respect to hypertension and left ventricular remodeling in aortic stenosis,

given the role that the RAS system also plays in driving myocardial hypertrophy, fibrosis, and the transition to heart failure.

CONCLUSIONS

Aortic stenosis is a common condition that is set to become an increasing health care burden. We lack effective medical therapies capable of slowing its relentless progression toward major surgery or adverse events. Recent insights into the pathophysiology of aortic stenosis have indicated that although lipid and inflammation may be important in establishing the disease (initiation phase), it is the self-perpetuating processes of calcification that are predominantly responsible for driving disease progression (propagation phase) (**Central Illustration**). On this basis, imaging modalities capable of quantifying aortic valve calcification will be best placed to predict its natural history, whereas novel anticalcific therapies hold major promise as methods of treatment. Randomized controlled trials of such agents, perhaps using imaging endpoints such as CT calcium scoring and ^{18}F-fluoride PET activity, are now required to establish their early efficacy.

REPRINT REQUESTS AND CORRESPONDENCE: Dr. Marc R. Dweck, British Heart Foundation/University Centre for Cardiovascular Science, Room SU 305, Chancellor's Building, University of Edinburgh, 49 Little France Crescent, Edinburgh EH16 4SB, United Kingdom. E-mail: marc.dweck@ed.ac.uk.

REFERENCES

1. Nkomo VT, Gardin JM, Skelton TN, et al. Burden of valvular heart diseases: a population-based study. Lancet 2006;368:1005–11.

2. Osnabrugge RL, Mylotte D, Head SJ, et al. Aortic stenosis in the elderly: disease prevalence and number of candidates for transcatheter aortic valve replacement: a meta-analysis and modeling study. J Am Coll Cardiol 2013;62:1002–12.

3. Rajamannan NM, Evans FJ, Aikawa E, et al. Calcific aortic valve disease: not simply a degenerative process. A review and agenda for research from the National Heart and Lung and Blood Institute Aortic Stenosis Working Group. Executive summary: calcific aortic valve disease—2011 update. Circulation 2011;124:1783–91.

4. New SE, Aikawa E. Molecular imaging insights into early inflammatory stages of arterial and aortic valve calcification. Circ Res 2011;108:1381–91.

5. Thanassoulis G, Massaro JM, Cury R, et al. Associations of long-term and early adult atherosclerosis risk factors with aortic and mitral valve calcium. J Am Coll Cardiol 2010;55:2491–8.

6. Stewart BF, Siscovick D, Lind BK, et al. Clinical factors associated with calcific aortic valve disease. Cardiovascular Health Study. J Am Coll Cardiol 1997;29:630–4.

7. Stritzke J, Linsel-Nitschke P, Markus MR, et al. Association between degenerative aortic valve disease and long-term exposure to cardiovascular risk factors: results of the longitudinal population-based KORA/MONICA survey. Eur Heart J 2009;30:2044–53.

8. Pachulski RT, Chan KL. Progression of aortic valve dysfunction in 51 adult patients with congenital bicuspid aortic valve: assessment and follow up by Doppler echocardiography. Br Heart J 1993;69:237–40.

9. Smith JG, Luk K, Schulz CA, et al., for the Cohorts for Heart and Aging Research in Genetic Epidemiology (CHARGE) Extracoronary Calcium Working Group. Association of low-density lipoprotein cholesterol-related genetic variants with aortic valve calcium and incident aortic stenosis. JAMA 2014;312:1764–71.

10. Thanassoulis G, Campbell CY, Owens DS, et al., for the CHARGE Extracoronary Calcium Working Group. Genetic associations with valvular calcification and aortic stenosis. N Engl J Med 2013;368:503–12.

11. Otto CM, Kuusisto J, Reichenbach DD, et al. Characterization of the early lesion of 'degenerative' valvular aortic stenosis. Histological and immunohistochemical studies. Circulation 1994;90:844–53.

12. Proudfoot D, Skepper JN, Hegyi L, et al. Apoptosis regulates human vascular calcification in vitro: evidence for initiation of vascular calcification by apoptotic bodies. Circ Res 2000;87:1055–62.

13. Kim KM. Calcification of matrix vesicles in human aortic valve and aortic media. Fed Proc 1976;35:156–62.

14. Nadra I, Mason JC, Philippidis P, et al. Proinflammatory activation of macrophages by basic calcium phosphate crystals via protein kinase C and MAP kinase pathways: a vicious cycle of inflammation and arterial calcification? Circ Res 2005;96:1248–56.

15. Moura LM, Ramos SF, Zamorano JL, et al. Rosuvastatin affecting aortic valve endothelium to slow the progression of aortic stenosis. J Am Coll Cardiol 2007;49:554–61.

16. Rajamannan NM, Subramaniam M, Springett M, et al. Atorvastatin inhibits hypercholesterolemia-induced cellular proliferation and bone matrix production in the rabbit aortic valve. Circulation 2002;105:2660–5.

17. Weiss RM, Ohashi M, Miller JD, et al. Calcific aortic valve stenosis in old hypercholesterolemic mice. Circulation 2006;114:2065–9.

18. Cowell SJ, Newby DE, Prescott RJ, et al., for the Scottish Aortic Stenosis and Lipid Lowering Trial, Impact on Regression (SALTIRE) Investigators. A randomized trial of intensive lipid-lowering therapy in calcific aortic stenosis. N Engl J Med 2005;352:2389–97.

19. Chan KL, Teo K, Dumesnil JG, et al., for the ASTRONOMER Investigators. Effect of lipid lowering with rosuvastatin on progression of aortic stenosis: results of the aortic stenosis progression observation: measuring effects of rosuvastatin (ASTRONOMER) trial. Circulation 2010;121:306–14.

20. Rossebø AB, Pedersen TR, Boman K, et al., for the SEAS Investigators. Intensive lipid lowering with simvastatin and ezetimibe in aortic stenosis. N Engl J Med 2008;359:1343–56.

21. Puri R, Nicholls SJ, Shao M, et al. Impact of statins on serial coronary calcification during atheroma progression and regression. J Am Coll Cardiol 2015;65:1273–82.

22. Capoulade R, Clavel MA, Dumesnil JG, et al., for the ASTRONOMER Investigators. Impact of metabolic syndrome on progression of aortic stenosis: influence of age and statin therapy. J Am Coll Cardiol 2012;60:216–23.

23. Mohler ER 3rd, Gannon F, Reynolds C, et al. Bone formation and inflammation in cardiac valves. Circulation 2001;103:1522–8.

24. El Accaoui RN, Gould ST, Hajj GP, et al. Aortic valve sclerosis in mice deficient in endothelial nitric oxide synthase. Am J Physiol Heart Circ Physiol 2014;306:H1302–13.

25. O'Brien KD, Shavelle DM, Caulfield MT, et al. Association of angiotensin-converting enzyme with low-density lipoprotein in aortic valvular lesions and in human plasma. Circulation 2002;106:2224–30.

26. Peltonen T, Napankangas J, Ohtonen P, et al. (Pro)renin receptors and angiotensin converting enzyme 2/angiotensin-(1-7)/Mas receptor axis in human aortic valve stenosis. Atherosclerosis 2011;216:35–43.

27. Capoulade R, Clavel MA, Mathieu P, et al. Impact of hypertension and renin-angiotensin

system inhibitors in aortic stenosis. Eur J Clin Invest 2013;43:1262–72.

28. Ducy P. CBFA1: a molecular switch in osteoblast biology. Dev Dyn 2000;219:461–71.

29. Rajamannan NM, Subramaniam M, Rickard D, et al. Human aortic valve calcification is associated with an osteoblast phenotype. Circulation 2003; 107:2181–4.

30. Pohjolainen V, Taskinen P, Soini Y, et al. Noncollagenous bone matrix proteins as a part of calcific aortic valve disease regulation. Hum Pathol 2008;39:1695–701.

31. Ganss B, Kim RH, Sodek J. Bone sialoprotein. Crit Rev Oral Biol Med 1999;10:79–98.

32. Liu AC, Joag VR, Gotlieb AI. The emerging role of valve interstitial cell phenotypes in regulating heart valve pathobiology. Am J Pathol 2007;171: 1407–18.

33. Aikawa E, Nahrendorf M, Figueiredo JL, et al. Osteogenesis associates with inflammation in early-stage atherosclerosis evaluated by molecular imaging in vivo. Circulation 2007;116:2841–50.

34. Aikawa E, Otto CM. Look more closely at the valve: imaging calcific aortic valve disease. Circulation 2012;125:9–11.

35. Watson KE, Bostrom K, Ravindranath R, et al. TGF-beta 1 and 25-hydroxycholesterol stimulate osteoblast-like vascular cells to calcify. J Clin Invest 1994;93:2106–13.

36. Tintut Y, Demer L. Role of osteoprotegerin and its ligands and competing receptors in atherosclerotic calcification. J Investig Med 2006;54: 395–401.

37. Garg V, Muth AN, Ransom JF, et al. Mutations in NOTCH1 cause aortic valve disease. Nature 2005;437:270–4.

38. Nigam V, Srivastava D. Notch1 represses osteogenic pathways in aortic valve cells. J Mol Cell Cardiol 2009;47:828–34.

39. Boström K, Watson KE, Stanford WP, et al. Atherosclerotic calcification: relation to developmental osteogenesis. Am J Cardiol 1995;75: 88B–91.

40. Yang X, Meng X, Su X, et al. Bone morphogenic protein 2 induces Runx2 and osteopontin expression in human aortic valve interstitial cells: role of Smad1 and extracellular signal-regulated kinase 1/2. J Thorac Cardiovasc Surg 2009;138: 1008–15.

41. Yang X, Fullerton DA, Su X, et al. Pro-osteogenic phenotype of human aortic valve interstitial cells is associated with higher levels of Toll-like receptors 2 and 4 and enhanced expression of bone morphogenetic protein 2. J Am Coll Cardiol 2009;53:491–500.

42. Caira FC, Stock SR, Gleason TG, et al. Human degenerative valve disease is associated with up-regulation of low-density lipoprotein receptor-related protein 5 receptor-mediated bone formation. J Am Coll Cardiol 2006;47:1707–12.

43. Chen JH, Chen WL, Sider KL, et al. β-catenin mediates mechanically regulated, transforming growth factor-β1-induced myofibroblast differentiation of aortic valve interstitial cells. Arterioscl Thromb Vasc Biol 2011;31:590–7.

44. Rajamannan NM. Oxidative-mechanical stress signals stem cell niche mediated Lrp5 osteogenesis in eNOS$^{-/-}$ null mice. J Cell Biochem 2012; 113:1623–34.

45. Kado DM, Browner WS, Blackwell T, et al. Rate of bone loss is associated with mortality in older women: a prospective study. J Bone Miner Res 2000;15:1974–80.

46. Pfister R, Michels G, Sharp SJ, et al. Inverse association between bone mineral density and risk of aortic stenosis in men and women in EPIC-Norfolk prospective study. Int J Cardiol 2015;178: 29–30.

47. Aksoy Y, Yagmur C, Tekin GO, et al. Aortic valve calcification: association with bone mineral density and cardiovascular risk factors. Coron Artery Dis 2005;16:379–83.

48. Demer LL, Tintut Y. Vascular calcification: pathobiology of a multifaceted disease. Circulation 2008;117:2938–48.

49. Persy V, D'Haese P. Vascular calcification and bone disease: the calcification paradox. Trends Mol Med 2009;15:405–16.

50. Hultgren HN. Osteitis deformans (Paget's disease) and calcific disease of the heart valves. Am J Cardiol 1998;81:1461–4.

51. Kaden JJ, Bickelhaupt S, Grobholz R, et al. Receptor activator of nuclear factor κB ligand and osteoprotegerin regulate aortic valve calcification. J Mol Cell Cardiol 2004;36:57–66.

52. Bucay N, Sarosi I, Dunstan CR, et al. *Osteoprotegerin*-deficient mice develop early onset osteoporosis and arterial calcification. Genes Dev 1998;12:1260–8.

53. Parhami F, Morrow AD, Balucan J, et al. Lipid oxidation products have opposite effects on calcifying vascular cell and bone cell differentiation. A possible explanation for the paradox of arterial calcification in osteoporotic patients. Arterioscl Thromb Vasc Biol 1997;17:680–7.

54. Demer LL. Vascular calcification and osteoporosis: inflammatory responses to oxidized lipids. Int J Epidemiol 2002;31:737–41.

55. Schurgers LJ, Uitto J, Reutelingsperger CP. Vitamin K-dependent carboxylation of matrix Gla-protein: a crucial switch to control ectopic mineralization. Trends Mol Med 2013;19:217–26.

56. Tantisattamo E, Han KH, O'Neill WC. Increased vascular calcification in patients receiving warfarin. Arterioscl Thromb Vasc Biol 2015;35:237–42.

57. Kaden JJ, Reinöhl JO, Blesch B, et al. Systemic and local levels of fetuin-A in calcific aortic valve stenosis. Int J Mol Med 2007;20:193–7.

58. Koos R, Brandenburg V, Mahnken AH, et al. Association of fetuin-A levels with the progression of aortic valve calcification in non-dialyzed patients. Eur Heart J 2009;30:2054–61.

59. Mohty D, Côté N, Pibarot P, et al. Reduced fetuin a serum level is associated with faster progression and increased valvular calcification in elderly patients with aortic stenosis. J Clin Exp Cardiol 2011;2:147.

60. Capoulade R, Côté N, Mathieu P, et al., for the ASTRONOMER Investigators. Circulating levels of matrix GLA protein and progression of aortic stenosis: a substudy of the Aortic Stenosis Progression Observation: Measuring Effects of rosuvastatin (ASTRONOMER) trial. Can J Cardiol 2014; 30:1088–95.

61. Côté N, El Husseini D, Pépin A, et al. ATP acts as a survival signal and prevents the mineralization of aortic valve. J Mol Cell Cardiol 2012;52:1191–202.

62. El Husseini D, Boulanger MC, Mahmut A, et al. P2Y2 receptor represses IL-6 expression by valve interstitial cells through Akt: implication for calcific aortic valve disease. J Mol Cell Cardiol 2014;72:146–56.

63. Baumgartner H, Hung J, Bermejo J, et al. Echocardiographic assessment of valve stenosis: EAE/ASE recommendations for clinical practice. Eur J Echocardiogr 2009;22:1–25.

64. Rosenhek R, Binder T, Porenta G, et al. Predictors of outcome in severe, asymptomatic aortic stenosis. N Engl J Med 2000;343:611–7.

65. Cioffi G, Mazzone C, Faggiano P, et al. Prognostic stratification by conventional echocardiography of patients with aortic stenosis: the "CAIMAN-ECHO score." Echocardiography 2013; 30:367–77.

66. Messika-Zeitoun D, Aubry MC, Detaint D, et al. Evaluation and clinical implications of aortic valve calcification measured by electron-beam computed tomography. Circulation 2004;110:356–62.

67. Jenkins W, Dweck M, Shah A, et al. 18F-NaF is a predictor of progression and outcome in aortic valve disease (abstr). J Am Coll Cardiol 2014;63 Suppl 12:A995.

68. Liu F, Coursey CA, Grahame-Clarke C, et al. Aortic valve calcification as an incidental finding at CT of the elderly: severity and location as predictors of aortic stenosis. AJR Am J Roentgenol 2006;186:342–9.

69. Koos R, Kühl HP, Mühlenbruch G, et al. Prevalence and clinical importance of aortic valve calcification detected incidentally on CT scans: comparison with echocardiography. Radiology 2006;241:76–82.

70. Aggarwal SR, Clavel MA, Messika-Zeitoun D, et al. Sex differences in aortic valve calcification measured by multidetector computed tomography in aortic stenosis. Circ Cardiovasc Imaging 2013;6: 40–7.

71. Dweck MR, Chin C, Newby DE. Small valve area with low-gradient aortic stenosis: beware the hard hearted. J Am Coll Cardiol 2013;62:2339–40.

72. Clavel MA, Messika-Zeitoun D, Pibarot P, et al. The complex nature of discordant severe calcified aortic valve disease grading: new insights from combined Doppler echocardiographic and computed tomographic study. J Am Coll Cardiol 2013; 62:2329–38.

73. Clavel MA, Pibarot P, Messika-Zeitoun D, et al. Impact of aortic valve calcification, as measured by MDCT, on survival in patients with aortic stenosis: results of an international registry study. J Am Coll Cardiol 2014;64:1202–13.

74. Feuchtner GM, Müller S, Grander W, et al. Aortic valve calcification as quantified with multislice computed tomography predicts short-term clinical outcome in patients with

asymptomatic aortic stenosis. J Heart Valve Dis 2006;15:494–8.

75. Koos R, Mahnken AH, Sinha AM, et al. Aortic valve calcification as a marker for aortic stenosis severity: assessment on 16-MDCT. AJR Am J Roentgenol 2004;183:1813–8.

76. Messika-Zeitoun D, Bielak LF, Peyser PA, et al. Aortic valve calcification: determinants and progression in the population. Arterioscl Thromb Vasc Biol 2007;27:642–8.

77. Dweck MR, Jenkins WS, Vesey AT, et al. 18F-NaF uptake is a marker of active calcification and disease progression in patients with aortic stenosis. Circ Cardiovasc Imaging 2014;7:371–8.

78. Nguyen V, Cimadevilla C, Estellat C, et al. Haemodynamic and anatomic progression of aortic stenosis. Heart 2015;101:943–7.

79. Dweck MR, Jones C, Joshi NV, et al. Assessment of valvular calcification and inflammation by positron emission tomography in patients with aortic stenosis. Circulation 2012;125:76–86.

80. Marincheva-Savcheva G, Subramanian S, Qadir S, et al. Imaging of the aortic valve using fluorodeoxyglucose positron emission tomography: increased valvular fluorodeoxyglucose uptake in aortic stenosis. J Am Coll Cardiol 2011;57:2507–15.

81. Dweck MR, Khaw HJ, Sng GK, et al. Aortic stenosis, atherosclerosis, and skeletal bone: is there a common link with calcification and inflammation? Eur Heart J 2013;34:1567–74.

82. Tahara N, Kai H, Nakaura H, et al. The prevalence of inflammation in carotid atherosclerosis: analysis with fluorodeoxyglucose-positron emission tomography. Eur Heart J 2007;28:2243–8.

83. Tawakol A, Migrino RQ, Bashian GG, et al. In vivo ^{18}F-fluorodeoxyglucose positron emission tomography imaging provides a noninvasive measure of carotid plaque inflammation in patients. J Am Coll Cardiol 2006;48:1818–24.

84. Tahara N, Kai H, Ishibashi M, et al. Simvastatin attenuates plaque inflammation: evaluation by fluorodeoxyglucose positron emission tomography. J Am Coll Cardiol 2006;48:1825–31.

85. Irkle A, Vesey AT, Lewis DY, et al. Identifying active vascular micro-calcification by 18F-sodium fluoride positron emission tomography. Nat Commun 2015;6:7495.

86. Otto CM. Calcific aortic stenosis—time to look more closely at the valve. N Engl J Med 2008;359:1395–8.

87. Price PA, Faus SA, Williamson MK. Bisphosphonates alendronate and ibandronate inhibit artery calcification at doses comparable to those that inhibit bone resorption. Arterioscl Thromb Vasc Biol 2001;21:817–24.

88. Fleisch H, Russell RG, Francis MD. Diphosphonates inhibit hydroxyapatite dissolution in vitro and bone resorption in tissue culture and in vivo. Science 1969;165:1262–4.

89. Rosenblum IY, Flora L, Eisenstein R. The effect of disodium ethane-1-hydroxy-1,1-diphosphonate (EHDP) on a rabbit model of athero-arteriosclerosis. Atherosclerosis 1975;22:411–24.

90. Kramsch DM, Chan CT. The effect of agents interfering with soft tissue calcification and cell proliferation on calcific fibrous-fatty plaques in rabbits. Circ Res 1978;42:562–71.

91. Sansoni P, Passeri G, Fagnoni F, et al. Inhibition of antigen-presenting cell function by alendronate in vitro. J Bone Miner Res 1995;10:1719–25.

92. Giraudo E, Inoue M, Hanahan D. An amino-bisphosphonate targets MMP-9-expressing macrophages and angiogenesis to impair cervical carcinogenesis. J Clin Invest 2004;114:623–33.

93. Lai TJ, Hsu SF, Li TM, et al. Alendronate inhibits cell invasion and MMP-2 secretion in human chondrosarcoma cell line. Acta Pharmacologica Sinica 2007;28:1231–5.

94. Elmariah S, Cimmino G, Fuster V, et al. Bisphosphonates prevent oxidized low- density lipoprotein-induced expression of osteogenic markers in aortic valve myofibroblasts (abstr). J Am Coll Cardiol 2010;55 Suppl 10A:A149.

95. Elmariah S, Delaney JAC, O'Brien KD, et al. Bisphosphonate use and prevalence of valvular and vascular calcification in women: MESA (The Multi-Ethnic Study of Atherosclerosis). J Am Coll Cardiol 2010;56:1752–9.

96. Innasimuthu AL, Katz WE. Effect of bisphosphonates on the progression of degenerative aortic stenosis. Echocardiography 2011;28:1–7.

97. Skolnick AH, Osranek M, Formica P, et al. Osteoporosis treatment and progression of aortic stenosis. Am J Cardiol 2009;104:122–4.

98. Sterbakova G, Vyskocil V, Linhartova K. Bisphosphonates in calcific aortic stenosis: association with slower progression in mild disease–a pilot retrospective study. Cardiology 2010;117:184–9.

99. Rapoport HS, Connolly JM, Fulmer J, et al. Mechanisms of the in vivo inhibition of calcification of bioprosthetic porcine aortic valve cusps and aortic wall with triglycidylamine/mercapto bisphosphonate. Biomaterials 2007;28:690–9.

100. Aksoy O, Cam A, Goel SS, et al. Do bisphosphonates slow the progression of aortic stenosis? J Am Coll Cardiol 2012;59:1452–9.

101. Dweck MR, Newby DE. Osteoporosis is a major confounder in observational studies investigating bisphosphonate therapy in aortic stenosis. J Am Coll Cardiol 2012;60:1027.

102. Cummings SR, San Martin J, McClung MR, et al., for the FREEDOM Trial. Denosumab for prevention of fractures in postmenopausal women with osteoporosis. N Engl J Med 2009;361:756–65.

103. Helas S, Goettsch C, Schoppet M, et al. Inhibition of receptor activator of NF-κB ligand by denosumab attenuates vascular calcium deposition in mice. Am J Pathol 2009;175:473–8.

104. University of Edinburgh. Study Investigating the Effect of Drugs Used to Treat Osteoporosis on the Progression of Calcific Aortic Stenosis (SALTIRE II). 2014. Available at: https://clinicaltrials.gov/ct2/show/NCT02132026. Accessed May 27, 2015.

105. Côté N, El Husseini D, Pépin A, et al. Inhibition of ectonucleotidase with ARL67156 prevents the development of calcific aortic valve disease in warfarin-treated rats. Eur J Pharmacol 2012;689:139–46.

106. Hung MY, Tsimikas S. What is the ultimate test that lowering lipoprotein(a) is beneficial for cardiovascular disease and aortic stenosis? Curr Opin Lipidol 2014;25:423–30.

107. Cowell SJ, Newby DE, Burton J, et al. Aortic valve calcification on computed tomography predicts the severity of aortic stenosis. Clin Radiol 2003;58:712–6.

108. Cueff C, Serfaty JM, Cimadevilla C, et al. Measurement of aortic valve calcification using multislice computed tomography: correlation with haemodynamic severity of aortic stenosis and clinical implication for patients with low ejection fraction. Heart 2011;97:721–6.

109. Utsunomiya H, Yamamoto H, Kitagawa T, et al. Incremental prognostic value of cardiac computed tomography angiography in asymptomatic aortic stenosis: significance of aortic valve calcium score. Int J Cardiol 2013;168:5205–11.

KEY WORDS aortic valve, calcification of, calcinosis, calcium, computed tomography, diphosphonates, positron emission tomography

OPEN

Optimization and Reproducibility of Aortic Valve 18F-Fluoride Positron Emission Tomography in Patients With Aortic Stenosis

Tania A. Pawade, MD; Timothy R.G. Cartlidge, MD; William S.A. Jenkins, MD; Philip D. Adamson, MD; Phillip Robson, PhD; Christophe Lucatelli, PhD; Edwin J.R. Van Beek, MD, PhD; Bernard Prendergast, DM; Alan R. Denison, MD; Laura Forsyth, BSc, PhD; James H.F. Rudd, MD, PhD; Zahi A. Fayad, PhD; Alison Fletcher, PhD; Sharon Tuck, BSc, MSc; David E. Newby, MD, PhD; Marc R. Dweck, MD, PhD

Background—18F-Fluoride positron emission tomography (PET) and computed tomography (CT) can measure disease activity and progression in aortic stenosis. Our objectives were to optimize the methodology, analysis, and scan–rescan reproducibility of aortic valve 18F-fluoride PET-CT imaging.

Methods and Results—Fifteen patients with aortic stenosis underwent repeated 18F-fluoride PET-CT. We compared nongated PET and noncontrast CT, with a modified approach that incorporated contrast CT and ECG-gated PET. We explored a range of image analysis techniques, including estimation of blood-pool activity at differing vascular sites and a most diseased segment approach. Contrast-enhanced ECG-gated PET-CT permitted localization of 18F-fluoride uptake to individual valve leaflets. Uptake was most commonly observed at sites of maximal mechanical stress: the leaflet tips and the commissures. Scan–rescan reproducibility was markedly improved using enhanced analysis techniques leading to a reduction in percentage error from ±63% to ±10% (tissue to background ratio MDS mean of 1.55, bias −0.05, limits of agreement −0·20 to +0·11).

Conclusions—Optimized 18F-fluoride PET-CT allows reproducible localization of calcification activity to different regions of the aortic valve leaflet and commonly to areas of increased mechanical stress. This technique holds major promise in improving our understanding of the pathophysiology of aortic stenosis and as a biomarker end point in clinical trials of novel therapies.

Clinical Trial Registration—URL: http://www.clinicaltrials.gov. Unique identifier: NCT02132026.

(*Circ Cardiovasc Imaging*. 2016;9:e005131. DOI: 10.1161/CIRCIMAGING.116.005131.)

Key Words: 18F-Fluoride ■ aortic valve stenosis ■ calcification ■ disease progression ■ echocardiography ■ positron emission tomography

Aortic stenosis is the most common form of valve disease in the Western world and a major healthcare burden that is set to treble by 2050. However, we currently lack any disease-modifying therapies. Calcification seems to be the predominant pathological process driving disease progression, leading to major interest in novel treatment strategies aimed at reducing calcification activity in the valve.[1] However, assessing the efficacy of new therapies requires large trials with prolonged follow-up to demonstrate an impact on disease progression and clinical end points.[2] A noninvasive imaging technique capable of measuring calcification activity in the valve would be highly desirable to assess treatment efficacy in phase 2 clinical trials.

See Editorial by Chang and Chareonthaitawee
See Clinical Perspective

18F-Fluoride is a positron-emitting radiotracer that binds to regions of newly developing microcalcification beyond the

Received May 18, 2016; accepted August 22, 2016.

From the BHF/Centre for Cardiovascular Science (T.A.P., T.R.G.C., W.S.A.J., P.D.A., D.E.N., M.R.D.), Clinical Research Imaging Centre, Queen's Medical Research Institute (C.L., E.J.R.V.B., A.F.), and Edinburgh Clinical Trials Unit, Western General Hospital (L.F.), University of Edinburgh, United Kingdom; Translational and Molecular Imaging Institute, Icahn School of Medicine at Mount Sinai, New York (P.R., Z.A.F.); Guy's and St Thomas' Hospitals NHS Foundation Trust, London, United Kingdom (B.P.); Institute for Education in Medical and Dental Sciences, University of Aberdeen, United Kingdom (A.R.D.); Division of Cardiovascular Medicine, University of Cambridge, United Kingdom (J.H.F.R.); and Wellcome Trust Clinical Research Facility, Western General Hospital Edinburgh, United Kingdom (S.T.).

The Data Supplement is available at http://circimaging.ahajournals.org/lookup/suppl/doi:10.1161/CIRCIMAGING.116.005131/-/DC1.

Correspondence to Tania Pawade, MD, BHF/Centre for Cardiovascular Science, Chancellor's Bldg, University of Edinburgh, 49 Little France Crescent, Edinburgh EH16 4SB, United Kingdom. E-mail tania.pawade@ed.ac.uk

resolution of computed tomography.[3] It is readily taken up by the valves of patients with aortic stenosis, and, on histology, correlates with markers of calcification activity.[4] Importantly, this technique predicts disease progression both with respect to echocardiography and computed tomography (CT) calcium scoring and with respect to adverse cardiovascular events.[5–7] 18F-Fluoride positron emission tomography (PET) imaging therefore holds major promise as a marker of calcification activity in aortic stenosis and is an exploratory secondary end point in the ongoing SALTIRE2 clinical trial (NCT02132026). Briefly, this is a randomized controlled trial investigating the ability of therapies targeting calcium metabolism (denosumab and alendronic acid) to modify disease progression in aortic stenosis.

Here, we sought to optimize 18F-fluoride PET scanning of the aortic valve, reduce the effects of cardiac motion, and assess the scan–rescan reproducibility of this technique to inform its future application as a novel biomarker of calcification activity in clinical trials.

Methods

Study Population

Patients aged >50 years with mild, moderate, and severe calcific aortic stenosis were recruited prospectively from outpatient clinics at the Edinburgh Heart Center. Aortic stenosis severity was determined by clinical echocardiograms and graded according to according to American Heart Association/American College of Cardiology guidelines. This is a substudy of the ongoing SALTIRE2 clinical trial (NCT02132026), and consequently patients had to meet the same exclusion criteria as those entering the main trial. These included renal failure and women of childbearing potential (full list in Table I in the Data Supplement). The study was approved by the Scottish Research Ethics Committee and has a Clinical Trial Authorization from the Medicines and Healthcare products Regulatory Authority of the United Kingdom. It was performed in accordance with the Declaration of Helsinki. All patients gave written informed consent.

Initial Image Acquisition and Analysis

Each patient underwent 18F-fluoride PET and CT scanning on 2 occasions. Patients were given 25 mg of oral metoprolol if their resting heart rate was >65 beats/min before being administered 125 MBq of 18F-fluoride IV. After 60 minutes, patients were imaged with a hybrid PET and CT scanner (Biograph mCT; Siemens). Attenuation-correction CT scans were performed before acquisition of PET data in list mode using a single 30-minute bed position centered on the valve in 3-dimensional mode. Finally, ECG-gated aortic valve CT calcium scoring and contrast-enhanced CT angiography were performed in diastole and in held expiration.

CT calcium scoring was performed by an experienced operator using dedicated software (Vitrea Advanced; Toshiba Systems) on axial views, with care taken to exclude calcium originating from the ascending aorta, left ventricular outflow tract, and coronary arteries. The calcium score was recorded in Agatston units.

Analysis was performed using an OsiriX workstation (OsiriX version 3.5.1 64-bit; OsiriX Imaging Software, Geneva, Switzerland). As previously reported, regions of interest were drawn around the perimeter of the valve on the fused nongated PET and noncontrast CT images.[6] These generated mean and maximum standard uptake values (SUV) for each slice. Averaging these values across the entire valve produced whole valve SUV_{mean} and SUV_{max} values, respectively. These SUV values were then corrected for blood-pool activity to generate tissue to background ratio (TBR): whole valve TBR_{mean} and TBR_{max}. The blood-pool uptake was determined using SUV_{mean} values averaged from across regions of interest drawn on 5 contiguous slices in the brachiocephalic vein. For consistency, the most caudal region of interest was positioned at the point where the innominate vein joined the brachiocephalic vein.[6]

To optimize the spatial localization and scan–rescan reproducibility of 18F-fluoride PET-CT imaging, we assessed different approaches to both image acquisition and image analysis.

Optimization of PET Image Acquisition

Contrast CT of Aortic Valve

Our original technique required the reorientation and coregistration of noncontrast CT images of the aortic valve. This technique posed several challenges, particularly with respect to aligning with the true plane of the valve and accurately defining its perimeter. Moreover, the structure of individual leaflets was not visible on these scans precluding more detailed localization of 18F-fluoride uptake. Contrast CT offered potential solutions to these challenges given its superior anatomic detail and the well-established methodology for finding the true plane of the valve[8] (Figure 1).

ECG-Gated PET Data

PET is susceptible to motion, limiting accurate coregistration and the spatial assessment of PET activity within the valve. As a solution, we used ECG gating of list-mode PET data. These data were reconstructed into 4 gates at 25% intervals of the cardiac cycle. Only data acquired between 50% and 75% of the RR interval were assessed because this period corresponds with diastole when cardiac motion is at a minimum. Given that 3 quarters of the PET data are therefore discarded, the bed-time was increased to 30 minutes to preserve signal to noise ratio.

Optimization of PET Image Analysis

Measurement of Blood-Pool Activity

The stability of blood-pool measurements in the SVC for 18F-fluoride–based tracers has recently been questioned,[9] and we were concerned about variation in the measured blood-pool activity at different levels of the brachiocephalic vein. We reasoned that this may be explained by the relatively small diameter of this vein rendering it susceptible to partial volume effects, amplified by the low PET signal in surrounding lung tissue (especially in the cranial aspects of the brachocephalic vein). We hypothesized that sampling blood-pool activity from the center of the right atrium (a much larger structure) may improve the ease and accuracy with which these measurements could be made and the consequent scan–rescan reproducibility. Using the same coregistered PET and CT images of the heart, reorientated to the plane of the valve, a 2-cm^2 region of interest was drawn in the center of the right atrium at the level of the right coronary ostium and again in the same position one slice superiorly. Averaging the mean SUV for these 2 slices gave an alternative measure of blood-pool activity, which was used to correct valvular uptake measurements using 2 different approaches. First, we used the conventional method of dividing aortic valve SUV measurements by the blood pool to generate TBR values. Second, we subtracted the blood-pool value from the valvular uptake, to generate the corrected aortic valve SUV as described recently.[9]

Most Diseased Segment and Whole Valve Approach

One of the biggest difficulties in quantifying uptake in the valve is defining its limits in the z-plane. To overcome this challenge, our original whole valve technique was compared with a most diseased segment (MDS) approach where the 2 contiguous slices with the highest SUV values (frequently in the center of the valve) were averaged to generate $SUV_{MDSmean}$, SUV_{MDSmax}, and corresponding TBR values. This is similar to the approach previously used for quantifying 18F-fluorodeoxyglucose uptake in carotid and aortic atheroma.[10]

Scan–Rescan Reproducibility

Scan–rescan repeatability and intra- and interobserver reproducibility of valvular 18F-fluoride PET quantification was assessed for each of the established and novel image analysis approaches described above. Two experienced operators (T.P. and T.C.) quantified uptake values on each of the scan pairs, on 2 occasions separated by ≥2-week

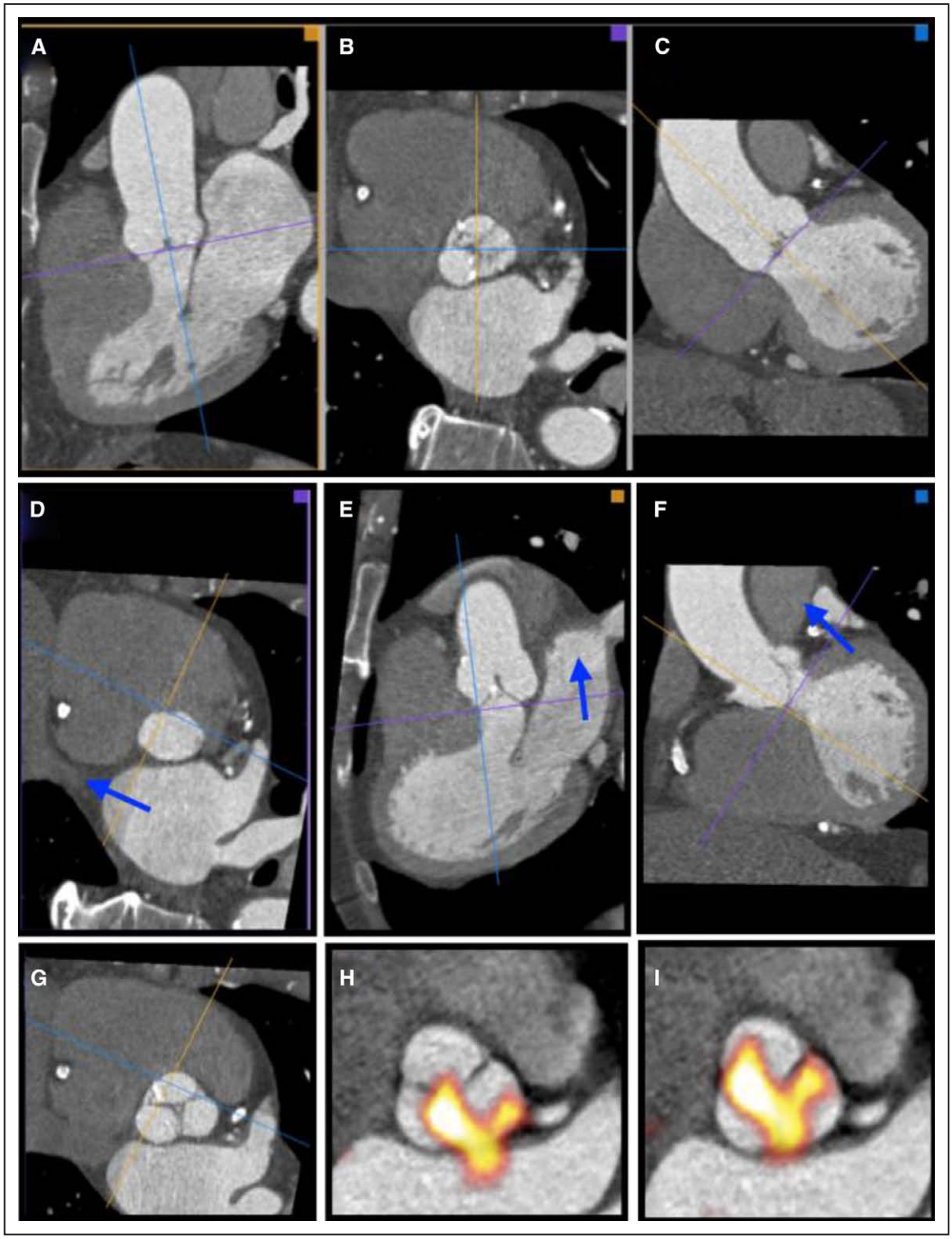

Figure 1. Creation of coregistered en face short-axis positron emission tomography (PET)/computed tomography (CT) images of the aortic valve. First, the CT angiogram is reorientated to get into the approximate plane of the aortic valve by lining up the axial cross hair (purple in this example) using the images in the coronal (**A**) and sagittal planes (**C**). This creates an approximate cross-sectional image of the aortic valve in the axial frame (**B**). Scrolling down in the axial frame, the center of the crosshairs is then placed over the exact point at which the right coronary cusp disappears, identifying the base of that leaflet (**D**). Similarly, the base of the noncoronary cusp is identified, and orthogonal planes adjusted so that the purple plane goes through the base of both these 2 cusps (**D**). Finally, the base of the left coronary cusp is found by rotation of the axial crosshairs so that first the cusp comes into view. The image is then slowly rotated in the opposite direction until the point where the leaflet first disappears (the base) is again found (**F**). This produces an en face image of the valve aligned with the base of all 3 leaflets (**G**). Adjacent 3-mm slices are then created in that plane and used for subsequent assessment. These slices are fused with the 18F-fluoride PET images (**H**) and careful coregistration performed in 3 dimensions to ensure accurate alignment between the PET and CT images (**I**).

interval to avoid recall bias. Observers were blinded to both their own previous measurements and those of the other operator.

Spatial Resolution

The effect of our modifications on spatial resolution and scan–rescan reproducibility were then assessed in comparison with the original approach. First, we assessed the ability of the technique to localize increased 18F-fluoride activity to individual valve leaflets and their different regions. This was done visually using a standardized method for windowing the fused PET/CT images that incorporated the blood-pool activity in right atrium as the minimum. Scan–rescan and observer agreements were assessed.

Statistical Analysis

Continuous variables were expressed as mean±SD, and categorical variables were expressed as total and percentage. Kappa statistics (with 95% confidence intervals) were used to measure the intraobserver and scan–rescan agreement in presence or absence of 18F-fluoride uptake across coronary cusps. The κ values were interpreted as follows: poor <0.20, fair 0.21 to 0.4, moderate 0.41 to 0.60, good 0.61 to 0.80, and very good >0.81.

Intraobserver, interobserver, and scan–rescan reproducibility of several 18F-fluoride PET uptake approaches were analyzed and presented using Bland–Altman analysis and percentage error.[11] Variability in the different techniques was expressed using the width of the 95% limits of agreement from Bland–Altman analyses. For the final approach, we considered the scan–rescan reproducibility to be good and acceptable for use in our future trial if the width of the 95% limits of agreement were within ±0.2 for the $TBR_{MDSmean}$ measurements. Percentage errors for the mean bias were calculated using twice the SD of the difference divided by the overall mean measurements. The intraclass correlation coefficient was used to examine the reliability for both intra and interobserver variability.

Statistical analysis was performed using SAS for Windows version 9.4. Graphs were produced using PRISM version 6.0 for Mac.

Results

Patient Characteristics

Fifteen patients (73±7 years, 67% men) had 2 scans (Table 1), 3.9±3.3 weeks apart between November 2014 and May 2015. Seven patients had mild aortic stenosis, 4 had moderate and 4 had severe aortic stenosis. In 3 participants, the between-scan interval exceeded 4 weeks (5 weeks, 8 weeks, and 14 weeks). The dose of 18F-fluoride was similar on each visit (123±8 and 125±4 MBq; *P*=0·49).

Altered PET Acquisition and Image Quality

Good image quality allowing complete image analysis was achieved on all 15 scan pairs. The prolonged bedtimes of 30 minutes did not result in increased patient motion during the 18F-fluoride PET scans. The impact of each stepwise change in the acquisition and analysis protocol on scan–rescan reproducibility is summarized in Table 2.

On visual assessment, contrast CT imaging of the valve provided much clearer anatomic detail of the leaflets and valve structure compared with noncontrast CT (Figure 2). This made it technically easier to get into the true plane of the valve and allowed more accurate regions of interest to be drawn around its perimeter (Figures 1 and 2). Coregistration with ECG-gated PET data then allowed localization of 18F-fluoride uptake to individual leaflets and their different regions. This was previously impossible using noncontrast CT and nongated PET. Most commonly increased activity was observed across all 3 coronary cusps (n=10), it involved 2 cusps in 4 patients and was isolated to 1 cusp in just 1 patient. The noncoronary cusp was involved in all patients apart from that latter case. Activity was most frequently observed at the valve commissures: the

Table 1. Patient Characteristics

	n (%) Total=15
Demographics	
Age	73.3±7.4
Male sex	10 (67)
Vital signs	
Body mass index, kg/m^2	29.7±5.6
Pulse, beats/min	67.7±15.5
Body surface area, m^2	1.9±0.2
Mean arterial pressure, mm Hg	100.1±9.3
Smoker status	
Current	1 (7)
Never	9 (60)
Ex	5 (33)
Symptoms	
Chest pain	4 (27)
Breathlessness	7 (47)
Syncope	2 (13)
Duration between scans	
Weeks	3.9±3.3
Relevant medical history	
Hypertension	11 (73)
CABG	2 (13)
PCI	4 (27)
Liver disease	1 (7)
Rheumatic fever	0 (0)
MI	3 (20)
Hypercholesterolemia	10 (67)
Diabetes mellitus	4 (27)
Renal disease	0 (0)
TIA/CVA	2 (13)
Laboratory results	
Serum creatinine, mg/dL	70.1±11.2
Normal eGFR	14 (93)
Concomitant medications	
ACE inhibitor	6 (40)
AIIRB	3 (20)
β-Blocker	7 (47)
Statin	9 (60)

ACE indicates angiotensin converting enzyme; AIIRB, angiotensin II receptor blocker; CABG, coronary artery bypass grafting; CVA, cerebrovascular accident; eGFR, estimated glomerular filtration rate; MI, myocardial infarction; PCI, percutaneous coronary intervention; and TIA, transient ischemic attack.

Table 2. Bland–Altman Values and Percentage Errors for Each Stepwise Change to the Image Acquisition and Analysis Technique

	Mean Values					Maximum Values				
	Overall Mean	Difference		95% Limits of Agreement	% Error	Overall Mean	Difference		95% Limits of Agreement	% Error
		Mean	SD				Mean	SD		
Original approach										
Whole valve, ungated PET, noncontrast CT										
Original standard uptake value	1.523	0.008	0.194	−0.373 to 0.389	26	1.955	0.094	0.263	−0.421 to 0.608	27
Original tissue to background ratio (using brachiocephalic)	1.439	0.047	0.451	−0.836 to 0.930	63	1.869	0.154	0.612	−1.045 to 1.354	65
RA blood-pool correction										
Corrected standard uptake value (subtracting RA)	0.425	0.008	0.091	−0.170 to 0.186	43	0.858	0.094	0.168	−0.236 to 0.423	39
Tissue to background ratio (using RA)	1.418	−0.002	0.086	−0.171 to 0.167	12	1.842	0.064	0.200	−0.328 to 0.456	22
Most diseased segment approach										
Standard uptake value	1.652	0.007	0.207	−0.400 to 0.413	25	2.129	0.131	0.265	−0.389 to 0.651	25
Tissue to background ratio (using RA)	1.547	−0.005	0.075	−0.151 to 0.142	10	2.012	0.107	0.145	−0.177 to 0.391	14
Final approach										
RA blood pool, most diseased segment, gated PET, contrast CT										
Final standard uptake value	1.662	0.044	0.291	−0.527 to 0.615	35	2.528	0.275	0.633	−0.966 to 1.515	50
Final tissue to background ratio (using RA)	1.546	−0.046	0.078	−0.199 to 0.107	10	2.385	0.111	0.439	−0.750 to 0.971	37

CT indicates computed tomography; PET, positron emission tomography; and RA, right atrium.

point where the valve cusps meet the aortic ring (n=10) and at the tips where the leaflets coapt during diastole (n=8; Figure 2).

When examining intraobserver reproducibility for detecting the presence or absence of 18F-fluoride uptake on individual valve leaflets, this was very good for the right coronary cusp (κ=1.00), good for the noncoronary cusp (κ=0.63), and moderate for the left (κ=0.58) coronary cusps. The scan–rescan agreement was good for the right coronary cusp (κ=0.76), good for the noncoronary cusp (κ=0.63), and very good for the left coronary cusp (κ=0.81) coronary cusps (Tables 3 and 4).

Effect of Altered Image Analysis on PET Reproducibility

Interobserver and intraobserver reproducibility was good using both the original and modified approaches as previously reported. Intraclass correlation coefficient values for intra- and interobserver reproducibility were 0.88 and 0.80, respectively (Table 5). However, the scan–rescan reproducibility of our original approach produced percentage errors of ±26% and ±27% for the mean and maximum SUV measurements, respectively (Table 2). Scan–rescan reproducibility for TBR measurements were disappointing with percentage errors of ±63% and ±65%.

Blood-Pool Measurements

The percentage error of our original TBR values was double that of the SUV values, suggesting a problem with our blood-pool measurements. Interestingly, a stepwise and nonphysiological reduction in our original brachiocephalic vein measurements was observed on moving cranially up the axial slices away from the heart and into the lung. On average, a 20% difference in values was observed between the top and bottom slices, but this difference could be as high as 66%. By comparison, blood-pool sampling from the right atrium was easier to perform, allowed larger regions of interest to be drawn, and was consistent, demonstrating a <1% difference in measurements acquired on adjacent slices (Figure 3).

Sampling the blood pool in the right atrium led to a substantial improvement in the scan–rescan reproducibility of all our TBR measurements. Indeed, after implementing this approach, the reproducibility of our TBR values consistently outperformed those for SUV values with percentage errors of between ±12% and ±22% for mean and maximum values, respectively. In contrast, the approach of subtracting the blood-pool uptake from the tissue SUV to produce corrected aortic valve SUV measures did not greatly improve reproducibility resulting in percentage errors of ±43% and ±39% for mean and maximum measurements, respectively, despite similar limits of agreement (Table 2).

Considerable variation was observed in 18F-fluoride blood-pool PET activity across our population (blood-pool SUV 1.10±0.35) and even between different scans on the same patients. This is likely related to physiological variation in the distribution of the tracer.

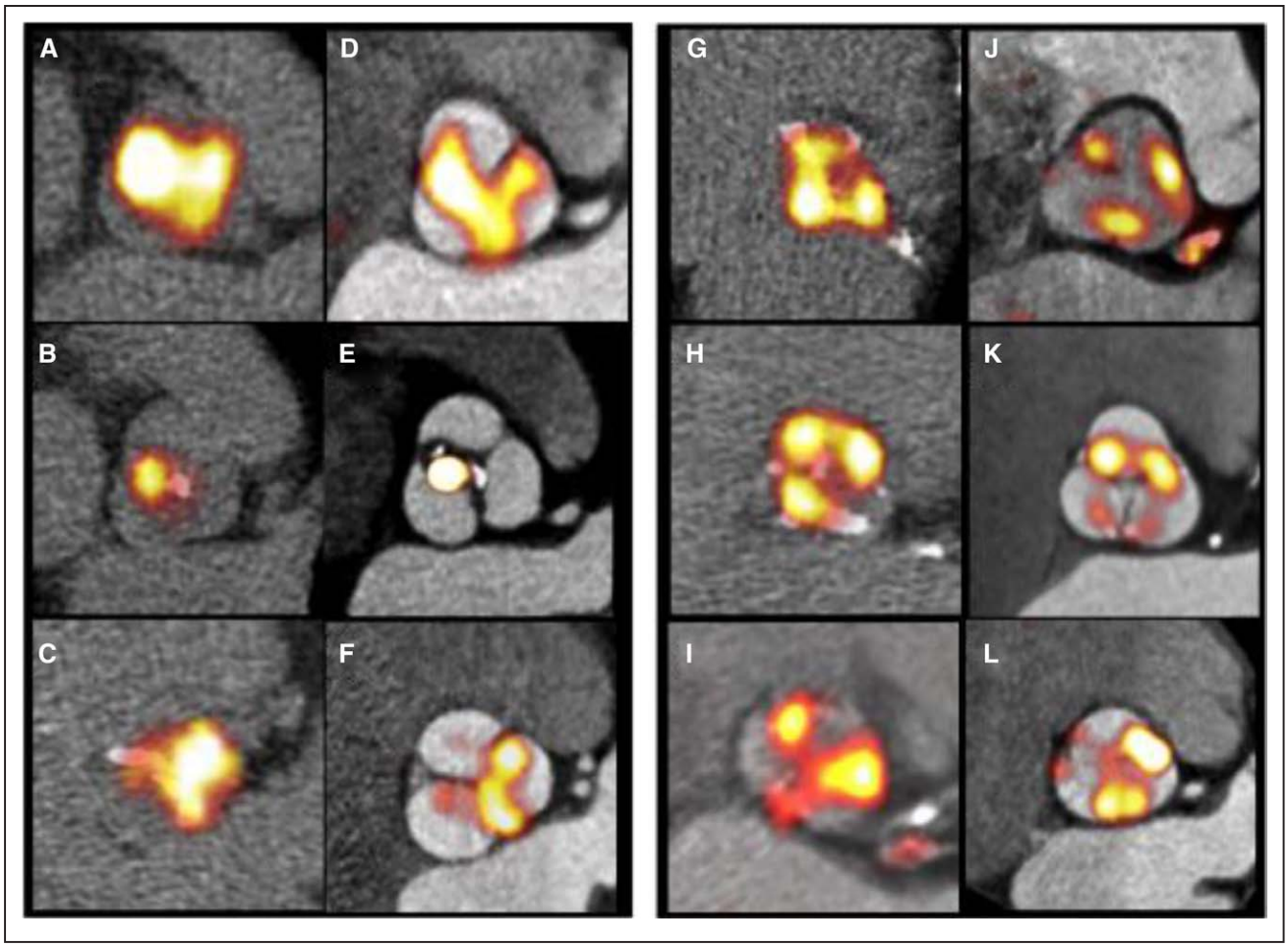

Figure 2. Improved localization of positron emission tomography (PET) signal within the aortic valve and its leaflets. Paired nongated, noncontrast PET/computed tomography (CT) scans (original approach **A**–**C** and **G**–**I**) and gated, contrast-enhanced PET/CT images (final approach **D**–**E** and **J**–**L**). Images demonstrate the typical distribution of the tracer uptake within the valve at sites of increased mechanical stress, that is, at the leaflet tips (**left**: **A**–**F**) and at the commissures (**right**: **G**–**L**).

MDS Approach

The MDS technique improved the technical ease of image analysis, removing the difficulty in deciding on the upper and lower limits of the valve in the z-plane. This translated into further improvements in scan–rescan reproducibility for mean TBR values with the percentage error for $TBR_{MDSmean}$ measurements reduced to ±10%. Similarly, maximum TBR values were optimized on addition of the MDS approach (percentage error TBR_{MDSmax} ±14%) as were the SUV measurements (percentage errors: $SUV_{MDSmean}$ ±25%; SUV_{MDSmax} ±25%; Table 2).

Final Approach: Addition of Contrast-CT and ECG-Gated PET

The addition of contrast CT and ECG-gated PET data, while markedly improving image quality as described above, did not have a major effect on scan–rescan reproducibility. Reproducibility of our final approach, however, remained good with a percentage error of ±10% for $TBR_{MDSmean}$ measurements (Figure 4). This, combined with its ability to localize PET uptake to individual leaflets, made the final approach our preferred strategy. $TBR_{MDSmean}$ values using the final approach did not show any proportional bias with disease severity (Figure I in the Data Supplement) and were again superior to the equivalent $SUV_{MDSmean}$ values (percentage error ±35%) and to measurements quantifying maximum valvular 18F-fluoride uptake, which were less reproducible after the addition of gated-PET and contrast-CT (percentage errors: SUV_{MDSmax} ±50% and TBR_{MDSmax} ±37%, respectively; Table 2).

Discussion

In this study, we have systematically investigated the acquisition and analysis of 18F-fluoride PET imaging of the aortic valve. First, we have improved the spatial localization of tracer uptake using ECG-gated PET data and contrast CT imaging, so that activity can now be localized to individual leaflets and regions within those leaflets. This has demonstrated that calcification activity is most commonly observed at sites of maximal mechanical stress: in particular, in regions of leaflet coaptation and at the commissures. Second, we have improved the scan–rescan reproducibility by using blood-pool sampling of right atrium and the MDS methodology and ultimately demonstrated good agreement for repeat $TBR_{MDSmean}$ measurements in the valve (percentage error ±10%). This has important implications for application to future clinical trials, indicating that 18F-fluoride might provide a useful imaging end point of drug efficacy.

Table 3. Scan–Rescan and Intraobserver Reproducibility for Presence or Absence of 18F-Fluoride Uptake

	Right Coronary Cusp			Noncoronary Cusp			Left Coronary Cusp		
Subject	1a	1b	2	1a	1b	2	1a	1b	2
1	+	+	+	+	+	+	+	+	–
2	+	+	+	+	+	+	+	+	+
3	+	+	+	–	+	+	–	+	–
4	+	+	+	+	+	+	+	+	+
5	+	+	+	+	+	+	+	+	+
6	+	+	+	–	–	–	–	–	–
7	+	+	+	+	+	+	+	+	+
8	–	–	–	+	+	+	+	+	+
9	+	+	+	+	+	+	+	+	+
10	+	+	+	+	+	+	+	+	+
11	–	–	–	+	+	+	+	+	+
12	+	+	–	+	+	+	–	–	–
13	+	+	+	+	+	+	+	+	+
14	+	+	+	+	+	+	+	–	+
15	+	+	+	+	+	+	+	+	+

Presence or absence of 18F-fluoride PET signal is denoted (+ and –, respectively) for each individual valve leaflet. The distribution of 18-fluoride signal on scan 1 images (1a) were reassessed (1b) to assess intraobserver reproducibility and compared with scan 2 (2) to determine scan–rescan reproducibility. PET indicates positron emission tomography.

In this study, we have modified our previous image acquisition protocol to include contrast-enhanced CT imaging of the aortic valve, thereby providing greater definition of the individual valve leaflets and their components. Moreover, we have included ECG-gated PET data to reduce the effects of cardiac motion and more accurately localize the pattern of activity on to the valve. The combined effect of these changes has been to improve the spatial localization of PET activity within the valve, which after accurate 3D coregistration, is now possible within specific regions of individual leaflets. This has demonstrated that 18F-fluoride activity predominantly localizes to sites of increased mechanical stress within the valve, supporting mechanical injury as a key driver to the disease process. For example, 18F-fluoride activity was observed at the edges of the valve leaflets exactly at the sites of leaflet impact during valve closure. Additionally, uptake was observed at the valve

Table 4. Kappa Statistics for Interobserver and Scan–Rescan Agreement for 18F-Fluoride PET Signal Distribution

		Scan 1 (Reading 2)				Scan 2	
		Absence	Presence			Absence	Presence
Right coronary cusp							
Scan 1 (first reading)	Absence	2	0	Scan 1 (first reading)	Absence	2	0
	Presence	0	13		Presence	1	12
Intraobserver agreement		1.00, 95% CI (0.00–0.00		Scan/rescan agreement		0.76, 95% CI (0.32–1.00)	
Noncoronary cusp							
Scan 1 (first reading)	Absence	1	1	Scan 1 (first reading)	Absence	1	1
	Presence	0	13		Presence	0	13
Intraobserver agreement		0.63, 95% CI (0.00–1.00)		Scan/rescan agreement		0.63, 95% CI (0.00–1.00)	
Left coronary cusp							
Scan 1 (first reading)	Absence	2	1	Scan 1 (first reading)	Absence	3	0
	Presence	1	11		Presence	1	11
Intraobserver agreement		0.58, 95% CI (0.07–1.00)		Scan/rescan agreement		0.81, 95% CI (0.47–1.00)	

The numbers of presence or absence of 18F-fluoride for right coronary cusp, noncoronary cusp, and left coronary cusp are provided. κ Statistics and 95% CIs for intraobserver (ie, scan 1 [first reading] vs scan 1 [second reading]) and scan–rescan (ie, scan 1 [first reading] vs scan 2) agreement are also shown. CI indicates confidence interval; and PET, positron emission tomography.

Table 5. Intra-/Interobserver Variability of 18F-Fluoride PET Uptake (Expressed as a Continuous Variable)

	Difference			
	Mean	SD	95% Limits of Agreement	ICC
Intraobserver*	0.053	0.124	−0.189 to 0.296	0.876
Intraobserver†	0.028	0.083	−0.134 to 0.190	0.979
Interobserver‡	−0.092	0.166	−0.418 to 0.234	0.796

ICC indicates intraclass correlation; and PET, positron emission tomography.
*Rater 1 scan 1 (first reading) vs rater 1 scan 1 (second reading).
†Rater 2 scan 1 (first reading) vs rater 2 scan 1 (second reading).
‡Rater 1 scan 1 (first reading) vs rater 2 scan 1 (first reading).

commissures where mechanical stress is concentrated before being transferred to the aortic wall.[12,13] Although these findings need to be confirmed in larger studies with further refinement of thresholding techniques, they here provide key insight into the triggers to calcification activity in aortic stenosis and the importance of mechanical injury. Recent data have indicated that the relationship between the valve calcium burden and hemodynamic obstruction is not perfect.[14,15] The ability of PET to accurately localize calcification activity may be useful in trying to understand whether calcium formation at different sites of the valve has different hemodynamic impacts.

We have modified our image analysis protocol, optimizing the scan–rescan reproducibility of 18F-fluoride imaging in the aortic valve using several different approaches. To date, it has been standard practice for 18F-fluorodeoxyglucose PET to measure the blood-pool SUV in the brachiocephalic vein.[16] This has the benefit of avoiding contamination of myocardial 18F-fluorodeoxyglucose uptake that would overestimate the blood-pool activity if measured in the heart. However, this benefit does not exist for 18F-fluoride, which has no background myocardial uptake. We, therefore, measured blood-pool activity in both the right atrium and the brachiocephalic vein. Measurements in the right atrium are easily performed on the en face (short-axis) images of the valve and resulted in much more consistent blood-pool measurements. Moreover, this approach led to a dramatic improvement in the scan–rescan reproducibility of our TBR measurements such that they then outperformed equivalent SUV measures. We think that sampling the blood-pool activity in the right atrium improved reproducibility because these measurements are less susceptible to the partial volume effects of adjacent lung tissue and because any minor inaccuracies in coregistration with the PET signal will not have a great impact. Furthermore, it seems important to correct for variations in background blood-pool activity that can occur between scans perhaps because of minor changes in renal function, tracer dose, and pharmacokinetic distribution. Chen et al[9] recently surmised that subtracting the blood pool from tissue SUV would improve accuracy. However, our study findings did not support this, and their approach produced lower TBR values, thereby increasing the percentage error of our repeat measurements.

Another major improvement in reproducibility was obtained using the MDS approach: measuring activity in the 2 hottest adjacent slices in the valve, rather than attempting to sample the entire valve. The major advantage of this technique is that it removes the considerable difficulty in deciding the limits and boundaries of the valve. Such uncertainty can lead to major differences in valve measurements because uptake is much lower at the extremes of the valve where the volume of tissue is small and inclusion of extraneous tissue will dilute down mean values.

In this article, although our stepwise changes to the protocol generally improved the reproducibility of mean measures of PET uptake, the effects on maximum measures were more variable. This finding is somewhat at odds with experience in oncology where the maximum values are often preferred. This may reflect the use of contrast-enhanced CT (not used in cancer imaging), which allowed accurate and reproducible regions of interest to be drawn around the perimeter of the valve, facilitating reproducible measurement of mean PET uptake. In addition, it may reflect ECG gating of the PET data, which discards 75% of the counts, potentially having a greater detrimental impact on maximum values (which rely on counts from only a few pixels and are therefore particularly susceptible to noise) than mean values. It is possible that advanced image analysis approaches that model and correct for cardiac motion without discarding any PET data will improve the reproducibility of TBR_{MDSmax} measurements as has recently been described for coronary 18F-fluoride activity.[17]

This is the first study to assess scan–rescan reproducibility for 18F-fluoride uptake in the aortic valve. For a technique to be clinically applicable, clinicians and clinical researchers need the reassurance that a given methodology is robust and reproducible. We have demonstrated this here. However, we acknowledge that scan–rescan reproducibility does not necessarily translate to accuracy and sensitivity. The value of 18F-fluoride as an imaging marker of calcification activity will ultimately be determined by its ability to predict disease progression and to detect changes in calcification activity in response to novel therapies. These aspects are both currently being studied within the SALTIRE 2 clinical trial. We have already shown that the $TBR_{MDSmean}$ can predict disease progression and clinical events in patients with aortic stenosis.[18] We can now report $TBR_{MDSmean}$ measurements, made using our optimized image acquisition and analysis protocols, can quantify valvular 18F-fluoride activity with good reproducibility and a 10% error. This translates directly into the requirement for low patient numbers for studies investigating the effects of interventions on 18F-fluoride PET uptake (as a marker of calcification activity), because any true effect will not be swamped by noise within the measuring technique. Indeed, based on our reproducibility data, we have provided estimates of the sample sizes required for different effect sizes (Figure 4). For example, 57 patients would be required in each group to detect a 10% difference in mean 18F-fluoride activity based on 80% power and an α error probability of 0.05. However, although these estimates provide a framework for minimum sample sizes, they should be interpreted with a degree of caution, because they assume a perfect agreement between changes in the $TBR_{MDSmean}$ signal and underlying changes in valve calcification activity.

Limitations

We acknowledge the small sample size in this study; however, it is similar to that used in previous studies examining the

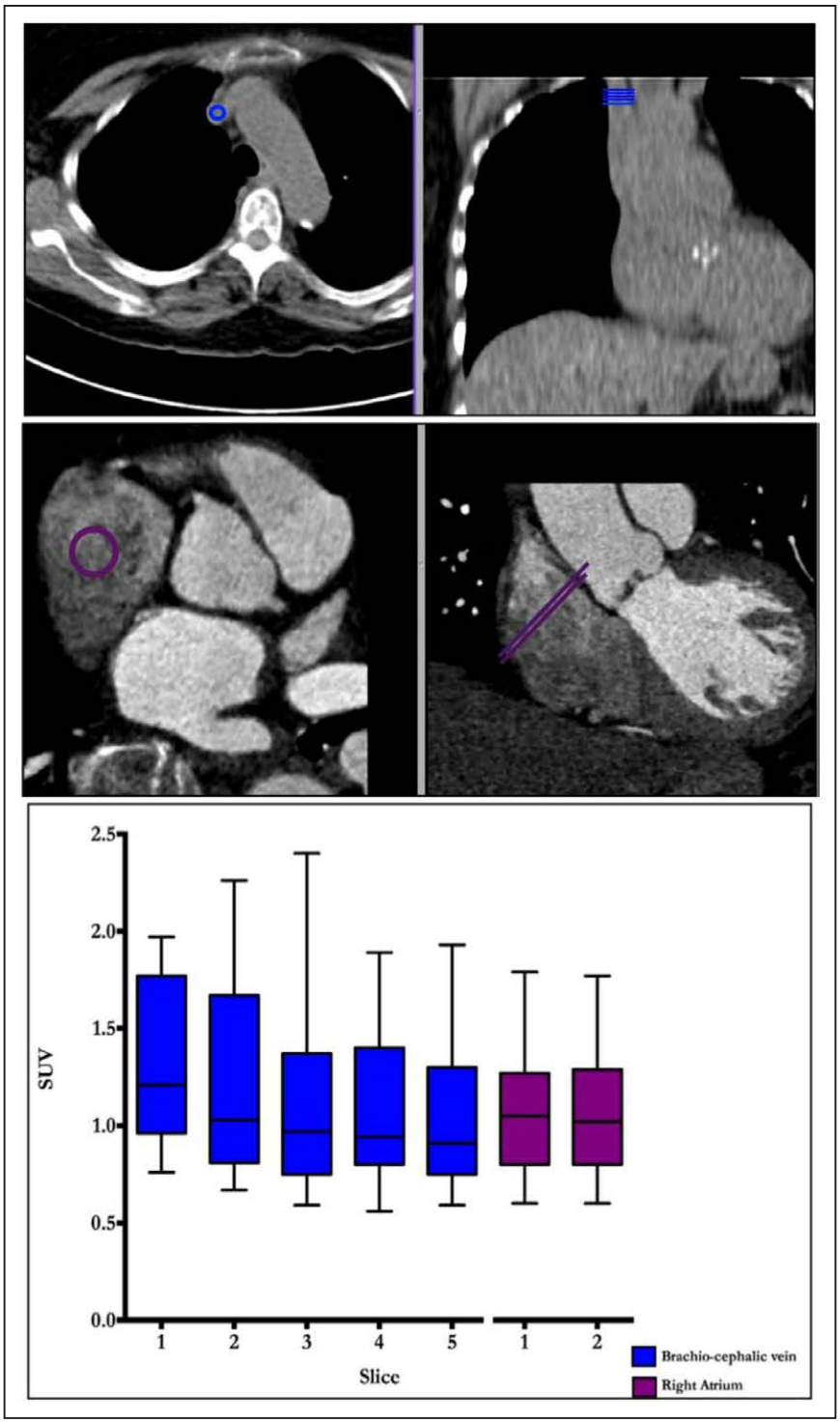

Figure 3. Measuring blood-pool activity in the brachiocephalic vein and the right atrium. Regions of interest for measuring blood-pool activity in the brachiocephalic vein (**top**) and right atrium (**bottom**) are shown in the en face of the valve (**left**) and coronal (**right**) planes. Note that the right atrium is a much larger structure allowing for larger regions of interest with less potential for partial volume artifact problems related to poor registration. Tukey plot demonstrates mean standard uptake values (SUV) for 5 contiguous slices from brachiocephalic (**blue**) and 2 from the right atrium (**purple**). Note the variation in brachiocephalic vein measurements between those taken most caudally vs those taken most cranially.

reproducibility of vascular PET[19]and, in part, reflects attempts to minimize the radiation exposure associated with repeat PET/CT imaging. Moreover, although previous studies have indicated that 18F-fluoride uptake correlates with histological markers of calcification activity and accurately predicts the progression in the CT calcium score, we currently lack data to show that 18F-fluoride is modifiable with drug therapy. Largely, this is because no drug has yet demonstrated an ability to reduce disease activity in aortic stenosis, and we lack reliable animal models of this condition.

In conclusion, we have optimized 18F-fluoride PET-CT imaging in the aortic valve. Excellent localization of the PET signal within the aortic valve is now possible, with uptake observed in regions of maximal mechanical stress. Moreover, quantification of valvular 18F-fluoride uptake is now possible with good scan–rescan reproducibility. 18F-Fluoride PET-CT holds major promise as a method to better understand calcification activity in aortic stenosis and as a surrogate end point in clinical trials assessing the efficacy of potential therapeutic interventions.

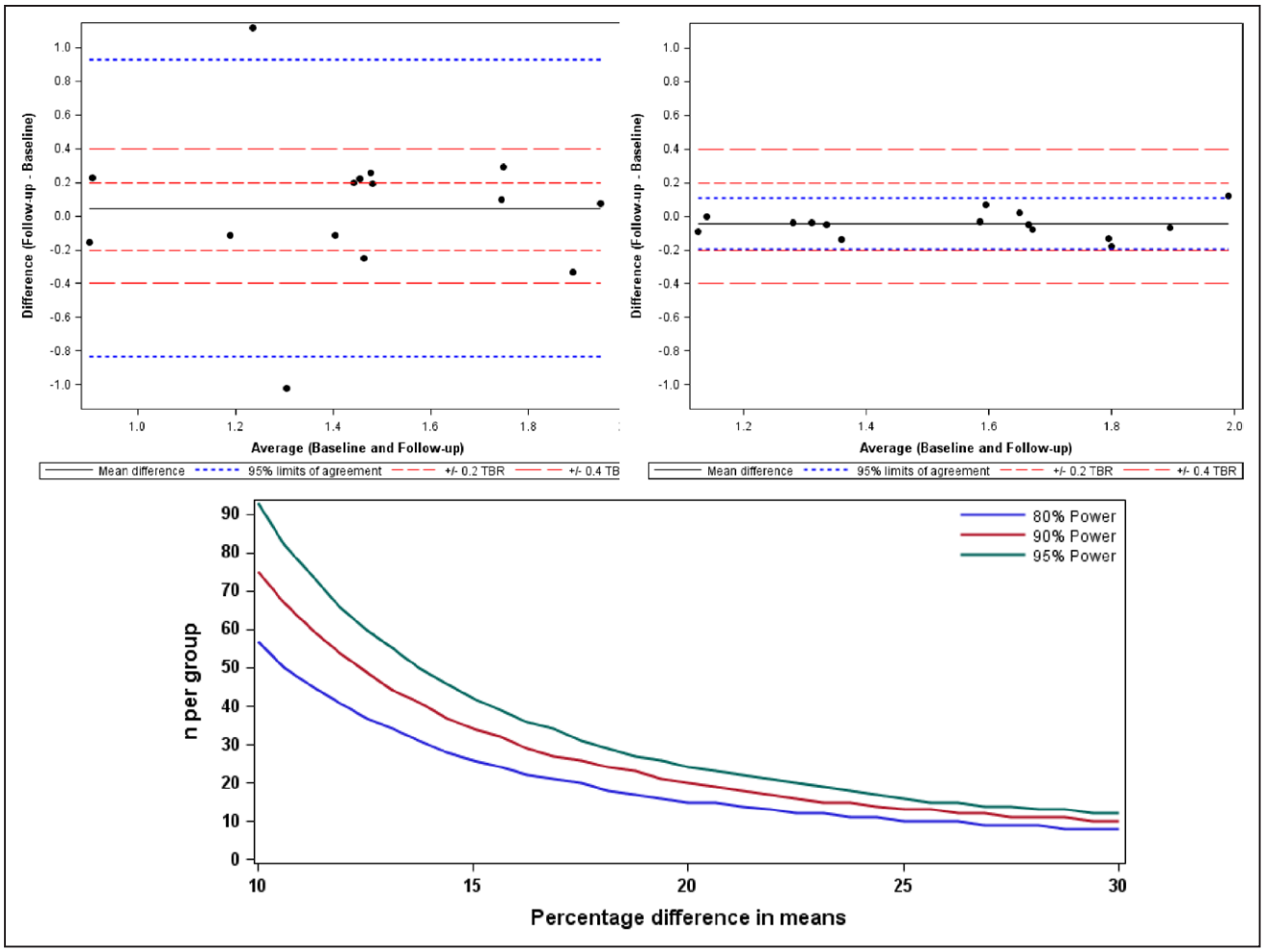

Figure 4. Scan–rescan reproducibility for 18F-fluoride positron emission tomography quantification in the aortic valve with consequent sample size estimates. Bland–Altman plots of scan–rescan reproducibility for tissue to background ratio $(TBR)_{MDSmean}$ measurements using the original image analysis and acquisition methods (**left**) and then using final method (**right**). Percentage error for the final method is less than ±10%. Graph (**below**) shows the sample size estimates needed to detect differences in means that range from 10% to 30% of the initial scan point estimate. The plot illustrates the sample size required to detect differences in means ranging from 10% to 30% with figures shown for 80%, 90%, and 95% power. In all cases, this assumes that the common SD is 18.75%. MDS indicates most diseased segment.

Acknowledgments

We acknowledge the support of staff at the Edinburgh Heart Centre at the Royal Infirmary of Edinburgh and the radiography and radiochemistry staff of the Clinical Research Imaging Centre. We also acknowledge the Edinburgh Clinical Trials Unit and the Trial Steering Committee for the SALTIRE 2 clinical trial.

Sources of Funding

The study was funded by the British Heart Foundation (FS/14/78/31020). Drs Pawade, Cartlidge, Jenkins, Dweck, and Newby are supported by the British Heart Foundation (SS/CH/09/002/26360, FS/13/77/30488, SS/CH/09/002/2636, FS/14/78/31020, and CH/09/002). Dr Newby is the recipient of a Wellcome Trust Senior Investigator Award (WT103782AIA). Dr Dweck is the recipient of the Sir Jules Thorn Award for Biomedical Research 2015. Dr Adamson is supported by New Zealand Overseas Training and Research Fellowship (1607) and Edinburgh and Lothians Health Foundation (50–534). The Wellcome Trust Clinical Research Facility and the Clinical Research Imaging Centre are supported by NHS Research Scotland (NRS) through NHS Lothian. Dr Rudd is partly supported by the NIHR Cambridge Biomedical Research Centre, the British Heart Foundation, and the Wellcome Trust.

Disclosures

None.

References

1. Pawade TA, Newby DE, Dweck MR. Calcification in aortic atenosis: the skeleton key. *J Am Coll Cardiol*. 2015;66:561–577. doi: 10.1016/j.jacc.2015.05.066.
2. Rossebø AB, Pedersen TR, Boman K, Brudi P, Chambers JB, Egstrup K, Gerdts E, Gohlke-Bärwolf C, Holme I, Kesäniemi YA, Malbecq W, Nienaber CA, Ray S, Skjaerpe T, Wachtell K, Willenheimer R; SEAS Investigators. Intensive lipid lowering with simvastatin and ezetimibe in aortic stenosis. *N Engl J Med*. 2008;359:1343–1356. doi: 10.1056/NEJMoa0804602.
3. Irkle A, Vesey AT, Lewis DY, Skepper JN, Bird JL, Dweck MR, Joshi FR, Gallagher FA, Warburton EA, Bennett MR, Brindle KM, Newby DE, Rudd JH, Davenport AP. Identifying active vascular microcalcification by (18)F-sodium fluoride positron emission tomography. *Nat Commun*. 2015;6:7495. doi: 10.1038/ncomms8495.
4. Dweck MR, Jenkins WS, Vesey AT, Pringle MA, Chin CW, Malley TS, Cowie WJ, Tsampasian V, Richardson H, Fletcher A, Wallace WA, Pessotto R, van Beek EJ, Boon NA, Rudd JH, Newby DE. 18F-sodium fluoride uptake is a marker of active calcification and disease progression in patients with aortic stenosis. *Circ Cardiovasc Imaging*. 2014;7:371–378. doi: 10.1161/CIRCIMAGING.113.001508.

5. Dweck MR, Jenkins WS, Vesey AT, Pringle MA, Chin CW, Malley TS, Cowie WJ, Tsampasian V, Richardson H, Fletcher A, Wallace WA, Pessotto R, van Beek EJ, Boon NA, Rudd JH, Newby DE. 18F-sodium fluoride uptake is a marker of active calcification and disease progression in patients with aortic stenosis. *Circ Cardiovasc Imaging*. 2014;7:371–378. doi: 10.1161/CIRCIMAGING.113.001508.
6. Dweck MR, Jones C, Joshi NV, Fletcher AM, Richardson H, White A, Marsden M, Pessotto R, Clark JC, Wallace WA, Salter DM, McKillop G, van Beek EJ, Boon NA, Rudd JH, Newby DE. Assessment of valvular calcification and inflammation by positron emission tomography in patients with aortic stenosis. *Circulation*. 2012;125:76–86. doi: 10.1161/CIRCULATIONAHA.111.051052.
7. Jenkins W, Pringle M, Cowie WJ, Richardson H, Fletcher A, Pessotto R, Boon NA, Rudd J, Newby D, Dweck M. 18F-NaF is a predictor of progression and outcome in aortic valve disease. *J Am Coll Cardiol* 2014;63. doi:101016/S0735-1097(14)60995-5.
8. Litmanovich DE, Ghersin E, Burke DA, Popma J, Shahrzad M, Bankier AA. Imaging in transcatheter aortic valve replacement (TAVR): role of the radiologist. *Insights Imaging*. 2014;5:123–145. doi: 10.1007/s13244-013-0301-5.
9. Chen W, Dilsizian V. PET assessment of vascular inflammation and atherosclerotic plaques: SUV or TBR? *J Nucl Med*. 2015;56:503–504. doi: 10.2967/jnumed.115.154385.
10. Fayad ZA, Mani V, Woodward M, Kallend D, Abt M, Burgess T, Fuster V, Ballantyne CM, Stein EA, Tardif JC, Rudd JH, Farkouh ME, Tawakol A; dal-PLAQUE Investigators. Safety and efficacy of dalcetrapib on atherosclerotic disease using novel non-invasive multimodality imaging (dal-PLAQUE): a randomised clinical trial. *Lancet*. 2011;378:1547–1559. doi: 10.1016/S0140-6736(11)61383-4.
11. Critchley LA, Critchley JA. A meta-analysis of studies using bias and precision statistics to compare cardiac output measurement techniques. *J Clin Monit Comput*. 1999;15:85–91.
12. Aikawa E, Nahrendorf M, Sosnovik D, Lok VM, Jaffer FA, Aikawa M, Weissleder R. Multimodality molecular imaging identifies proteolytic and osteogenic activities in early aortic valve disease. *Circulation*. 2007;115:377–386. doi: 10.1161/CIRCULATIONAHA.106.654913.
13. Deck JD, Thubrikar MJ, Schneider PJ, Nolan SP. Structure, stress, and tissue repair in aortic valve leaflets. *Cardiovasc Res*. 1988;22:7–16.
14. Clavel MA, Messika-Zeitoun D, Pibarot P, Aggarwal SR, Malouf J, Araoz PA, Michelena HI, Cueff C, Larose E, Capoulade R, Vahanian A, Enriquez-Sarano M. The complex nature of discordant severe calcified aortic valve disease grading: new insights from combined Doppler echocardiographic and computed tomographic study. *J Am Coll Cardiol*. 2013;62:2329–2338. doi: 10.1016/j.jacc.2013.08.1621.
15. Dweck MR, Chin C, Newby DE. Small valve area with low-gradient aortic stenosis: beware the hard hearted. *J Am Coll Cardiol*. 2013;62:2339–2340. doi: 10.1016/j.jacc.2013.08.1620.
16. Tawakol A, Migrino RQ, Bashian GG, Bedri S, Vermylen D, Cury RC, Yates D, LaMuraglia GM, Furie K, Houser S, Gewirtz H, Muller JE, Brady TJ, Fischman AJ. *In vivo* 18F-fluorodeoxyglucose positron emission tomography imaging provides a noninvasive measure of carotid plaque inflammation in patients. *J Am Coll Cardiol*. 2006;48:1818–1824. doi: 10.1016/j.jacc.2006.05.076.
17. Rubeaux M, Joshi NV, Dweck MR, Fletcher A, Motwani M, Thomson LE, Germano G, Dey D, Li D, Berman DS, Newby DE, Slomka PJ. Motion correction of 18F-NaF PET for imaging coronary atherosclerotic plaques. *J Nucl Med*. 2016;57:54–59. doi: 10.2967/jnumed.115.162990.
18. Jenkins WS, Vesey AT, Shah AS, Pawade TA, Chin CW, White AC, Fletcher A, Cartlidge TR, Mitchell AJ, Pringle MA, Brown OS, Pessotto R, McKillop G, Van Beek EJ, Boon NA, Rudd JH, Newby DE, Dweck MR. Valvular (18)F-fluoride and (18)F-fluorodeoxyglucose uptake predict disease progression and clinical outcome in patients with aortic stenosis. *J Am Coll Cardiol*. 2015;66:1200–1201. doi: 10.1016/j.jacc.2015.06.1325.
19. Rudd JH, Myers KS, Bansilal S, Machac J, Rafique A, Farkouh M, Fuster V, Fayad ZA. (18)Fluorodeoxyglucose positron emission tomography imaging of atherosclerotic plaque inflammation is highly reproducible: implications for atherosclerosis therapy trials. *J Am Coll Cardiol*. 2007;50:892–896. doi: 10.1016/j.jacc.2007.05.024.

CLINICAL PERSPECTIVE

18F-Fluoride positron emission tomography (PET) is being increasingly used as a research tool to study calcification activity in the vasculature. It binds preferentially to regions of newly developing microcalcification beyond the resolution of computed tomography (CT) and, in aortic stenosis, correlates closely with calcification activity on histology (alkaline phosphatase staining). Moreover, clinical 18F-fluoride PET-CT in aortic stenosis offers accurate prediction of disease progression and adverse cardiovascular events. 18F-Fluoride PET-CT, therefore, has major potential to improve our understanding of the role of calcification in aortic stenosis and also as a surrogate end point in studies of novel therapies for this condition. This article adds to current literature demonstrating that optimized 18F-fluoride PET-CT in aortic stenosis can localize calcification activity to individual leaflets and regions of the valve associated with increased mechanical stress. Moreover, it shows that the scan–rescan reproducibility of aortic valve PET measurements is good, with a percentage error of ±10%. These data strongly support the use of 18F-fluoride PET-CT as a tool to study the mechanisms underlying aortic stenosis and also as an end point in novel therapies for this common condition.

Circulation
Cardiovascular Imaging

Optimization and Reproducibility of Aortic Valve 18F-Fluoride Positron Emission Tomography in Patients With Aortic Stenosis

Tania A. Pawade, Timothy R.G. Cartlidge, William S.A. Jenkins, Philip D. Adamson, Phillip Robson, Christophe Lucatelli, Edwin J.R. Van Beek, Bernard Prendergast, Alan R. Denison, Laura Forsyth, James H.F. Rudd, Zahi A. Fayad, Alison Fletcher, Sharon Tuck, David E. Newby and Marc R. Dweck

Circ Cardiovasc Imaging. 2016;9:
doi: 10.1161/CIRCIMAGING.116.005131
Circulation: Cardiovascular Imaging is published by the American Heart Association, 7272 Greenville Avenue, Dallas, TX 75231

Print ISSN: 1941-9651. Online ISSN: 1942-0080

SUPPLEMENTAL MATERIAL

Table 1. Full list of inclusion and exclusion criteria

Inclusion Criteria	Age >50 years
	Peak aortic jet velocity of >2.5 m/s on Doppler echocardiography
	Grade 2-4 calcification of the aortic valve on echocardiography
Exclusion Criteria	Women of childbearing potential who have experienced menarche, are premenopausal,
	Women who have not been sterilized or who are currently pregnant.
	Women who are breastfeeding
	Renal failure (estimated glomerular filtration rate of <30 mL/min)
	Inability to undergo scanning
	Allergy or contraindication to iodinated contrast
	Inability or unwilling to give informed consent
	Likelihood of non0compliance to treatment allocation or study protocol.
	Anticipated or planned aortic valve surgery in the next 6 months,
	Life expectancy less than 2 years,
	Treatment for osteoporosis with bisphosphonates or denosumab.

	Known allergy or intolerance to alendronate or denosumab, or any of their excipients
	Abnormalities of the oesophagus or conditions, which delay oesophageal/gastric emptying.
	Inability to sit or stand for at least 30 minutes.
	Hypocalcaemia
	Regular calcium supplementation
	Dental extraction within 6 months
	Long term corticosteroid use.
	History of osteonecrosis of the jaw
	Poor dental hygiene
	Major or untreated cancers

Figure 1. Linear regression analysis of scan-rescan reproducibility versus calcium burden. The mean difference between 18F-Fluoride TBRMDSmean measures for the 15 scan pairs is plotted against the log-transformed Computed Tomography calcium score (log_{10} Agatston Units). No proportional bias is observed.